Technical Transactions

Czasopismo Techniczne

Contents

Julia Kurek
Justyna Martyniuk-Pęczek
justyna.martyniuk-peczek@pg.edu.pl
Faculty of Architecture, Gdańska University of Technology

Forecasted climate changes and their influence on cities and regions in 2050 in terms of extreme hydrological events

Prognozowane zmiany klimatyczne i ich wpływ na miasta i regiony w 2050 roku w kontekście ekstremalnych zjawisk hydrologicznych

Abstract

Global climate change is a problem which arises numerous theories and uncertainties, especially in terms of speculated human impact. Independent from the fact, what is the main driver for the changes, some of the climate shifts are visible already nowadays. Both contemporary and future cities will have to face such problems. Although climate change may cause numerous effects on different fields, a special stress in this article is laid on hydrological events – which are possible to observe even in these days. The purpose of this article is to indicate the main approaches both to the issue of climate change and activities undertaken by cities in relation to hydrological threats.

Keywords: climate change, extreme weather events

Streszczenie

Kwestia zmian klimatycznych jest tematem, wokół którego narastają liczne teorie i niepewności, w szczególności odnośnie spekulowanego wpływu antropogenicznego. Niezależnie od tego, co jest ich główną przyczyną, niektóre z prognozowanych zmian można już zaobserwować współcześnie. Pomimo że skutki zmian klimatycznych można obserwować na wielu polach, w tym artykule nacisk położony jest na ekstremalne hydrologiczne zjawiska klimatyczne, których narastanie można zaobserwować już w chwili obecnej. Miasta, zarówno obecnie, jak i w przyszłości, będą się musiały z tego typu problemami zmierzyć. Celem tego artykułu jest wskazanie głównych podejść zarówno do kwestii zmian klimatycznych, jak i działań podejmowanych przez miasta w związku ze zmieniającym się klimatem i zagrożeniami hydrologicznymi.

Słowa kluczowe: zmiany klimatyczne, ekstremalne zjawiska pogodowe

1. Introduction

Global climate change and its consequences are becoming today's most pressing issue. Despite numerous international investigations, the exact mechanism of their occurrence is ambiguous and accordingly, universal climate change adaptation strategies have not yet been developed. The cities and regions are especially vulnerable in terms the factor of water.

Numerous investigations conducted by NASA [9] and other organizations of International Climate Change Panel confirm the flux of our climate [1]. The scientists claim that since the 1950s the changes in the climate are extraordinary. The mean temperatures have risen what is visible in the atmosphere, ocean levels and melting glaciers. Given the complexity of climate no confident prediction about future global mean temperature or its impact can be made [1].

Nowadays the approach towards architecture and urban planning is based on the sustainable development rules which are understood as a proper balance between environmental, social and economic aspects. There are many approaches being developed to deal with climate change hazards, especially in terms of water, as they strongly influence the relation between water and city.

The aim of this article is to draw attention to urgent problems of climate change and extreme weather events in terms of water along with providing examples of possible approaches to the problem.

2. The evidence of global climate change and its characteristics

In terms of climate change and anthropogenic influence there are many often contradictory theories arising. Climate change as a complex topic, apart from scientific insight gained some interest of different groups dealing with it on daily basis.

We can distinguish three main groups of people dealing with the climate change problems: the scientists form IPCC (International Panel of Climate Change, organized by United Nations), the second group consisting of scientists called skeptics and the third group- politicians, environmentalists and media. According to scientists from IPCC, climate change is caused by burning fossil fuels like oil, coal and natural gas. Because of that the emission of CO_2 is arising and may dangerously heat the planet. This group also supports the view on anthropogenic influence of climate change [11].

As stated by second, sceptic group of scientists – there are many reasons why the climate changes – like sun position, cloud and ocean movements along with other numerous complex inputs. None of them is fully understood and there is no evidence that anthropogenic CO_2 emissions are the dominant factor in climate change. One of them is American atmospheric physicist known for his work in the dynamics of the middle atmosphere, retired professor from Massachusetts University of Technology, who regularly confirms his thesis on research articles and scientific books [7, 8].

For the third group global warming alarmism provides most favorable aspects – for politicians it is money and power whereas for environmentalists these are finances for their organizations and confirmation of their devotion to the idea that man is destructive force acting upon nature [11].

2.1. The acknowledged facts of climate change

Regardless of the fact if we agree on anthropogenic influence on climate change or not, there is some unquestionable information about it.

First of all, the climate has been always changing. The proof for this is visible on charts presenting climate changes since ages. Another fact is that CO_2 is a greenhouse gas without which life on earth is not possible, but increased concentration of it to atmosphere should lead to global warming. Atmospheric levels of CO_2 have been increasing since the middle ice-age. Apart from this, by 1800–2000 global mean temperature has increased slightly and erratically by 1°C*. But only since 1960s has man's greenhouse emissions been sufficient to play a role.

Given the complexity of climate no confident prediction about future global mean temperature or its impact can be made [11].

2.2. Forecasted climate changes – potential ways of climate shifts
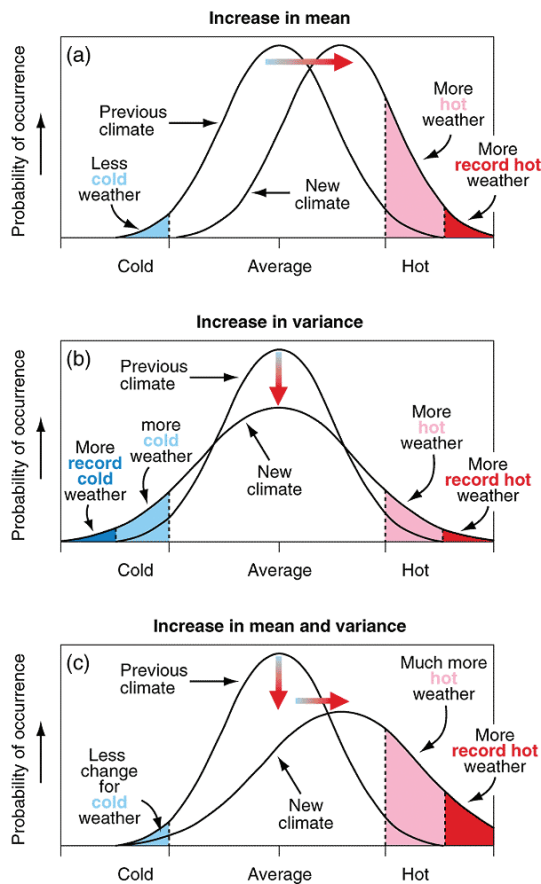
Fig. 1. Schematic presenting possible changes in climate and the effect on extreme temperatures (source: [3])

The schematic above is showing the effect on extreme temperatures. If considered potential climate changes, three different results can be expected. When for a normal distribution of temperature, the mean temperature increases it can lead to longer seasons (without transitional seasons), for example longer summer growing season and longer winter season almost without existence of autumn and spring. In the situation when the variance increases extreme weather events can grow i.e. extreme precipitation and droughts. There is also a possibility of growth both the mean and variance increase what can result in both in prolonging the seasons without transitional seasons and increase in extreme weather events [3].
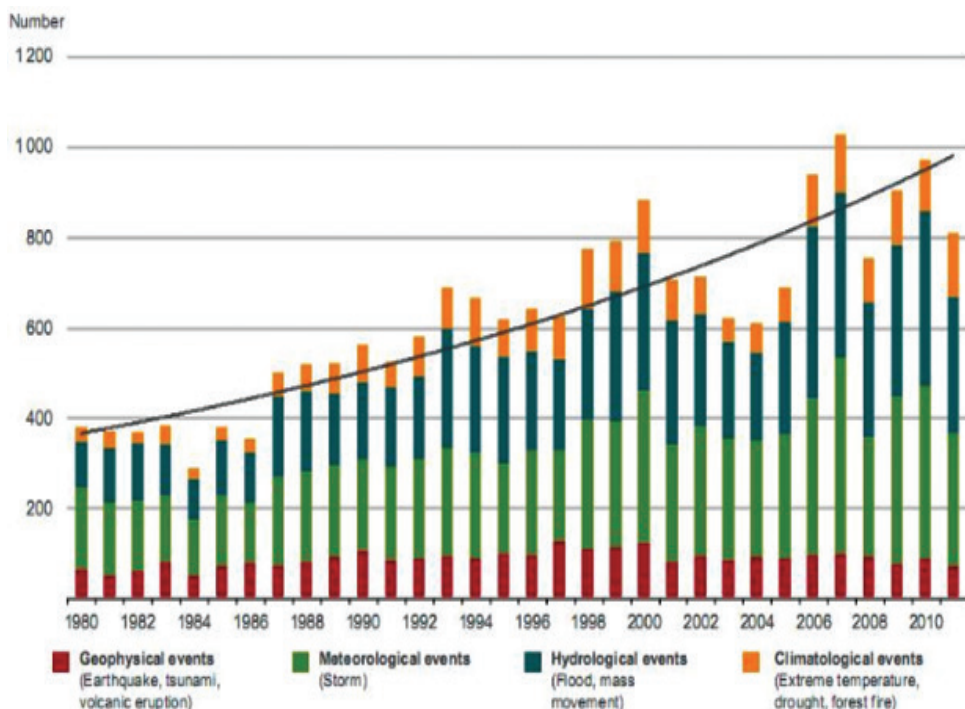
Fig. 2. Natural catastrophes worldwide 1980–2011. Number of events with trend (source: [16])

If we consider the natural catastrophes worldwide at the time 1980-2011 a tendency of a slight growth of natural catastrophes worldwide is observed (according to the chart [16]. The number of hydrological events grew remarkably).

3. The sustainability context of climate change

Contemporary approach towards planning involves attempts towards sustainable development – finding the right balance between social, economic and environmental issues. As one of the UN Habitat sustainable development goal climate action has been indicated, which confirms the significance of the problem and the need to undertake sever steps on regular basis.
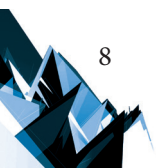
3.1. Social aspects of climate change – the problem of awareness

It is important to note that, not only economic and ecological aspects play crucial role in terms of climate change. Not less important is the underestimated social factor.

At both the business and household levels information is needed about beliefs, knowledge and attitudes towards energy use, climate change science and policy, as well as current behaviors regarding energy use. Information is needed about strategies that will be most effective at encouraging households and businesses to reduce energy use. Information is also needed about strategies that will be most effective at helping households and businesses adapt to changes in climate.

At the community, local and state government levels research is needed to understand and measure communities' state of readiness for managing the impacts of climate change; how communities are currently affected by climate change; and how community design can be altered to better prepare communities for further climate change [30].

4. Cities and regions most threatened with climate change in 2050 in terms of hydrological events

Although climate change may cause numerous effects on different fields, a special stress in this article is laid on hydrological events – which are possible to observe even in these days.
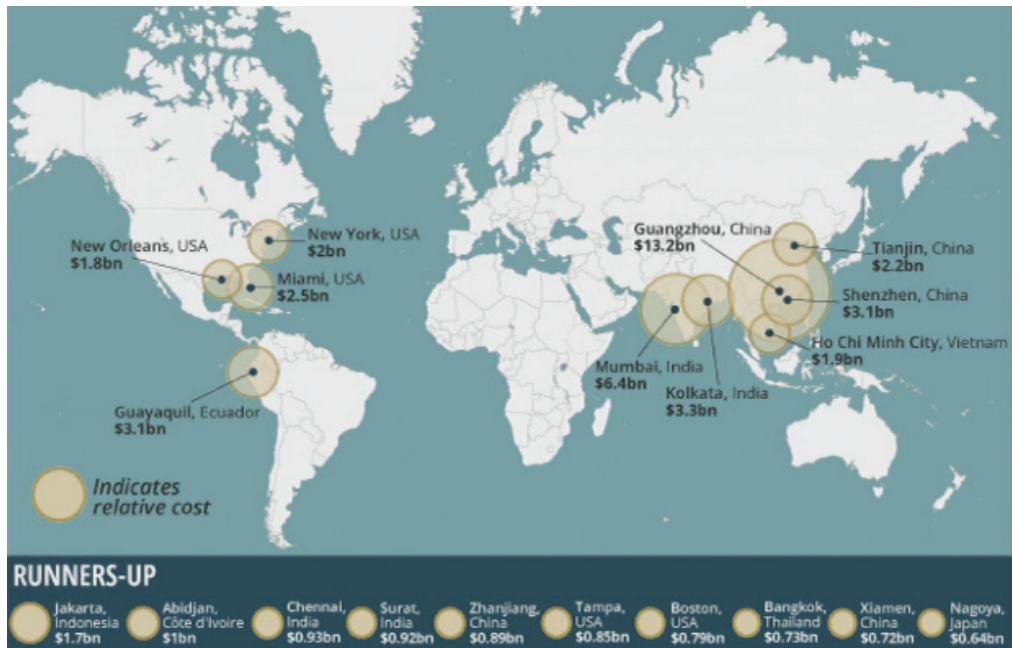
Fig. 3. Cities with the ten highest annual flood costs by 2050 (source: [2])

Water Stress by Country: 2040

ratio of withdrawals to supply

- Low (< 10%)
- Low to medium (10-20%)
- Medium to high (20-40%)
- High (40-80%)
- Extremely high (> 80%)
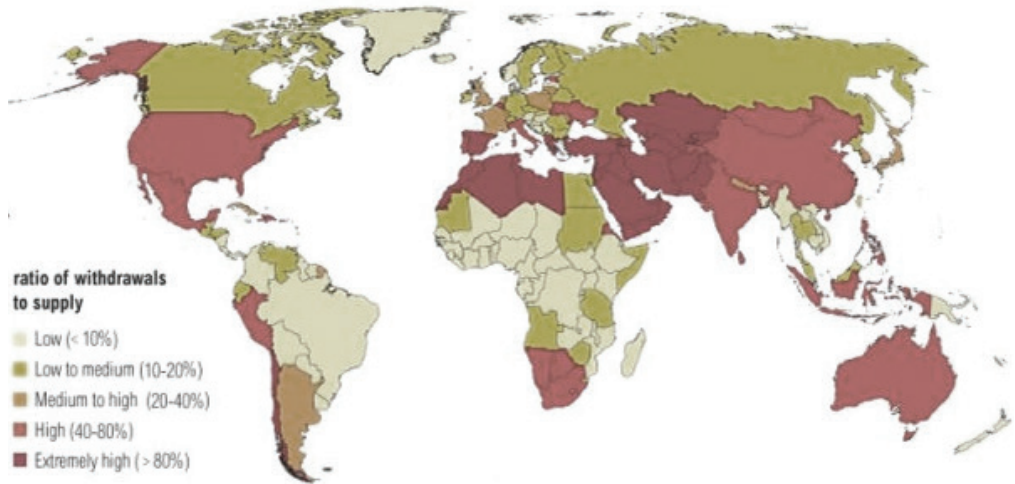
NOTE: Projections are based on a business-as-usual scenario using SSP2 and RCP8.5.

For more: ow.ly/RiWop

WORLD RESOURCES INSTITUTE

Fig. 4. Water Stress by Country 2040 (source: [5])

Fig. 5. Climate change impacts around the world (source: [15])

The map above presents cities with the ten highest annual flood costs by 2050. Most at risk are the safety and the economic development of communities in Small Island Developing States, Least Developed Countries, African countries, and other countries that have significant populations who are vulnerable to the impacts of climate change. The world's 136 largest cities could be facing annual flood losses of US $1 trillion (1,000,000,000,000$) by 2050 [5].

If we consider water stress by country 2040 [6], nearly 634 million people – one tenth of the global population – live in at-risk coastal areas, just a few meters above existing sea levels. Three quarters are located in Asian flood-prone densely-populated river deltas or in low-lying small island states.

Climate change has a remarkable impact specially on hydrological events such as: wildfires, species impact, floods, sea level rise, water stress, melting ice and crop changes. The changes can be observed around the whole world [15] It is also projected to increase the frequency and severity of climate-related hazards, such as: storms, extreme precipitation, flooding, sea-level rise, heat waves increase in the spread of vector borne diseases [10] This all leads to the conclusion, that severe actions at all levels need to be undertaken to deal with those issues.

Although Poland is not remarkably threatened with extreme hydrological events, an increase of some of the can be observed already in a form of extreme precipitations and floods. These are increasing in frequency in recent years.

5. Adaptation and mitigation strategies and actions of the cities and regions

Although the terms of climate adaptation strategy and contingency measures, solutions for climate change may seem similar it is important to distinguish between on the spot, contingency solutions which are just dealing with existing problems and long term adaptation strategies which are prevention of problems.
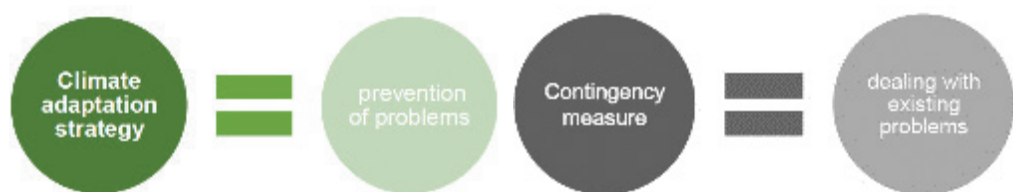
Fig. 6. schematic showing of possible approaches of cities towards climate change

5.1. Contingency measures for hydrological events caused by climate change

A few contingency measures can be differentiated in dealing with climate change in terms of water. If the need is to direct the water into desired direction, there are dikes or sandbags used. In terms of reduction of water masses these are usually rainwater retention basins. In order to collect rainwater, the water is used for building or watering the fields. An extreme solution, but still present is surrending from the effects: escape, move out from a certain location or even region.

5.2. Adaptation strategies for hydrological events caused by climate change

Both architectural and urban concepts can take into account the role of the climate factor in specific design solutions – adaptation strategies. Scientists around the world develop numerous strategies helping to deal with climate hazards like floods. One of the solution is green street storm water planter. This constitutes a typical adaptation strategy approach. Thanks to storm water Planter in Philadelphia the excess water can be quickly piped. While drought, the planted greenery prevents form excess heating. Green streets utilize green storm water infrastructure (GSI) to capture storm water at its (source and minimize the amount of pollutants that reach the river, and the many tributary streams within the city. Green streets are a key component of the City of Philadelphia's Green City, Clean Waters initiative, an innovative program to achieve federal water quality mandates by managing storm water from impervious surfaces citywide utilizing green storm water management practices [16]
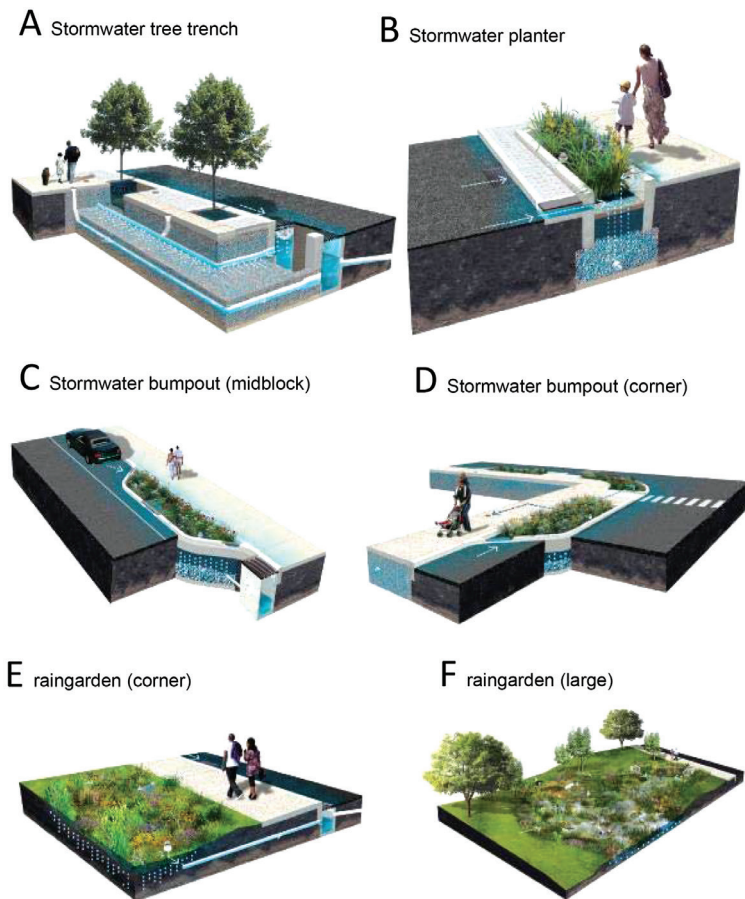
Fig. 8. Storm water Management Practices, Philadelphia (source: [17]): A.Stormwater tree trench, B) Stormwater planter, C) Stormwater bumpout (midblock), D) Stormwater bumpout (corner), E) raingarden (corner) F) raingarden (large)

5.2.1. Stormwater management practices on the example of Philadelphia

The city of Philadelphia developed several stormwater management practcies configurations, which are visible on the pictures below. They shape an overlook of accessible and diverse methods avalaible for contemporary cities interested in in climate adaptation in terms of hydrological events. The methods developed by Philadelphia Water Department rely on bioinfiltration and bioretention processes. They consist of vegetated depressions or basins that use surface storage (such as vegetation, planting soil, outlet controls) and other components to treat, detain, and retain stormwater runoff. These practices enable reducing stormwater volume and pollution thanks to filtering runoff through a vegetated soil medium that promotes evapotranspiration. In terms of diversity, a variety of configurations can be distinguished from relatively large and open vegetated basins to small-scale configurations contained within flow-through planter boxes [18].

5.2.2. Amphibious house system

Another promising solution against flooding are amphibious houses. One of such solutions has been proposed by the architects from BACA. UK's first amphibious house developed by them is able to float on floodwater like a boat [15]. It has been designed on the flood-prone river island near Marlow in Buckinghamshire.

While floods the building can raise and float on the water with no damage to the structure itself. As floodwaters fill the fixed "dock" beneath the three-bedroom home, the water levels push the buoyant house upwards. The structure is attached to four guideposts that extend upwards and allow for a 2.5-meter-high floodwater clearance, to ensure that the home does not float away.
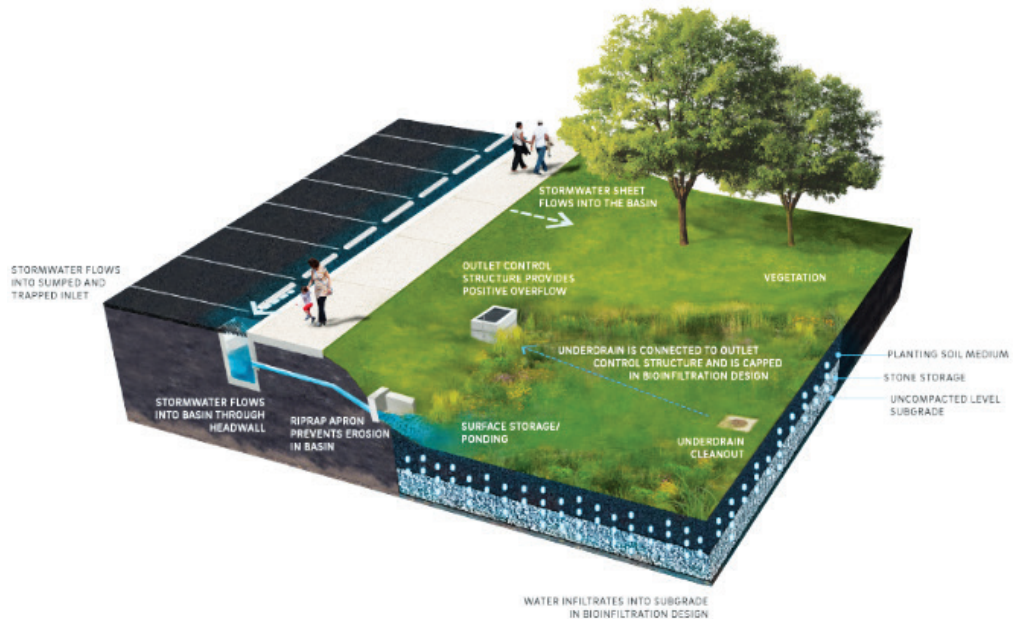
Fig. 9. Bioinfiltration/Bioretention Basin with Typical Features (source: [18])

Fig. 10. Flow-Through Planter Box with Typical Features (source: [18])

Coutts from baca architects explains that, the design was developed according to the Archimedes principle: "the house's mass and volume are less than the equivalent of water, and that's what creates buoyancy".

The form of the house is traditional, lightweight timber-framed structure. Inside the structure there is an excavated "wet dock" made from steel sheet piling with a mesh base to allow water to enter and escape naturally.

The structure of clad in zinc shingles with glazed gables structure is independent of the house. It faces a small garden, which slopes up from the edge of the river and is designed to provide an early warning of flooding.

Fig. 11. Site plan and view of amphibious house, BACA architects (source [19])
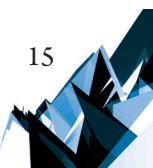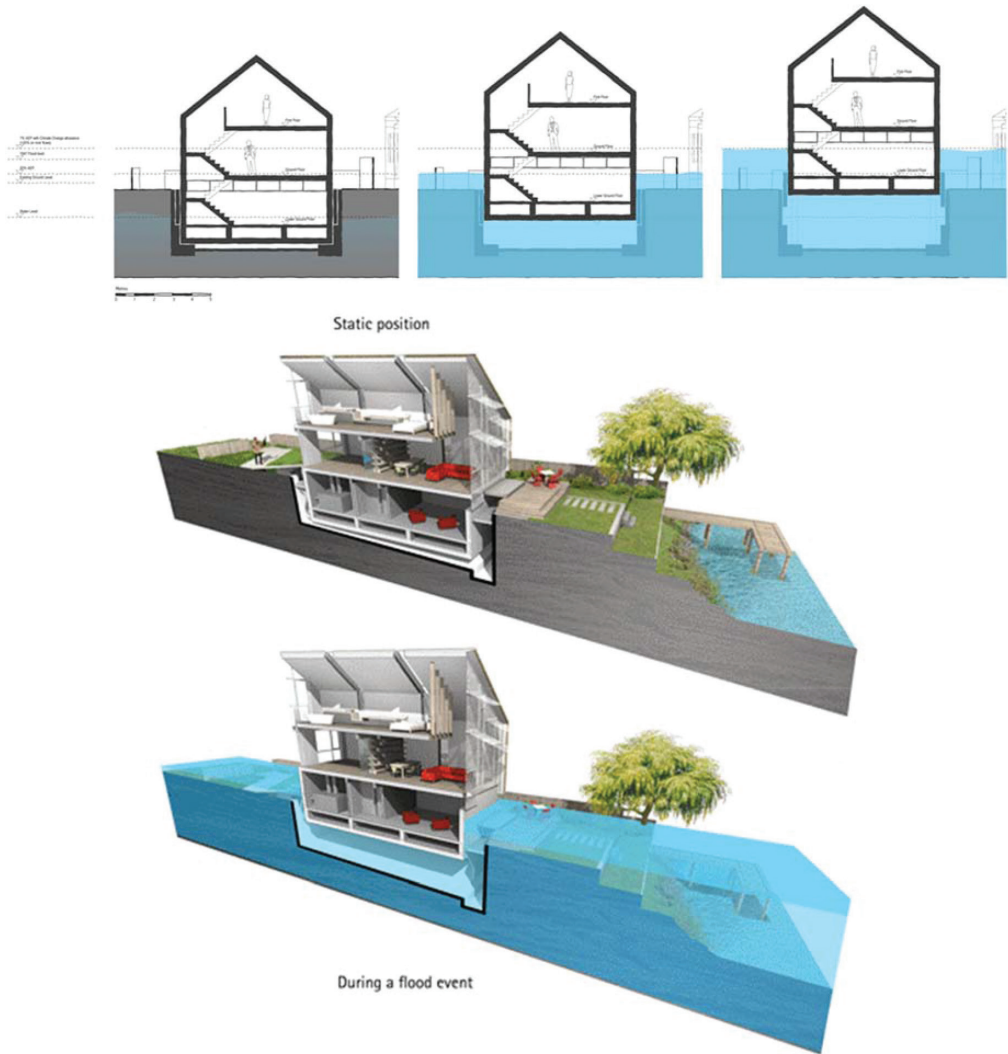
Fig. 12. Amphibious house at resting position and flood event (sources: [15, 19])

5.2.3. Shade balls

To prevent from evaporation consitently often the shade balls over water pool are being used. The plastic balls, which can save water and protect water quality, are an attempt to cope with severe droughts [14] The shade balls used in water basins threatened with droughts are made of high-density polyethylene (HDPE) with carbon black additive to protect the plastic from ultraviolet radiation. Adding carbon black also prevents the formation of bromate, which causes stomach problems when water contaminated with it is consumed.

Fig. 13. Shade Balls, California (source: [14])
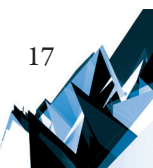
It is predicted that the use of shade balls could save millions of gallons of water. This This rather new concept incorporates small, black, plastic balls floating on the water's surface. Their aim is to help reducing about 90 percent of the total evaporation and maintain respectable water quality. The balls have been successfully used in several locations during extreme droughts such as Ivanhoe Reservoir, the Elysian Reservoir or Upper Stone Canyon Reservoir. In each of those locations, the slowing of natural evaporation brought significant improvement.

The ball:

DIMENSIONS
About 4 inches in diameter and weighs approximately 245 grams

PLASTIC MATERIAL
The .04 inch walls are made of high density polyethylene, the same material used to mold milk jugs. BPA free and NSF certified for contact with drinking water

WATER BALLAST
Filled with air, with some holding about 205 grams of water so they are more deeply immersed and do not blow away

MELTING POINT
Typically in the range 120 to 180 °C (248 to 356 °F)

DEGRADATION
May split in half or fail at the seams after 10 years, at which point they will be removed and fully recycled

SURFACE
Covered in black surface because that color is UV resistant to heat, and also prevents the production of algae and a carcinogen called bromate

STORMS
Apparently can withstand bad weather like rainstorms and have done so successfully in the past

Fig. 14. Shade Balls, infographic- basic parameters (source: [21])

5.2.4. Flood–resistant garage on the example of Deggendorf, Germany

Another method of adaptation to climate change was developed in Germany by the Raumzeit office located in Berlin. It is a flood-resistant garage, located in Deggendorf in the South of Germany in the flood-prone location.

Fig. 15, 16. The view of flood–resistant garage (source: [22])
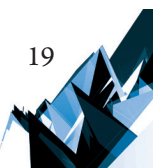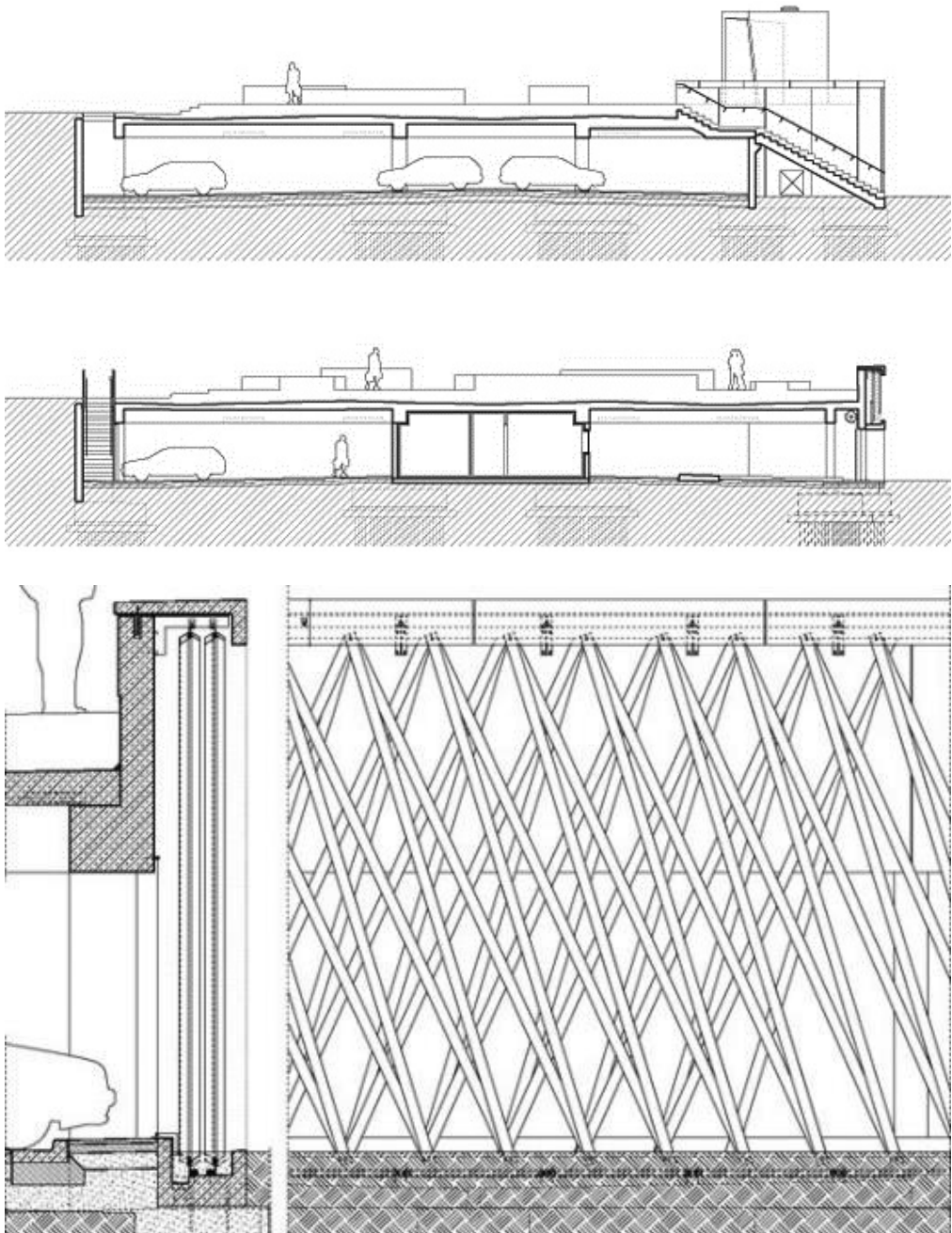
Fig. 17, 18. Flood–resistant garage – construction sections (source: [22])

The parking deck is conceived as an urban infrastructure in the landscape area: with a length of 345 meters, the building runs along the flood dike, passes under a federal highway and connects the city park with the new pedestrian bridge over the Danube.

The terrain slope along the flood dike is used to make it possible for the large volume of construction to disappear in the landscape. A new public park could thus be created on the roof of the parking deck: as show the so-called dike gardens, which have been designed by K1 Landschaftsarchitekten. With the green roof of the parking deck, the parking area is recovered in the long term as a landscape space.

The parking deck extends 330 meters along the flood dike and undercuts the highway. The facade in the direction of Ackerloh consists of green and yellow aluminum bars, which are arranged so that a wave pattern is created. Waves should also appear on the roof: There is currently a park landscape created with paths, flowerbeds and lawns in waveform – the so-called dike gardens. The 11,000 square meters become an integral part of the garden show grounds, which are protected from floods.

The ground-breaking ceremony for the dike parking deck took place on April 15, 2011, together with the official ground-breaking ceremony. About two years later, towards the end of April 2013, the dikes were almost completely poured out. And the view from one of the two-meter-high dikes already held at this time, which the concept has promised: The perspective on the exhibition contributions changes, the "real" flood dikes, which were relocated to give the Danube more room at high tide, are clearly visible with a small turn around its own axis.

Definitely, there are many more adaptation strategies against the mentioned factors, and the several strategies mentioned are just a tip of an iceberg showing the complexity of the problem. The researchers are still conducting new investigations and developing new ideas of how to successfully mitigate or adapt to climate change hazards.

6. Urban and regional adaptation strategies for hydrological events caused by climate change

In terms of developing urban resilience, the ability to deal effectively with current social, economic and ecological problems – like climate change hazards – there is a well-known initiative of 100 most resilient cities. As the approach to the sustainable development was insufficient in some cases, the concept of resilient cities was developed. Cities called resilient successfully faced not only the sustainability problems, but also developed their own strategy for dealing with alarming problems of our times like poverty, immigration or natural disasters.

There is an international competition where the cities can compete to become the most resilient ones, but they can also share the strategies. The aim of this is to help cities with building their resilience to the physical, social, and economic challenges that are a growing part of the 21st century. Cities in the 100RC network are provided with the re(sources necessary to develop a roadmap to resilience along main pathways [12].

Due to the complexity of the issues they are dealing with, only one of them will be mentioned, referring to various goals of sustainable development and as one of final effects solving also the problems related to climate problems.

However, it should be emphasized that there are numerous other crucial urban adaptation strategies and they can be an interesting basis for further considerations and inspirations for other cities.

The cities example show that climate change and extreme weather events can be treated as a driver for development rather than the (source of problem. An example for this the Danish city of Vejle, projected to be totally underwater in future years. With the help of experts and specialists it developed interesting strategy triggering the city development.

Water in Vejle is seen both as an asset and a challenge. As this city is designated as one of ten Danish risk areas where there is a significant flood risk due to rising sea levels, increasing rainfall and flooding. The assets which are most vulnerable to climate change, belong the harbour, the coastal area, the urban core and some of our infrastructure (small bridges and tunnels in west side urban core). Although the water and sewage system are not prepared for heavy rain and flooding, some of the energy transformer stations and communication

Fig. 19. 'Fjordbyen' in Vejle – prospective laboratory for water management (source: [23])

infrastructure in the city are also vulnerable to flooding, today the city has a well-functioning emergency response capability, as well as climate and risk management action plans

Vejle's assets and communities are threatened by flooding from the fjord. Therefore the main aim of the city is providing the city's edges to be safe and protected during storms and rising water levels.

There was a plan to use 'Fjordbyen' as a laboratory to improve water management by exploring innovative and integrated solutions such as retrofitting new public spaces. The aim is to encourage economic growth whilst reducing risk. This action is also included in the City Development Plan. Reductions the risk of flooding will be met by the city be means of following measures such as designing flood defenses to encourage investment, development and real estate value. Moreover, it was planned to use Østbykvarteret as a demonstration area where flood management interventions have a recreational and community value. Apart from this, there was also a plan of Protect the hinterland areas of the Grejs River by installing integrated flood solutions along the road infrastructure to decrease the waterflow.

The aim of Vejle was to show how small cities can solve big problems and show great responsibility, which can be a good- role model for other cities.

Along with Vejle there are numerous other cities dealing with extreme hydrological events in creative way (such as Rome, Singapore and others), treating them as a challenge and opportunity for future development. Their strategies, along with Vejle are available on the webpage of the organizers 100 resilient cities

7. Conclusions

The impact of global climate change on cities and regions is unequivocal. Climate change may have major and unpredictable effects on the extreme weather conditions and the results brought about. For these reasons the climate change needs to be properly respected in urban planning process.

Consequently, the importance of climate change in sustainable planning cannot be underestimated. While planning process the environmental factors and their changeability need to be seriously taken into consideration. Although, there are numerous strategies developed and implemented, particular problems following extreme hydrological events definitely need further investigation and profound insight in terms of mitigation and adaptation.

Moreover, one ideal solution or adaptation strategy for regions threatened with alarming environmental problems does not exist. Each area should be treated individually and requires distinctive approach. Definitely, new environmental challenges of the cities in the early 21st age require not only new technical and technological solutions, administrative in crisis planning or cost recalculation, but also of the new socio-ecological reflectivity and new empathetic urban policy.

The essay is limited to certain networks of relationships, draws attention to the particular processes, and the directions of research, that I suggest, require further thoughts and refine.

References

[1] Field, C.B., Barros V.R., Dokken D.J., Mach K.J., Mastrandrea M.D., Bilir T.E., Chatterjee M., Ebi K.L., Estrada Y.O., Genova R.C., Girma B., Kissel E.S., Levy A.N., MacCracken S., Mastrandrea P.R., White L.L., Climate Change 2014: *Impacts, Adaptation, and Vulnerability. Summaries, Frequently Asked Questions, and Cross-Chapter Boxes. A Contribution of Working Group II to the Fifth Assessment Report of the Intergovernmental Panel on Climate Change*, IPCC, World Meteorological Organization, Geneva, Switzerland 2014.

[2] Hallegatte S., Green C., Nicholls R.J. & Corfee-Morlot J., *Future flood losses in major coastal cities,* Nature Climate Change, Vol. 3, 2013, Map: McDonnell T. https://www.washingtonpost.com/news/wonk/wp/2013/08/20/these-20-cities-have-the-most-to-lose-from-rising-sea-levels/?utm_term=.51ed36abce55 (online: 4.12.2017).

[3] Intergovernmental Panel on Climate Change. Climate Change 2001: The Scientific Basis. *IPCC Third Assessment Report.* Cambridge Univ. Press, 881 pp. www.grida.no/publications/other/ipcc_tar/ (online: 4.12.2017).

[4] Intergovernmental Panel on Climate Change (IPCC), Climate Change, *Synthesis Report Summary for Policy-Makers IPCC, 2014: Climate Change 2014: Synthesis Report. Contribution of Working Groups I, II and III to the Fifth Assessment Report of the Intergovernmental Panel on Climate Change* [Core Writing Team, R.K. Pachauri and L.A. Meyer (eds.)]. IPCC, Geneva, Switzerland 2014.

[5] International Institute for Environment and Development. "Climate change: study maps those at greatest risk from cyclones and rising seas", March 28, 2007, http://www.iied.org/climate-change-study-maps-those-greatest-risk-cyclones-rising-seas (online: 4.12.2017).

[6] Luo T., Young R., Reig P., *Aqueduct Projected Water Stress Country Rankings*, World Resource Institute, 2015.

[7] Lindzen R., *Global warming and the irrelevance of science*, The Global Warming Policy Foundation, 2016.

[8] Lindzen R., Choi Y.-S., On the Observational Determination of Climate Sensitivity and Its Implications, The Korean Meteorological Society and Springer 2011.

[9] Schmidt G. A., Arndt D., *Annual Global Analysis of temperatures for 2016, NOAA/NASA,* January 2017.

[10] Xiaoxu Wu, Yongmei Lu, Sen Zhou, Lifan Chen, Bing Xu, *Impact of climate change on human infectious diseases: Empirical evidence and human adaptation,* Environment International 86, 2016.

[11] Richard Lindzen R., MIT, https://www.youtube.com/watch?v=OwqIy8Ikv-c (online: 4.12.2017).

[12] http://www.100resilientcities.org (online: 19.12.2017).

[13] www.a2rinitiative.org (online: 19.12.2017).

[14] http://news.nationalgeographic.com/2015/08/150812-shade-balls-los-angeles-California-drought-water-environment (online: 19.12.2017).

[15] http://www.bbc.com/news/science-environment-26810559 (online: 4.12.2017).
[16] https://www.munichre.com/us/property-casualty/home/index.html (online: 4.12.2017).
[17] https://ppntestblog.files.wordpress.com/2018/04/page-58-59-smp-types_pwd1.jpg (online: 2.10.2018).
[18] https://www.pwdplanreview.org/manual/chapter-4/4.1-bioinfiltration-bioretention (online: 2.10.2018).
[19] https://www.baca.uk.com/amphibious-house.html (online: 2.10.2018).
[20] https://www.dezeen.com/2014/10/15/baca-architects-amphibious-house-floating-floodwater (online: 2.10.2018).
[21] http://time.com/3998554/shade-balls-graphic (online: 2.10.2018).
[22] http://www.raumzeit.org/NewFiles/parkdeck_deggendorf_01.html (online: 2.10.2018).
[23] Vejle's Reslirnt Strategy: http://100resilientcities.org/wp-content/uploads/2018/01/Vejles_resilience_strategy_webquality_160317.pdf (online: 2.10.2018).
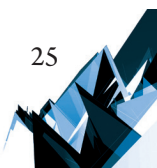
Cecilia Maria Roberta Luschi orcid.org/0000-0002-7777-5360

cecilia.luschi@unifi.it
Dipartimenti di Aarchitettura, University of Florence

Among the archaeologists and the designers: a critical survey of Sant'Andrea of Acre in Israel

Wśród archeologów i projektantów: krytyczna ankieta kościoła Sant'Andrea Akko w Izraelu

Abstract

We propose a historical architectural study of the hypogeum of the church of Sant'Andrea in Akko (Israel), which promoted new reflections on the urban historical fabric and at the same time provided concrete data for a redesign of part of the structure in line with the historical role and the building Hierarchy that made it a cornerstone for navigation and orientation at sea. The discovery of its architectural composition led the design to an extended dimension in addition to the building itself. We intend to propose a violation of contemporary architecture as a daughter of history and not as an assertion of modernity often detached from the context. In this case we try to recover the role and monumentality of the building, the urban context and the sea front.

Keywords: Izrael, archeology, historical research

Streszczenie

Artykuł stanowi opis historycznego studium architektonicznego hipogeum kościoła Sant'Andrea w Akko (Izrael), promujący nowe refleksje na temat miejskiej tkanki historycznej i dający konkretne dane do przeprojektowania części konstrukcji zgodnie z historyczną rolą i budową. Odkrycie kompozycji architektonicznej doprowadziło do rozszerzenia projektu poza sam budynek. Proponuje się rozumienie współczesnej architektury jako córki historii, a nie jako twierdzenie o nowoczesności często oderwanej z kontekstu. W tym konkretnym przypadku proponuje się odzyskanie roli i monumentalność budynku w kontekście miejskim i morskim.

Słowa kluczowe: Izrael, archeologia, badania historyczne

The work which is presented, in addition to being an advanced historical research, represents a more geometric and proportional route to the mediaeval project.

The geometric relationships and composition compared with the functional hypothesis of the structure, give us a knowledge of the architectural design of the building.

The road that follows is that of being able to recover all the historical and cultural heritage of the artefact itself, and to be able to propose its preservation and its functional reuse within the historical logic. There seems to be a step towards a new type of enhancement that provides dignity to the building and especially to what it has been through the ages.

Around Sant'Andrea, gradually, there are many interests that have added up. What prompted us to deepen the knowledge of the church of Sant'Andrea is a famous text that reads as follows:

> *Acri è golfo et bom porto e qua è uno scollio che fai lo porto.*
> *Alli quali scolli potete stare a prodese en fondo de iiij passi.*
> *E de ver terra ferma è la torre delle mosche. La 'ntrata de lo porto è entre la dicta torre e li scolli.*
> *Se venite a lo dicto porto, va lontano a la città, coè a ssavere a la macone dello templo et alla chiesa de lo sancto Andrea iiiij, prodesi per la secca che ède sopre Sancto Andrea. E quando averete la mancone che fo de lo Conestavele a dericto de la torre de le mosche, podete far la via a lo porto dericta. E quanno entrarete a lo porto, va tanto entro che aibate la citta de Cayfas en mecca poppe da levante, e la torre delle mosche per mecca proda. E così girate allo porto nepto della dicta secca* [1].

> *Acri is a gulf and good port, and here there is a reef that protects the port.*
> *You can in stand by to be moored with a bow and a 140 metre-long rope.*
> *On the mainland is the tower of flies. The entrance to the port is between the tower and the rocks. If you arrive at this port, go far from the city, that is, off the Templar Matter and the church of Sant'Andrea because there is a bank in front of Sant'Andrea.*
> *When you have aligned the tower of the temple with the Tower of the Flies, you can go straight in parallel. To enter the port you must navigate until Haifa is half aft from the east, and the Tower of the Flies in the middle of the bow.*
> *And so you enter the port avoiding the reefs* (Fig. 1).

It is the most ancient Mediterranean Portolan text to be used as a Compass to navigate, anonymous and undated, the historian mediaevalist Bacchisio R. Motzo found it over thirty years ago in an archive of Alghero in Sardinia. The Compass is recommended to navigate four miles away from Saint Andrew's shoal and look over the Templar mansion and the church of Sant'Andrea to get into the port without damage. As just reported, giving importance to the church is no longer local but becomes an excellent land marker and a sea warning for navigation.

It becomes the meeting point between land and sea and all that is represented by architecture. We enter then into the depths of the underground site and architecture studied, and try to understand it as it appears.

Direct survey now seems obsolete in favour of high technologies like 3D surveys, but in reality it has a unique potential, which is to confront the structures for a long time and look at
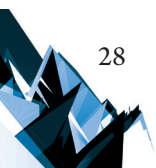
them and see them day by day, interrogate them stone by stone and pillar after pillar. The need to get caught between the building structures and to be immersed in the structural design, promotes a different understanding and a different approach to the cognitive process. At this time we would like to present this kind of observation and investigation that does not exclude the methodological rigour and metrical precision, but adds a personal feeling towards the architecture.

From the above, a method follows that does not rely on preconceived ideas. Often it is better to know nothing of the structure that is to be investigated, to be free to read every possible architectural variant that arises, (for this assertion I apologize to historians and archaeologists, who I read a lot, always after my analyses).

A matter to be clarified concerns the measurement concept in the classical or mediaeval period. Today, the measure for us has a value in metres and starts from zero. But this can only happen in an environment where zero is known.

The measure for a classical or mediaeval manufacturer starts from 1 and contemplates a quantity the 1 is already a quantity itself [2, 3][1].

The other problem is the irrational quantity such as the 2 radical or the radical 3, known as the diagonal of a square or a cube. But in geometry those measures are rational, they join two opposite corners of a square or a cube. Rationalization of irrational numbers passes directly from the use of the Pythagorean triples identifying square numbers which are in turn the sum of square numbers.

Given these premises, we can now enter the suggestive space of the Church of dell'ipogeo of Sant'Andrea in Acre.

After a day of observation, the architects definitively identify three types of different structures in terms of walls and floors (Fig. 2).

There are barrel covers lowered in the first room to the right of the access corridor.

Then we find the cross lounge, with a perimeter rib, excluding the first left evidently rebuilt in the following period.

In addition to this wide dizzying heights room, we find a narrow transverse corridor, which is parallel to the four newly outdated bays, divided by those from a wall with a sizeable section. We realize that the wall is independent of the main structure of the trusses that rest instead of pillars, except for the first left and the last to the right, where the trusses rest on extroflexions of the wall itself.

Entering into the hallway, a series of three ogival openings are arranged telescopically and narrow between the two septa which are not lying parallel to one another.

Besides this atypical and very curious structure, we know that there are two tanks that stand about 5 metres below and have no direct communication with these compartments.

We have chosen to focus on two main issues. The cisterns on one side and the underground vaulted on the other side.

---

[1]   In the western world, the indi numbers was introduced for the first time, with the addition of zero to perform the positional calculation. Before then and until the modern era, Roman numerals were used with a base nomenclature of 5. (V; X; L; C; D; M –5; 10; 50; 100; 500; 1000).

The cross vaults have the characteristic to download the forces in accordance with the diagonal. The Forces are then collected from the wide section pillars. So the static calculation of the effort must be computed according irrational magnitudes and more with complex operations such as multiplication and division. The workers who do not know the numbers and then work with Roman numerals, definitely used a geometry protocol for static estimate. For correct critical investigation you should know that the measures taken orthogonally are often misleading with respect to the protocol implemented in the presence of cross structures so complex. The search for the geometric program must be carried out according to the diagonal, and still more difficult, should contain a quantity that is not accessible, or the section of the wall

Once consolidated the forces that could have compromised the immobility of the upper structures, it seems to have been decided to chain the crosswise structure by sacrificing one bay.[2]

It was decided to reinforce the transversality with a wall which, however, has an inclined trend respect to the system rationalized according to the diagonals of vaults of discharge. The reason for a structural redundancy of this kind is the need to be separated from the structure. That is, the bays fit across into the wall and exploits discharges like a vice.

The result is that the building wedge has no chance to slip or rotate, and has an autonomous foundation, thanks to the crosspieces, which divide the two septa.

As the net of openings could still exist between the two environments, we wondered why it was necessary to reestablish a part of the structure, (which also took place after seeing the confinement of the pillars and the building of a new one to support time). Something had to be changed in the management of the upper floors or at least the intention of making a remarkable rise buildings has led to a severe structural re-foundation.

The presence of the vacuum of the cisterns must have been known, with regard to the existing well within the inner section of the second span to the left, the opening surprised the builders that have changed the compositional design to avoid the wall leaning on the cisterns. They put in place then an ancient and effective, such as that used for example for the Ardica of Theodoric, or the so-called cryptoporticoes of Roman style foundation. A technique that raises the facade in complete autonomy with respect to the remainder of the building structure.

The façade in fact was not, as we now think, part of the structure of the body of the building, but was itself a separate building. It was the part of the building that spoke on the outside and was structured according to the monastic rules often borrowed from dall'ordini.

To sum up the facade of the church is a body composed of the western area arcades; it was open or closed (or Galilean or paradisum) and two knight towers to finish the scope of the construction.

What today is called Westwerk [4][3].

Let us read again the structure that we found, and try to see its composition better.

We said earlier that on the left of the entrance there is a small room with no connection to the rest of the structure, it might be the foundation of the left tower. To the right a "full" leads us to think that there may be the foundation of the tower on the right.

---

[2]   The relief and critical reading of the structures, highlight the cut of the span with the continuous wall of plug. It is almost aligned with the current façade of the church on the upper floor

[3]   The Westwerk is simply the representation of the Gate of the celestial Jerusalem, and the architectural paradigm are the gates of the city of Rome

The ogival portion with its massive pillars, is the area that supports the Galilean superiorly, and the facade is brought from the foundation structure as we have seen, The façade, or the ardica, is located behind the line of the towers.

This outlines a fascinating piece of mediaeval period, two knight towers that defend the only central access.

The defensive structure in this case seems to be explicit and reasonable given the historical period and location, but as in all research there is always a "but." If this was the shape of the facade, it would collide with the iconographic sources we have of St. Andrew, and then a dislocation problem opens that is not insignificant.

St. Andrew is like each other access to a Templar mansion that is proposed its rider with two towers to defend access.

However, today, this is the church of Saint Andrew and respecting the historical dynamics, we should work on the awareness that the current church perhaps occupies the historic Templar mansion. However, the studies carried out can provide a framework of territorial relationships that a project of reconstituting the façade can fix and involve [5].

The design of ancient buildings, according to the contemporary feel, is often relegated to a contagious museographic aspect. With conservation we propose a way that draws a lesson from the past. To refurbish sites where there is the possibility, it is a proposal to be evaluated. The Sant'Andrea of Acre, after having thoroughly studied its design genesis, has become an example of a study for refunctionalization.

The need for a new facade to the current church, draws its geometry and dimensions directly from the ancient structures, resting on them and protecting them.

The decentralized access is re-proposed as a verifiable limit for embarking on a journey between history and contemporaneity. The Church of Sant'Andrea appropriates ancient structures by using them and forming according to mediaeval design rules in a contemporary reading. The experimental proposal, and as such it must be interpreted, wants to promote a process of knowledge that becomes a driving force for the project of recovery and design. Everyday life from new life and sharing in the historical city and absolves its lesson of tradition and identity with the possibility of dialogue with the re-born context in a modern way.

Carlo Scarpa once said: I want to confess: I would like a critic to discover in my works certain intentions that I have always had. That is to say, an enormous desire to be within tradition, but without making capitals or columns, because they can no longer be done. Even a god would not invent an Attic base today[4].

Work in September 2016, responsible Cecilia Luschi, Shally Peleg, Israeli Authority Authorities, with the kind permission of Father Andrea Baccus responsible for the church of Sant'Andrea in Akko.

Project proposal that starts from the elaborated historical data, with the purpose of reconstituting the prospect of the current church of Sant'Andrea is to recreate the hierarchy of the sea front and the dimensional relationships of the various building realities.

---

[4]   Carlo Scarpa Mille Cipressi, Conference in Madrid 1978, in F. Dal Co G. Mazziarol "Carlo Scarpa Opera Completa" Electa 1984–1992).

Fig. 1. From the descriptive installation of the Torsello a further map was written by J. Picard, in the 16th century with an overlapping plan of the navigation scheme of the Pisan portulan XIII sec.

SCALE 1:50

UNIVERSITÀ DEGLI STUDI FIRENZE

ISRAEL ANTIQUITIES AUTHORITY

7

SECTION CC'

WITH QUOTES AND PHOTOMOSAIC

scala 1:50

scala 1:50

UNIVERSITÀ DEGLI STUDI FIRENZE

ISRAEL ANTIQUITIES AUTHORITY

10

Fig. 2, 3. Plan and Section of the ground floor on the archaeological level of the current church of Sant'Andrea

33

Study of alignments according to the module of the cubit
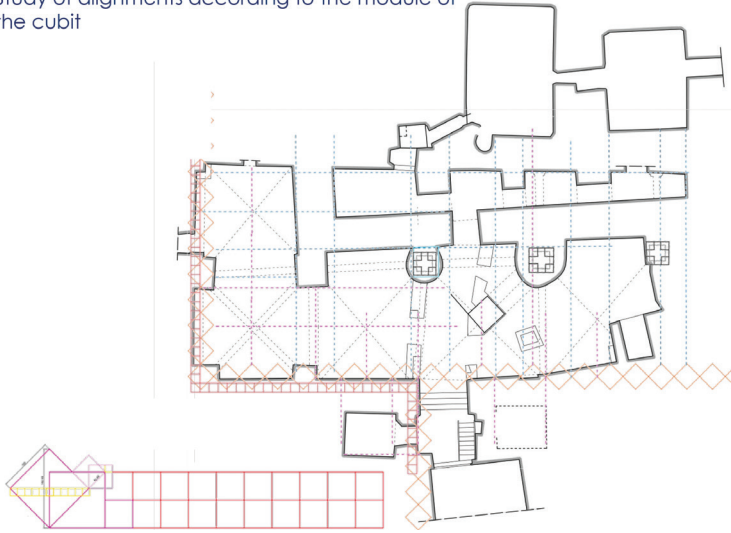
Fig. 4. Geometric schemes of equivalence between the Roman foot and the Royal Cubit, with geometrical relations for the realization of vaults and bays (elaborated by the author)
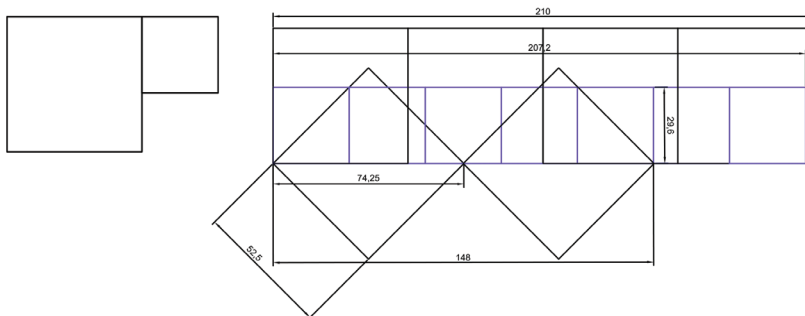
Fig. 5. Study according to the geometric protocol of the Sant'Andrea hypogeum, application of the original geometric proportions (elaborated by the author)
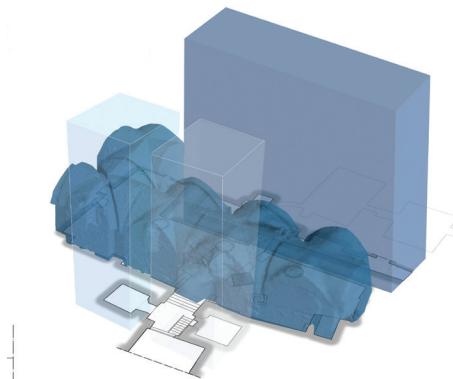
Fig. 6. Ardica di Teodorico (Ravenna), an example of the foundation of a façade in the late ancient period (author's photo)

Fig. 7

Fig. 8. The corridor of the hypogeum of the Sant'Andrea of Akko, which seems to populate the same foundation system designed to support a higher construction, today partly elided (author's photo)

Functional division of the compound foundation

Cisterns

Ardica Fondation - Facade sant'Andrea (?)

Portico area Like a Galilea

Towers area Lake westwerck Torri Cavaliere (?)
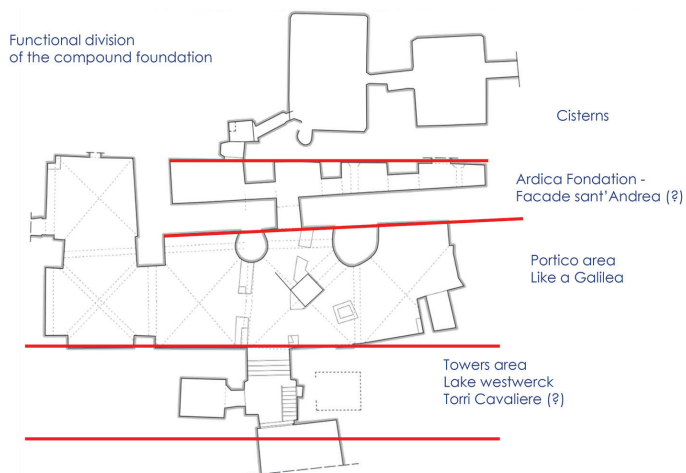
Fig. 9. Functional hypothesis of spaces. The transversal wall cuts the most ancient span going to form the corridor described above (elaborated by the author)
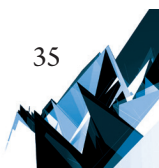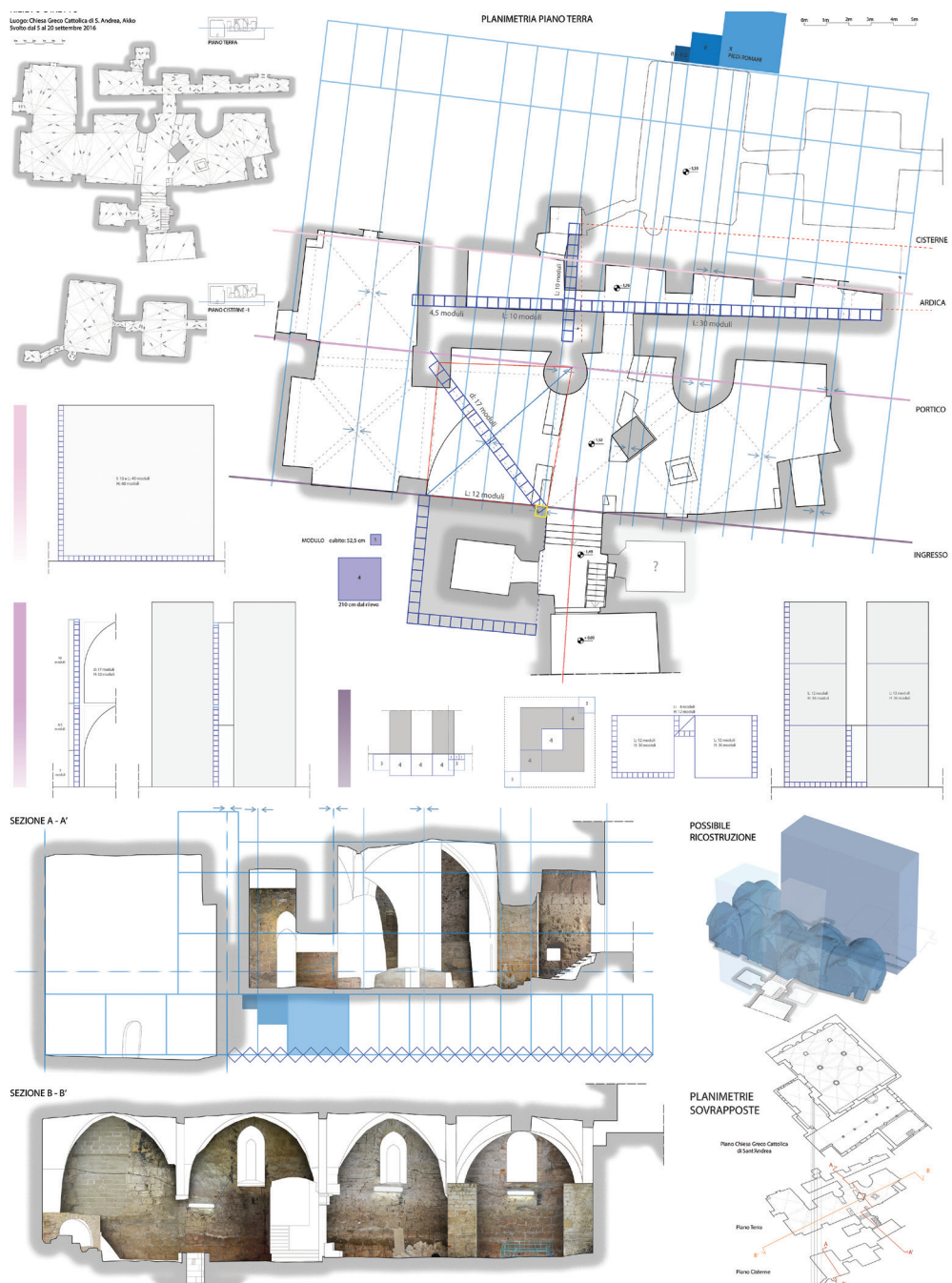
Fig. 10. Reconstructive hypothesis of the rises by calculating the ratios between the masonry section and the height of each element (author's study)
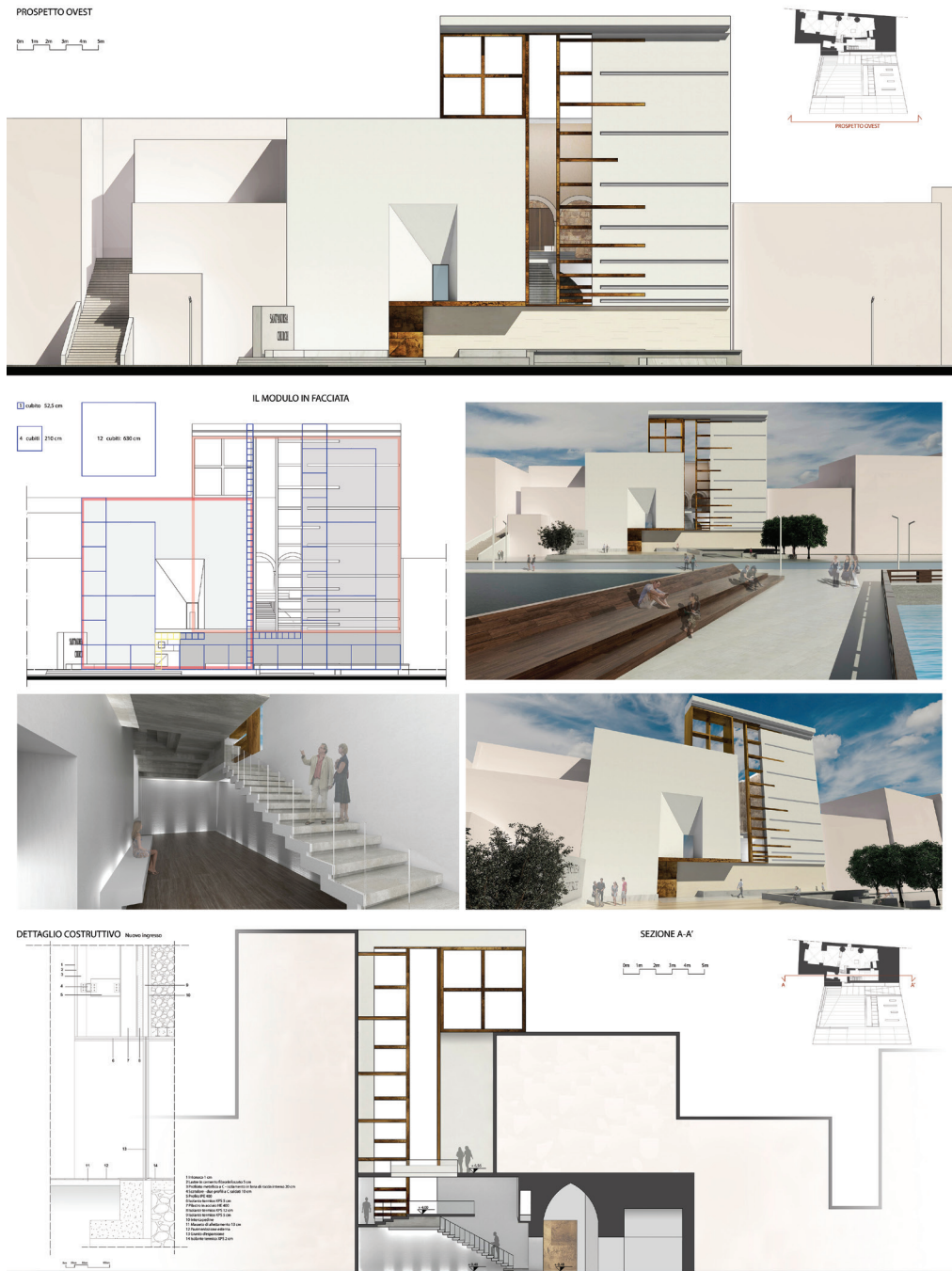
Fig. 11. Overall geometric analysis program, with direct relationships between wall sections and heights and subsequent reconstructive hypothesis (study by Luschi Cecilia and Alessandra Vezzi)

References

[1] *Lo Compasso da Navigare*, ed. C. Hamilton 396, study by A. Debanne, P.I.E. Peter Lang, Bruxelles 2011.
[2] Sigler L.E., *Fibonacci's Liber Abaci. A translation into modern english of Leonardo Pisano's book of calculation*, New York, Springer, 2003.
[3] Luschi C.M.R., *Sui rapporti numerico matematici alla maniera di Federico II. Il castello di Prato. in MATEMATICA E RCHITETTURA, Metodi analitici, metodi geometrici e rappresentazione in Architettura*, Alinea editrice, Firenze 2001.
[4] Luschi C.M.R., *La Mistagogia del Monastero fra sintassi teologica e composizione Liturgica*, Aracne editrice, Roma 2015.
[5] Carlo Scarpa Mille Cipressi, Conference in Madrid 1978, [in:] F. Dal Co G. Mazziarol, *Carlo Scarpa Opera Completa*, Electa 1984–1992.
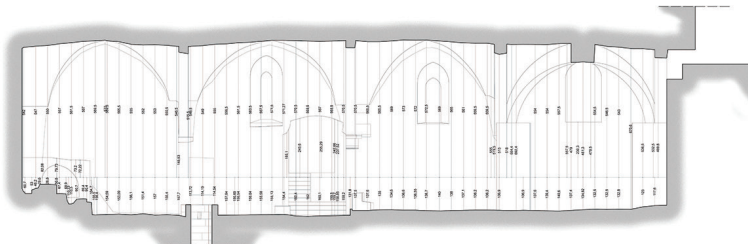[6] Luschi C.M.R., *La mistagogia del monastero fra sintassi teologica e composizione architettonica*, Arcane editrice, Roma 2015.

Krzysztof Petrus orcid.org/0000-0002-3836-6804
kpetrus@pk.edu.pl
Institute of History of Architecture and Monument Preservation, Faculty of Architecture,
Cracow University of Technology

The restitution of Garbary, Cracow's largest suburb, after the destruction caused by the invasion of archduke Maximilian Habsburg in 1587

Restytucja Garbar, największego krakowskiego przedmieścia, po zniszczeniach w czasie najazdu arcyksięcia Maksymiliana Habsburga w roku 1587

Abstract

This paper presents an outline of the history of spatial transformations of Cracow's largest suburb in the years 1587–1655. So far, this topic has not been given due attention and the published works only present the history of Garbary up to the invasion of Archduke Maximilian Habsburg in 1587. However, the siege of Cracow by supporters of the representative of the House of Habsburg, who aspired to the throne, closed an extremely successful stage in the history of the suburb, and the liquidation of existing buildings forced its residents to undertake a quick and intensive reconstruction. Furthermore, the paper contributes to further research into the suburb's development at the end of the 16th century and in the first half of the 17th century, thus filling a considerable gap in research on the development of the urban system of Cracow.

Keywords: Garbary (Tanner's Suburb), Cracow, suburbs, urban planning, history of spatial development

Streszczenie

W niniejszym artykule przedstawiono zarys historii przemian przestrzennych największego krakowskiego przedmieścia w latach 1587–1655. Tematowi temu nie poświęcono dotąd należnej uwagi, a opublikowane prace przedstawiają historię Garbar jedynie do najazdu arcyksięcia Maksymiliana Habsburga w roku 1587. Tymczasem oblężenie Krakowa przez zwolenników habsburskiego pretendenta do tronu zamknęło niezwykle pomyślny etap w dziejach przedmieścia, a dokonana wówczas likwidacja zabudowy zmusiła jego mieszkańców do szybkiej i intensywnej odbudowy. Artykuł stanowi również przyczynek do dalszych badań nad zabudową przedmieścia pod koniec XVI i w pierwszej połowie XVII stulecia, wypełniających istotną lukę w aktualnym stanie wiedzy o rozwoju urbanistycznym krakowskiego zespołu miejskiego.

Słowa kluczowe: Garbary, Kraków, przedmieście, urbanistyka, historia rozwoju przestrzennego

The 16th century was a particularly favourable period in the history of Cracow. Before 1587 the city was safe from warfare and it did not suffer any unrest in the times of the first and second interregnums in the years 1572–73 and 1574–76. As the capital city of a powerful country, Cracow constituted a political and economic European centre – a place where celebrations of a definitely supraregional character were held, where royal coronations, weddings, and funerals took place, where events attended by the most prominent dignitaries of the state were held, such as the homage paid by the City Council to Sigismund I in 1507, the arrival of Duke Konstanty Ostrogski in 1514 after the battle of Orsha, the ceremony of the installation of the City Council and the arrival of Queen Bona in 1518, the Prussian Homage in 1525, the arrival of Hetman Jan Tarnowski in 1535 after the battle of Obertyn, the reception of Sigismund Augustus in 1543, the arrival of Henry of Valois and his reception of the homage of the Cracow townspeople in 1574, the festive arrival preceding the coronation of Stephen Báthory in 1576, or the wedding of Chancellor Jan Zamoyski in 1583.

Cracow in the 16th century was also an arena where transformations in the economy and production system manifested themselves earlier and more visibly than at the rest of the country [5, p. 20]. As a supraregional centre of trade and craftsmanship, as well as one of the important economic centres in Central Europe, from at least the 15th century Cracow was a wealthy city that constantly improved its standing. The population increased considerably and the city itself changed radically, although the changes did not relate to its territory, which was limited by the city walls. Year after year, the city became more and more beautiful, with exquisite new additions: modern palaces were erected, Gothic tenement houses were reconstructed and combined into bigger complexes [see e.g. 13, pp. 85-98], a new edifice of the town hall was erected, the Cloth Hall was radically rebuilt after a fire, and the Market Square was rearranged and its surface levelled.

The residents of Krakow were very fond of the arts of the Renaissance and the architectural developments they inspired in the transformation of the city's skyline. Thanks to the presence of a royal court and a university, the city quite quickly earned the status of a supraregional cultural centre and the most important artistic, social, and scholarly centre in the country. The Renaissance prosperity of Cracow was particularly clearly visible during the reign of the last representatives of the Jagiellonian dynasty, which was aptly grasped by Jan M. Małecki, who wrote: "The times of Sigismund, often referred to as the golden age in the history of Poland, were also a golden age in the history of Cracow, particularly in all circles of its culture, in the royal court, the bishop's court, at the university, amongst townspeople, and in the Jewish ghetto" [5, p. 155].

The golden age of prosperity acted as leverage for development, not just for Cracow, but also for towns adjacent to the city (Kazimierz and Kleparz), its suburbs, semi-rural settlements, and *iuridicas*, which were situated outside the city walls. Despite institutional differences, they were in close economic relationships with Cracow, creating a fragmented, mutually complementary, and largely harmoniously functioning urban system. The dynamic pace of its transformations in the 16th century was not slowed down by street riots, which were quite frequent at the time, religious unrest, and rebellions of the common people; nor was it hampered by numerous natural disasters: floods in 1515, 1528, 1533, 1534, 1542,
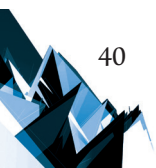
1570, fires in 1504 (Kazimierz), 1509 (Stradom suburb), 1522 (Stradom), 1523 (Cracow, Stradom), 1528 (Cracow and Kleparz), 1530 (Cracow), 1535 (Kazimierz), 1539 (Kleparz), 1546 (Kazimierz, Cracow), 1555 (fire of the Cloth Hall), 1556 (Kazimierz), and plagues in 1508, 1515, 1543, and 1555–1556 [5, pp. 41–43].

Amongst the suburbs surrounding Cracow, a leading role was played by Garbary (Tanners' Suburb), referred to as the suburb "in front of the Szewska Gate", or later on as Piasek. It was the oldest and largest *iuridica* located in the vicinity of Cracow – a settlement with its own separate administrative and judicial structures, located in the direct vicinity of the city or within its territory, but excluded from the city's jurisdiction under a royal charter or a foundation act authorised by the ruler. It occupied an area to the west of the city walls, between today's streets of Straszewskiego, Podwale, Dunajewskiego, Łobzowska and Słowackiego and Mickiewicza avenues, and the rear limits of the plots in the northern frontage of today's Piłsudskiego street (near Jabłonowskich street)[1].

In contrast to numerous *iuridicas* administered by the nobility, the governor, and the church, Garbary was a municipal *iuridica,* a type encountered much less frequently. It was founded in the location of early medieval gardens on the outskirts of the city and was a place of craftsmen's workshops and other services and production. Nevertheless, as early as the mid-14th century, Cracow City Council transferred most of Garbary's rights to the suburb's residents, allowing it to achieve a considerable degree of independence.

This initially small settlement of craftsmen very soon transformed into a specialised production complex; in the 16th century it obtained the status of the best-developed *suburbium* of Cracow and one of the most important production centres in the region of Małopolska[2]. The production infrastructure was developed on a scale which was unprecedented at the time; the layout of the suburb was intensified and densified, and the population growth could be stopped even by the plagues that raged in 1543, 1555, and 1571, which were particularly severe for the suburb [29, p. 23], [5, p. 43]. Therefore, there were no harbingers of a rapid fall after two hostile invasions, seventy years apart: the siege of Cracow by the troops of Archduke Maximilian Habsburg in 1587 and the Swedish invasion in 1655.

On 12 December 1586, Stephen Báthory died in Grodno. During a stormy period of the third interregnum, after several months of disputes, the divided nobility led a double election during the assembly held in Wola near Warsaw. On 19 August 1587, supporters of the chancellor and the Great Crown Hetman proclaimed a Swedish prince, Sigismund Vasa, a king, and on 22 August the dignitaries focused around the Borowski brothers elected Archduke Maximilian Habsburg, Emperor Rudolf II's brother, as king. A civil war started in which it was not the military forces of individual sides that were to decide who would take the

---

[1]   One of the few cartographic documents depicting the area of the tanners' *iuridica* is a city map by Józef Kromer from 1784. See: *Wymiar geometryczny miasta Krakowa z przyległościami dopełniony w roku 1783 przez Józefa Kromera Geometrę Przysięgłego…*. The original was lost but a copy made by J. Czech in 1792 is in the National Archives in Cracow, Cartographic Collections, ref. No. II-18 (former ref. No. II-7c).

[2]   More on the foundation, functioning, architecture, and spatial development of Garbary in the first centuries of its existence. See: [25–29].

throne, but the effectiveness, promptness, and accuracy of decisions made by representatives and supporters of the candidates.

Similarly to the previous interregnums, a key role in the dispute over the crown was to be played by Cracow. Kazimierz Lepszy quite aptly described it when he wrote: "Whoever was seen in the splendour of the crown by the dignified walls of Cracow cathedral could be certain of the support of thousands of noblemen passionate about politics" [19, p. 9]. This time, however, there were fears of a military intervention. Therefore, the city authorities prepared the capital for defence as effectively as they could, considering their financial capacity. The armament was completed as early as the spring of 1587, and in July of the same year repairs of the fortifications were launched: first the Szewska Gate, then sections of the city walls, the Floriańska Gate, and the Grodzka Gate. Cannons were renovated and retrofitted, gun powder and cannon balls were gathered. Nearly all entrances to the city were closed, leaving only the Floriańska gate (from the north) and the Grodzka gate (from the south) open for use [19, pp. 13, 17].

On 24 August 1587, on behalf of the king-to-be, envoys of Sigismund Vasa pledged *pacta conventa* – contracts drawn up by the election assembly. This, however, did not calm the municipal authorities of Cracow, who reckoned with the risk of a military invasion by the other candidate. These fears were shared by Chancellor Zamoyski, an avid advocate of the Swedish prince. The tense internal situation and the vicinity of the Habsburg empire prompted him to urgently convene the assembly of the Małopolska nobility and to set off for Cracow, which he reached on 8 September. It was a very prescient decision, as several days later, on 27 September, Maximilian pledged *pacta conventa* in Olomouc and set off for the capital too.

On 29 September, Zamoyski received an oath of allegiance from the townspeople, and on 9 October preparations for the defence of the city began: houses adjacent to the city fortifications were knocked down and cannons were mounted on the walls [5, p. 158]. On 14 October, Maximilian's troops reached Zielonki; the next day they quartered in Tonie, and then, awaiting reinforcements from Germany, Bohemia, Moravia, and Silesia, they settled in the Cistercian Abbey in Mogiła. It was then that Garbary faced the threat of a complete planned liquidation for the first time. According to the strategy adhered to at the time, in the face of danger defenders were to knock down the buildings of the suburbs, which shielded the attackers and made fighting them difficult. Nevertheless, Hetman Zamoyski, who was in charge of the defence of the city, decided to leave them be, hoping that having fortified the *suburbium* he could use it as an additional shield for the city.

This concept, however, did not save Garbary. On 24 November 1587, Maximilian's army attacked Cracow from the west, setting fire to the suburban buildings. The chronicle of the Cracow townspeople of 1575–1595 (*Kronika mieszczanina Krakowskiego z lat 1575–1595*) reads: "On the day given above, at 1 o'clock at night, Garbary was set on fire and the entire suburb was ablaze. The fire was horrible, huge, like in Sodom and Gomorrah, nobody could remember such a huge, severe, horrible fire like that one. At the time of the fire there was such a strong wind that a man could not stand up but was knocked down by it. A man could not see another man, they did not know what to do, as they had to beware of the fire and of the enemy, who was on the alert. St. Mary's church in Piasek was burnt down – fire took it over from all
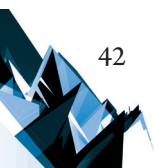
sides, and it finally caught fire; many beautiful buildings were destroyed and tenement houses burnt down completely. Vaulted chambers, granges, beautifully arranged gardens – everything was looted over one day. And on the third day, everything turned to ash" [15, pp. 46–47][3]. After heavy fighting in the area of the Carmelite monastery, caused by the betrayal of city residents of German descent[4], the attack on the city was fended off. But the situation "in front of the Szewska gate" was not back to normal for a long time. Over subsequent days Polish city residents murdered 50 German tanners there and 23 more were beheaded under a ruling of the city authorities; on 26 November 1587, the few surviving buildings were burnt down, both as an act of revenge and in fear of a new assault. On 29 November Maximilian started to retreat towards Silesia, and on 9 December Sigismund Vasa arrived at the capital city. A period of peace commenced that was unfavourable for Cracow, during which the city was slowly but surely losing its political and economic significance.

The destruction of the times of the Habsburg invasion was the greatest calamity suffered by Garbary thus far. Nevertheless, the suburb residents who survived the turmoil quite quickly started its reconstruction. Krystyna Pieradzka writes that the layout of the *suburbium* was not changed then [29, p. 27]; it is known, however, that certain plots were demarcated anew, giving rise to disputes which continued until 1597[5].

There is no doubt as to the road layout, which remained unchanged. Besides the then streets of Garncarska[6], Szeroka[7], Czarna[8], and Półwsie[9], in the period of restitution the streets of Krupników[10], Różana[11], Mała[12], and Grzebiennicza[13] were maintained, and a tax register from 1601 mentions a road "from the stone mill towards a wide street" that is today's

---

[3] The history of the warfare related to the invasion of Archduke Maximilian Habsburg is also extensively described in [19, 41].

[4] During the attack, tanners who supported Archduke Maximilian hid two German troops in the suburb, which attacked the rear of the Polish army during a pretended retreat of the Habsburg troops

[5] E.g. in 1597 a dispute was recorded in Garbary relating to inappropriate demarcation of a plot belonging to Wojciech Kawalec. See: *Quartaliensium Recognitiones Et Divisiones…*, manuscript, National Archives of Cracow, Early Files, ref. No. 1377, p. 646, item 647; [16, part III, pp. 232–233].

[6] A road in the place of today's Krupnicza street, mentioned for the first time in the first half of the 15th century. See e.g.: [18, p. 346; 38, p. 86].

[7] A road which largely coincides with the eastern section of today's Karmelicka street (between Plant Park and the Carmelite monastery), mentioned under this name for the first time in 1392. See e.g.: [17, p. 190, item 1541; 38, pp. 70–71].

[8] A road after the extension of the then Szeroka street, largely coinciding with the western section of today's Karmelicka street (between the Carmelite monastery and Słowackiego and Mickiewicza avenues), mentioned for the first time in 1326. See e.g.: [23, p. 83, item 815; 38, p. 71].

[9] A road in the place of today's Łobzowska street, perhaps derived from the local section of a route to Silesia from before the town's incorporation. See e.g.: [40, p. 176; 38, pp. 96–97].

[10] A road in the place of today's Garncarska street, mentioned several times in 1470–80. See e.g.: [42, p. 694; 38, pp. 53–54].

[11] A road of an unknown layout, most probably oriented towards the west, mentioned for the first time in 1485. See e.g.: [42, p. 694].

[12] A small alley, parallel to the city walls, the precise layout of which has not yet been defined, mentioned for the first time in 1431. See e.g.: [29, pp. 40–41].

[13] A road in the place of or in the direct vicinity of today's Rajska street, initially nameless, mentioned for the first time as Grzebienna street in 1560. See e.g.: [29, p. 41; 42, pp. 693, 704].
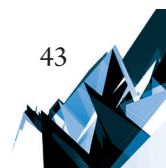
Garbarska street [1, pp. 56–57]; [29, p. 29]; [16, part III, pp. 165–166]; [16, part IV, pp. 23, 229][14]. At the end of the 16th century we also encounter information on tracts within the area of Krupniki[15], Kawiory[16], and Rybitwy[17], most probably referring to the former streets of Rybacka[18], Paśników[19], and – perhaps – the western section of the then Garncarska street, separating the settlement of groats makers from the old Jewish cemetery [29, p. 29]; [1, p. 57]; [16, part IV, pp. 14–15][20].

The lack of any essential changes in the suburban traffic layout is also confirmed by the list of buildings offering accommodation to visitors arriving at the coronation assembly of Władysław IV Vasa, drawn up in 1632 (*Rejestr gospód w Krakowie)*. It mentions the then streets of Różana, Garncarska (today's Krupnicza street), Grzebienna (today's Rajska street), Szeroka and Czarna (today's Karmelicka street), "a street called Tasemberk, running from St. Mary's church in Piasek to the Biskupie" (today's Garbarska street), "behind St. Peter's" (the then Półwsie street, today Łobzowka street), the roads "in Czarna Wieś", "in Rybitwy behind the gate of St. Ann's", and "in Kawiory", as well as Pańska street, which is a certain mystery, located within the triangle of today's Dunajewskiego, Karmelicka, and Garbarska streets or in the place of today's Asnyka street or Basztowa street [34, pp. 89–103].

---

[14] See also: *Quartaliensium...* p. 598, item 587; p. 674, item 672; p. 809, item 871; *Acta scabinalia suburbii Cerdonum…* , manuscript, National Archives in Cracow, Files of Cracow Iuridicas, ref. No. Jur. IV-12, pp. 851, 965; *Acta scabinalia suburbii Cerdonum…* , manuscript, *ibid.,* ref. No. Jur. IV-13, p. 505, *Quartale Figulorum* (ca. 1590), manuscript, *ibid.*, Early Files, ref. No. 2556, pp. 24, 36; *Quartuale Slawkoviense anni Domini 1601*, manuscript, *ibid.*, ref. No. 2566, pp. 166–174.

[15] The name of the area of today's Garncarska street, derived from the colony of craftsmen producing groats, established there most probably at the turn of the 14th century. See: [18, pp. 336–337].

[16] An area within the limits of the tanners' *suburbium*, at least from the second half of the 16th century, coinciding with the territory of Krupniki and different from the area referred to using this name in the 19th and 20th century; most probably there was a Jewish cemetery located in tanners' Kawiory or in its direct vicinity, situated close to today's Krupnicza and Czysta streets, mentioned many times in the years 1311–1460. See e.g.: [23, p. 20, item 167; 42, pp. 693, 694; 29, p. 45].

[17] The name of the settlement of Pobrzeże, mentioned since 1436, a village built for the Vistula fishermen, confirmed in the sources for the first time in 1315; after 1375 residents of Pobrzeże ran the so-called Fish Guard *(Stróża Rybna)*, a company of a considerable size, engaged in the storage of fish intended for sale, located in the area of the western part of today's Humberta, Krupnicza, or Czysta streets, perhaps in the place of today's Mickiewicza avenue and the edifice of the AGH University of Science and Technology. See e.g.: [18, pp. 315, 322, 337; 29, pp. 38, 56].

[18] A road within the territory of tanners' Rybitwy, nowadays of an unspecified location, perhaps located in the vicinity of today's Czysta street or Mickiewicza avenue. See e.g.: [29, p. 39]; cf.: *Acta dominorum scabinorum ante valvam sutorum…* , manuscript, National Archives in Cracow, Files of Cracow Iuridica, ref. No. Jur. IV-4, p. 205; *Exactio sacrae regiae magestatis anno 1553. Quartale Figulorum…* , manuscript, National Archives in Cracow, Early Files, ref. No. 2510, p. 26

[19] A road within the territory of tanners' Kawiory – Krupniki, today's location unknown, leading towards the grassland and suburban meadows, perhaps in the place of today's Wenecja and Piłsudskiego streets, or the western section of Krupnicza street. See e.g.: [40, p. 181]

[20] See also: *Quartaliensium...* p. 668, item 667; cf.: *Przedmieście wiertelu garnczarskiego*, manuscript, National Archives in Cracow, Early Files, ref. No. 2562, pp. 3–20; *Quartale Figulorum* (ca. 1590), manuscript, *ibid.*, ref. No. 2556, p. 37; *Acta scabinalia suburbii Cerdonum…* , manuscript, National Archives of Cracow, Files of Cracow Iuridicas, ref. No. Jur. IV-12, pp. 870, 981.

As some properties were demarcated anew, the dimensions of several suburban plots were recorded in the municipal documents. The preserved descriptions suggest that they had irregular, often polygonal or trapezoidal shapes [e.g. 16, part III, pp. 26–27, 117, 136–137]; [e.g. 16, part IV, pp. 18, 62–64, 250][21]. At the same time, there is no reason to believe that the plots were ever demarcated in a modular or repetitive way, and the layout of their limits was determined by certain permanent land development elements, roads, and the river bed of the Młynówka Królewska river, sometimes referred to as the Rudawka river, which intersected the *suburbium*[22].

The suburban water network was not in very good condition. In 1598, a heavily damaged dam that was used by a smithy was recorded before the Upper Mill [16, part IV, pp. 31–32][23], and in 1604 the fact that wastewater was drained from plots of land, privies, and pigsties to a branch of the Młynówka river, which supplied water to the municipal pipeline, was noted [16, part IV, p. 176][24]. Most probably some major renovation works were undertaken on this waterway only in the 1630s [4, p. 164].

Although the reconstruction of the suburb was progressing swiftly and most damage was noted in 1588 [16, part II, pp. 219–220, 221, 222–223, 224–225][25], we can read about areas destroyed by the fire (ruins and empty, unkept yards) in documents even from the first decade of the 17th century [e.g. 16, part IV, pp. 136–138, 222, 253][26]. Simultaneously, tax registers from the years 1591–1632 imply that a considerable number of the residential and production buildings of the *iuridica* was restored as early as in the last years of the 16th century. The structure of the development did not change then, and in the years 1613–1614 nearly 90% of houses registered in the city records were located to the south and west from the then Szeroka street (today Karmelicka street).

In comparison to previous years, the development density did not change a lot in the vicinity of the city walls and at Różana street (ca. 16–18% tanners' plots), in Kawiory, which was also known as Krupniki, (17–21%), and at Grzebiennicza street (8–12%); it was reduced, on the other hand, in the area of "Dębny" Mill (4–5%) and in Rybitwy (ca. 6%). A certain density of houses was recorded at the then Garncarska and Szeroka streets (27–32%) and in Czarna Wieś[27] (13–17%); nevertheless, it is worth remembering that after 1598 no structures

---

[21]   See also: *Quartaliensium...* p. 486, item 482; p. 560, item 547; pp. 567–568, item 561; pp. 670–671, item 670; pp. 692–693, item 709; p. 825, item 892.

[22]   Młynówka was built under a privilege granted to Cracow-based Dominicans by Leszek the Black in 1286 – more on the project and associated structures in [14, pp. 25–33; 4, pp. 138–172; 32, pp. 19–29; 33, pp. 7–16; 26, pp. 142–143].

[23]   See also: *Quartaliensium...* pp. 677–678, item 681; the Upper Mill was located in the place of today's building at 3 Łobzowska street.

[24]   See also: *Quartaliensium...* pp. 769–770, item 823.

[25]   See also: *Quartaliensium...* p. 380, item 387; p. 381, item 389; pp. 382–383, item 391; pp. 384–385, item 394.

[26]   See also: *Quartaliensium...* p. 743, items 784, 785; p. 804, item 862; p. 828, item 896.

[27]   A settlement located between Pobrzeże and Czarna street along the axis of today's Czarnowiejska street, mentioned for the first time in 1358; due to its complicated ownership-related situation (the village was administered by Cracow governors, but a considerable part of the land belonged to the city, private owners, and church institutions), Czarna Wieś was not incorporated into the administrative limits of Garbary and in subsequent centuries it remained administratively separate. See e.g.: [21, pp. 439–441; 18, p. 323].

were demarcated on Czarna street and in the area of St. Peter's church, as these were recorded in the registers of the neighbouring areas[28].

The lack of any radical changes in the structure of the suburban development is also confirmed in the register referred to above, which in 1632 mentions a total of 245 properties in Garbary and Czarna Wieś [34, pp. 89–103]. In the following decade this number slightly increased: tax registers from 1642 mention 244 developed plots in the suburb (including 228 houses, 3 mansions, 9 tenement houses, and 4 gardens), but these numbers do not take Czarna Wieś into account[29].

At the turn of the 16th century, the suburban residential and production development was still not particularly diverse in terms of the materials and technologies applied. A vast majority were wooden buildings with a log frame or half-timbered structure; brick or mixed buildings were a true rarity. The initially small number of suburban "tenement houses" slightly grew over time: in 1601 only one such building was recorded in Garbary[30], and in 1609 there were already eight of them[31].

Documents dating back to the period of restitution also seem to point to the fact that the houses built after the defeat of Maximilian Habsburg largely repeated the layouts developed in the previous decades. A typical suburban house from the years 1587–1655 was, therefore, at least a 2-storey double- or triple-bay building, with one or two rooms at the front, chambers at the back, and several rooms on the first floor. A very distinctive element was a hallway that frequently connected to the kitchen; it led to a utility and production yard with a well, surrounded with numerous workshops, sheds, stables, and other utility buildings [e.g. 16, part III, pp. 136–137][32].

Most probably one of the first types of structure reconstructed after the Habsburg invasion was suburban religious buildings. After the disasters that had affected their church, the Carmelite Friars residing in Garbary not only rebuilt it very soon, but also spared no efforts to

---

28   See: manuscripts in the National Archives in Cracow, Early Files: *Quartuale Figulorum* (ca. 1590), ref. No. 2556, pp. 17–39; *Przedmieście wiertelu garnczarskiego* (1598), ref. No. 2562, pp. 3–20; *Quartuale Slawkoviense anno Domini 1598*, ref. No. 2563, pp. 54–57; *Quartuale Slawkoviense anno Domini 1598*, ref. No. 2564, pp. 118–129; *Quartuale Figulorum…* (1602), ref. No. 2568, pp. 81–155; *Quartuale Figulorum…* (1602), ref. No. 2569, pp. 79–155; *Figulorum quartuale 1607*, ref. No. 2571, pp. 31–51; *Quartuale Slawkoviense anno Domini 1607*, ref. No. 2572, pp. 137–161; *Exactio quartualis Figulorum…* (1609), ref. No. 2575, pp. 89–159; *Quartuale Slawkoviense* (1609), ref. No. 2576, pp. 75–82; *Exactio contributionis vulgo szosz dictae pro anno Domini 1612. Quartuale Figulorum*, ref. No. 2578, pp. 24–27; *Quartuale Slawkoviense anno Domini 1612*, ref. No. 2579, pp. 169–196; *Quartuale Figulorum* (1613), ref. No. 2581, pp. 70–157; *Quartuale Slawkoviense anni Domini 1613*, ref. No. 2582, pp. 51–58; *Slawkoviense. Exactores duplicis contributionis szosz appelatae…* (1613), ref. No. 2583, pp. 48–53; *Exactores simplae quintuplicis… Quartale Figulorum* (1614), ref. No. 2588, pp. 93–166; *Exactores simplae quintuplicis… Quartuale Slawkoviense* (1614), ref. No. 2589, pp. 32–36; cf.: [25, pp. 159–160, 164–165].

29   See: manuscripts in the files of the National Archives in Cracow, Early Files: *… Exactia pozwolona… Quartuale Figulorum* (1642), ref. No. 2614, pp. 14–28; *…Exactia pozwolona… Quartuale Slawkoviense* (1642), ref. No. 2616, pp. 19–25; cf.: *Regestrum Figulorum 1642, ibid.*, ref. No. 2615, pp. 21–48

30   *Quartuale Slawkoviense anni Domini 1601*, manuscript, National Archives in Cracow, Early Files, ref. No. 2566, p. 170.

31   *Exactio quartualis Figulorum…* (1609), manuscript, National Archives in Cracow, Early Files, ref. No. 2575, pp. 94–96, 128, 129.

32   See also: *Quartaliensium...* pp. 567–568, item 561; cf.: [25, pp. 158–159, 163–164].

set up a filial monastery within the perimeter of the city walls, near St. Thomas's church in the place of the former Arian church[33].

At the end of the 16th century, the tanners' St. Peter's church was restored[34]; according to the documents recording the visitation of the Cracow Bishop, Jerzy Radziwiłł, for the year 1599, it was built with half-timbered technology [1, pp. 111–113][35]. Despite its rather small size, it was an extremely important building for the *suburbium* residents, as services were officiated there in German [31, p. 113, item. 40]. Manuscripts of Ambroży Grabowski contain also a laconic mention, based on an entry in the tax register, relating to an attempt to establish an unspecified nunnery in Garbary in 1609; nevertheless, nothing is known about it besides its hypothetical location[36].

At the end of the 1630s, another religious complex was erected in Garbary: a church and a monastery of the Franciscans of Primitive Observance. Representatives of this religious community came to Cracow in 1642 or at the beginning of 1625 in search of a founder and a location for a new seat that was close to the bishop's court[37]. The monks quite quickly narrowed down their search to the suburbs; the elements that were decisive in this respect were the better availability of land and the limitations imposed by a royal decree of 1624. Eventually, they chose Garbary, where on 16 January 1625 a plot of land with a garden was purchased. According to their records, it was a plot accommodating a wooden and a brick building that was situated in the vicinity of the city walls in the area of today's Kapucyńska and Podwale streets [24, p. 17].

In the purchased houses the monks soon set up a private chapel, living spaces, a refectory, and a small infirmary; in mid-1626 they also commenced efforts to set up a chapel that was open to the public. On 13 December 1627, the monks were granted a royal foundation privilege, and in the second half of 1628, on the grounds extended by an adjacent plot, the foundations for individual parts of the complex were laid[38]. For financial reasons the construction was delayed considerably and only the presbytery was built before 1638, while the entire complex was completed within the following two years[39].

---

[33]   The transfer of valuable archives and library collections to the branch of the monastery within the city limits protected them against destruction during the Swedish deluge. See: [5, p. 282].

[34]   A small church from the early 16th century, located in the place of today's monastery and church of Resurrectionist Fathers at Łobzowska street, disassembled in 1801. It was a filial church of St. Stephen's church at Szczepański square, and it was surrounded by a public cemetery, a precursor of the municipal necropolis in Cracow; more on this complex. See e.g.: [42, p. 694; 40, p. 176; 29, p. 53; 27, pp. 157–158].

[35]   Cf.: [35, p. 115].

[36]   A. Grabowski, *Kraków i okolice (zbiór notat i wiadomości do opisu miasta Krakowa)*, vol. III, manuscript, National Archives in Cracow, ref. No. 29/679/9 (former ref. No. E 17), p. 727.

[37]   More on the religious community of Franciscans of Primitive Observance in Małopolska and the history of their first monastery in Garbary. See: [24, pp. 13–35].

[38]   According to the author, due to the lack of funds it was decided to build the monastery first, and only later the church. See: [24, p. 20].

[39]   *Descriptio authentica erectionis duorum conventuum in Civitate Cracoviensi*, manuscript in the collections of the Archives of the Province of Franciscans of Primitive Observance in Cracow, p. 3; *Monimentum seu archivum Conventus Civitatis Metropolitanae Cracoviensis ad S. Casimirum 1625–1753*, manuscript, *ibid.,* p. 29.

The tanners' *iuridica*, rebuilt after the destruction of 1587, survived in the form described above for sixty years. In 1652 the *suburbium* residents were decimated by a plague, but what proved to be a true calamity was the siege and the subsequent occupation of Cracow by the Swedish army. Even before the arrival of the enemy, on 25 September 1655, Stefan Czarniecki, who was in charge of the defence of the city, ordered that all the buildings located to the north and west from the city be burnt down. Garbary, Biskupie, and Kleparz fell victim to the fire; even Cracow itself faced the threat of the flames – the fire raging outside the city walls also consumed the nunnery of the Dominican Sisters in Gródek, the church of the Franciscan Friars, the municipal pipeline, the furriers' tower, a part of the bishop's palace, and the attics of Wawel castle. Only quick firefighting action saved Collegium Maius[40].

Over subsequent months the remains of the old buildings were used in the construction of barricades and disassembled to get fuel; the few buildings that survived were plundered and burnt down. In September 1656, under a decree of the Swedish governor, Paul Wirtz, the final liquidation of the suburban development was ordered as it constituted a potential shelter for attackers. According to Janina Bieniarzówna and Jan M. Małecki, "on 13 November 1656 Smoleńsk, Retoryka, Wesoła, Podbrzezie, Błonie, Czarna Wieś, Krowodrza, Zwierzyniec, and Łobzów were burnt down. (…) Ruins of suburban churches were smashed as they could have offered shelter to attackers, thus completing the work of destruction begun by Czarniecki in September 1655. Church walls, e.g. of the Carmelites in Piasek, were demolished by means of battering rams brought there especially for this purpose" [5, p. 384].

After capitulation, announced on 25 August 1657, and after the Swedish army abandoned the city, the suburbs of Cracow were in a deplorable condition. Ludwik Sikora writes that to the west of the city walls only two little houses survived in Podzamcze, "in Piasek not even one house was left out of several hundred, all that was left of the mill and the Carmelites' monastery was a heap of debris" [37, p. 119]. The technical infrastructure was razed to the ground; roads and waterways were devastated; mills, fulling mills, baths, and the municipal pipeline were utterly destroyed. The layout of the *iuridica* returned to the one from the times before the incorporation, and the political economic, and social conditions of the 17th century offered no hope for a quick reconstruction.

After the retreat of the Swedish troops Garbary never regained its former glory; nevertheless, the liquidation of its development carried out in the years 1655–1657 did not bring an end to the history of the suburb. Although its development changed radically after the retreat of the Swedish army, it still constituted an attractive location for craftsmen's workshops, wayside inns, religious buildings, suburban residences, gardens, and orchards. Less than a half of the suburban development was recovered from the damage, and the area "in front of the Szewska Gate" had to wait until the mid-19th century for another period of prosperity.

---

[40] An extensive description of the history of the Swedish deluge is presented by Ludwik Sikora in his work. See: [37].

References

[1] *Akta wizytacji dekanatu krakowskiego z r. 1599, przeprowadzonej z polecenia kardynała Jerzego Radziwiłła – część I*, published by Cz. Skowron, Lublin 1965.

[2] *Atlas historyczny miast polskich*, collective work, ed. R. Czaja, vol. V Małopolska, issue 1, Kraków 2007

[3] Banach J., *Dawne widoki Krakowa*, Kraków 1983.

[4] Bąkowski K., *Dawne kierunki rzek pod Krakowem*, „Rocznik Krakowski", vol. V, 1902, pp. 138–172.

[5] Bieniarzówna J., Małecki J.M., *Kraków w wiekach XVI–XVIII, Dzieje Krakowa*, vol. 2, Kraków 1984.

[6] Bieniarzówna J., Piotrowski A.T., *Sanktuarium maryjne w kościele OO. Karmelitów na Piasku w Krakowie. Dzieje kultu i kaplicy*, Kraków 1983.

[7] Friedberg M., *Kraków w dobie Odrodzenia (wiek XVI i pierwsza połowa XVII)* [in:] *Kraków. Studia nad rozwojem miasta*, collective work, ed. J. Dąbrowski, Kraków 1957, pp. 189–227.

[8] *Garbary* [in:] *Encyklopedia Krakowa*, collective work, ed. A. H. Stachowski, Warszawa–Kraków 2000, pp. 228–229.

[9] Grabowski A., *Przedmieścia i okolice Krakowa. Wypisy z Dzieł*, Kraków 2007.

[10] Kęder I., Kęder W., *Kościoły nieistniejące* [in:] *Encyklopedia Krakowa*, collective work, ed. A. H. Stachowski, Warszawa–Kraków 2000, pp. 450–451.

[11] Kolak W., *Inwentarz akt jurydyk krakowskich 1412–1809*, Warszawa 1968.

[12] Kolak W., *Jurydyki Krakowskie*, „Archeion", vol. XXXVIII, 1962, pp. 219–240.

[13] Komorowski W., Krasnowolski B., Średniowieczne i renesansowe pałace krakowskie [in:] *Mecenat artystyczny a oblicze miasta*, collective work, ed. D. Nowacki, Kraków 2008, pp. 77–99.

[14] Krasnowolski B., *Młynówka Królewska – geneza i przekształcenia*, „Rocznik Krakowski", vol. LXIX, Kraków 2003, pp. 25–32.

[15] *Kronika mieszczanina Krakowskiego z lat 1575–1595*, published by H. Barycz, Kraków 1930.

[16] *Księga wiertelnicza krakowska*, published by K. Jelonek-Litewka, A. Litewka, Ł. Walczy, part I (1568–1577), Kraków 1997; part II (1578–1591), Kraków 1998; part III (1592–1597), Kraków 1999; part IV (1598–1606), Kraków 2000.

[17] *Księgi Ławnicze Krakowskie 1365–1376 i 1390–1397. Acta scabinalia Cracoviensia 1365–1376 et 1390–1397*, published by S. Krzyżanowski, Kraków 1904.

[18] Laberschek J., *Rozwój przestrzenny krakowskiego zespołu osadniczego extra muros XIII–XVIII w.* [in:] *Kraków. Nowe studia nad rozwojem miasta*, collective work, ed. J. Wyrozumski, Kraków 2007, pp. 297–354.

[19] Lepszy K., *Oblężenie Krakowa przez arcyksięcia Maksymiliana w 1587*, Kraków 1929.

[20] Leszczyńska–Skrętowa Z., *Czarna Ulica* [in:] *Słownik historyczno-geograficzny województwa krakowskiego w średniowieczu*, part 1, vol. 3, Wrocław–Łódź 1985, pp. 438–439.

[21] Leszczyńska–Skrętowa Z., *Czarna Wieś* [in:] *Słownik historyczno-geograficzny województwa krakowskiego w średniowieczu*, part 1, vol. 3, Wrocław–Łódź 1985, pp. 439–441.
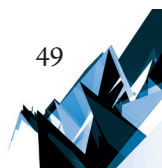
[22] Małecki J.M., *Życie gospodarcze XVI-wiecznego Krakowa* [in:] *Szkice z dziejów Krakowa od czasów najdawniejszych do pierwszej wojny światowej*, collective work, ed. J. Bieniarzówna, Kraków 1968, pp. 89–128.

[23] *Najstarsze księgi i rachunki miasta Krakowa od 1300 do 1400*, published by F. Piekosiński and J. Szujski, Kraków 1878.

[24] Pasiecznik J., *Kościół i klasztor Reformatów w Krakowie*, Kraków 1978.

[25] Petrus K., *Analiza piętnasto- i szesnastowiecznej zabudowy zachodnich przedmieść Krakowa przykładem badań nad zaginioną architekturą miasta / Analysis of the 15th- and 16th-century building development of the western suburbs of Cracow as an example of research into the lost architecture of the town*, "Czasopismo Techniczne – Technical Transactions", No. 6-A/2015, issue 9, year 112, pp. 155–166.

[26] Petrus K., *Największe przedmieście Krakowa. Zarys rozwoju przestrzennego Garbar*, part I, „Czasopismo Techniczne", No. 5-A/2011, issue 16, year 108, pp. 139–151.

[27] Petrus K., *Największe przedmieście Krakowa. Zarys rozwoju przestrzennego Garbar*, part II, „Czasopismo Techniczne", No. 5-A/2011, issue 16, year 108, pp. 153–163.

[28] *Piasek* [in:] *Encyklopedia Krakowa*, collective work, ed. A. H. Stachowski, Warszawa–Kraków 2000, pp. 747.

[29] Pieradzka K., *Garbary, przedmieście Krakowa (1363–1587)*, Kraków 1931.

[30] *Prawa przywileje i statuta Miasta Krakowa 1507–1795*, published by F. Piekosiński, vol. I, Kraków 1885; vol. II, Kraków 1890.

[31] *Przewodnik abo kościołów krakowskich krótkie opisanie*, Kraków 2002.

[32] Rączka J.W., *Młyny królewskie w krajobrazie Krakowa, cz. 1*, „Teka Komisji Urbanistyki i Architektury", vol. XII, year 1978, pp. 19–29 .

[33] Rączka J.W., *Młyny królewskie w krajobrazie Krakowa, cz. 2*, „Teka Komisji Urbanistyki i Architektury", vol. XIII, year 1979, pp. 7–16.

[34] *Rejestry gospód w Krakowie z lat 1632 i 1649 ze zbiorów Biblioteki Naukowej PAU i PAN w Krakowie i Biblioteki Jagiellońskiej*, published by K. Follprecht, Kraków 2005.

[35] Rożek M., *Nieistniejące kościoły Krakowa*, „Biuletyn Biblioteki Jagiellońskiej", year 33, 1983, pp. 95–120.

[36] Sikora F., *Dębny Młyn* [in:] *Słownik historyczno – geograficzny województwa krakowskiego w średniowieczu*, part 1, vol. 3, Wrocław–Łódź 1985, pp. 538–539.

[37] Sikora L., *Szwedzi i Siedmiogrodzianie w Krakowie, 1655–1657*, Kraków 1908

[38] Supranowicz E., *Nazwy ulic Krakowa*, Kraków 1995.

[39] Tobiasz M., *Jak powstały przedmieścia Krakowa?*, Warszawa–Kraków 1972.

[40] Tomkowicz S., *Ulice i place Krakowa w ciągu dziejów, ich nazwy i zmiany postaci*, Kraków 1926.

[41] Wimmer J., *Odparcie najazdu arcyksięcia Maksymiliana w 1587–88*, Warszawa 1955.

[42] Wiśniewski J., *Garbary* [in:] *Słownik historyczno – geograficzny województwa krakowskiego w średniowieczu*, part 1, vol. 4, Wrocław–Łódź 1986, pp. 693–706.

[43] Włodarczyk W., *Kościół Karmelitów na Piasku*, „Rocznik Krakowski", vol. XXXVI, 1963, pp. 127–148.

ULICA POŁWSIE

"ZA ŚW. PIOTREM"

CZARNA ULICA

ULICA CZARNA

DROGA NA CZARNEJ WSI

CZARNA WIEŚ

ULICA GRZEBIENNICZA

ULICA TASEMBERK

ULICA PAŃSKA

ULICA SZEROKA

ULICA MAŁA

RYBITWY

ULICA GARNCARSKA

KRAKÓW

12

KAWIORY

ULICA RÓŻANA

ULICA KRUPNIKÓW

KRUPNIKI

OGRODNIKI

- A
- B
- C

0   100
        M
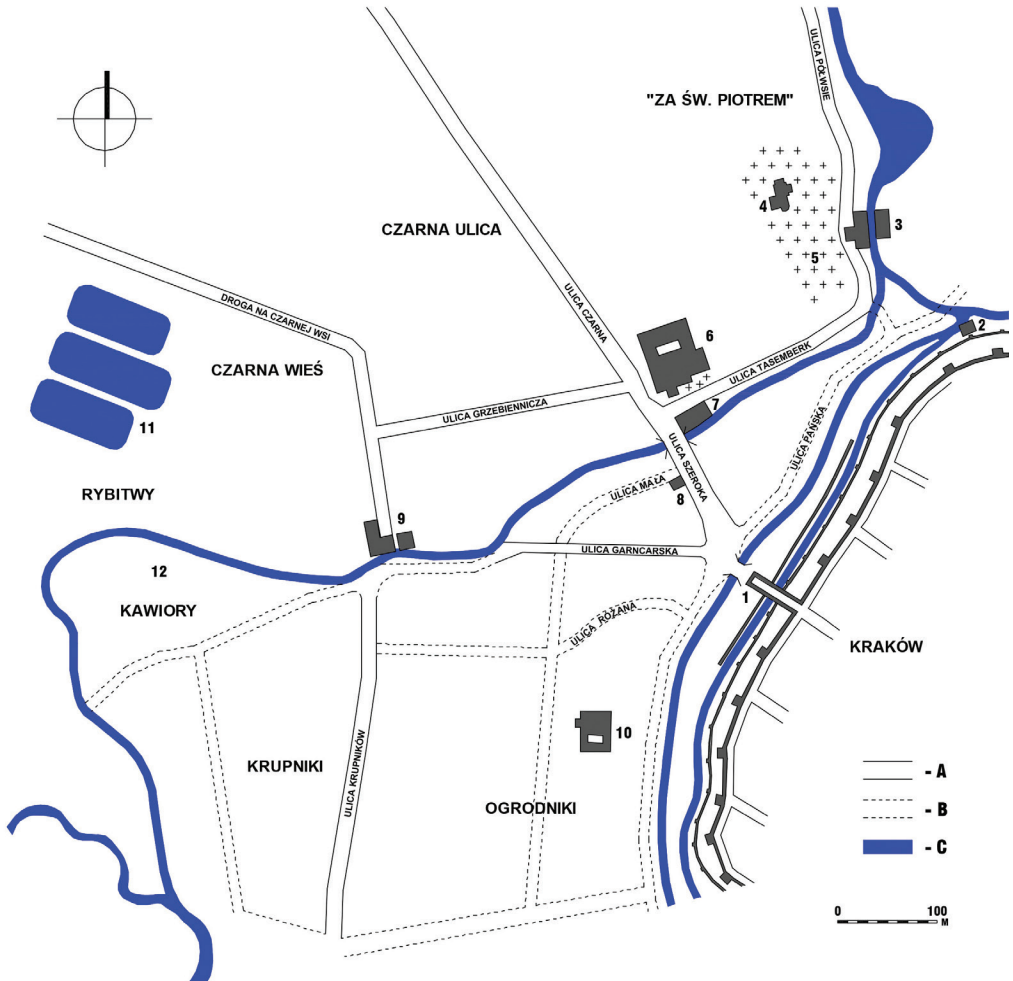
Fig. 1. Garbary in the years 1587–1655: A – streets with a layout confirmed in the sources; B – streets with a hypothetical layout, not confirmed in the sources; C – waterways and bodies of water. More important buildings and development elements of the suburb: 1 – "Szewska" Gate; 2 – water pipeline; 3 – Upper Mill; 4 – St. Peter's church; 5 – public cemetery; 6 – Carmelite Fathers' church and monastery; 7 – "Dębny" Mill; 8 – town hall of the *iuridica*; 9 – Lower Mill; 10 – church and monastery of the Franciscans of Primitive Observance; 11 – probable location of the Fish Guard; 12 – probable location of the old Jewish cemetery (prepared by K. Petrus)
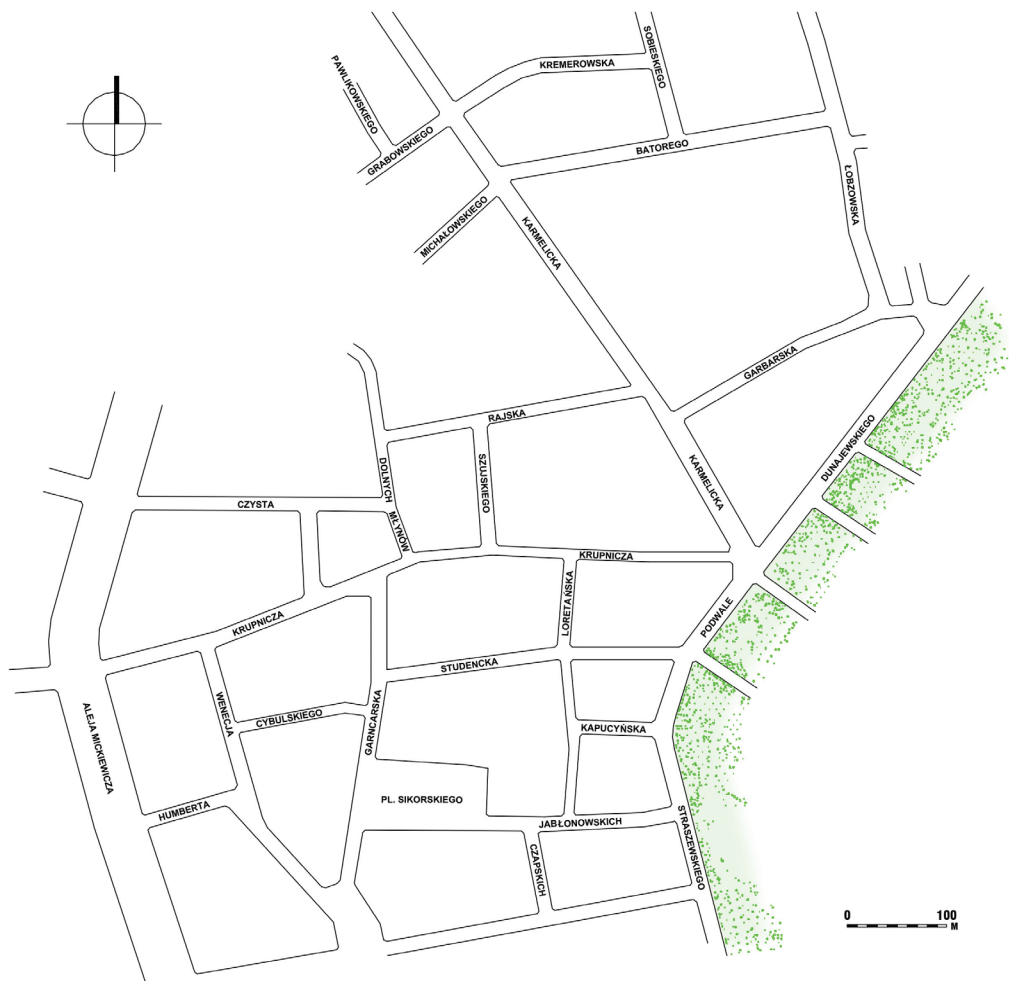
Fig. 2. Current road grid within the area of the former tanners' *iuridica* (prepared by K. Petrus)

Mariusz Twardowski

patwardo@cyf-kr.edu.pl

Institute of Urban Design, Faculty of Architecture, Cracow University of Technology

Football Stadiums – Icons of Sports Architecture

Stadiony piłkarskie – architektoniczne ikony sportu

Abstract

Modern stadiums constitute a challenge to urban planning, architects and buildings. The exceptional character of these enormous structures is, on the one hand, highlighted by their unique massings and the innovative materials that they employ, while on the other, their composition within the space of the city and its skilful blending into its context causes them to become icons and landmarks. Three different examples demonstrate that the requirements presented above can be fulfilled. Modern forms have been fitted into the scale of cities of various size and adapted to their surroundings. Functional solutions were well-thought out and circulation and access have been placed so that events would not block traffic in the city each time they are held.

Keywords: stadium, Eisenman, Arroyo, Herzog & de Meuron, Munich, La Coruña, Barakaldo, icon

Streszczenie

Nowoczesne stadiony to wyzwanie dla urbanistyki miasta, architektów i budowniczych. Wyjątkowość tych dużych budowli z jednej strony podkreślana jest niespotykaną bryłą i zastosowanymi nowatorskimi materiałami. Z drugiej strony, ich kompozycja w przestrzeni miasta i umiejętne wpisanie w jego kontekst sprawiają, że stają się one ikonami i punktami orientacyjnymi. Trzy zróżnicowane przykłady ukazują, że powyższe wymagania mogą być spełnione. Nowoczesne formy wkomponowane zostały w skale różnej wielkości miast i w dostosowane do otoczenia. Rozwiązania funkcjonalne przemyślano a komunikację i dostęp usytuowano w sposób taki, by każdorazowe wydarzenia nie blokowały ruchu w mieście.

Słowa kluczowe: stadion, Eisenman, Arroyo, Herzog & de Meuron, Monachium, La Coruña, Barakaldo, ikona

1. Introduction

Football is the national sport of many of the world's countries, as well as of the majority of European states. The quality of an arena for such a sport is decided by not only its form, but also the variety of function, technological and material solutions, as well as those that support sustainable development.

Stadiums most often become landmarks on the scale of the city, while sometimes they become dominants within the surroundings in which they have been built. The owners of sports clubs who build these structures want them to become the icons of cities. When writing about form and composition we can analyse ideas concerning site development and the unique shape of architecture. When discussing function, we should remember not only about accompanying functions, which are going to operate practically only during matches organised at the stadium, but also about circulation, access and the space for spectators itself. Flexible solutions make it possible to organise other events than football matches. Technology and material solutions complement the form and composition and cause a given structure to become unique. Solutions that are friendly to the environment reduce energy consumption and generate lower maintenance costs. They are also friendlier to the environment. It would be appropriate to analyse in what manner do the referenced solutions placed in cities of various size operate and what requirements should we set for the designs of these complicated buildings in order to meet the criteria below: a large city – a large stadium – city limits, average-sized city—medium-sized stadium – city centre, small city – a small stadium.

Exceptional architectural solutions

In order to find quality in the architecture of sports stadiums, the author described three examples of arenas: in Munich, Barakaldo near Bilbao and in La Coruña. Two of them have been built, while the third remains in its design phase. The examples that were selected show the problem being discussed in a scale appropriate to the localities in which they had been placed. Their cubature and spectator capacity has been appropriately thought through and selected in relation to the size of the city, the significance of the matches [2][1] and the popularity of clubs whose teams play on these arenas. The large stadium in Munich found its place on the border of the city. The site on which it was built had sufficient potential for the construction of a large stadium, parking lot, train station and a connection with nearby highways. The small Barakaldo stadium was placed within the context of a small city. The arena in La Coruña is a large structure in the centre of an old town district. It is meant to replace the currently used stadium.

---

[1] Bayern Munich, apart from playing in the Bundesliga, plays in the Champions' League. This league's matches gather an exceptionally large audience. Deportivo is one of the best teams of the Spanish La Liga and regularly plays in the European League.

2. Allianz-Arena, Munich, Germany, design by Jacques Herzog and Pierre de Meuron

For many years, two of Munich's clubs have been using the same stadium. The Olympic Stadium (69256 seats), designed by world-famous architects Günter Benisch and Otto Frei, with the first match to be played on it taking place on the 26th of May 1972 between the national teams of Germany and the Soviet Union, was used up to 2005. Since the 2005/2006 season, the local Bayern and TSV 1860 teams have been competing on the new Allianz-Arena stadium. The future of the Olympic Stadium is a bit of a mystery, however, as concerts and other large events take place there and it has been opened to visitors on weekdays. The previous Grünwalder stadium (12 500 seats), on which matches were played prior to 1972, served the amateur and junior teams of both clubs up to 2017. In 2017 the contract between the management of Allianz-Arena and the TSV 1860 sports club was terminated. The club was demoted to the regional league and returned to the older Grünwalder stadium [2].

The idea for the construction of Allianz-Arena crystallised on the occasion of Germany entering the competition to become the host country of the World Cup Tournament in 2006. In 2001 a referendum was organised, asking the residents' opinion on the matter of the construction of the new stadium [2]. In 2002 an international architectural competition was announced for the design of a stadium meeting the requirements of the football federation of Germany, UEFA and FIFA, as well as functional requirements concerning the safety of spectators, fire safety and the use of the structure, in addition to not limiting it to serving solely as a football stadium once every two weeks. The competition jury, composed of acclaimed architects from all over the world, representatives of football federations, the owners of the structure and the sponsor, selected a design by the Swiss design company Herzog & de Meuron[2]. It was decided that their work fulfilled the conditions described above and that it would also become a hallmark of the city, an interesting stadium of the upcoming World Cup and an excellent advertisement for the sponsor – the Allianz company. Its representatives stated that the see-through cladding that towers above a plateau would be identified with the company in the best possible manner.

Despite the fact that the form and the materials can appear futuristic, the architects, through the adoption of "transparency", referred to tradition by reminding us of the suspended tent-like structures of the Olympic Stadium of 1972. The building is a play of light, which is to elicit "otherworldly" emotions. The lighting fitted to structural elements, by illuminating the semi-translucent shell, creates an illumination of colours, which "introduces the building into the magical meaning of poetry" [29]. It was also stated that, due to the fact that the Allianz-Arena was meant to be the host stadium for both of Munich's clubs, they could identify with the stadium through its highlighting with light and colour. Thus, when one team plays, the stadium is lit red, when the other plays – it is blue.

---

[2]   Jacques Herzog and Pierre de Meuron are well-known and acclaimed architects whose built projects can be found in Switzerland, Germany, France, Italy, Austria, Great Britain, Spain, Japan and the United States. They are the laureates of architectural competitions from all around the world. They are invited to deliver lectures at the best architectural universities. In 2001 they were awarded the greatest distinction in architecture – the Pritzker Prize. From: [61].
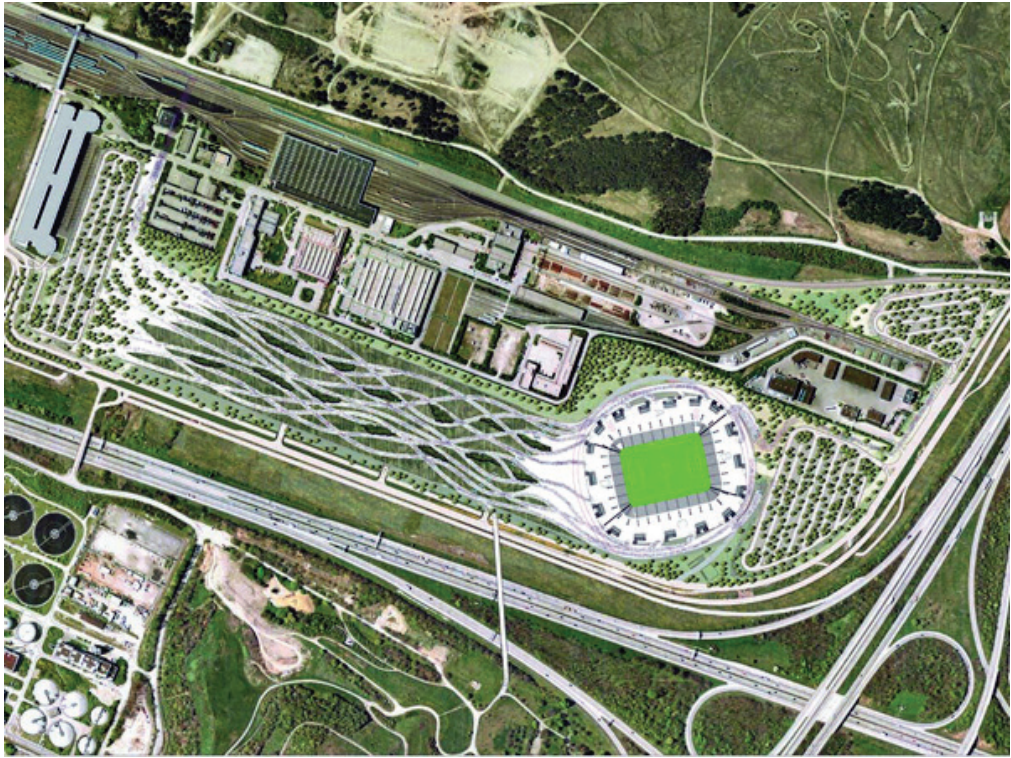
Fig. 1. Allianz Arena in Munich, top-down view (source: [58])

Fig. 2. Allianz Arena in Munich, construction on the stadium (source: [2])

Fig. 3. Allianz Arena in Munich, proposals of the illumination of the stadium depending on which football club is currently playing (source: [28])

Jacques Herzog and Pierre de Meuron had uniquely solved the functional matters of the stadium, which was another point that convinced the jurors and the sponsor. The illumination of the pitch was suspended from the roof covering the spectator stands of all teams. The stadium can house 66,000 spectators on three levels of stands, including seats for journalists and guests of honour. Persons with disabilities can use 200 places for themselves and their caregivers on the lower stand. A parking lot for 11,000 cars (including 350 spaces for buses and 1,200 spaces underneath the stadium) was placed on both sides of the complex, in addition to stores with club merchandise, as many as 400 kiosks and two restaurants for the fans of Munich's teams, located on opposite sides of the stadium and isolated from one another. Allianz-Arena (in accordance with competition guidelines) has not resisted commercialisation. In order for the project to be profitable, a shopping gallery was placed underneath the passages (entry from one of the parking lots).

Thanks to its appropriate placement on the site, the parking lot has been quite easily integrated with the city's bypasses. The project was completed in 2005.

The project presents itself impressively: 66,000 spectators, 171,000 m^2 of floor surface area, a shopping gallery and parking spaces for 11,000 cars. However, that which is essential in such an enormous project is that the architects elegantly and delicately ("semi-translucently") blended the building into the surrounding infrastructure and the flat landscape surrounded only by forests, meadows, the nearby highway intersections and the buildings of the city visible in the distance.
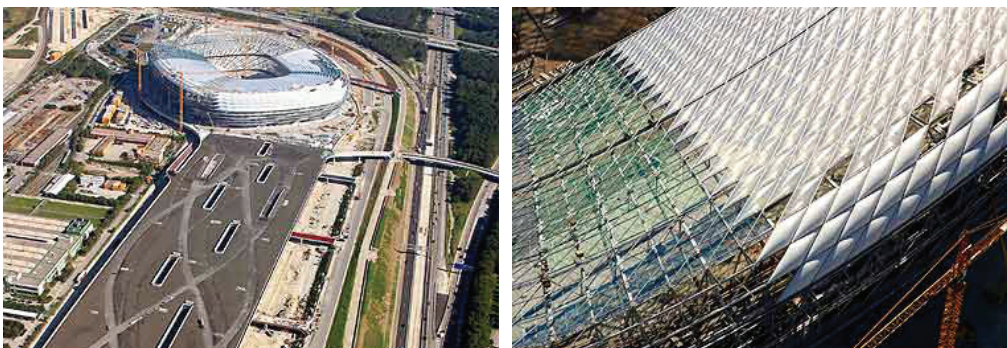

Fig. 4. Allianz-Arena in Munich, photographs of the construction site (source: [71])

Fig. 5. Allianz-Arena in Munich (photo by Mariusz Twardowski)

3. Lasesarre Barakaldo, Barakaldo, Spain, design by No.MAD Arquitectos, Eduardo Arroyo

The stadium of the local team is considered to be one of the best – as well as best-looking – examples of sports arena architecture. The Spanish architect Eduardo Arroyo[3] proposed the use of geometric forms made from semi-transparent materials in order to preserve the contact of the modern massing with nature.

One would be very hard pressed to find any excessive decorations and details in the design. The only decoration are the large, almost one-and-a-half-metre tall white letters – the name of the complex and the city, located on semi-transparent panels on the outer wall of the stadium.

Transparency and a connection with nature and the surroundings were also highlighted through grates separating the interior of the stadium from the street. They were built in a modular manner, as if forming a pattern – a print on the material and thanks to their slightly sculptural shapes, refer to nature. This measure also caused the gates composed from elements designed in this manner to cease to be negatively associated with entrances to the stadium, their only purpose being protection from aggressive football fans.

---

[3]   Eduardo Arroyo belongs to a young generation of Spanish architects. Born in Bilbao, he graduated from the Faculty of Architecture in Madrid in 1988, where is currently a professor. He also teaches at the best architecture schools around the world. He has received many awards and honorary mentions in competitions, he took part in the EXPO 2000 international exhibition in Hanover as a representative of Spain, as well as in the most prestigious architectural exhibition in the world – the Biennale in Venice, also in 2000. One of his last designs is the football stadium in Saragossa (2002). From: [41, p. 42].

The illumination of the pitch was fitted to geometric columns (covered, similarly to the entire stadium, with semi-transparent panels from Plexiglas). It should be added that this solution in terms of lighting columns was its architect's homage to the history of the stadium. Lighting columns are no longer used on stadiums, as they are considered obsolete solutions. Eduardo Arroyo replaced the old lighting columns with "new" ones.

Once again highlighting the connection with nature, the architect designed the pitch of the stadium in such a way so that it blends in with the spectator stands. In some places it "slides in" between the stands, curving slightly upwards.

The seats for spectator stands are another reference to nature. As the author asked – how difficult it is to paint anything like a rainbow in today's world [44]. It was placed in such a manner so that the spectators sitting in the closest rows to the pitch "play" together with their team. In addition, the designer planned the planting of 1,000 trees near the stadium, composed using a modular grid.

The stadium presents completely different aesthetic qualities in the evening. The semi-translucent surfaces start to shine in their own, highly sensitive and delicate manner. As a result, the architect obtained an extraordinary impression of the stadium's lightness, which has been "elevated" above the surrounding urban context in this manner.

Fig. 7. Lasesarre Barakaldo Stadium, Barakaldo, the stadium against the background of the city's buildings, (source: [8])
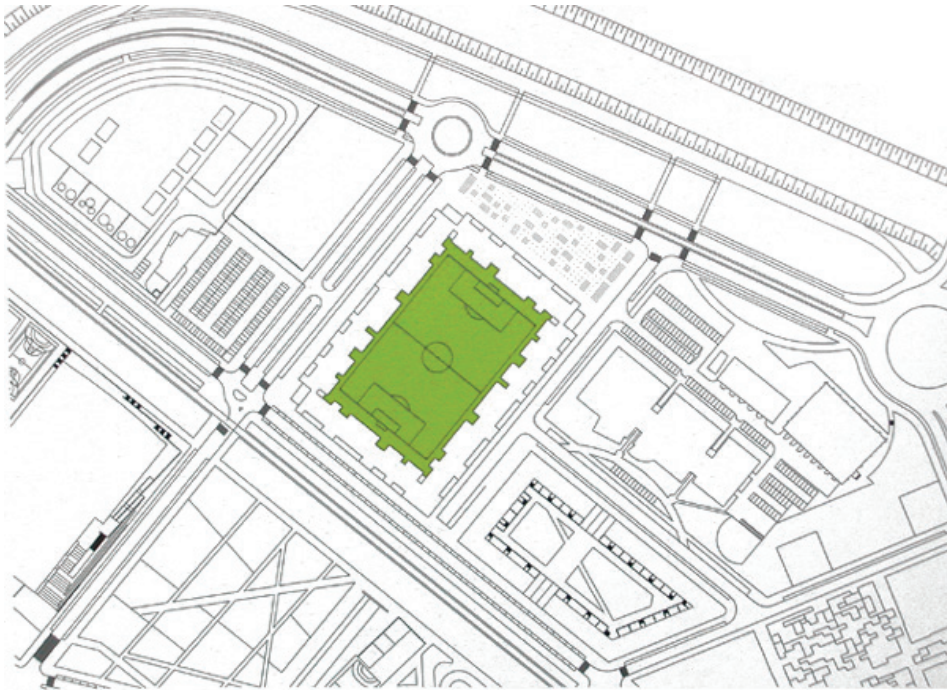
Fig. 6. Lasesarre Barakaldo Stadium, Barakaldo, site development plan (source: [41, p. 44])

Fig. 8. Lasesarre Barakaldo Stadium, Barakaldo, facade with semi-transparent, backlit panels and steel grates, phot. by Roland Halbe (source: [43])

Fig. 9. Lasesarre Barakaldo Stadium, Barakaldo, illumination of the stadium during a match, phot. by Roland Halbe (source: [48])

Fig. 10. Lasesarre Barakaldo Stadium, Barakaldo, the cameral space of the interior of the stadium, phot. by Roland Halbe (source: [43])
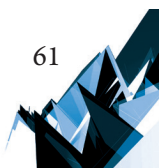
Fig. 11. Lasesarre Barakaldo Stadium, Barakaldo, Interior illuminated by the sun entering through the sculptural grates, which result in an extraordinary interplay of light and shadow, phot. by Roland Halbe (source: [17])

The designer, using very simple means, organised the circulation and access to each of the stadium's sectors, able to house a total of 10 thousand spectators. The layout of the entrance gates around the structures directs the spectators directly to small sectors without causing a commotion during entering and leaving the arena. Every sector is a sort of repeated "building" with its own organisation of the spectator stands, its own toilets, gastronomic establishments and stores with football club merchandise. Every element of this building "proves" that it is a fragment of an immeasurably well-thought out composition.

The stadium, built in 2003 in Barakaldo, which has a population of 96 thousand and is located 8 km away from Bilbao, has become a hallmark of the city and is one of the permanent features of guided tours visiting the city.

4. Estadio de Riazor, Deportivo La Coruña, Spain, design by Peter Eisenman

Real Club Deportivo La Coruña is not perhaps as famous as Real Madrid or F.C. Barcelona, but it has its own illustrious traditions as well. Since the 1990's it has always been in the leading portion of the Spanish La Liga, celebrating its national cup title in 2000.

"Art does not try to be sublime, beautiful or grand. It is rather a commentary on the current events of the present... The spectator observes the grey and ordinary, oftentimes ugly architecture. However, sometimes it so happens that he sees quite remarkable things. In order
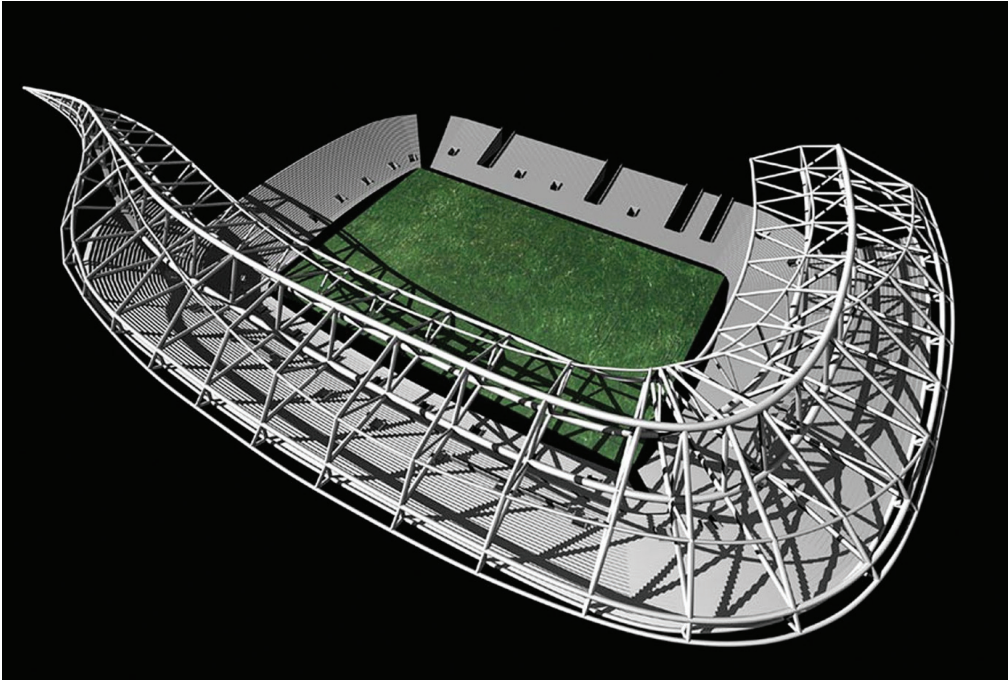
Fig. 12. Stadion de Riazor, La Coruña, visualisation by Peter Eisenman Studio, source: materials made available to the author by Peter Eisenman

to be called original, they break away from those already devised with their form. At the same time, they build beauty" [69]. Peter Eisenman's design is exactly such an image of subtle architectural compositions.

The American architect Peter Eisenman[4] was selected to develop the design of the new stadium, which was to meet the extremely strict requirements of the club's board and shareholders. The author of the design performed admirably in the task he had been given. The design of the new Estadio de Riazor presents two directions of thought: obtaining a model of a professional club with a modern stadium and of the future and development of the city. A private developer, in cooperation with the city and the region, as the hosts of

---

[4] Peter Eisenman, born in 1932 in Newark, New Jersey, USA, is an architect and academic teacher. He studied at Cornell and Columbia University, defending his doctoral dissertation in Cambridge, Great Britain. He received three honorary doctorates. He currently teaches at the faculties of architecture of Cambridge, Princeton, Yale, Ohio State and Harvard universities, as well as at ETH in Zurich and IUAV in Venice. He wrote around a dozen books and publications. For such a popular architect, only a small number of his projects have been built. His latest built projects include the Holocaust museum in Berlin, the Arizona Cardinals NFL stadium in Phoenix, the City of Culture in Santiago, Spain. Most of his built projects are the results of winning architectural competitions. He is regularly selected as the representative of the United States to participate in exhibitions held during the Biennale in Venice. He is one of the world's most famous architects, a representative of the New York-based group of architects "New York Five": Peter Eisenman, John Heyduk (died in 2000), Michael Graves (died in 2015), Charles Gwathmey (died in 2009) and Richard Meier, which paved the way for a new perspective of architectural theory and of architecture as an art. From: [70, p. 100].

Fig. 13. Estadio de Riazor, La Coruña, mock-up by Peter Eisenman Studio, source: materials made available to the author by Peter Eisenman

the football club, decided that the existing stadium no longer fitted the image of the club. It was neither about the number of seats[5] nor its size, but rather about the internal functional layout, the flexibility of solutions and the possibility of proposing various additional functions (e.g. residential, commercial or hotel spaces).

In the design, Eisenman presented a sophisticated architectural critique of the surrounding compositional ever-day reality. Eisenman won over the board of the club not only with the immensity of the structure's multi-functionality, but also with the three-dimensionality of its architecture, a philosophical depth very rarely encountered in architectural designs and the fact that

---

[5]   The existing stadium houses 34,600 seats, while the new one is meant for 36 000 spectators. Information from Peter Eisenman.

only a mature patron of the arts could appreciate the work, understand it and afford such a design. Eisenman claimed that in order to treat him seriously, to take him literally and believe him, it was necessary to become lost. He said faith made it possible to move forward, with temporarily "losing oneself" enabling an outlook on and evaluation of a work without negative contexts or habits [51, p. 25]. Eisenman, as a leading representative of deconstructivism in architecture, attempted to depict a conflict of two formal principles in the design: of instability against stability and the changing of time against the unchanging space. He depicted these conflicts by elevating the building above the ground and designing the structure of the stadium in the form of three-dimensional, spatial trusses and its storeys as surfaces suspended from different heights. The building becomes as fleeting as unrecorded time. The stable structure unstably permeates into the area of the city and through its winding form reaches the bay. Apart from philosophical discussions concerning the proposed building, in effect the architectural form must refer to logic. It if really is so then we can compare Eisenman's work with the previously described designs.

Peter Eisenman added over one hundred and fifty thousand square metres of multi-functional spaces to the basic sports-related function (the stadium, a swimming pool, tennis and squash courts, gyms, etc.). They feature a museum of the history of the club and exhibition spaces, restaurants, a hotel for 200 guests with conference halls, a restaurant and the necessary facilities, a community centre with exhibition halls, a commercial section with shops and
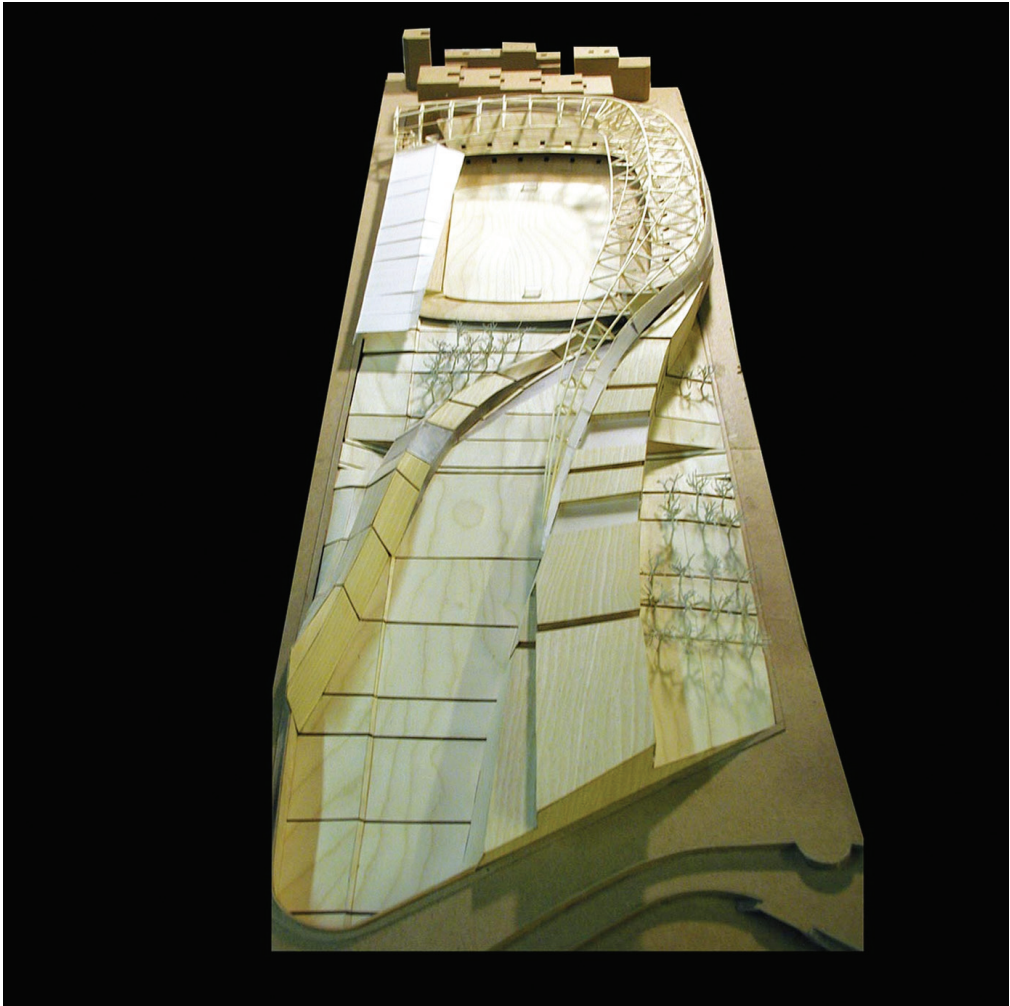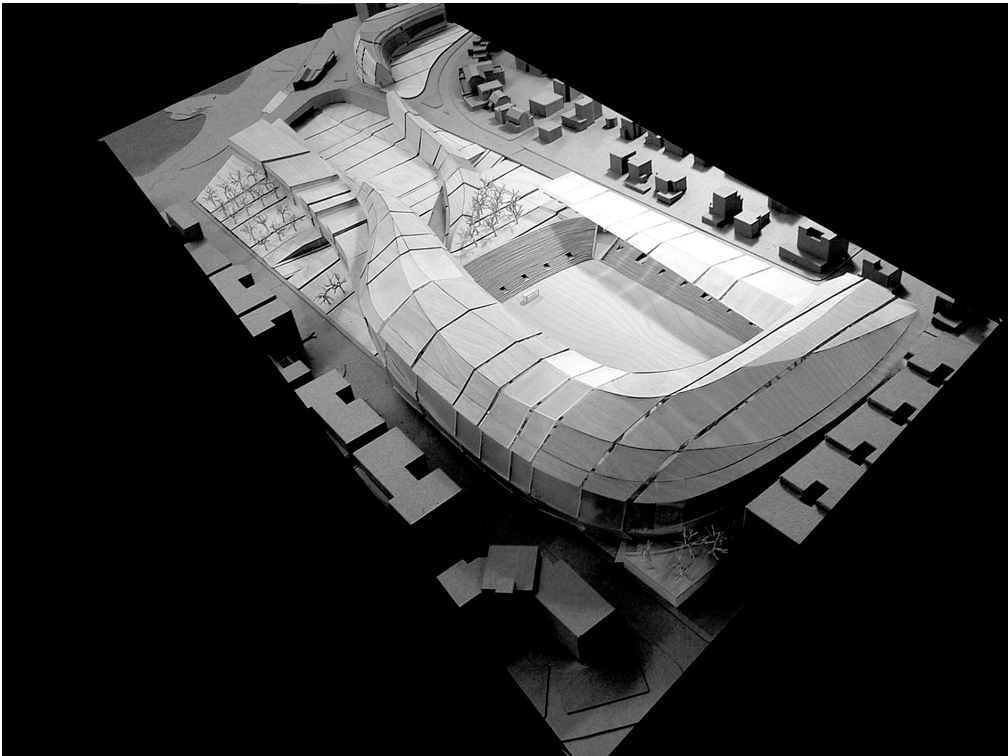

Fig. 14. Estadio de Riazor, La Coruña, mock-up by Peter Eisenman Studio
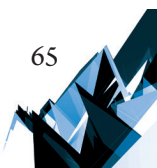(source: materials made available to the author by Peter Eisenman)

65

Fig. 15. Estadio de Riazor, La Coruña, wizualizacja Peter Eisenman Studio (source: materials made available to the author by Peter Eisenman)

boutiques, a park for children – a place, where entire families could reside and where parents could leave their children under care if they need to – as well as office spaces, green spaces with gardens and a park, an enormous parking facility and apartments meant both for sale and for rent (the entirety featuring an impressive floor area of 250,000 m^2)[6]. Each of the elements of the additional space has been carefully designed in order to reconstruct existing urban structures in such a way as to cast a new light on them, to calibrate them anew with the newly designed ones, as well as the existing context in order to underscore the innovative aspects of the entire layout.

In this design the author searched for a new expression for urban space by using the natural beauty of the forms of the nearby bay and its port. The architect contained the stadium, the hotel and retail spaces in an organic massing of dynamically elevating surfaces [52]. After its construction the building could, without a doubt, become an icon of the city. The subtlety of the form of the stadium, however, has not been fully appreciated by the developers and this design from 2001 has not been built. We should only hope that the cost[7] of the construction of the entire complex will not exceed the financial capabilities of the club, whose conflicts with the municipal authorities are postponing the project.

[6]   Information from Peter Eisenman.
[7]   The cost of the stadium's construction is estimated at 85 million dollars, while that of ancillary functions – 155 million. Information from Peter Eisenman.

5. Conclusion

The examples that have been described present three cases of designs placed in completely different locations. Each of them became or could become an orientation point on the scale of the city. They introduce modernity into the tissue of the city on each of its scales. Each of the forms has a different context, however, all of them have prospered in their surrounding conditions. Regardless of whether it is an open space in Munich, with a population of one and a half million, the multi-family buildings of small Barakaldo with one hundred thousand residents or the centre of an old town district in La Coruña with a population of two hundred and fifty thousand, all of the buildings blend into their varied surroundings. At the same time their functional variety meets the requirements of football club owners and city governors, which see profit in the use of stadiums[8]. The wealth of complementary functions makes it possible to draw additional income financing sports operations. Flexible solutions concerning spectator stands and their appropriate layout around the pitch make it possible to use the pitches and spectator stands for other entertainment-related and commercial purposes. The technologies used in the designs cause the individuality of each stadium to be unique. They lower energy consumption and the cost of their occupancy.

Difficult stadium complexes of varying scale have become pretexts for the authors of all of the presented buildings to pursue beauty. They presented greater values in their designs than those that are usually attributed to such structures and the architecture of these stadiums can cause them to become icons of sports architecture.

References

[1] Alexander Ch., *Język wzorców Miasta*, Gdańsk 2008.
[2] *Allianz Arena*, https://allianz-arena.com/en/arena/facts/the-making-of-the-allianz-arena (access: 19.05.2018).
[3] *Arene*, Area 2004, Iss. 75.
[4] Arnheim R., *Sztuka i percepcja wzrokowa. Psychologia twórczego oka*, transl. J. Mach, Warszawa 1978.
[5] Augé M., *Nie-Miejsca. Wprowadzenie do antropologii nadnowoczesności*, Teksty Drugie 2008, 4.
[6] Aymonino C., *Il significato delle città*, Marsylia 2000.
[7] Aymonino C., *Per Un'Idea di Citta*, Cluva 1984.
[8] *Barakaldo CF, Pagina Oficial*, http://barakaldocf.com/localizacion/ (access: 27.09.2012)
[9] Bonenberg W., *Architektura ostatnich dziesięcioleci XX wieku*, Stowarzyszenie Psychologia i Architektura, Poznań 2001.

---

[8] Only in the case of Estadio de Riazor in La Coruña has the lack of agreement between the owners of the club and the city caused the construction of the stadium to be postponed for many years.

[10] Borowska M., *Estetyka i poszukiwanie znaczeń w przestrzeniach architektonicznych*, Semper, Warszawa 2013.

[11] Broto C., *New urban design*, Barcelona 2000.

[12] Cassirer E., *Filosofia Delle Forme Simboliche*, La Nuova Italia, 1961.

[13] *Changing Cities*, Area 2008, Iss. 100.

[14] *Definiowanie przestrzeni architektonicznej*, materiały Międzynarodowej Konferencji Naukowej IPA WA PK, Kraków 2000–2008.

[15] Eco U., *Historia brzydoty*, Poznań 2007.

[16] Espuelas F., *Il. Vuoto. Riflessioni sullo spazio in architettura*, Marinotti 2004.

[17] *Estadio De Futbol De Lasesarre / NO.MAD* [w:] Plataforma Arquitectura, 18.11.2013, https://www.plataformaarquitectura.cl/cl/02-310227/estadio-de-futbol-de-lasesarre-no-mad/52897f45e8e44ea3db0000d4-lasesarre-football-stadium-no-mad-photo (access: 21.05.2018)

[18] Focillon H., *Vita Delle Forme*, Einaudi, 1987.

[19] Franta A., *Adaptable City*, Czasopismo Techniczne, 2-A/2014, 81–102.

[20] Gehl J., Życie między budynkami. Użytkowanie przestrzeni publicznych, transl. M. A. Urbańska, RAM, Kraków 2009.

[21] Grassi G., *Architettura, Lingua Morta*, Electa, 1988.

[22] Gregotti V., *Architettura e postmetropoli*, Einaudi, Turin 2011.

[23] Gregotti V., *Città visibile*, Einaudi, Turin 1993.

[24] Gyurkovich J., *Architektura w przestrzeni miasta. Wybrane problemy*, Wydawnictwo Politechniki Krakowskiej, Kraków 2010.

[25] Gyurkovich J., *Znaczenie form charakterystycznych dla ksztaltowania* i percepcji przestrzeni, Monograph, Series: Architektura, Wydawnictwo Politechniki Krakowskiej, Kraków 1999.

[26] Gyurkovich M., *Hybrydowe przestrzenie kultury we współczesnym mieście europejskim*, Monograph, Series: Architektura, Wydawnictwo Politechniki Krakowskiej, Kraków 2013.

[27] *Herzog & de Meuron, Arupsport Allianz Arena* [in:] Divisare 23.09.2009, https://divisare.com/projects/91395-herzog-de-meuron-arupsport-duccio-malagamba-allianz-arena

[28] *Herzog&de Meuron*, https://www.herzogdemeuron.com/index/projects/complete-works/201-225/205-allianz-arena.html (access: 12.03.2008)

[29] Adam H., *Allianz-Arena – Gralsburg und Hexenkessel*, [in:] Next Room, Vienna 28.05.2005, www.nextroom.at/building.php?id=655 (access: 18.05.2018).

[30] Jagiełło-Kowalczyk M., *Zrównoważone osiedla bez samochodów… i bez mieszkańców*, Środowisko Mieszkaniowe, Wydawnictwo Politechniki Krakowskiej, Kraków 2014.

[31] Jałowiecki, B. (ed.), *Czy metropolia jest miastem?*, Wydawnictwo Naukowe Scholar, Warszawa 2009.

[32] Kadłuczka A., *Architektoniczne "reguły gry" w przestrzeni historycznych centrów miejskich*, International Symposium Protection and Management of UNESCO Cultural World Heritage in East Central Europe, Warsaw, Zamość, Cracow, September 14–18 1994.

[33] Kantarek A.A., *O orientacji w przestrzeni miasta*, Monografia, Wydawnictwo Politechniki Krakowskiej, Kraków 2013.

[34] Kobylarczyk J., *Wpływ nowych rozwiązań architektoniczno-urbanistycznych na tożsamość miast*, [in:] *Tożsamość miasta w dobie globalizacji: Problemy tożsamości metropolii i dużych miast*, Wydawnictwo Politechniki Poznańskiej, Poznań 2009.

[35] Koolhaas R., *Junckspace*, Quodlibet, 2006.

[36] Koolhaas R., *S, M, L, XL*, Monacelli Press, New York 1995.

[37] Kosiński W., *Człowiek – wartości – piękno – miasto – architekt – kompozycja*, Czasopismo Techniczne. 2-A/2014, 121–193.

[38] Kosiński, W., *Miasto i piękno miasta*, Wydawnictwo Politechniki Krakowskiej, Kraków 2011.

[39] Krier R., *Architectural Composition*, London 1988.

[40] Krier L., *Architektura, wybór czy przeznaczenie*, Warszawa 2001.

[41] Krier R., *Lo spazio della citta*, Cluva, Milano 1982.

[42] Kucza-Kuczyński K., *Czwarty wymiar architektury miasta*, Arkady, Warszawa 1982.

[43] *Lasesarre Football Stadium / NO.MAD* [in:] ArchDaily, 20.11.2013, www.archdaily.com/449637/lasesarre-football-stadium-no-mad (access 20.05.2018)

[44] *Lasesarre Football Stadium* [in:] MacContext, Chicago, issue 30–31, www.mascontext.com/issues/30-31-bilbao/lasesarre-football-stadium/ (access: 12.08.2015).

[45] *Learning from cities*, 10. Mostra Internazionale di Architettura, Marsilio, Venezia 2006.

[46] Lynch K., *The Image Of The City*, Cambridge 1960.

[47] *New Lasesarre Football Stadium, Barakaldo, Spain* [inw:] AREA, Arene, iss. 75, Firenze 2004,

[48] No.Mad, www.nomad.as/html%20css/ (access: 20.05.2018).

[49] Norberg-Schultz, Ch., *L'Abitare: L'Insediamento, Lo Spazio Urbano, La Casa*, Electa, 1984.

[50] Norberg-Schulz Ch., *Bycie, przestrzeń, architektura*, transl. B. Gadomska, Warszawa 2000.

[51] *One Madison*, Cetra/Ruddy, www.cetraruddy.com.

[52] Eisenman P., *House X*, Rizzoli, 1982.

[53] *Phaidon Atlas*, Phaidon Press Ltd, London 2015.

[54] Czasopismo Techniczne, 1-A/1/2012, Politechnika Krakowska, Kraków 2012.

[55] Rossi A., *Considerazioni sulla morfologia urbana e la tipologia edilizia*, 1964.

[56] Rossi A., *L'architettura della citta*, 1966, Officina Edizioni, Roma 1976.

[57] Saarinen E., *The City. Its Growth, Its Decay, Its Future*, MIT Press, Cambridge 1966.

[58] Staten S., *Case Study: Allianz Arena – Munich, Germany, Parametric Modelling* [in:] ARCH 653 – BIM Modeling in Architecture 26.03.2013 https://sstamu.wordpress.com/2013/03/26/parametric-modeling/ (access: 21.05.2019)

[59] Schneider-Skalska G., *Kształtowanie zdrowego środowiska mieszkaniowego: wybrane zagadnienia*, Monograph 307, Wydawnictwo Politechniki Krakowskiej, Kraków 2004.

[60] Szpakowska E., *Architektura miasta idealnego*, Kraków 2011.
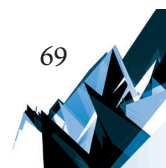
[61] *The Pritzker Architecture Prize*, 2001, www.pritzkerprize.com/laureates/2001 (access: 18.05.2018)

[62] Ventur, R., *Complexity and Contradiction in Architecture*, New York 1966.

[63] Wejchert K., *Elementy kompozycji urbanistycznej*, Warszawa 1971.

[64] Węcławowicz-Bilska E., *Kierunki współczesnego rozwoju przestrzennego miast europejskich*, Czasopismo Techniczne, 3-A/2011, 147–172.

[65] Węcławowicz-Gyurkovich, E., *Czy najnowsza architektura może upiększyć miasto?*, [in:] *Odnowa krajobrazu miejskiego: uroda miasta*, Wydział Architektury Politechniki Śląskiej i Komitet Architektury i Urbanistyki PAN, Gliwice 2009.

[66] Woodehouse L., *Architecture Since 1945*, Kinko's, Knoxville 1992.

[67] Ahmed Y.M., *Allianz Arena – Football Stadium | Herzog & de Meuron* [in:] arch20, https://www.arch2o.com/allianz-arena-football-stadium-herzog-de-meuron/

[68] Zuziak Z.K., *Od architektury do urbanistyki i od urbanistyki do architektury*, [in:] *Definiowanie przestrzeni architektonicznej. Architektura dziś*, vol. 1, Wydawnictwo Politechniki Krakowskiej, Kraków 2010.

[69] Materiały konferencyjne „Definiowanie przestrzeni architektonicznej", *Co z tym pięknem architektury współczesnej*, ed. M. Misiągiewicz, D. Kozłowski, Kraków 2007.

[70] *TSA CardinalsMultipurpose Facility, Glendale, Arizona* [in:] AREA, Arene, iss. 75, Firenze 2004.

[71] *Framepool RightSmith Company*, http://footage.framepool.com/es/shot/965080678-herzog-&-de-meuron-aparcar-allianz-arena-construccion-de-edificios (access: 16.01.2014).

Elżbieta Węcławowicz-Bilska ![orcid](orcid.org/0000-0002-3537-7348)
eweclawowicz-bilska@pk.edu.pl
    Faculty of Architecture, Cracow Uniwersity of Technology

Martin Vaščak
archmva@gmail.com
Ing. architect, authorized architect of Slovakia Chamber of Architects

Contemporary transformation of traditional Polish health resorts against the background of changes observed in balneological centers around the world

Współczesne przekształcenia tradycyjnych uzdrowisk polskich na tle zmian obserwowanych w ośrodkach balneologicznych na świecie

Abstract

The dynamic development of health resorts is cause for the comparison of the tendencies in the changes observed in terms of the development and arrangement of the space in therapeutic complexes and their adjacent localities. Studies demonstrated differences both in the programme of these complexes, as well as in their formal solutions.There are the result of civilizational differences, conditions of the natural environment or of the state of affluence of citizens. there can constitute an inspiration for the development of Polish layouts of spa, In conditions of competitive development, the increase in the wealth of society and the care for health and good physical fitness, the fully justified are improvment of standards quality of public spaces and increasing the amount of green areas.

Keywords: health resorts, spatial development, urban planning

Streszczenie

Dynamiczny rozwój uzdrowisk jest przyczyną porównania tendencji zmian obserwowanych pod względem rozwoju i aranżacji przestrzeni w kompleksach terapeutycznych i przyległych miejscowościach. Badania wykazały różnice zarówno w programie tych kompleksów, jak i w ich formalnych rozwiązaniach. Są one wynikiem różnic cywilizacyjnych, warunków środowiska naturalnego lub stanu zamożności obywateli. Może to stanowić inspirację dla rozwoju polskich układów uzdrowiskowych. W warunkach konkurencyjnego rozwoju, wzrostu zamożności społeczeństwa oraz dbałości o zdrowie i dobrą kondycję fizyczną w pełni uzasadnione są poprawa standardów jakości przestrzeni publicznych i zwiększenie ilość terenów zielonych.

Słowa kluczowe: uzdrowiska, zagospodarowanie przestrzenne, urbanistyka

1. Introduction

The sudden increase in the amount of health, rehabilitation, spa, wellness and other types of resorts associated with the improvement of man's physical and psychological fitness that has been observed since the 1990's around the world is based on varied spatial layouts – including traditional, restored and completely new ones, erected in various locations. At around the same period Poland saw the beginning of changes to its economic system and ongoing changes to the principles of the functioning of balneological therapeutic centres. The goal of the article is the comparison of efforts that are being undertaken around the world towards the improvement of the attractiveness of these types of centres, the localities tied with them, their competitive development and urban planning tools that are used in the achievement of this development, with Polish examples. The article demonstrates differences in tendencies in the development and arrangement of main public and urban spaces between balneological therapeutic centres in our country in relation to health resort layouts in other parts of the world. The article also notes the standards of the organisation of these spaces in both groups of examples that were compared. Conclusions can be useful in the planning and spatial development of health resort localities in Poland.

2. The essence of a health resort

When discussing spatial changes that have been observed in recent years in health resorts, it would be appropriate to remind ourselves what health resorts are and what the goal of their establishment has been. Even though the first of these types of centres were established in ancient times[1], the overarching principle of their founding has always been the need to cure various illnesses with the use of natural materials. Such was the case in some centres that operated in ancient times, such as Asclepeion[2] on the Greek island of Kos or Epidaurus, located in the eastern part of the Peloponnese. Therapies were being provided in therapeutic centres arranged specifically for this purpose. Health resort complexes were often placed on several terraces and were made up of a number of buildings, such as, for instance, a temple or medical schools, complexes of sports pitches and stadiums, as well as areas of greenery like flowery meadows combined with places of residence, like in the aforementioned complex on the island of Kos.

During subsequent periods a clearer increase in the precision of the shape of the space of health resorts took place, while divisions and classifications were introduced as well, however, the main idea behind the establishment of these types of complexes remained unchanged – the providing of conditions for conducting therapy through the use of natural curative

---

[1] Numerous treatment centres were established in ancient times that are today described as health resorts. Particularly many were established in areas occupied by Rome, both on the Apennine Peninsula, as well as in the entire area of Europe, Asia Minor and North Africa. Many of them fell to ruin after the fall of the Roman Empire.

[2] Asclepeion was a name used for Greek sanctuaries of the god Asclepius, who focused on curing people. These types of complexes were built near thermal or mineral water springs, as well as in places with a special climate.

Fig. 1. View of the medicinal establishment's terraces in Aesklepeion (photo by M. Vaščak 2017)

materials in rather attractive spaces. This is because patients, as a rule, should reside in a healthy environment, spending a lot of time in an open space filled with attractively arranged areas of greenery. This is why today places where the use of various natural curative factors – mineral, climatic, natural and aesthetic ones – is possible are considered the basis for the operation of these types of centres. Therapies are conducted in conditions of high comfort, ensured both by highly effective technical machinery used to obtain the curative elements, as well as to secure the natural environment from destruction, and high-quality open spaces and structures. This is why health resorts are currently considered places of balance between natural and cultural factors.

3. Contemporary directions of the development of health resorts

The intensive development of curative complexes using natural materials has currently been observed around the world since the two final decades of the twentieth century. A number of general directions of the transformation of historical and traditional centres and the establishment of new complexes can be distinguished in these efforts, such as:

- ▸ the restoration and regeneration of historical complexes,
- ▸ the competitive development of health resorts associated with the globalisation of the phenomenon,
- ▸ the construction of unique, avant-garde complexes designed by outstanding designers,
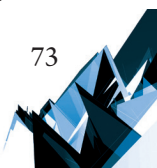
- ▸ the establishment of health resort therapeutic centres in natural surroundings,
- ▸ the establishment of multi-functional centres combining health resorts, tourist and holiday destinations [see: 10, p. 112].

The article presents the main tendencies that are being applied in all sorts of variants. However, the most essential is the fact that in the aforementioned period a clear return to *spending time at the baths* has taken place, although it currently has a different dimension than it had during the period of the *belle* époque. Another phenomenon that is being observed is the globalisation[3] in both the establishment of centres of balneological treatment and various complexes meant for relaxation, rehabilitation and herbal medicinal treatment around the world.

4. The restoration and regeneration of historical complexes

It is based on the restoration of historical and traditional health resorts and their modernisation, reconstruction and urban regeneration in numerous European countries[4]. The end of the twentieth century, perhaps on the wave of ecological interests, was a period of a return to natural treatment methods, including balneotherapy, hence interest in health resorts and their one or two-hundred-years' worth of history and their past. During this time there has not only been a large number of books published on the occasion of round anniversaries of the founding of these structures, but efforts were being made concerning the conservation and renovation of historical structures and complexes within health resorts, such as, for instance, the meticulous renovation of the water drinking space, casino and imperial baths in Baden-Baden, Gellert's Hotel[5] and the Szechenyi baths in Budapest[6] or the systematically performed renovation and partial reconstruction of the Czech health resort Františkovy Làznĕ[7], which was severely neglected during the period of socialism, and has been carried out since the 1990's, as well as the restoration of numerous buildings in the health resorts of the former GDR that has been ongoing in the twenty-first century, such as the Baltic baths at Bad Heringsdorf, Bad Albeck and others. The most interesting efforts covering not only the health resort centre itself, but the entire city of Vichy and its

---

[3] Health resorts and particularly spas (centres in which the main therapeutic factor is water) have been established in Europe for centuries and the set of behaviours associated with spa therapies, as well as the principles of the design of such centres were developed here.

[4] For instance, such efforts were conducted in the 1970's and the 1980's in France, as well as in the 1980's in Styria, Austria, where several new centres of spa-treatment were established as a result of drilling in search of thermal springs, fully taking the principles of competitive development into consideration. In Campania, Italy, in turn, a project from the start of the twenty-first century, funded by the Regional Operational Programme, featured the regeneration of ancient health resorts located in the vicinity of the Bay of Naples, such as Oplontis, Pozzuolli, Stabie and others.

[5] The building was thoroughly cleaned and the entire complex on Gellert's Hill was restored in accordance with the original plans by A. Sebastyen, A. Hegedus and I. Stark from 1911, including the modernist changes from the 1930's.

[6] In this case prof. G. Czigler's original design was faithfully restored.

[7] The southern lands of Germany financially participated in the renovation of the health resort from the start.
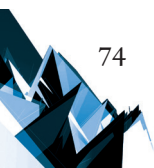
agglomeration have been made with varying intensity since the 1960's[8]. In recent years the redevelopment has been based on strong economic foundations due to the extension of the Ladry university and technology pole located in the immediate vicinity of the baths park. The income the city receives from innovative operations constitutes the basis for its renewal and redevelopment[9]. In many health resorts, due to the improvement of the quality of therapy conditions, historical complexes are being adapted to other functions and therapy is being administered in newer and more comfortable facilities.

5. Competitive development of health resorts associated with the globalisation of the phenomenon

The globalisation of the phenomenon of the development of baths, thermal baths and therapeutic complexes is primarily based on the fact that complexes used for such therapies, rehabilitation and the improvement of the physical and psychological fitness of man have started appearing in many areas of the world in which such activity has never been performed, such as work associated with the establishment of health resorts in the 1970's in Juzan and Al-Lith near the Red Sea in Saudi Arabia, as well as in the mountainous and highland areas of Iraq, in addition to Algeria, Venezuela and Ecuador. They were also associated with the results of geological[10] studies conducted in the search of energy resources, as well as due to civilisational changes resulting in the increase of the amount of free time, the promotion of youthful fitness, the mass character of recreation and the widespread care for one's appearance.

One interesting example of marketing activities in the competitive development of health resorts was the French project Chaine Thermale du Soleil Compagne, undertaken at the turn of the 1970's and the 1980's, which featured the promotion of systemic solutions supporting economically weaker health resorts through having some of them form a sort of consortium. Economic efforts in these complexes were based on encouraging patients to undergo therapies

---

8   It was then, during the term of mayor P. Coulon, during the turn of the 1960's and the 1970's, after the abandonment of the health resort by patients from Maghreb, that holiday-making functions were developed. After the damming of the Alier River and building the Park du Lac bathing facility, the Agglomeration Vichyssoise was established in the Alier River Valley, building a complex of open-air pools, a hippodrome and the Complex Omnisport sports and recreation centre in the localities placed on the bank of the river opposite the health resort.

9   Efforts conducted in the years 1989–2010 by mayor C. Malhuert caused, among others, the expansion of the Lardy University Technological Pole, the construction of a promenade in the centre of the city, the arrangement and reintroduction of Rue de Paris, which connects the train station with the health resort complex, to pedestrian traffic, the reconstruction and renovation of therapeutic facilities and the balneotherapy centre, as well as a reconstruction of the congress centre with the use of the existing historical buildings of the Casino and Opera.

10 From: A. Issadi, *Presentation de la carte des eaux thermominerales de l'Algerie*; M. Taher Hussein, A.G. BAzuhair, M. Hanza, *Thermal springs in Jizan and Al.-Lith Areas, Saudi Arabia*; M.Fricke, *Curative and Natural Water Potential of Iraq*; E. Eguireune, *News from Argentina*; M.A. Puente, *News from Ecuador*, [in:] [5]; and F. Urbani, *Geothermal News from Venezuela* [in:] [6].

only at associated health resorts[11], as well as the gradual introduction of non-invasive industry utilising natural curative materials into the vicinity of health resort towns. In Austria, in turn, local traditions were employed in the development of health resorts, such as the story of the love between Sissi and the young emperor Franz Joseph in Bad Ischl, while Baden used references to nineteenth-century meetings between monarchs, politicians and aristocrats, with Salzburg, which lives on Mozart's music, organising theatrical and musical workshops, while spectacles can be watched at every square of the city.

Supported by European funds and government subsidies in the 1980's, the renovation and modernisation of small private historical health resorts in Spanish Galicia led to several tens of complexes resuming their operations. In Austrian Styria, in turn, due to drilling in search of hot springs, a number of new therapeutic health resorts have been opened while fully taking into consideration the principles of competitive development, as in, for instance, the Rogner Bad Blumau complex which is a completed version of the fairy-tale design by Friedensreich Hundertwasser, Bad Waltersdorf – a cameral therapeutic facility located amidst a complex of greenery, Bad Radkersburg – which has been built in the form of an enormous, compact complex of buildings and therapeutic and recreational facilities, Erlebnis Therme – is a complex of open and partially covered thermal pools beautifully blended into the steep slope of a hill, while Loipersdorf has been arranged as a thermal bathing complex enclosed in a single structure.

In Italy in Campania, as a part of a project financed by the Regional Operations Programme, which has been carried out already at the start of the twenty-first century, the urban regeneration of ancient health resorts located in the vicinity of the Bay of Naples has been planned, such as Pozzuoli, Oplontis, Stabie and others.

6. The construction of unique, avant-garde complexes designed by outstanding authors

As a result of the mass development of health resort centres around the entire world, their developers often commission the best designers to develop the individual therapeutic or hotel buildings or even entire layouts in order to improve the attractiveness of the site. Thus, extraordinarily interesting structures designed by outstanding artists have started to appear in many centres of balneological treatment.

A number of structures designed by famous authors have been built in Swiss health resorts in recent years. The most often presented one is the purist thermal facility in the small health resort of Valz, with an austere purist form and flat stone facades. The large complex of the Tschuggen Berg Oase Spa Centre in Arosie[12] was designed at a height of almost 2000 metres

---

[11] An almost three-fold increase in the number of patients in associated health resorts was observed in relation to other health resorts in the region as a result of these efforts. The experiences of this project were employed in the establishment of new health resorts in Tunisia, Algeria, Morocco, Spain, as well as in the Americas [3].

[12] The design from 2003, built in 2006 with a cubature of 27,000 m³, is composed of a three-storey natural treatment service building and hotel buildings.

Fig. 2. Tschuggen Berg Oase w Arosie. project by. Mario Botta (Photo by: Pino Musi, source: [12])

above sea level by Mario Botta. The element that defines its visual expression is a set of around a dozen semi-circular, tall and illusory skylights, whose glazed facades refer to the branches of trees in a dramatic rocky landscape through the outline of their muntins.

The largest singular health resort complex in Europe in the last 30 years was built in the small town of Bad Blumau in Styria, designed entirely by Friedensreich Hundertwassr, in the artist's distinct manner featuring colourful, irregular forms and green roofs as if taken from a dream about the gardens of paradise. A single hotel building by him has also been built there, occupying an urban block in the health resort of Bad Soden near Frankfurt, as a new, attractive element of the public space of the city.

Jean Nouvel also built a number of hotel buildings in health resorts, such as the environmentally friendly Pleide building and Odyssée Residences in Nice in 2015 or the Life Marina on Ibiza from the years 2005–2011. He is the laureate in the competition for the new Espace Santé et Baeaute bathhouse in the historical health resort of Vichy[13], as well as the natural therapy facility Hotel Les Thermes built in the middle of the 1990's, located in the centre of the therapeutic complex in the vicinity of the Adour River in the small health resort town of Dax in Aquitaine.

---

[13]   Design from 1988, unbuilt but placed in accordance with the competition guidelines in the baths park, featured a balneotherapy centre, a beauty institute, public swimming pools, gyms, as well as a four-star hotel with 180 rooms, restaurants and conference halls.

7. The establishment of therapeutic health resort centres in natural surroundings

Many places around the world have seen the development of therapy centres in areas that are extraordinarily attractive because of their nature, and even in extreme areas, such as the Blue Lagoon baths complex in Grindavik, Iceland[14], located inside a volcanic crater, naturally flooded with water of an extraordinary blue colour, or in national parks, like the Turkish Pamukkale, where natural terraces created from limestone sediment on the slope of Cökelez mountain were used to provide free baths. A similar centre is located in the Italian town of Saturnia. Close to the renowned Saturnia Terme health resort there are two waterfalls that have been made available to tourists and which feature sulphur-rich water: Cascate del Mulino and Cascate del Gorello. The natural stone pools of the terraced cascades are used for open-air bathing. The Termas Geométricas Hot Springs Complex, located in a narrow gorge in the Villarica national park in Chile[15], with its clearly outlined orange timber bridges, built in a traditional manner without the use of nails, separates the curative space from the rich greenery that grows here in the vicinity of its hot springs.

Fig. 3. Termas Geométricas Hot Springs Complex project by. German del Sol (Photo by Guy Wenborn, source: [13])

---

[14]   The complex was designed by VA Arjitektar Reykjavik in 1999.
[15]   The complex, built in 2009 in accordance with a design by Germàna del Sol at an elevation of almost 2 000 metres above sea level, between the localities of Coñaripe and Pucón.

8. Polish health resorts

Polish spas were largely established and formed in the nineteenth century[16]. The period of the Second Republic saw, among other things, the mandatory obligation to rest, which led in an extraordinary manner to the development of tourism, holiday destinations and health resorts. All of them became nationalised after the Second World War. The largest and most renowned ones in particular were expanded during the period of socialism both through the placement of large sanatoriums or holiday homes and complexes of multi and single-family residential buildings, which led to the urbanisation of these centres. In addition, small renovation works were performed on some guesthouses, converting them to community apartments. Many health resorts became the seats of communities and even *powiats* (equivalent to a county – transl. note)[17], while some became administratively incorporated into neighbouring large cities. Some of the centres did not obtain the status of a health resort and, as a result, their development became based on other functions[18].

After independence was regained, a discussion was initiated on the subject of new precepts of the organisation of health-resort-based therapeutics and spatial regulations concerning their shape and organisation. It was only the new health resorts act[19], approved twenty five years later, that regulated these matters.

Various efforts aimed at increasing the effectiveness of the operations of P. P. Uzdrowiska Polskie, which governed all centres of balneotherapy, had been made already prior to the act entering into force. The process of their privatisation took place in several stages. It was initially associated with a conversion into state-owned companies, followed by the return of property to some inheritors, as well as, primarily in the years 2008–2015, their sale. Certain reparatory efforts concerning the quality of the public and historical space of health resorts were made earlier, already in the 1970's and the 1980's. The first efforts after the regaining of independence were based on improving the conditions of lodgings for patients, which was based on the remodelling of socialist sanatoriums and improving their standards. In the years that followed, already in the twenty-first century, efforts in traditional and historical health resorts and their neighbouring localities concerned the following changes:
- ▶ the renovation and modernisation of the cultural heritage of health resorts,
- ▶ the progressive urbanisation of health resorts,
- ▶ new projects after the privatisation or communalisation of health resorts,
- ▶ the commercialisation of the space of a health resort or its neighbourhood.

[16] Spa-therapy was conducted earlier in only a few of them, for instance, in Swoszowice, Iwonicz, Szkło [9].

[17] At present, from among forty six statutory health resorts only eleven do not feature community offices (Czerniawa-Zdrój, Dąbki, Długopole-Zdrój, Przerzeczyn, Wapienne, Wieniec Zdrój, Wysowa and Żegiestów, while Swoszowice and Cieplice Śląskie-Zdrój were administratively incorporated into Krakow and Jelenia Góra, respectively, during the period of the People's Republic of Poland.

[18] After the Second World War twenty four localities were not granted the status of a health resort despite the fact of possessing it during the period of the Second Republic, in addition to being public use facilities or despite being considered health resorts whilst in German borders or providing balneotherapy in already existing spa facilities, although not all of them exhausted their natural curative resources.

[19] Act concerning spa-therapy, health resorts and areas of health resort protection and health resort communities of 28.07.2005.

The renewal and modernisation of the cultural heritage of health resorts began already towards the end of the 1970's, as a result of placing nineteenth-century structures under conservation. In the majority of Polish health resorts, particularly Carpathian ones, timber structures, whose lifecycle is limited by the qualities of the material itself, are dominant. The model example here was the reconstruction of the burned-down mineral water drinking facilities in Szczawno Zdrój and of the Witoldówka guesthouse in Krynica, whose structure was built out of durable materials, but the external timber cladding of the facades constituted a faithful copy of the originals. Szwajcarka in Krakow's Swoszowice was renovated in a similar manner, however the discussion on the subject of conservation doctrine concerning the principles of the conservation of the timber architecture of health resorts is still ongoing[20]. Meanwhile in many privatised health resorts or spa centres which function in former masonry spa therapeutics centres, the modernisations and renovations performed there have restored buildings such as Zakład Mateczny in Krakow to their glory, with similar examples to be found in Busko-Zdrój, Iwonicz-Zdrój, Krynica, Ciechocinek and other health resorts. At the same time the process of the renovation and refurbishment in many cases also applied to historical timber and masonry guesthouse buildings, such as the structures at Jana Wiktora Street in Szczawnica and in Krynica along Kościuszki Street. Efforts aimed at the reconstruction of lost historical buildings have also found themselves to be a part of the tendency of caring for the historical space of health resorts, with such measures being taken in Wysowa through the reconstruction of an old mineral water drinking facility that had been destroyed by a fire or in Szczawnica, where the inheritors of the Stadnicki family restored the building of Dworzec Gościnny in the second decade of the twenty-first century.

The progressive urbanisation and commercialisation of health resorts, as it has already been mentioned, began in the 1960's. It was based on the construction of so-called Workers' Estates for the employees of health resorts. These complexes of multi-family residential buildings that were at least five-storeys-high and featured forms typical of inner cities were located on sunny slopes, in the vicinity of therapeutics centres, which now causes them to dominate in the panoramas of these localities, like in, for instance, Krynica, Piwniczna, Rabka, Iwonicz Zdrój and others. The construction of company-owned holiday homes, also featuring forms that did not refer to those already existing in health resorts, started to be built a little later, particularly in reputable centres. Numerous such buildings were built in Krynica, for instance: Hajduczek, Leśnik, Silesia; in Szczawnica they were Hutnik, Górink, Chemik, or in Ciechocinek, e.g. Frezja. After a wave of criticism, particularly in health resorts in mountainous areas, attempts were made to refer to rock-based forms, which, coupled with poor quality workmanship, resulted in massings that were too heavy and unattractive, like, for instance, those of the Połoniny and Nauczycielskie sanatoriums in Szczawnica, although successful attempts did appear, such as the Budowlani sanatorium in Krynica. In recent years reputable health resorts have been seeing further urbanisation through the construction of various complexes of apartment buildings and further residential developments, most often

---

[20]   An example of this is the discussion concerning the restoration of timber villas and guesthouses along Lipowa Avenue in Nałęczów.

including single-family buildings, typically in an organised form. The commercialisation of health resorts pertained not only to changes in the accessibility of Patients to treatment and housing, but also to an increase in the economic activity of private entities, particularly concerning services. In addition, in the pursuit of finding employment for residents and increasing profits, many health resorts have started to dynamically grow their mineral water bottling industries[21]. After the privatisation of health resorts, particularly those reclaimed by inheritors of their former owners, **new development projects** have appeared in numerous health resorts. In many cases these were construction projects featuring buildings, line in, for instance, Solec-Zdrój, where new owners, after making the Malinowy spring available, erected two new therapy centres, that make use of its waters, on both sides of the baths park. Unfortunately, these buildings were not incorporated into the original complex in terms of composition.

In Wysowa, in turn, a new indoor swimming pool facility was built recently in the baths park, in the vicinity of the rebuilt mineral water drinking building. The most dynamic reconstruction and redevelopment took place in Szczawnica, where the new owners,

Fig 4. Fragment of the spa park in Muszyna (Photo by E. Węcławowicz-Bilska, 2010)

---

[21] It appears that the community of Muszyna appears to be in the lead in this regard, in which there are several large new mineral water bottling plants, in: Złockie, in Milik, two in Muszyna and an additional one in Powroźnik.

employing French architects, systematically and attractively redeveloped the individual areas of the health resort. These efforts have restored Szczawnica's charm and brought it on par with the standards of a European resort[22].

Significant development-related changes have also affected Żegiestów, where the new owner restored the former Prometeusz, Warszawianka, Wiktor as well as other sanatoriums, in addition to new guesthouses also being built in the northern part of the health resort. However, it appears that projects associated with the establishment and attractive development of arranged green spaces are the most valuable to health resorts, as the situation in Inowrocław and Busko-Zdrój has demonstrated.

Currently such work is being consistently performed in Muszyna in the Zapopradzie region, where a very large complex of greenery featuring a sports-related, recreational and cultural function, in addition to a baths park with an area of around a dozen hectares, has been built. Work is currently being performed on the arrangement of a science park in Zapopradzie as well.

Fig. 5, 6. The rally of old Polish cars on the promenade in Krynica on May 12
(Photo by E. Węcławowicz-Bilska, 2018)

The commercialisation of the space of health resorts and their vicinity is based not only on the fact that the very process of therapy and residing in a health resort itself is being commercialised, which manifests itself in a clear increase in various types of services and, as a result, in ever-present advertisements appearing in various places around health resorts.

The commercialisation of space pertains primarily the use of the most attractive public spaces of health resorts, including therapeutic spaces, such as promenades in the immediate vicinity of natural therapy centres, baths and mineral water drinking facilities, to organise various types of international meetings and congresses, such as the most prestigious Economic Forum in Krynica, mass events like old-timer car shows on the walking promenade in Krynica[23] and others.

---

[22] These projects have come to a halt in recent years. the modernist natural treatment facility designed by Andrzej Gliszczyński has so far not been dismantled and a new structure referring to the traditional architecture of the Pieniny Mountains has not been built. There are voices in the conservation community concerning the necessity to protect modernist architecture.

[23] Cars drive to the place of the show using pedestrian alleys and are parked right near carefully cultivated flower beds along the Old Spa House.

It also often manifests itself in the arrangement of temporary structures, such as beer drinking or gastronomic establishments, in which meals are being prepared using outdoor grills. Crowds of onlookers gather in therapeutic spaces, which is often accompanied by chaos, optic agitation, the pollution of space with noise, smells and in the case of old-timer car conventions – engine exhaust. Temporary installations placed for marketing purposes featuring a poor aesthetic are placed randomly and do not improve the appearance of the most representative spaces of the localities.

Fig. 7. Kudowa-Zdrój advertising along the main street leading to the spa center
(Photo by E. Węcławowicz-Bilska, 2018)

Numerous Polish health resorts are situated in the immediate vicinity of the state border, both in mountainous and lowland areas[24]. On the one hand this provides the possibility of shaping attractive walking and cycling trails to neighbouring localities, as it has taken place in, among others, Szczawnica, while on the other the proximity of vehicular and rail transit routes constitutes a source of inconvenience.

Furthermore, numerous commercial companies and warehouses locate their facilities close to the border, often in special economic zones, with constantly increasing indoor and

---

[24]   Here we can mention: Gołdap, Kudowa, Lądek-Zdrój, Muszyna, Piwniczna, Supraśl, Szczawnica, Świnoujście, Żegiestów and others.

outdoor storage spaces negatively affecting the immediate surroundings of health resorts. The impact of these areas on protected sites – such as health resorts – through both vehicular traffic and ostentatious advertisement and marketing activity can be clearly observed.

9. Conclusion and summary

In the past dozen years or so a clear increase in development activity has taken place in Poland, including in the country's health resorts. However, observations have shown that in each health resort the process and strategy of development is shaped independently, which leads to a situation in which similar or identical services including sports, recreation and their associated spatial solutions appear in several centres[25]. Due to the various phases and types of privatisation and reprivatisation of health resorts in Poland, the degree of their redevelopment is also varied.

So far efforts associated with the establishment of consortiums of several therapeutic centres offering similar therapeutic profiles have not been undertaken. Large projects aimed at the activation of health-resort based therapeutics, holiday-making and tourism within a broader region, such as, for instance the Poprad River Valley or in the Kłodzko Valley, where complexes of health resorts are present, or in other ones, have not been implemented.

In Polish health resorts there is a lack of modern structures and larger natural therapy complexes designed by outstanding authors. During the interwar period many avant-garde structures were erected according to designs by, for instance, Adolf Szyszko-Bohusz[26], Bohdan Pniewski[27] or, particularly in Carpathian centres, by the professors of the Lviv University of Technology[28], which constitute significant structures in these complexes to this day.

It appears that traditional and historical balneotherapy centres, despite changes that have been described above, still constitute interesting complexes that can be used to provide therapy using natural curative substances.

References

[1] Dryglas D., Golba J., *Determinanty funkcjonowania i rozwoju uzdrowisk w Europie. Studium przypadku Polska*, PWN, Warszawa 2017.
[2] Kita J., *Zapomniane polskie uzdrowiska*, Księży Młyn, Łódź 2016.

---

[25] For instance downhill skiing slopes and bicycle trails in health resorts in mountainous areas or highlands.
[26] Here we can mention the establishment of the natural therapy facility in Zegiestów-Zdrój, the military sanatoriums in Busko Zdrój and Krynica and others.
[27] The Jan Kiepura "Patria" Guesthouse in Krynica
[28] E.g. in Krynica the design of the New Mineral Baths by Władysław Klimczak, the design of the New Spa Building by Witold Minkiewicz or the Wiktor sanatorium by Jan Bagieński and Zbigniew Wardzała in Żegiestów.

[3] *Le Courire de la Chaine Thermale di Soleil Compagne.* Française du Thermalisme, Paris-Lille 1984, 1985, 1990, 1996.

[4] *Recreational use of geotermal water in Visegrád Grroup coutries,* edited by M. Dej, M. Huculak, W. Jarczewski, Kraków 2013.

[5] SITH „Publicationes News Actualités", No. 3., Septembre 1994

[6] SITH „Publicationes News Actualités", No. 4, Decembre 1995.

[7] *Spa design,* Daab Cologne, London, New York 2006,

[8] Wdowiarz-Bilska M., *Spa resorts in the age of knowledge based economy,* Technical Transactions, 4-A/2014.

[9] Węcławowicz-Bilska E., *Historyczne założenia zdrojowisk w kształtowaniu współczesnych ośrodków balneologicznych w Polsce,* Kraków 1990.

[10] Węcławowicz-Bilska E., *Uzdrowiska Polskie. Zagadnienia programowo przestrzenne,* Kraków 2008,

[11] Wójcikowski W., *Obszary strategicznej interwencji w regionie uzdrowisk popradzkich, Strategic areas of intervention in the Poprad spa resort,* Czasopismo Techniczne, 1-A/2011.

[12] https://www.archiportale.com/news/2007/08 (online: 3.09.2018).

[13] http://www.germandelsol.cl (online: 3.09.2018).
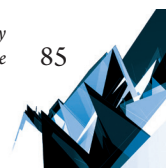
Kazimierz Furtak
kfurtak@pk.edu.pl
Faculty of Civil Engineering, Cracow University of Technology

The effect of changing loads on the deflection of RC beams reinforced with ribbed bars

Wpływ obciążeń zmiennych na ugięcia belek żelbetowych zbrojonych prętami żebrowanymi

Abstract

The paper presents a way of taking account of the effect of changing loads on the deflection of RC beams reinforced with ribbed bars. The proposed solutions were verified experimentally, based on the results of tests performed by the author. The beams were subjected to multiple repeatable loads. The deflection increment dependent on the value of the basic parameters characterising the changing loads (cycle maximum load M_{max}, stress ratio R, number of load cycles N_i). The increment of the deflection of RC beams reinforced with ribbed bars subjected to changing loads increases with increases in the number of load cycles N_i ($\log N_i$, to be more accurate), and is greater for higher values of ratio κ and lower values of ratio R ($\kappa = M_{max}/M_n$; $R = M_{min}/M_{max}$; M_{min} – minimal moment of cycle; M_{max} – maximal moment of cycle; M_n – failure moment under short-term loads). The relations for the number of load cycles N_i are similar.

Keywords: changing loads, deflection of beams, ribbed bars, RC beams

Streszczenie

W pracy podano sposób uwzględniania wpływu obciążeń zmiennych na przyrost ugięć belek żelbetowych zbrojonych prętami żebrowanymi. Podane rozwiązana poddano weryfikacji doświadczalnej. Wykorzystano przy tym wyniki własnych badań doświadczalnych Badane belki były poddane obciążeniom wielokrotnie powtarzalnym Przyrost ugięć uzależniono od wartości podstawowych parametrów charakteryzujących obciążenia zmienne (wartość obciążenia maksymalnego cyklu M_{max}, współczynnik asymetrii cyklu R, liczba cykli obciążenia N_i). Przyrost ugięć belek żelbetowych zbrojonych prętami żebrowanymi poddanych obciążeniom zmiennym wzrasta wraz ze wzrostem liczby cykli obciążenia N_i (a ściślej $\log N_i$) i jest większy dla większych wartości współczynnika κ oraz dla mniejszych wartości współczynnika R ($\kappa = M_{max}/M_n$; $R = M_{min}/M_{max}$; M_{min} – moment minimalny cyklu, M_{max} – moment maksymalny cyklu, M_n – moment niszczący przy obciążeniach doraźnych). Podobne są zależności dla danej liczby obciążeń N_i.

Słowa kluczowe: obciążenia zmienne, ugięcia belek, pręty żebrowane, belki żelbetowe

1. Introduction

Reinforced beams have been investigated by researchers of reinforced concrete ever since this type of structure came into use. Both standard recommendations and the literature on the subject, however, have dealt primarily with short-term loads (immediate) or – much less frequently – long-term loads (now called quasi-long-term) [6, 7, 9–12]. The research works that cover the effect of changing loads on reinforced beam deflections are exceptionally rare. This results not only from both the economic and time-related costs of tests, but mainly from the fact that the number of structures subjected to repeated changing loads which may affect the deflections of the elements in question is rather limited.

Changes to the deflection of reinforced concrete beams under changing loads are caused by several factors including:

- the formation and propagation of microcracks in the zone under tension between the cracks,
- the widening of cracks due to larger sections of loss of concrete-rebar bond (particularly in the zone of predominant action of bending moment, and – to a much lower extent – to shearing forces) [1, 2, 4, 5],
- a lower value of concrete modulus of elasticity under the loads in question (3). The extent of the second of the aforementioned factors depends on the type of reinforcing bars (plain, ribbed).

This paper presents a method of taking into account the effect of changing loads on the deflection of RC beams reinforced with ribbed bars. The proposed solutions were verified experimentally, based on the results of tests performed by the author. The beams were subjected to multiple repeatable loads. The deflection increment was dependent on the value of the basic parameters characterising changing loads (cycle maximum load, stress ratio, the number of load cycles). Beam deflections were not the primary purpose of the experiments described in [3]. Nevertheless, on their basis, certain conclusions can be drawn and the formula covering the effect of parameters and the number N ($\log N$) i.e. the number of load cycles on RC beams deflection can be verified.

2. Experimental section

2.1. Test specimens

The tests were performed on seventeen reinforced concrete beams of dimensions and reinforcement as shown in Fig. 1. Each beam was 15 cm wide. In one group of beams (Fig. 1a) in the zone of action of bending moment of a constant value from the programme load the omission of stirrups is intentional to avoid introducing inclusions that would change the beam cracking image [3]. In the other groups of beams, stirrups and top longitudinal bars were applied along the entire length of the beams (Figs. 1b & 1c).

In the article, the results of tests performed on beams reinforced with ribbed bars made from 18G2 steel are presented (the tests were done when the given denotation of steel was valid). All the beams were reinforced with bars with a diameter of 16 mm ($\mu = 1.48\%$). In each series, the beams were cured in natural conditions (the production plant and the laboratory: temperature $t = 18\pm3°C$; air relative humidity RH = $60\pm10\%$).

The beams were made from concrete with a mean compressive strength 'f_{cm}' and tensile strength (splitting tests) 'f_{ctm}' of: f_{cm} = 27.96 MPa, f_{ctm} = 2.78 Mpa. The standard deviation values were s_{cm} = 1.09 MPa, s_{ctm} = 0.12. Young's modulus of elasticity of the concrete was on average 28.09 GPa. The mean tensile strength of the steel was 529.23 Mpa, the yield point was 390.43 MPa.

The test period for each beam was up to four days and this is why concrete shrinkage and creep were not included. With such a short test time, the effect of these rheological factors is negligibly small and was disregarded in the analysis.
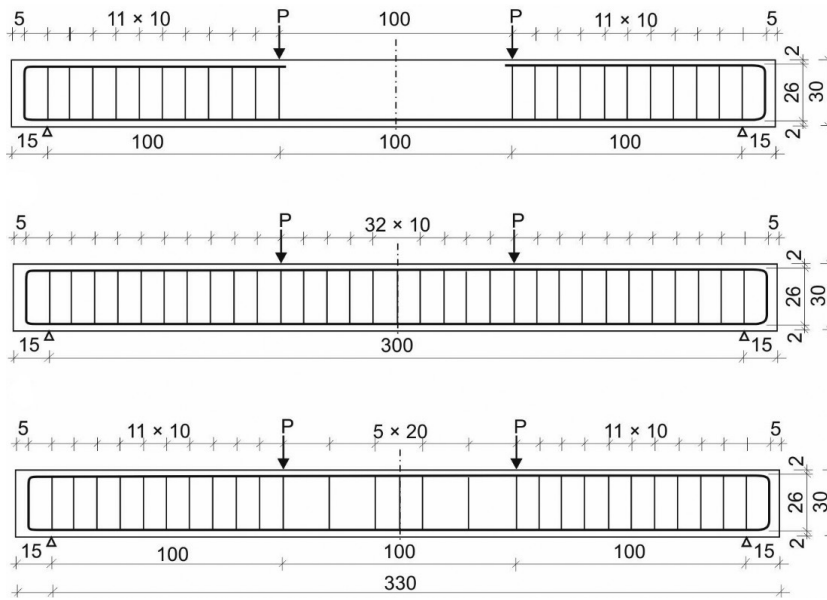
Fig. 1. Dimensions [cm] and beam reinforcement method: a – with no stirrups in the middle zone; b – with stirrups at larger spacing in the middle zone; c – with stirrups at constant spacing along the entire length of beam

2.2. Program and test description

The beams were subjected to multiple repeatable loads: two concentrated loads applied on one third of the beam span. The ZD-40 PU testing machine was used. The loading variation frequency was constant at 6.67 Hz.

The loading cycle parameters adopted were:

▸ ratio κ of maximum bending moment in cycle (M_{max}) to failure moment (M_n); $\kappa = M_{max}/M_n$

- stress ratio R, equal to minimum moment (M_{min}) to maximum moment (M_{max}) ratio; $R = M_{min}/M_{max}$
- The values of bending moments M_{min}, M_{max}, M_n correspond to loads: minimum P_{min}, maximum P_{max} and failure load P_n.

The values of ratio $\kappa = M_{max}/M_n$ were adopted as 0.45 and 0.60. The stress ratio $R = M_{min}/M_{max}$ was: 0.15; 0.30; 0.60. The values of failure moments M_n for particular types of beams were determined experimentally by static tests performed on identical specimens (identical reinforcement, identical concrete mix).

The deflections were measured at the midpoint of the beam spans (and in support sections for verification) with dial test indicators of 0,01 mm scale The measurements were taken after a certain number of load cycles N_i for the minimum load M_{min} (P_{min}) and maximum load M_{max} (P_{max}) of the cycle. In the analysis, deflections measured for the cycle maximum load M_{max} (P_{max}) were taken into account.

3. Analytical solution of the task

To begin the solution of the task, the recommendations of Eurocodes [9, 10] were adopted. In general, beam deflection a can be calculated from formula [9]:

$$a = \alpha_k \frac{M_{Sd,lt}\, l_{eff}^2}{B_\infty} \tag{1}$$

where:

α_k – coefficient dependent on load configuration and support conditions,

l_{eff} – effective span,

$M_{Sd,lt}$ – value of bending moment; for the in calculation of real deflections adopted as characteristic value;

$$B_\infty = \frac{E_{c,eff} I_{II}}{1 - \beta \left(\dfrac{M_{cr}}{M_{Sd,lt}} \right)^2 \left(1 - \dfrac{I_{II}}{I_{I}} \right)} = B \tag{2}$$

β – coefficient (for ribbed bars $\beta = 1.00$),

M_{cr} – cracking moment,

$M_{Sd,lt}$ – moment of inertia of reduced cross section (uncracked cross section – phase I),

I_{II} – moment of inertia of cracked section (phase II),

$E_{c,eff}$ – effective modulus of elasticity of concrete equal;

$$E_{c,eff} = \frac{E_{cm}}{1 + \phi(\infty, t_o)} \tag{3}$$

E_{cm} – secant value of concrete mean modulus of elasticity,

$\phi(\infty, t_o)$ – creep coefficient (included in the case of long-time loads).

In this context, it should be emphasised that adopting the coefficient $\beta = 0.5$ in formula (2) does not generate deflection calculation results compatible with those of experimental tests.

The effect of changing loads on the modulus of elasticity can be described by formula [3]:

$$E_{cm\,N_i} = E_{cm}\left(1 - 0{,}30\frac{N_i}{N}\right) \tag{4}$$

where:

    N_i – number of load cycles for which the value of modulus of elasticity is being determined,

    N – limit number of load cycles corresponding to concrete fatigue compressive strength.

In the case of the beams analysed, applying the given load parameters and the values of stress in the zone of concrete under compression, resulting from these parameters, this effect can be disregarded since $N_i <<< N$.

A detailed analysis of the effect of changing loads on RC beam deflection was preceded by a comparison of the values of deflections calculated from formulae (1) and (2) with the values of coefficients $\beta = 1.0$ and $\beta = 0.5$. The corresponding bending moments were calculated for the geometric and load parameters characteristic of the tested beams. The ratio of the calculated deflections $a(\beta = 0.5)/a(\beta = 1.0)$ did not exceed 5%, which was several times less than indicated by experimental tests. Consequently, it can be stated that the effect of changing loads on RC beam deflection cannot actually be taken into account by changing the value of coefficient β from 1.0 to $\beta = 0.5$.

Keeping valid the general formulation of the equation provided in norms, it would be easiest to include the effect of load variation on RC beam deflection by introducing an additional coefficient γ_f in the second term of the denominator in formula (2). The value of this coefficient should depend on the parameters and the number of load cycles.

A general formula for the calculation of γ_f was adopted as:

$$\gamma_f = 1 + b(1 - cR)^d \log N_i \tag{5}$$

where:

    R – stress ratio,

    N_i – number of load cycles,

    b, c, d – coefficients determined on the basis of experiment results.

The values of parameters b, c and d which would yield a good compatibility between calculated beam deflections and those obtained from tests could not be determined by way of an analysis of the tests performed by the author. Therefore, a formula describing the complete increment of deflections is proposed below. This formula takes the form:

$$\gamma = 1 + b(1 - R)^c (0{,}5 + \kappa)^d \log N_i \tag{6}$$

where (as in the previous formula):

    R – stress ratio,

    κ – maximum cycle load to failure load ratio,

N_i – number of load cycles,

b, c, d – coefficients whose values can be adopted from test results.

To determine the values of the coefficients in formula (5) the results of tests on group of beams whose load parameters were: $\kappa = 0.25, 0.45, 0.60, 0.75$ and $R = 0.15, 0.30, 0.50, 0.60$. The results of tests on the other beams were used for the verification of the correctness of the final formula.

Using the test results, the values of parameters for formula (5) were determined as: $b = 0.036$, $c = 1.18$, $d = 1.30$. The final formulation was adopted:

$$\gamma = 1 + 0{,}036(1-R)^{1,18}(0{,}5+\kappa)^{1,30}\log N_i \tag{7}$$

Formula (7) must have a practical restriction, since at $N_i \to \infty$ the value of the coefficient also increases to infinity. The number of cycles $N_i = 10^7$ can be adopted as such a restriction. In the conditions of effective loads, this number is practically impossible to reach.

4. Analysis of solution and its experimental verification

The results of the analysis of formula (7) are shown in Figs. 2–6.

Figure 2 illustrates the experimental verification of formula (7). 'The results of tests on the beams used for verification (those that were not employed for the determination of parameters for formula (6)) are indicated on the graphs plotted on the basis of this formula.

Figures 3–6 refer to the effect of particular parameters of load cycles and their number on coefficient γ. The graphs in Fig. 3 indicate a deflection increment with increases in the number of load cycles N_i at higher values of ratio κ (for a given value of R). The effect of stress ratio R is inverse; the lower its value, the greater the effect of changing loads on RC beam deflection, which is proved by the plots in Fig. 4.

On the basis of the analysis results presented graphically in Fig. 5, it can be stated that the deflection increment after a specified number of load cycles N_i (in Fig. 5, $N_i = 10^6$ was adopted) increases with increases in the value of ratio κ. On the basis of the plots in Fig. 9, in turn, it can be concluded that with the increase of R, the increment of RC beam deflections under changing loads decreases.

5. Remarks and final conclusions

The aim of this paper was to propose a formula for including the effect of changing loads on the deflection of RC beams reinforced with ribbed bars. The proposed formula was verified in experimental tests performed by the author (see Fig. 2). The test scheme was also employed for the specification of the values of coefficients for equation (6). It should be emphasised that for the calibration of the coefficients, the results for different beams were used than for the assessment of the correctness of formula (7). However, the correctness of formula (7) can be verified by the results of independent investigation.

Regardless of the degree of formula (7) accuracy with regard to quantity, it can be used as a basis for the formulation of unequivocal remarks and conclusion in terms of quality. The analysis of graphs and results of tests shown in Figs. 2-6 proves that the increment of the deflection of RC beams reinforced with ribbed bars under changing loads is affected by parameters $(\kappa = M_{max}/M_n$, $R = M_{min}/M_{max}$; M_{min} – minimal moment of cycle, M_{max} – maximal
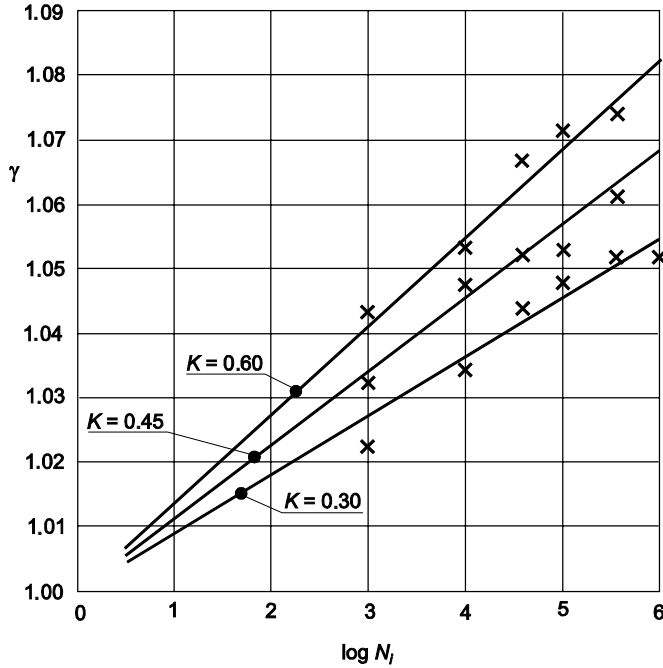

Fig. 2. Experimental verification of formula (7)
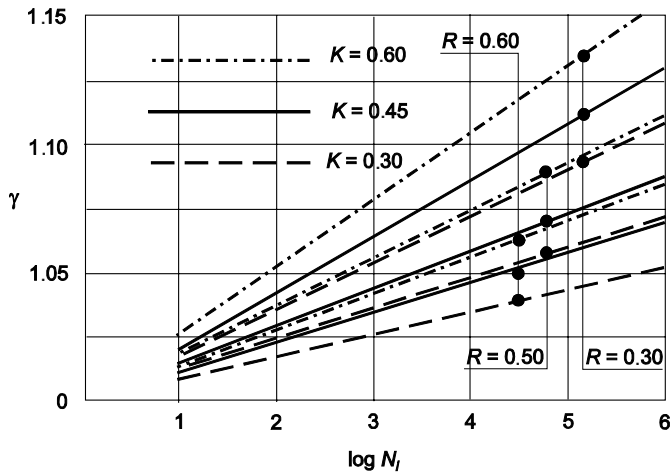
Fig. 3. Effect of the number of load cycles N_i and ratio κ on deflection increment
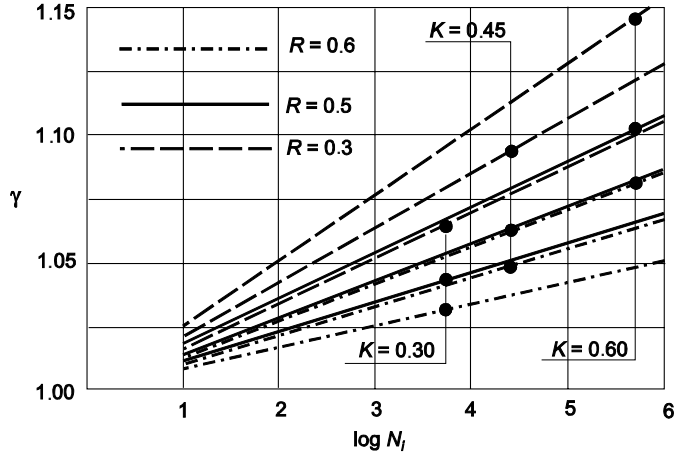
Fig. 4. Effect of the number of load cycles N_i and ratio R on deflection increment
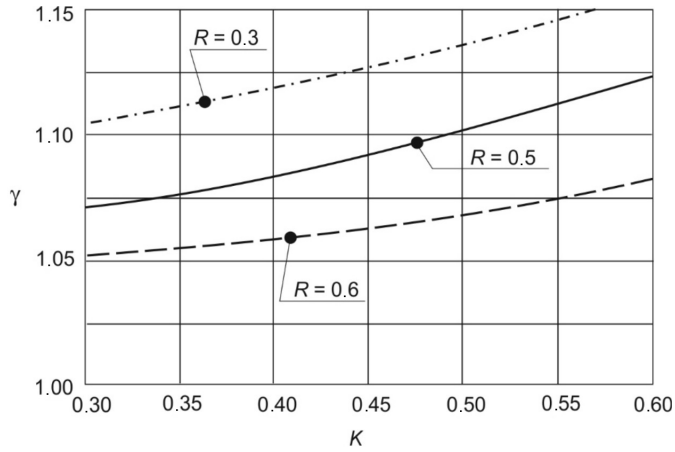
Fig. 5. Effect of ratio κ on deflection increment for some values of ratio R for $N_i = 10^6$
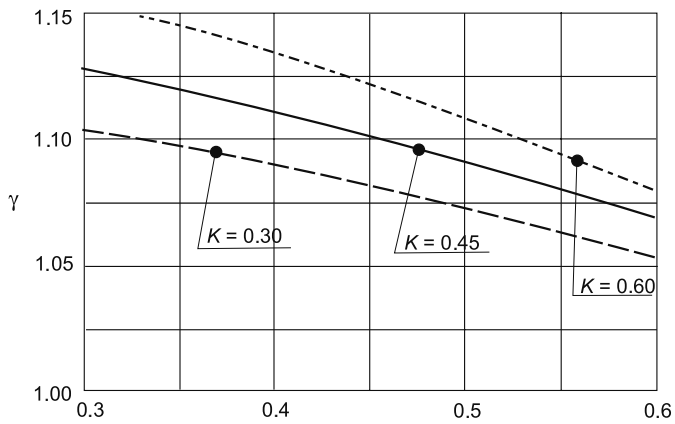
Fig. 6. Effect of ratio R on deflection increment for some values of ratio κ for $N_i = 10^6$

moment of cycle, M_n – failure moment under short-term loads) and number of load cycles N_i (to be more precise, logN_i).

The increment of deflection of RC beams reinforced with plain bars subjected to changing loads increases with increases in the number of load cycles N_i (logN_i, to be more accurate), and is greater for higher values of ratio κ (see Fig. 3) and lower values of ratio R (see Fig. 4). The relationships for the number of load cycles N_i are similar (see Figs. 5 & 6).

References

[1] Dyba M., *Wpływ parametrów technologicznych na przyczepność betonu wysokowartościowego do stalowych splotów sprężających,* (in Polish). Praca doktorska, Politechnika Krakowska, Kraków 2014.

[2] Dybeł P., *Wpływ składu i właściwości betonów wysokowartościowych na przyczepność do stalowych prętów zbrojeniowych* (in Polish). Praca doktorska. Politechnika Krakowska, Kraków 2013.

[3] Furtak K., *Nośność przekrojów normalnych w zginanych elementach żelbetowych poddanych obciążeniom zmiennym ze szczególnym uwzględnieniem obiektów mostowych* (in Polish). Politechnika Krakowska, Zeszyt Naukowy Nr 4, Kraków 1985.

[4] Furtak K., *Ocena wpływu zmienności obciążeń na szerokość rozwarcia rys w belkach żelbetowych* (in Polish), Czasopismo Techniczne, 6-B/1995.

[5] Furtak K., *Wpływ obciążeń zmiennych na wysokość rys prostopadłych w belkach żelbetowych* (in Polish), Czasopismo Techniczne, 6-B/1995.

[6] Kamiński M,. Pędziwiatr J., Styś D., *Projektowanie konstrukcji żelbetowych,* (in Polish). Dolnośląskie Wydawnictwo Edukacyjne, Wrocław 2007.

[7] Knauff M., *Obliczanie konstrukcji żelbetowych według Eurokodu 2,* (in Polish). Wydawnictwo Naukowe PWN, Warszawa 2012.

[8] Lachiewicz-Złotowska A., *Wpływ obciążeń stałych i zmiennych na wytrzymałość zmęczeniową betonu rozciąganego,* (in Polish), Praca doktorska, Politechnika Krakowska, Kraków, 1999.

[9] Łapko A., *Projektowanie konstrukcji żelbetowych,* (in Polish), Arkady, 2003.

[10] PN-EN1992-1-1: Projektowanie konstrukcji z betonu. Część 1-1: Reguły ogólne i zasady dla budynków) (in Polish).

[11] PN-EN1992-2*:* Projektowanie konstrukcji z betonu. Część 2: Mosty z betonu. Obliczanie i reguły konstruowania (in Polish).

[12] Starosolski W., *Konstrukcje żelbetowe według PN-B-03264 i Eurokodu 2,* (in Polish), Wydawnictwo Naukowe PWN, Warszawa 2007.
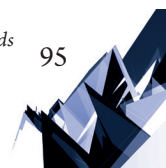
Piotr Woźniczka orcid.org/0000-0002-5471-9526
pwozniczka@pk.edu.pl

Marek Piekarczyk orcid.org/0000-0003-0566-4749
Institute of Building Materials and Engineering Structures, Faculty of Civil Engineering,
Cracow University of Technology

The fire resistance of steel plate girders with slender webs – a comparative study

Odporność ogniowa stalowych blachownic z cienkościennymi środnikami – studium porównawcze

Abstract

A comparative study of the load-bearing capacity of selected steel plate girders with slender webs under fire action is presented in this paper. Typical plate girders and girders with corrugated webs are considered. Stiffeners are only placed at the ends of cantilever beams so the shear buckling is a possibility. Fire resistance of the analysed members was estimated using two separate FEM software packages. Moreover, the computational approach applied for each case was different, thus validation of the software was possible. Failure modes, critical temperatures and deformations for steel plate girders subject to fire temperatures are also presented.

Keywords: fire resistance, steel plate girder, corrugated webs, local buckling

Streszczenie

W artykule przedstawiono studium porównawcze nośności wybranych blachownic stalowych ze smukłym środnikiem poddanych oddziaływaniom pożarowym. W analizie uwzględniono typowe blachownice oraz blachownice z falistym środnikiem. Żebra umieszczono tylko na końcach wspornika, w związku z czym możliwa była utrata stateczności przy ścinaniu. Odporność pożarową analizowanych elementów oszacowano za pomocą dwóch niezależnych pakietów oprogramowania bazujących na metodzie elementów skończonych. Co więcej, podejście obliczeniowe zastosowane w obu przypadkach było różne, w związku z czym możliwa była walidacja użytych pakietów oprogramowania. Zaprezentowano również modele zniszczenia, temperatury krytyczne oraz deformacje dla blachownic stalowych poddanych działaniu temperatury pożarowej.

Słowa kluczowe: odporność pożarowa, blachownica stalowa, środniki z blachy profilowanej, utrata stateczności miejscowej

1. Introduction

The development of lightweight steel structures and the current trend to use thin-walled members allows obtaining reductions in both material consumption and the overall costs of construction projects; however, their use demands a more thorough knowledge of the behaviour of structures in the event of fire.

Experimental research is without any doubt the best way to evaluate the performance of a structure during conditions of elevated temperature resulting from fire. However, this is too inconvenient and expensive to be commonly used. Instead, in normal practice, a set of design rules are recommended for the purpose; these may also be aided by computer technology. Numerical simulations with validated programmes can be used to check the accuracy of measured dimensions and/or observe the behaviour of a structure in conditions of fire.

Design rules given in the current standard EN 1993-1-2 [4] for the 4th class of cross sections are limited to a certain range of temperatures. According to the standard for this type of cross section, the critical temperature is always 350°C and the standard does not, for example, consider the degree of utilization of selected parts of the steel member. Such an approach seems to be conservative. Even taking into account data that could be found in [7] (i.e. some additional verifications of fire resistance that are not covered by [4]) the assessment of the load-bearing capacity of steel plate beams or columns with slender webs is still not fully recognised in conditions of elevated temperature. To investigate this situation, extended research has been recently performed in a few European countries. Some of the most important results in this field have been obtained for shear buckling [14, p. 34–43] and lateral-torsional buckling [2, p. 410–421], [13, p. 2–18]. The outcomes of experimental investigations concerning the behaviour of columns are presented in [5] while outcomes for research on beams with corrugated webs are provided in [12, p. 69–78]. Generally, in almost all the previously mentioned papers, computer simulations have been validated by full-scale tests. This approach seems to be the most appropriate in order to obtain high-quality results of computer simulations, but it is also quite expensive and time-consuming. Another fairly common way how to validate computer calculations is to use at least two numerical methods based on different theoretical foundations (e.g. theories of plastic flow etc.) and obtain similar effects [1, p. 83–142]. In this paper such approach is presented. The two advanced software packages SAFIR [6, p. 300–323] and ABAQUS [9] are used here for this purpose.

2. Comparative study

2.1. Computer simulations performed using the Abaqus program

Three different cantilever beams were considered. One was a typical steel plate girder with flanges measuring 250 mm wide and 20 mm thick, a web measuring 750 mm high and 5 mm thick. The two other beams were steel plate girders with corrugated webs (SIN type) marked as WTA750 and WTC750. Their flange dimensions were the same as for the plate beam but
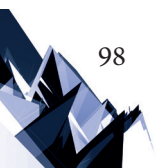
the thicknesses of the webs were 2 mm and 3 mm, respectively. Each beam was 3.1 m long and the live load at the end of the cantilever is 25 kN. The flanges were made of S235JRG2 steel grade with a yield strength of f_y=240 MPa and webs were made of S235JR with a yield strength of f_y=215 MPa. The stress-strain relationship and reduction factors were exactly the same as those given by EN 1993-1-2 [4]. The beams were modelled with the use of shell elements (S4R5) which are 4 node elements with 5 degrees of freedom in each node. The web depth in the case of the SIN profiles was divided into 16 elements, which gives 3,008 elements in total for the whole beam. For the plate girder, these values are 26 and 4,784, respectively. The view of a model prepared using ABAQUS software [9] is presented in Fig. 1. The cross section was heated according to the natural fire curve shown in Fig. 2. For simplicity, it was assumed that temperature of the web was always equal to the gas temperature, while the temperature of the flanges was calculated according to EN 1993-1-2.

In order to estimate the load-bearing capacity of a cantilever beam under fire action, the Riks method is used. This approach is valid for the unstable, geometrically nonlinear collapse of structures. The nonlinear properties of materials are also taken into consideration. The described method consists of several successive steps that form the analysis as a whole. For each step, all the steel properties are determined for the given temperature and only the load parameter is raised. If the obtained load is higher than the required 25 kN, the simulation goes to the next step and is repeated once again using reduced properties of steel for the next higher temperature value. Otherwise, when the required load (P = 25 kN) cannot be reached, the simulation stops and the fire resistance is taken as the value for the last fully completed step. All calculations presented in this paper were performed in [15].

The described methodology does have some disadvantages. For example, during a typical fire episode, it is usual for the dead and live loads to have been added to the structure before the rise of the temperature took place. In the result some parts of strains caused by mechanical loads are developed at ambient temperature. Moreover, following increase of strains during a fire should be calculated using steel properties that depends on elevated values of temperature. However, as previously mentioned, for comparison reasons, the material properties for separate simulations are constant and the force parameter is increased. The other significant disadvantage here is the computational cost of the simulation which must be performed many times before the final estimation of fire resistance is obtained.

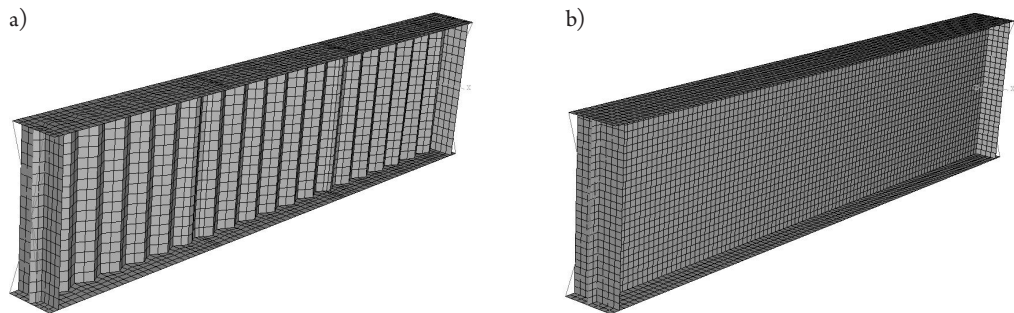a)   b)

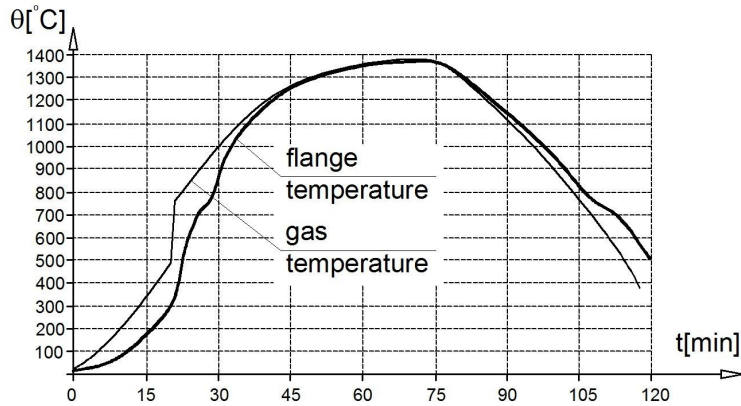Fig. 1. Analysed models prepared using Abaqus software: a) SIN profiles; b) plate girder

Fig. 2. Temperature during the considered natural fire

2.2. Computer simulations performed using the Safir program

The same beams analysed with Abaqus were analysed again using the Safir software program [6, p. 300-323]. As before, the steel properties and reduction factors were taken from EN 1993-1-2; however, the method used for conducting the analysis was quite different. Firstly, a dynamic approach was applied to overcome local instabilities. The mass matrix was included explicitly, while the damping matrix was introduced as so-called 'numerical damping' and Newmark's method was used to solve the governing equation. The time step for the analysis was automatically selected by the program and the come back factor was 0.0001 sec. The shell elements are quadrangles based on four nodes, each bearing three translations and three rotations. A relatively fine mesh was set in the model with an element size of around 25 x 25 mm, which gave a total of 7,072 elements for the plate girder. The load achieved from the last converged step of the Abaqus analysis was taken into account so the load values were 40.76 kN for the plate girder, 26.44 kN for the WTC type and 24.1 kN for the WTA girder type. Recommended biaxial plane stress material type STEELEC32D was applied in the simulations.

As the used software package is specified for simulations of a structure's behaviour under fire action, it has some further features that should be mentioned here. This especially applies to the fact that, unlike the previous case, the temperature is calculated numerically across the section. As a result, the temperature varies along the thickness of the steel plate and this may lead to additional stresses. Moreover, dead and live loads were added to the structure during the first twenty seconds of analysis and only after this period did the temperature significantly increase. One can notice that this approach is much closer to the real behaviour of structures in conditions of fire than the method adopted for the previously described Abaqus simulations. Models created with the use of Safir software are presented in Fig. 3. More details regarding the exact properties and limitations of the software can be found in [6, p. 300-323] and [7].
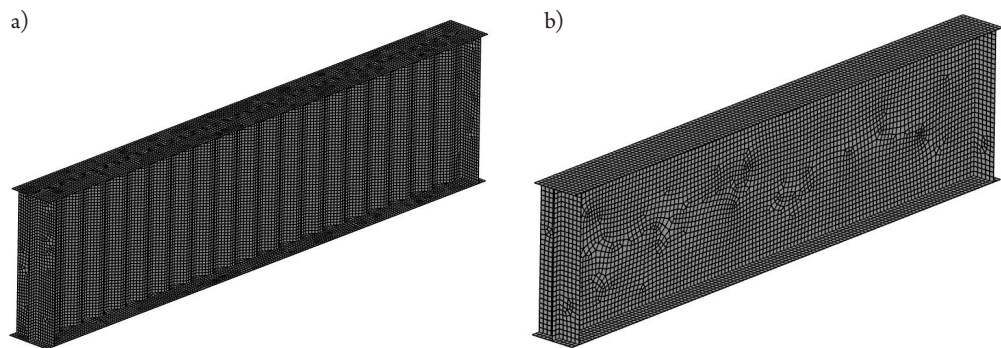
a)   b)

Fig. 3. Analysed models prepared using Safir software: a) SIN profiles; b) plate girder

2.3. Results of the analyses

The main results obtained for the both described calculation methods are: fire resistance – expressed by the time after which the collapse of the beam occurs; critical temperature of the web and the flanges; final deflections; types of failure modes. A comparison of these results is presented in Table 1 for the steel plate girder, in Table 2 for the WTA SIN type girder and in Table 3 for the WTC SIN type girder.

Table 1. Results – steel plate girder

	Critical temperature – flange [°C]	Critical temperature – web [°C]	Maximum deflection [mm]	Fire resistance [min]
SAFIR	640	800	16	24
ABAQUS	656	848	12.5	25

Table 2. Results – SIN WTA type girder

	Critical temperature – flange [°C]	Critical temperature – web [°C]	Maximum deflection [mm]	Fire resistance [min]
SAFIR	590	746	83	23
ABAQUS	450	771	10	22

Table 3. Results – SIN WTC type girder

	Critical temperature – flange [°C]	Critical temperature – web [°C]	Maximum deflection [mm]	Fire resistance [min]
SAFIR	670	815	96	24.5
ABAQUS	627	835	10	24.5

It is clearly shown that for all the simulations, nearly no differences in the predicted fire resistance occurred. However, it should be stressed once more that the estimated collapse time for the same tests using the ISO curve [3] might lead to significantly lower results. For the plate girder and the SIN WTC type girder, the critical temperatures of the web and flanges given by both software programs are practically the same. The highest disagreement is as much as 10%. This is not the case for the flange of the WTA girder. However, this outcome can be easily justified when we look at the time-temperature relationship presented in Fig. 2. The failure occurs at the same time when a flashover takes place (vertical part of the gas temperature graph somewhere around t = 22.5 min) so the changes of the temperature are very high over an extremely short period of time. Therefore, even a small difference in the heating calculation method, which is obvious according to the previously described facts (see clauses 2.1 and 2.2), leads to inaccuracy in the estimation of flange temperature. This is not that visible for the web because of its thickness – for such a plate, its temperature is always almost equal to the temperature of the fire environment regardless of the calculation methodology.

The deflections obtained using the Safir software are higher than those obtained for the Abaqus simulations – this is due to using the dynamics approach in Safir. The Riks method stops immediately when some instability is detected while the dynamics approach can overcome this point and calculations are continued for some additional time. However, the analysed structure is statically determinate, therefore the only advantage of the dynamic approach is a better insight into the beam's post-buckling behaviour. For indeterminate structures where redistribution of forces appears and the impact on fire resistance may be crucial, a dynamic approach in the incremental analysis is recommended.
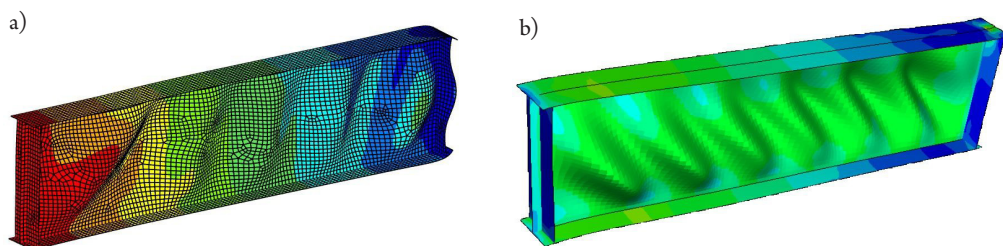
a)

b)

Fig. 4. Failure modes for steel plate girder: a) Safir software (fixed support on the right side of the beam); b) Abaqus software (fixed support on the left side of the beam)
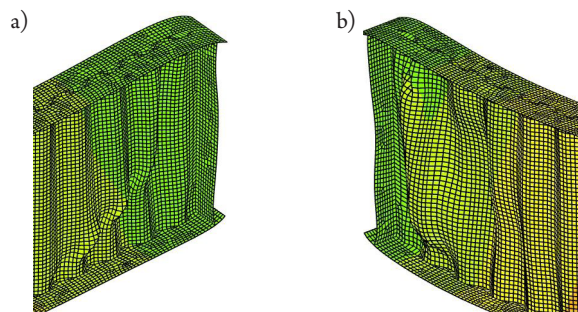
a)   b)

Fig. 5. Failure modes near the support obtained using Safir software for: a) SIN WTA girder; b) SIN WTC girder
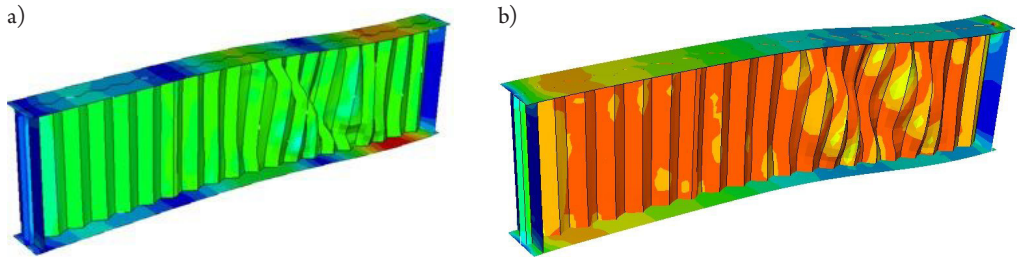
a)

b)

Fig. 6. Failure modes obtained with Abaqus software (fixed support on the left end of the beam) for:
a) SIN WTA girder; b) SIN WTC girder

The failure modes for the girders are presented in Figs. 4-6. Once again, results for the plate girder are very close to each other. Firstly buckling appears for the web due to compression developed by temperature differences between the web and the flanges. However, this deformation does not affect the load-bearing capacity of the whole beam. The structure remains stable until the web buckling near the support occurs. This phenomenon is more visible for the model created using Safir software (Fig. 4a). Furthermore, the observed shape of deformations is quite similar to those observed in the steel structures after the real fire (see Fig. 7 [8, p. 51-66]).

The failure modes obtained for the SIN type profiles are more varied. In the case of the Abaqus software, web destruction occurs near the middle of the span. This cannot be easily explained and further investigation is required here. The form of web buckling presented in Fig. 5 (and especially in Fig. 5b) should be recognised as the correct one. Firstly, it appears near the support where the bending and shear forces reach maximum values. Secondly, this type of web buckling is similar to the results of experimental research obtained by Kuchta [10] for ambient temperatures (Fig. 8).

Fig. 7. Deformations of steel beams after real fire exposure [8, p. 51-66]

Fig. 8. Failure mode for the SIN type profile according to [10]

3. Conclusions

The comparison of computer simulations performed for different types of steel girders affected by fire action was analysed. Two separate approaches to the calculations and two separate software programs were used to estimate the fire resistance of cantilever beams and to validate the computational software. The results obtained for a steel plate girder are satisfactory and both software programs predict very similar data with regard to time when the failure occurs, deflections and failure modes.

A few more significant differences for SIN type profiles can be observed; however, most of these were expected and can be easily explained. Moreover, it is clearly shown that the load-bearing capacity of 4th class cross sections cannot be limited to the critical temperature of 350°C (15 minutes) and simple fire unprotected structures could survive nearly 25 minutes of natural fire. Similar conclusions for other types of steel members have also been drawn by other researches e.g. [11, p. 370–382].

References

[1]   Arbocz J., *Post-buckling behaviour of structures. Numerical techniques for more complicated structures*, Buckling and Post-Buckling. Lecture Notes in Physics, Vol. 288. Springer-Verlag, Berlin, Heidelberg, 1987, 83–142.

[2]   Couto C., Vila Real P., Lopes N., Zhao B., *Numerical investigation of the lateral-torsional buckling of beams with slender cross sections for the case of fire*, Engineering Structures, Vol. 106, 2015, 410–421.

[3]   European Committee for Standarization, *EN 1991-1-2: Eurocode 1: Actions on structures. Part 1–2: General actions - Actions on structures exposed to fire,* Brussels, Belgium 2002.

[4]   European Committee for Standarization, *EN 1993-1-2: Eurocode 3: Design of steel structures. Part 1–2: Structural fire design,* Brussels, Belgium 2005.

[5]   Franssen J-M., Fohn T., *FIDSEC4: Fire behaviour of steel members with class 4 cross sections under axial compression and axial compression with eccentricity*, Report of the experimental tests performed at the University of Liege, 2013.

[6]   Franssen J.-M., Gernay T., *Modelling structures in fire with SAFIR: Theoretical background and capabilities*, Journal of Structural fire Engineering, Vol. 8 issue 3, 2017, 300–323.

[7]   Franssen J.-M., Vila Real P., *Fire design of steel structures 2nd edition*, ECCS Press and Ernst & Sohn Wiley Company, 2015.

[8]   Gwóźdź M., Woźniczka P., Tkaczyk A., *The reconstruction of fire-damaged industrial steel halls*, Safety&Fire Technique, Vol. 44, Issue 4, 2016, 51–66.

[9]   Hibbit, Karlsson & Sorensen Inc., *Abaqus: Analysis user's manual*, Volumes I–IV, version 6.10, 2010.

[10]   Kuchta K., *Nośność i sztywność blachownic o falistych środnikach*, Politechnika Krakowska, 2004. Rozprawa doktorska.

[11]   Maia E., Couto C., Vila Real P., *Critical temperatures of class 4 cross-sections,* Journal of Constructional Steel Research, Vol. 121, 2016, 370–382.

[12]   Maślak M., Łukacz M., *Interactive shear resistance of corrugated web in steel beam exposed to fire*, Journal of Structural Fire Engineering, Vol. 7, Issue 1, 69–78.

[13]   Prachar M., Hricak J., Jandera M, Wald F., Zhao B., *Experiments of class 4 open section beams at elevated temperature*, Thin-Walled Structures, Vol. 98, 2016, 2–18.

[14]   Reis A., Lopes N., Vila Real P. *Shear-bending interaction in steel plate girders subjected to elevated temperatures*, Thin-Walled Structures, Vol. 104, 2016, 34–43.

[15]   Tatara Z., *Design of workshop hall (24 x 42 m) with crane transportation. The influence of thermal load on carrying-capacity of chosen steel members.* Brandenburg Technical University Cottbus, Cracow University of Technology, Diploma Work, 2006.

Wojciech Czuchra
wczuchra@pk.edu.pl

Bartosz Woszczyna orcid.org/0000-0002-2355-4175
bwoszczyna@pk.edu.pl

Department of Traction and Traffic Control, Faculty of Electrical and Computer
Engineering, Cracow University of Technology

Measurement and simulation testing of harmonics in the on-board power grid of traction vehicles

Pomiary i badania symulacyjne harmonicznych w napięciu pokładowej sieci zasilania w pojeździe trakcyjnym

Abstract

The requirements relating to the emission of auxiliary AC supply sockets in traction vehicles have been extended in standard PN-EN 50121-3-2:2015 by voltage harmonics measurement. This applies to the public on-board AC supply grid which is accessible to all passengers. It is concerned with providing the quality of power supply which is required by computer devices and mobile phone rechargers. This article presents the requirements and test methods resulting from extended standard scope. Normative factors, for which levels of permissible voltage harmonics in the public supply grid of traction vehicle have been defined are discussed. Examples of comparative results obtained from measurements and analyses of voltage harmonics within on-board supply grids are also presented. The presented results include extended calculations of distortion factors for groups and subgroups of supply voltage harmonics. In order to improve the quality of voltage within the on-board grid, which did not meet the requirements, simulation calculations were performed and an additional output sinusoidal filter was proposed.

Keywords: electromagnetic compatibility, power quality, voltage harmonics, total harmonic distortion

Streszczenie

Wymagania dotyczące emisji portów pomocniczego zasilania AC w pojazdach trakcyjnych zostały w normie PN-EN 50121-3-2 z 2015 roku rozszerzone o pomiar w zakresie harmonicznych napięcia. Dotyczy to publicznej sieci zasilania pokładowego ogólnie dostępnej dla pasażerów. Związane jest to z zapewnieniem jakości zasilania, która jest wymagana dla urządzeń komputerowych oraz zasilaczy telefonów komórkowych. W artykule przedstawiono wymagania oraz metody badań wynikające z rozszerzonego zakresu normy. Omówiono normatywne współczynniki, dla których określone są poziomy dopuszczalne emisji harmonicznych w napięciu publicznej sieci zasilania w pojeździe trakcyjnym. Przedstawiono również przykładowe wyniki porównawcze uzyskane na podstawie pomiarów i analiz harmonicznych w napięciu pokładowej sieci zasilania. Prezentowane wyniki obejmują rozszerzone obliczenia współczynników odkształceń dla grup i podgrup harmonicznych napięcia zasilania. W celu poprawy jakości napięcia w sieci pokładowej, która nie spełniała wymagań normatywnych wykonano obliczenia symulacyjne i zaproponowano dodatkowy wyjściowy filtr sinusoidalny.

Słowa kluczowe: Kompatybilność elektromagnetyczna, jakość energii, harmoniczne w napięciu

1. Introduction

The requirements relating to the emission of auxiliary AC supply sockets in traction vehicles have been extended in standard PN-EN 50121-3-2:2015 by voltage harmonics. This applies to the public on-board AC supply grid which is accessible to all passengers. It is concerned with providing the quality of power supply which is required by computer devices and mobile phone rechargers.

The requirements on emission limits are specified in detail in PN-EN 50121-3-2 [1]; specific guidelines for conducting tests of voltage harmonics are specified in detail in PN-EN 61000-4-30 [2]. The supplement referred to in standard [2] is a general guideline for harmonics and interharmonics measurement PN-EN 61000-4-7 [3]. The issue of harmonic emission in traction vehicles has been the subject of a number of publications; however, the vast majority of these refer to harmonic distortion in traction current [6]. This is directly related to traffic safety due to the possible negative effects of higher frequency current signals on railway traffic control circuits [5, 8]. Therefore, the results of tests and analytical calculations of harmonic distortions in power supply in traction vehicles have been widely presented in publications [4, 7].

This article presents requirements and test methods resulting from the extended scope of the referenced standard. The standard factors for which harmonic emission limits in the public supply grids of traction vehicles are specified are discussed herein. Examples of comparative results obtained from measurements and analyses of voltage harmonics within on-board supply grids are also presented. The presented results calculations of the distortion factor for groups and subgroups of supply voltage harmonics. In order to improve the quality of voltage within on-board grids which did not meet the requirements, simulation calculations were performed and an additional output sinusoidal filter was proposed.

2. Methods of measurement of harmonic distortion in the supply voltage

The guidelines for harmonics measurements in AC voltage on-board grids in traction vehicles are specified in standard [1]. Two main measurement classes (A and S) and an additional class (B) are specified therein. The scope of parameters which should be determined in the test varies depending on the class used in the measurements. The measurement tools used in tests can measure either individual or all the parameters required in the standard but within the same class for all parameters. An example of the standard measurement chain with signal indication is shown in Fig. 1.

The most commonly used measurement tool is a LEM voltage transducer with galvanic isolation of an input and output circuit. This is an important element of the measurement path, and its parameters should meet the requirements of standard [1] in the scope of frequency band and phase response. The measurement unit (Fig. 1) is usually an analogue-to-digital transducer with an option to record the measured signal. An advanced software program with the option for FFT analysis is the used for the verification of measurements and compliance with the standard.
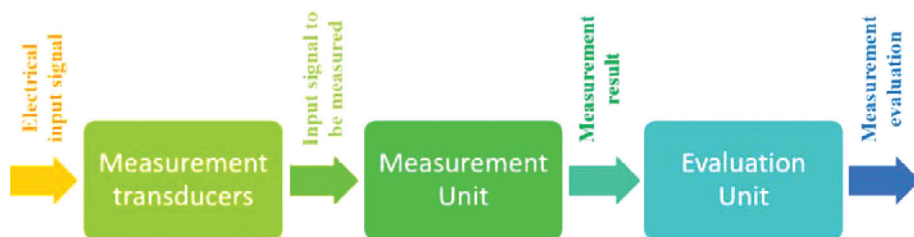
Fig. 1. Block diagram of measurement chain

Harmonic measurements can be made in single-phase or multi-phase power supply systems and, depending on the system and the needs, the following voltages can be determined: phase-neutral, phase-phase, phase-ground and neutral-ground. For traction vehicles, measurements are limited to a single-phase grid. Depending on the measurement class both in harmonic and interharmonic measurements, the standard specifies the maximum measurement order, the number of cycles included in the analysis, the required measurement uncertainty and the measurement range of the applied tools. Due to a huge number of measurement data items which require transmission recording, analysis and filing, data reduction is allowed using statistical methods or recording only the highest or average values.

3. Extended guidelines for the investigation of voltage harmonics in on-board supply grid

With regard to on-board AC supply grid in traction vehicle accessible to all passengers, the requirements relating to voltage harmonic emissions are included in PN-EN 50121-3-2. According to the standard, harmonic emission should be determined within the frequency range of 50 Hz to 2 kHz, whilst the indicator for the signal levels is total harmonic distortion (THD). The limit value of harmonic distortion is THD = 8%. The basic standard to carry out measurements in this scope is PN-EN 61000-4-30; however, the details are specified in PN-EN 61000-4-7.

THD is defined as:

$$THD = \sqrt{\sum_{n=2}^{H} \left(\frac{U_n}{U_1} \right)^2} \qquad (1)$$

where:

U_n – effective (r.m.s.) value of the nth harmonic,
U_1 – effective (r.m.s.) value of fundamental harmonic,
n – harmonic order,
H – maximum harmonic order.

In addition to the basic definitions of harmonic and interharmonic effective (r.m.s.) values, PN-EN 61000-4-7 introduces the effective values of a harmonic group and subgroup, as well as the effective values of an interharmonic group and subgroup. The corresponding

definitions of total distortion factors are also specified therein. The introduction of the effective value of a harmonic group and subgroup, which is calculated as a square root of the sum of squares of the harmonic value and its neighbouring spectral components, aims to improve the measurement accuracy in order that, for example, in the case of the effective value of the harmonic subgroup include the impact of fluctuations of values such as measured voltage.
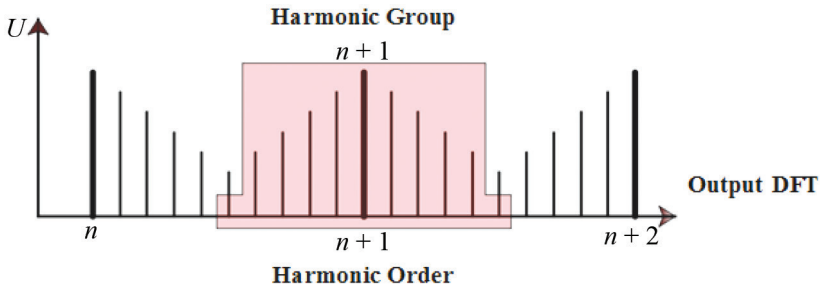

Fig. 2. Illustration of the harmonic group for a 50 Hz power supply network

The resultant r.m.s. value of the voltage harmonic group $U_{g,n}$ is defined as:

$$U^2_{g,n} = \frac{U^2_{k-5}}{2} + \sum_{i=-4}^{4} U^2_{k+i} + \frac{U^2_{k+5}}{2}$$

(2)

where:

U_{k+i} – r.m.s value of spectral component.
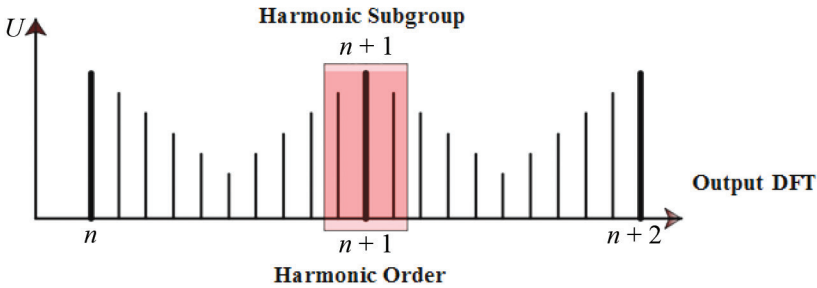
Fig. 3. Illustration of the harmonic subgroup for a 50 Hz power supply network

The resultant r.m.s. value of the voltage harmonic subgroup $U_{sg,n}$ is defined as:

$$U^2_{s,g,n} = \sum_{i=-1}^{1} U^2_{k+i}$$

(3)

where:

U_{k+i} – r.m.s. value of spectral component.

The group total harmonic distortion THDG is:

$$THDG = \sqrt{\sum_{n=2}^{H}\left(\frac{U_{gn}}{U_{g1}}\right)^2} \qquad (4)$$

where:

U_{gn} – effective (r.m.s.) value of the n*th* harmonic group,
U_{g1} – effective (r.m.s.) value of the group fundamental,
n – harmonic order,
H – maximum harmonic order.

The subgroup total harmonic distortion THDS is:

$$THDS = \sqrt{\sum_{n=2}^{H}\left(\frac{U_{sgn}}{U_{sg1}}\right)^2} \qquad (5)$$

where:

U_{sgn} – effective (r.m.s.) value of the n*th* harmonic group,
U_{sg1} – effective (r.m.s.) value of subgroup fundamental,
n – harmonic order,
H – maximum harmonic order.

4. Test results of supply voltage harmonic distortion in on-board grid

The presented measurement results derive from the tests which have been carried out for several selected on-board power supply grids in traction vehicles. The measuring setup consisted of a LEM voltage transducer with galvanic isolation, a DEWE43 analogue-to-digital transducer with the option to continuously record signals on an external computer and an autonomous power supply system. The obtained results of voltage measurements to determine the harmonics were subjected to FFT analysis in Matlab software and compiled on charts for the purpose of comparison. Calculations included 10 cycles of voltage signal using a rectangular-shaped window and the maximum harmonic order was 40. The indicators for determining the compliance of power supply parameters with standard [1] were calculated.

Time waveform and voltage supply harmonic distortion (Us1) in the 230 V AC on-board grid in the traction vehicle, in which the sinusoidal wave-forming methods were not applied are shown in Fig. 4. The results for on-board grids (Us2 and Us3) in which output filtering systems were applied are shown in Figs. 5 & 6. To compare time waveforms and on-board voltage supply harmonic distortions; Figs. 7 & 8 show the results obtained for typical power supply (Us4) and uninterruptible power supply UPS (Us5), respectively.
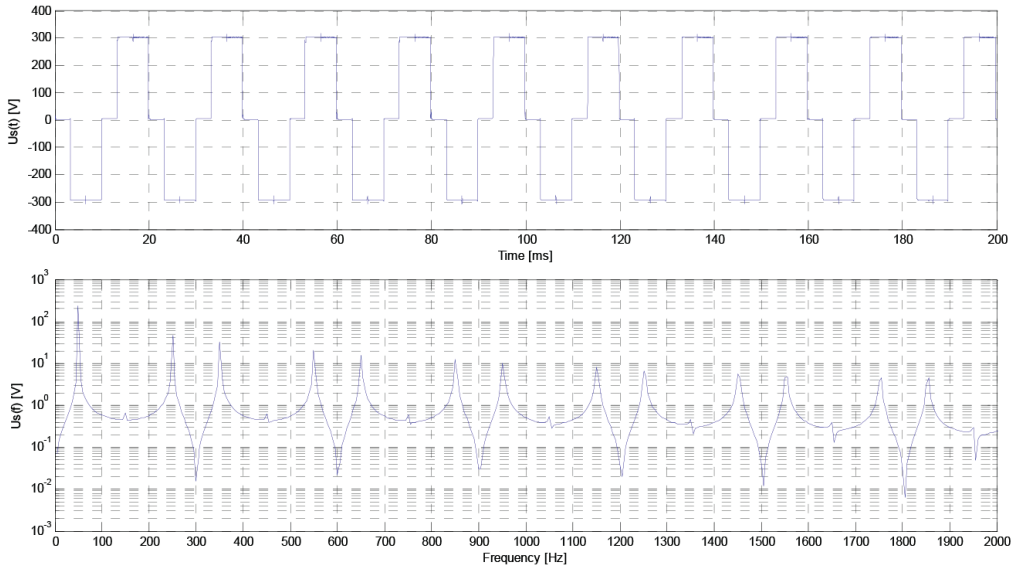
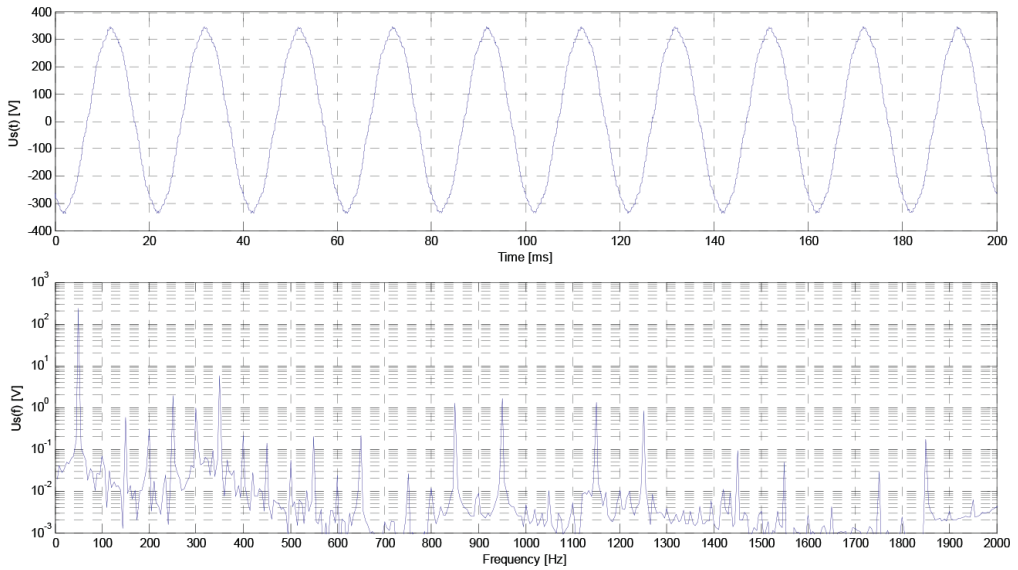Fig. 4. Variable component of voltage supply and voltage harmonic spectrum (Us1)

Fig. 5. Variable component of voltage supply and voltage harmonic spectrum (Us2)

Fig. 6. Variable component of voltage supply and voltage harmonic spectrum (Us3)

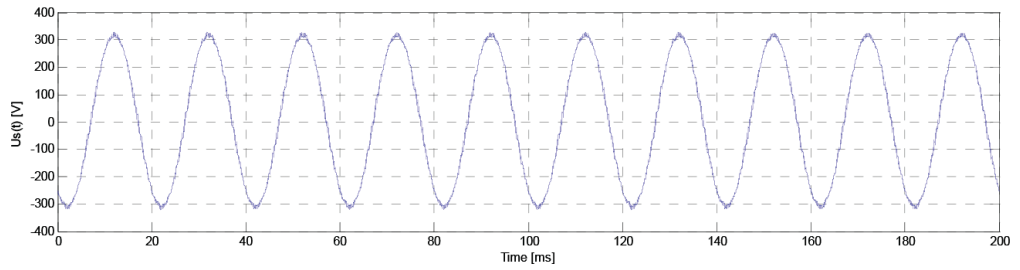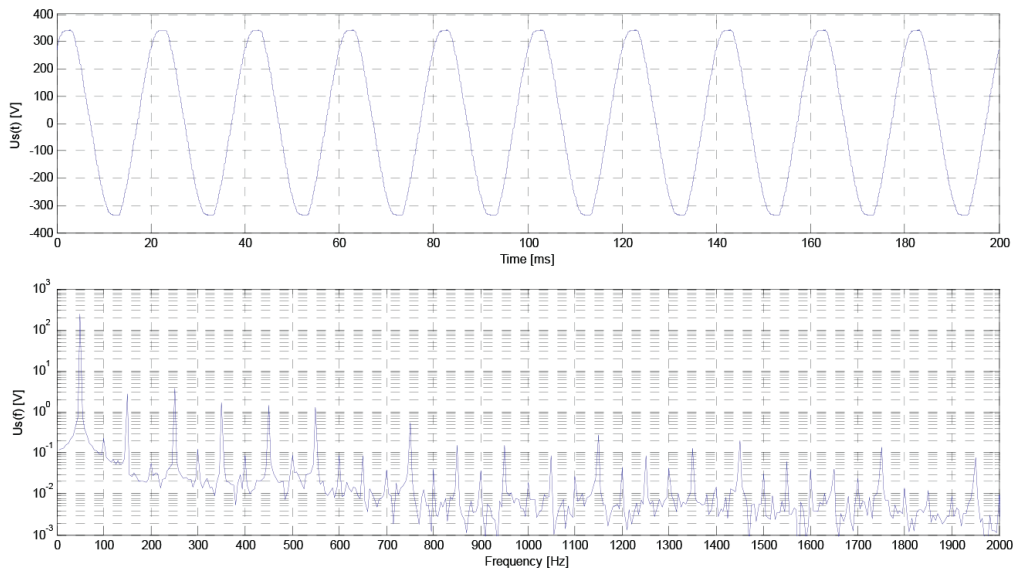

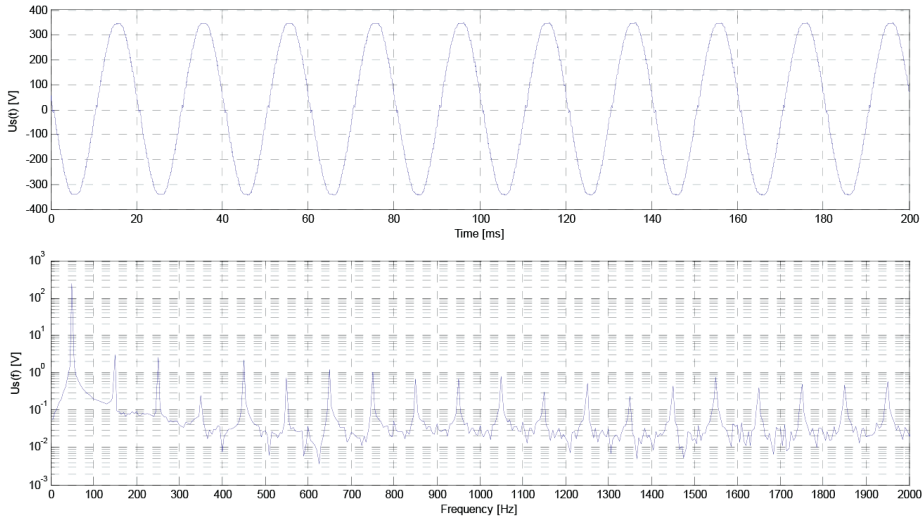Fig. 7. Variable component of voltage supply and voltage harmonic spectrum (Us4)

Fig. 8. Variable component of voltage supply and voltage harmonic spectrum (Us5)

A summary of the results of the individual harmonics for the three selected on-board power supply grids in traction vehicles is shown in Fig. 9. The comparison refers only to odd harmonics due to their dominant share in the spectrum.

Based on the determined levels of individual harmonics, the factors characteristic of total harmonic distortion in the 230 V AC supply in traction vehicles were calculated and are shown in Table 1. In addition to the basic THD factor, the group total harmonic distortion (THDG) and subgroup total harmonic distortion (THDSG) factors were also determined. For the purpose of comparison, the table also includes the total harmonic distortion for a typical power supply and an uninterruptible power supply.
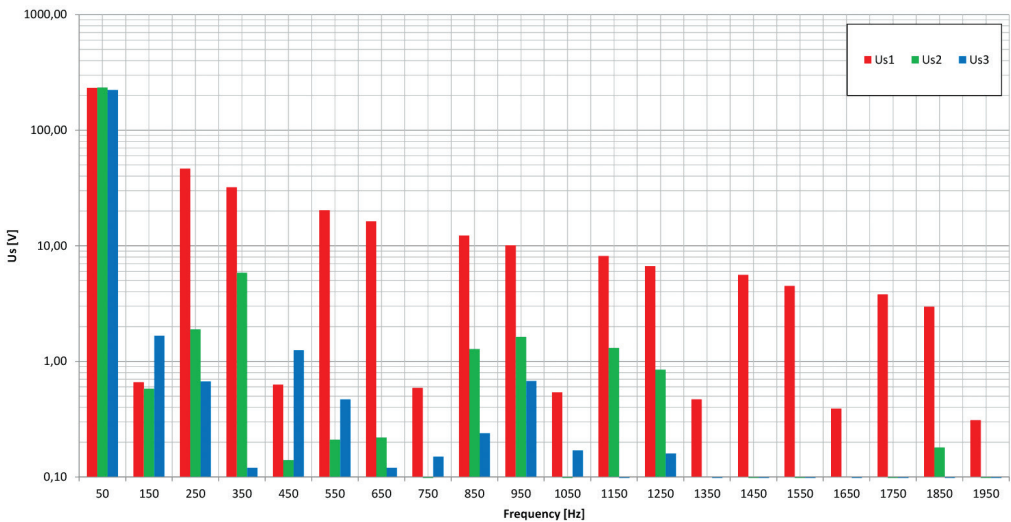
Fig. 9. Comparison of harmonic distortion in the on-board supply voltage

Table 1. Factors characteristic of harmonic distortion in selected grids

Factor	Us1	Us2	Us3	Us4	Us5
THD [%]	28.22	2.89	1.09	2.25	2.15
THDG [%]	29.66	2.89	1.11	2.25	2.21
THDSG [%]	29.23	2.89	1.09	2.25	2.17

The determined harmonic distortion factors in the investigated 230 V AC on-board grid in traction vehicles (Us1, Us2, Us3) show significant variation. Odd harmonics have a key impact on the value of this factor for all tested grids. The collation of THD for on-board supply with THD for the typical power supply (Us4) and the uninterruptible power supply UPS (Us5) shows that the THD for on-board supply grid in which output waveforming systems are applied (Us2 and Us3) is comparable to the THD for a typical power supply. In one case, for grid Us3 the THD is even better than the THD for a typical power supply. The results for on-board grids with output filtering systems meet the requirements of PN-EN 50121-3-2, as the determined THD factors are less than 8%. Further calculations of THDG for group harmonic distortion and THDSG for subgroup harmonic distortion have confirmed that in a properly conducted FFT analysis, no significant differences are observed. It does not mean, however, that the methods of harmonic grouping presented herein, and detailed in PN-EN 61000-4-7, cannot be useful for improving the accuracy of determining both voltage harmonics as well as harmonic distortion. The impact of the methods on the result is dependent upon the type of supply grid, its parameters and the applied FFT analysis.

5. Simulation testing of an additional input filter

As part of the tests a solution was proposed to improve the quality of the on-board voltage of the traction vehicle. The 230 V AC on-board voltage is obtained from the three-phase $3 \times 400/230$ V output of the auxiliary converter powered by full-line overhead contactors. This converter supplies the three-phase voltage primarily to the main drive cooling fan motors and to the heating system blower motors. Due to the high harmonic content of the 230 V AC on-board power grid and the THD value of 28.22%, which does not meet the requirements of PN-EN 50121-3-2 (THD < 8%), the output filter was proposed. The output sinusoidal filter is an example of a passive low pass second order LC filter. The filter shapes the sinusoidal voltage by suppressing the higher harmonics in the on-board grid. The resonance frequency of the filter falls between the primary supply frequency and the lowest harmonic frequency resulting from the control algorithm. The capacity of the filter capacitor should compensate for the reactive power of the engine connected to this power supply grid and for the fall in voltage in the filter inductance. In addition to a smoothed sinusoidal waveform, this filter protects both the engine and engine cable against high du/dt values and overvoltage by limiting further losses in the engine. This generally improves the reliability of the converter drive system. Due to the electrical structure of the on-board grid subjected to testing, in which a three-phase isolation transformer at the output of the inverter was applied, the selection

of the filter had to take into account the influence of the parameters of this transformer. Converter loads are inductive engines operating in variable configurations that have been replaced in the simulation by one substitute. A flowchart of the converter system modelled in Matlab Simulink is shown in Fig. 10. In order to represent the actual shape of the voltage obtained from the measurements for grid 1 (Fig. 4), the waveform (Fig. 11) was outlined in the simulation, the parameters of which reflect the actual waveform. After the selection and activation of the sinusoidal filter to the system shown in Fig. 10, a sinusoidal phase voltage waveform was generated as shown in Fig. 12. The analysis of the obtained waveform showed a significant decrease in the level of higher harmonics (Fig. 13) and the THD factor (Table 2). The results of the simulations show that the use of a properly selected output sinusoidal filter enabled sinusoidal shaping of voltage in the 230 V AC on-board network as well as reducing the THD = 2.73% to a level acceptable by PN-EN 50121-3-2.
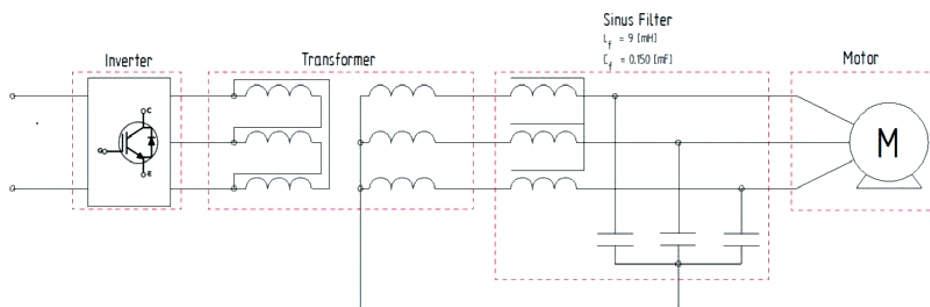
Fig. 10. Flowchart of the converter system modelled in Matlab Simulink
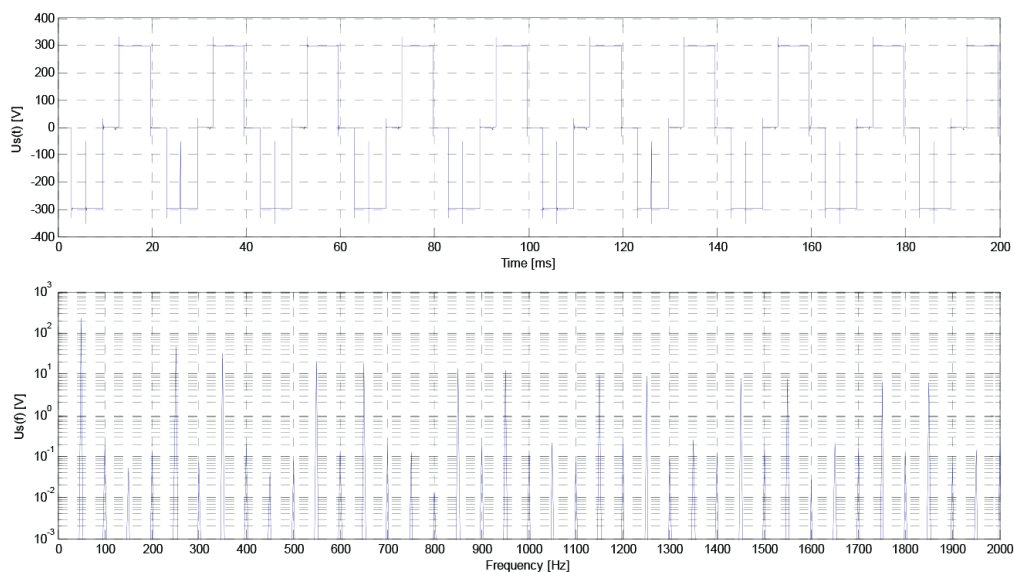
Fig. 11. Variable component of voltage supply and voltage harmonic spectrum – simulation without filter
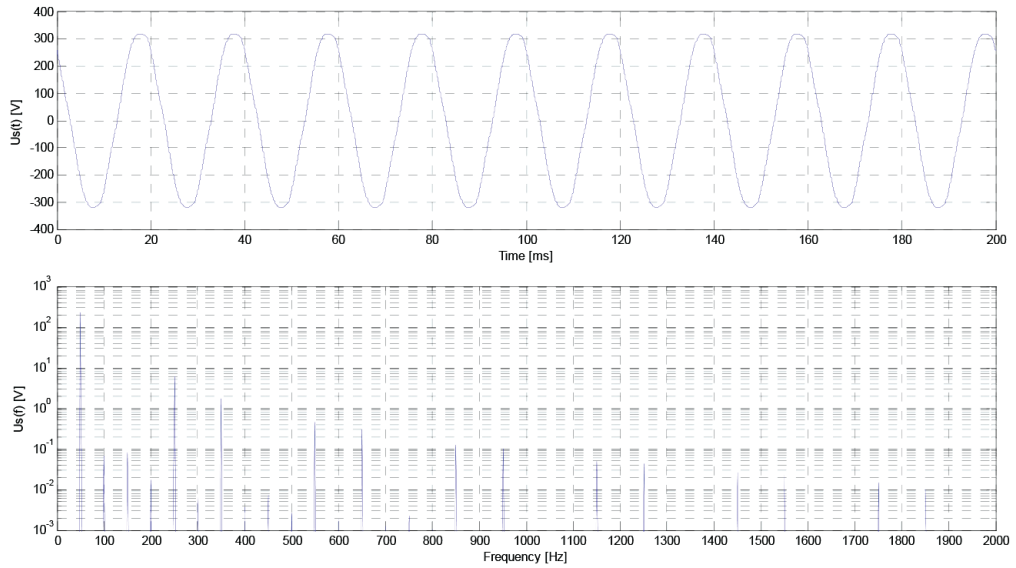
Fig. 12. Variable component of voltage supply and voltage harmonic spectrum – simulation with filter
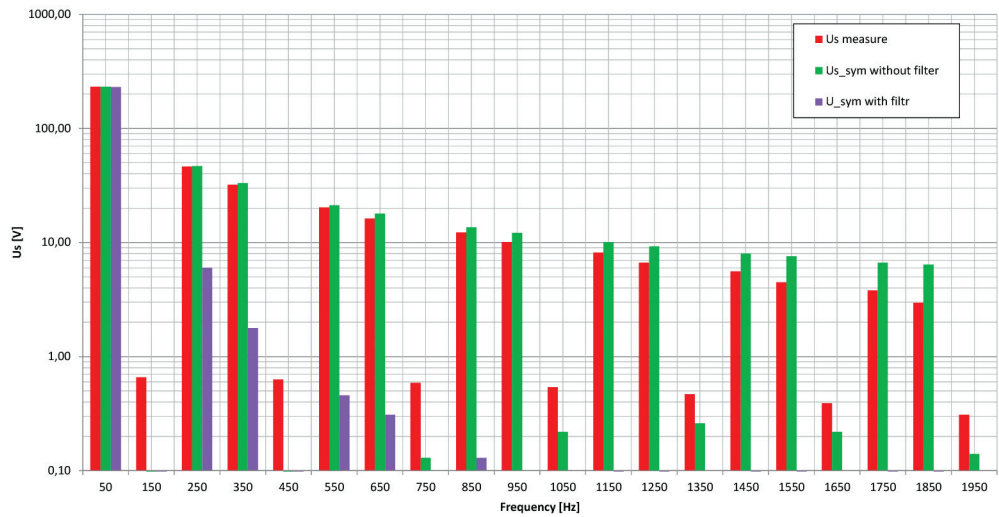

Fig. 13. Comparison of harmonic content in on-board power supply – measurement, simulation without filter, simulation with filter

Table 2. Factors characteristic to harmonic distortion – measurement, simulation without filter, simulation with filter

Factor	Us1	Us without filter	Us with filter
THD [%]	28.22	29.76	2.73
THDG [%]	29.66	29.76	2.73
THDSG [%]	29.23	29.76	2.73

6. Summary

The guidelines outlined in this article for testing the quality of an on-board 230 V AC grid and the results of the measurements conducted for the selected grids provide an overview of the need to ensure the required quality of power supply. The tests performed for selected on-board grids in traction vehicles in which sinusoidal output voltage waveforming methods were applied meet the requirements of PN-EN 50121-3-2. The results of the calculation of the total harmonic distortion for these grids show a comparable quality of voltage for both a typical power supply and an uninterruptible power supply. Further calculations for group harmonic distortion and subgroup harmonic distortion have shown that in properly conducted FFT analysis, no significant differences are observed. The harmonic grouping methods presented herein and detailed in PN-EN 61000-4-7 may, however, be useful for improving the accuracy of the determination of both voltage harmonics and harmonic distortion. The results of the simulations show that the use of a properly selected output sinusoidal filter enabled sinusoidal shaping of voltage in the 230 V AC on-board network as well as reducing the THD to the level acceptable by PN-EN 50121-3-2.

References

[1] PN-EN 50121-3-2: Railway applications. Electromagnetic compatibility. Part 3-2: Rolling stock. Apparatus.

[2] PN-EN 61000-4-30: Electromagnetic compatibility (EMC). Part 4-30: Testing and measurement techniques. Power quality measurements methods.

[3] PN-EN 61000-4-7: Electromagnetic compatibility (EMC). Part 4-7. Testing and measurement techniques. General guide on harmonics and interharmonics measurements and instrumentation, for power supply systems and equipment connected thereto.

[4] Skarpetowski G., Zając W., Czuchra W., *Analytical Calculation of Supply Current Harmonics Generated by Train Unit*, 12th International Power Electronics and Motion Control Conference EPE-PEMC 2006, Portoroż 2006.

[5] Białoń A., Czuchra W., Zając W., *Research of the interference effects caused by locomotives with asynchronous motors on rail traffic control equipment*, International Symposium on Electromagnetic Compatibility EMC EUROPE 2002, September 9–13, Sorrento, Italy, Conference Materials, Vol. 2, 1027–1030.

[6] Zając W., Czuchra W., *Computer modelling of a system: supply circuit – locomotive with AC motors in order to determine current harmonics*, 10thInternatinal Power Electronics and Motion Control Conference EPE-PEMC 2002 Cavtat & Dubrovnik 9–11 September 2002, Croatia, Conference Materials, Vol. 1, pp. 285 (summary), Full text – CD-ROM.

[7] Czuchra W., Zając W., *Time-frequency analysis of traction vehicles' supply current,* [in:] *Electrical engineering in traction applications,* Cracow University of Technology 2014, 73–83.

[8] Jiao J., Wen Y., Li M., Rao J., *Research on Vehicle Onboard Measurement System of Traction Harmonic Current for Analyzing Interference on Track Circuit,* 2015 IEEE 6th International Symposium on Microwave, Antenna, Propagation, and EMC Technologies (MAPE), 475–478.

117

Marek Dudzik
marekdudzik@pk.edu.pl

Janusz Prusak
Faculty of Electrical and Computer Engineering, Cracow University of Technology

Sławomir Drapik
ELECTREN S.A.

Valeriy Kuznetsov
Dniepropetrovsk National University of Railway Transport (DIIT), Ukraine

The efficiency of using artificial feedforward neural networks with a single hidden layer of eight neurons for the analysis of overload conditions of selected tramway traction substations

Efektywność wykorzystania sztucznych sieci neuronowych, typu feedforward o jednej warstwie ukrytej ośmio-neuronowej, do analizy przeciążeń wybranej tramwajowej podstacji trakcyjnej

Abstract

This paper presents further results of research on the load variability of rectifier units for the selected tram traction substation. Actual measurements were used in the performed analysis. This time, the analysis was focused on the characteristics of maximum loads and overloads for time periods of five minutes and sixty minutes, for a number of selected cases. The second part of the article discusses the effectiveness of the use of artificial neural networks of the feedforward type with one hidden layer with eight neurons to analyse the overloads of the traction substation over a longer time scale. The obtained positive results indicate that this type of research should be continued, using different variants of artificial neural networks.

Keywords: loads and overloads of tram traction substation, artificial neural network

Streszczenie

W artykule przedstawiono kolejne wyniki badań zmienności obciążeń zespołów prostownikowych wybranej tramwajowej podstacji trakcyjnej. Do analiz wykorzystano rzeczywiste wyniki pomiarów. Tym razem zwrócono uwagę na specyfikę maksymalnych obciążeń i przeciążeń w odcinkach czasowych 5 min i 60 min – dla kilku wybranych przypadków. W drugiej części artykułu przedstawiono efektywność wykorzystania sztucznych sieci neuronowych, typu feedforward o jednej warstwie ukrytej z ośmioma neuronowami, do analizy przeciążeń dla eksploatacji podstacji trakcyjnej w dłuższej skali czasowej. Uzyskane pozytywne wyniki wskazują na konieczność kontynuowania tego typu badań, m.in. wykorzystując inne warianty sztucznych sieci neuronowych.

Słowa luczowe: obciążenia i przeciążenia tramwajowej podstacji trakcyjnej, sztuczne sieci neuronowe

1. Introduction

Rectifier systems in tramway traction substations undergo varying loads [3, 15, 20]. The studies conducted by the authors [1, 2, 4, 6–8, 16, 17] have confirmed this hypothesis. It has also been found that DC power supply systems of the electric traction have some power redundancy resulting from the required overrating e.g. parameters of rectifier systems forming the basic equipment of the substations in question *with this sentence structure – it is unclear exactly what this is an example of – this needs rephrasing*. Further studies and analyses of traction load details should aid the development of load description tools to better perform engineering calculations. The development of engineering tools to better *'better' is very vague and subjective – for the sake of clarity, consider choosing something more specific and objective* describe possible traction loads of improved power supply units is a comprehensive task. One of the aspects of key importance in this regard is presented below

2. Particulars of loads occurring in the traction sub-station concerned

The registered loads taken to analysis and described to some extent below occurred to the tramway traction substation located almost in the middle of a large city with a rail and road traffic hub of high traffic density [5, 9–11]

2.1. Examples of momentary traction load values

Figure 1 shows some graphs of momentary traction current values which occurred in the rectifier units of the abovementioned tramway traction substation. One normal working
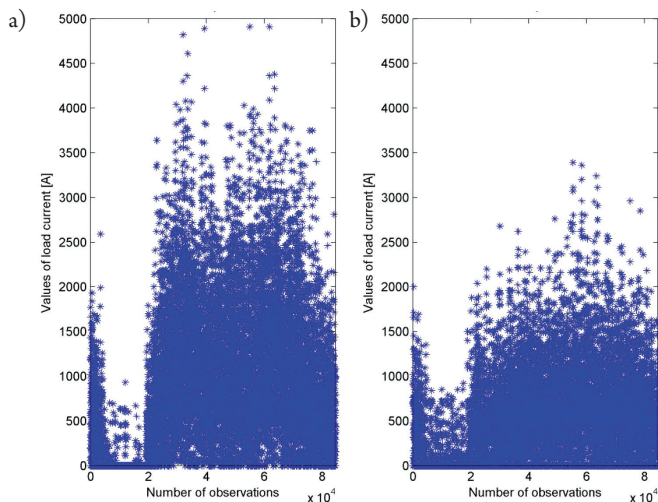

Fig. 1. Registered momentary values of load current in the 'Czyżyny' traction substation on: a) 23rd Oct 2013 (Wed), b) 27th Oct 2013 (Sun) [5, 11, 22]

day (23rd Oct 2013 – Wednesday) and one public holiday (27th Oct 2013 – Sunday) were considered for the presentation. The provided results refer to two days which cover approx. 0.55% of the calendar year, and currently used engineering tools are based on the assessment of annual power consumption. Much longer periods of time are considered later in this paper.

These results show that the 'Czyżyny' traction substation was not fully loaded within the considered days [5, 11]. For example, the load applied to the substation was equal to the continuous power of the four rectifier units the substation is equipped with for a total of only six minutes and the substation (rectifier units) remained load free for a total duration of almost five hours within the working day. All four transformers of the rectifier units consumed power from the grid within this time only to cover idle running losses.

2.2. Examples of momentary traction load values

The measurement results provided in this section of the paper and selected aspects of their analysis refer to the period of time [9, 22] covering sixteen consecutive calendar weeks within an autumn and winter season (from 1st Sept 2014 to 21st Dec 2014). Some parts of the submitted results were subsequently subject to analysis performed using artificial neural networks (Chapter 3). Figure 2 shows the average values of traction load currents occurring in the individual weeks of the test period.
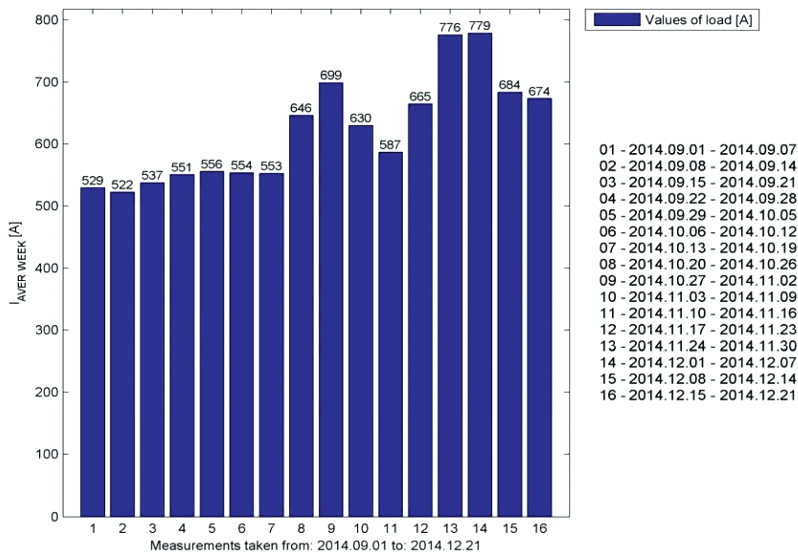
Fig. 2. Average values of traction load currents occurring in the individual weeks [9]

The above figure shows that the substation was subject to a varying load during the individual weeks of the test period. The highest average current value (i.e. the largest power consumption) occurred during the 14th week and amounted to 778.74 A, which is 1.25 times more than the average current value for this period (621.61 A).

Figure 3a shows the average values of traction load current occurring on the individual days (with a 24-hour period); Figure 3b shows a graph of these loads in a descending order, from the highest value (965.38 A) to the lowest value (304.11 A).
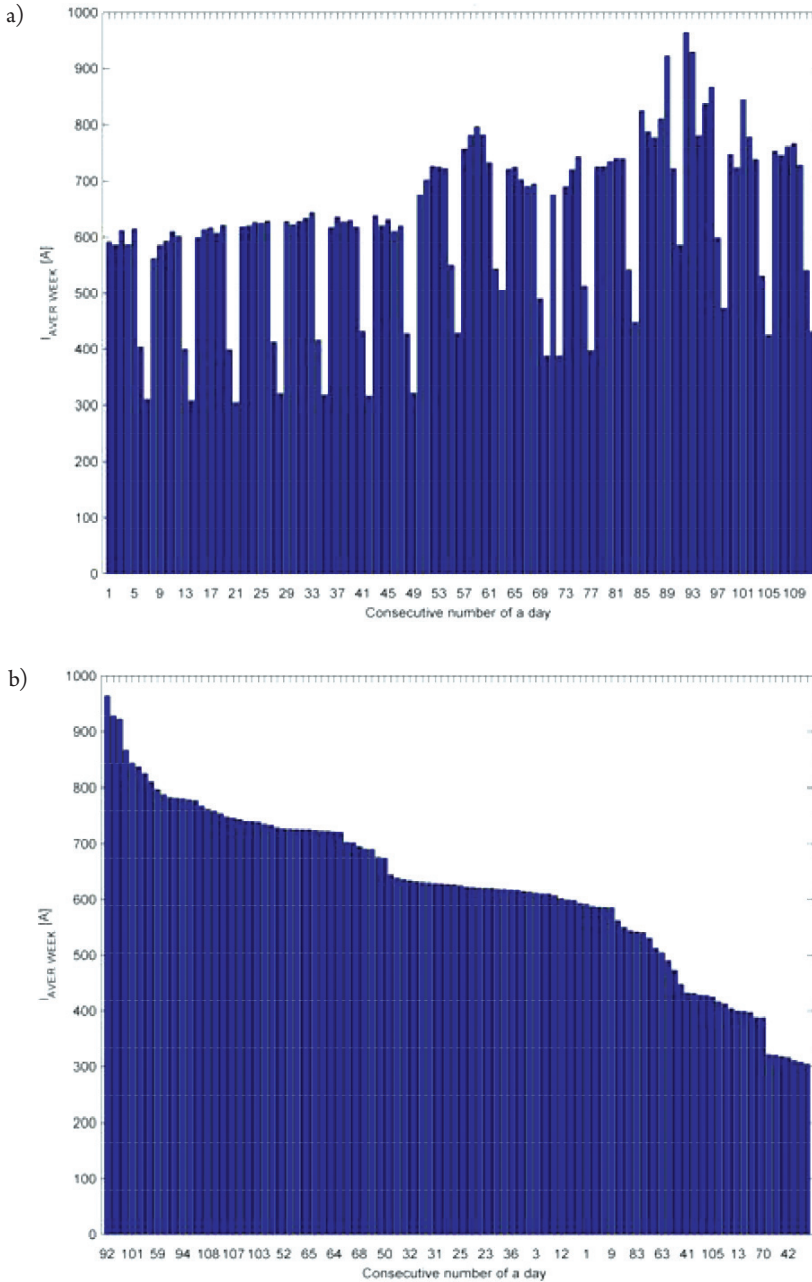

Fig. 3. Average values of traction load currents occurring on individual days:a) in the order in which they occurred, b) in descending order [9]

Additional figures show the graphs of momentary values of load currents occurring in the traction units selected by the following criteria:

- ▸ Figure 4 shows the graph of maximum average current value occurring within a five-minute timespan of all five-minute timespans within the 112 analysed days,
- ▸ Figure 5 shows the graph of current occurring within a five-minute timespan among all five-minute timespans in the 24-hour period in which the five-minute overload factor was the highest,
- ▸ Figure 6 shows the graph of maximum average current values occurring within a sixty-minute timespan of all sixty-minute timespans within the 112 analysed days,
- ▸ Figure 7 shows the graph of current occurring within a sixty-minute timespan among all sixty-minute timespans in the 24-hour period in which the sixty-minute overload factor was the highest.
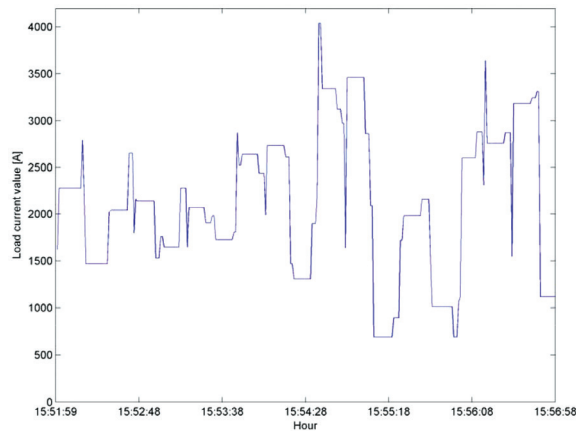
Fig. 4. The graph of load current for a 5-min. timespan in the day (24 hr) within which the maximum 5-min. overload falls (the authors' own elaboration)
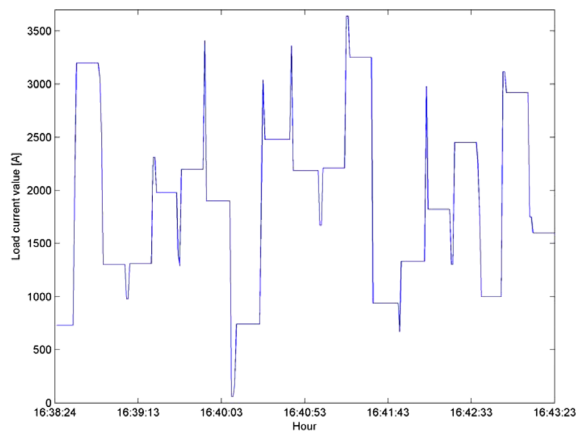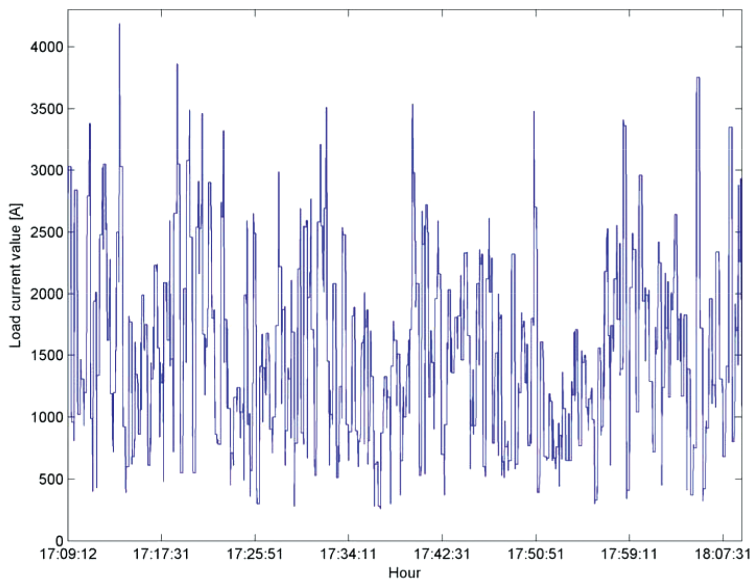

Fig. 5. The graph of load current for a 5-min. timespan in the day (24 hr) within which the maximum 5-min. overload falls (the authors' own elaboration)

For the purposes of this section, the overload is the ratio of the maximum average current value in the given timespan (either 5 or 60 mins) and the average current value in the given day (24-hour period). This factor is designated by the authors as 'α'.

Quantitative comments to the graphs plotted in the above figures are provided in Table 1.

Fig. 6. The graph of load current for a 60-min. timespan in the day (24 hr) within which the maximum 60-min. overload falls (the authors' own elaboration)
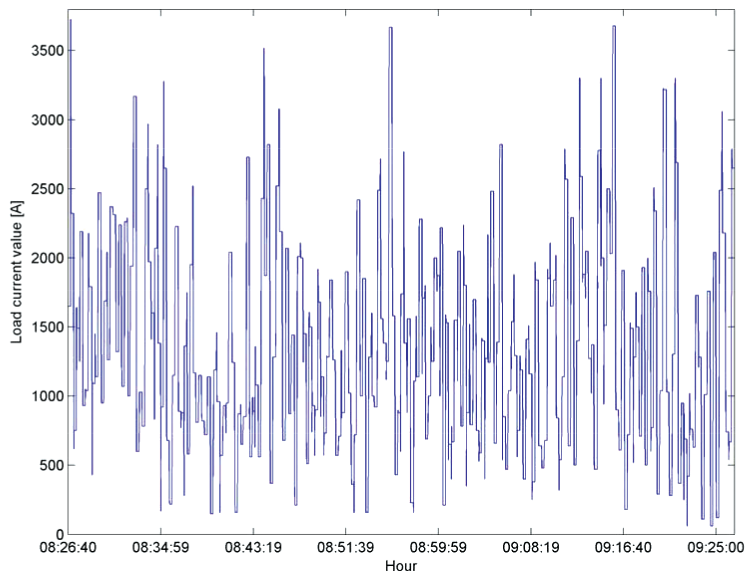
Fig. 7. The graph of load current for a 60-min. timespan in the day (24 hr) within which the maximum 60-min. overload falls (the authors' own elaboration)

Table 1. Parameters for graphs of loads for the 5- and 60-min. timespans within the days (24 hr) of highest and maximum loads within the selected span (the authors' own elaboration)

Item	Timespan	Determinant	Consecutive day number	Date	Time of occurrence	Max. value [A]	Average value [A]	Effective value [A]	Form coefficient [-]	Peak coefficient [-]
1.	5 min	Maximum load	89	28/11/2014	15:51:59 15:56:58	4,040	2,126	2,260	1.0630	1.7873
2.	5 min	Maximum overload factor	18	18/09/2014	16:38:24 16:43:23	3,640	1,890	2,048	1.0835	1.7767
3.	60 min	Maximum load	92	01/12/2014	17:09:12 18:09:11	4,190	1,518	1,686	1.1100	2.4851
4.	60 min	Maximum overload factor	43	13/10/2014	08:26:40 09:26:40	3,730	1,327	1,518	1.1436	2.4566

The above figures show that in-spite of noticeable fluctuations, the traction load currents did not fall to zero. Figure 3 demonstrates the highest average value of traction load occurring within day 92 (1st Dec 2014). Table 1 also shows that, for example, the 60-min. timespan with the highest average load value of all 112 analysed days (Fig. 6) also falls on day 92; this occurred in the late afternoon (17:09:12 – 18:09:11).

The other three cases indicated in Table 1 fell on the other days in which the load was lower than the load which occurred on day 92. This observation as well as the other results provided in the table additionally confirm that the traction load fluctuates and is of a complex nature.

Further studies on this matter should enable better investigation of the properties and nature of traction loads. The results obtained should facilitate the development of better engineering tools and/or new solutions for DC traction power supply units [14].

3. Introductory information and input data

The calculations were performed using Matlab version R2011B. The input data for the ANN analysis was 112 pairs of numbers. In each pair, one of the numbers (input) was the temperature value and the other number (output) was the substitute thermal factor corresponding to the temperature.

Measurement data processing was performed using a two-layer feedforward neural network implemented in Matlab. Figure 8 shows the neural network block created in the Simulink environment.
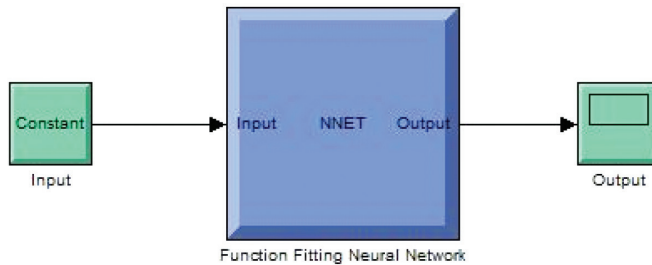

Fig. 8. The neural network block created in the Simulink environment; own work

Figure 9 depicts the created neural network structure. This structure had one hidden layer consisting of four neurons. There were no delays implemented on the input for this layer. The activation function for the hidden layer was tangensoidal (tansig). The output layer had a linear activation function.
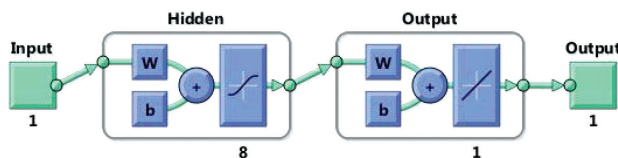

Fig. 9. The created neural network structure; own work

The aim of the study was to approximate the function that would relate the temperature factor value for each thermal coefficient corresponding to the temperature.

The results shown below in Section 4 were obtained for the following ANN training settings:

- ▶ maximum number of epochs to train: 1000
- ▶ performance goal: 0
- ▶ learning rate: 0.01
- ▶ maximum validation failures: 12
- ▶ momentum: 0.9
- ▶ minimum performance gradient: 10^{-10}
- ▶ epochs between displays: 25
- ▶ maximum time to train in seconds: infinite

In order to teach the designed artificial neural network, one-way network (up to three layers) training was used according to the Leveneberg-Marquardt algorithm.

4. Computation

Figure 10 depicts results obtained from the training, validation and test of the ANN in the form of an error histogram.
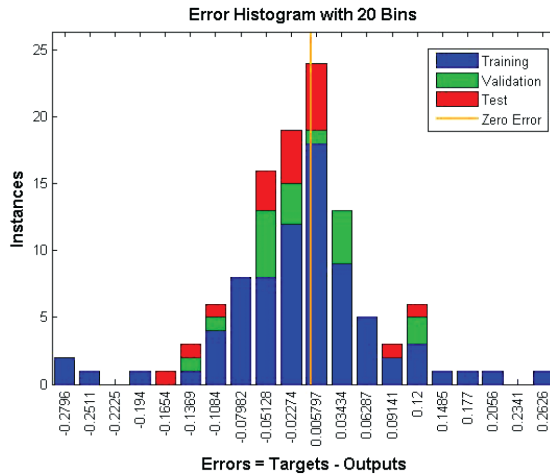

Fig. 10. Error histogram (own work)

Figure 11 presents an illustration of the performance of the ANN for successive learning epochs.

Figure 11 presents the artificial neural network performance graph during learning. The ordinate axis refers to the ANN performance function values. The mean square error ('MSE') was chosen as the performance function. The horizontal axis corresponds to learning epochs. The system reached the best neural network validation of the ANN performance for the fifth epoch and it was '4.5551'·10^{-3}. One can observe that the neural network system continued the
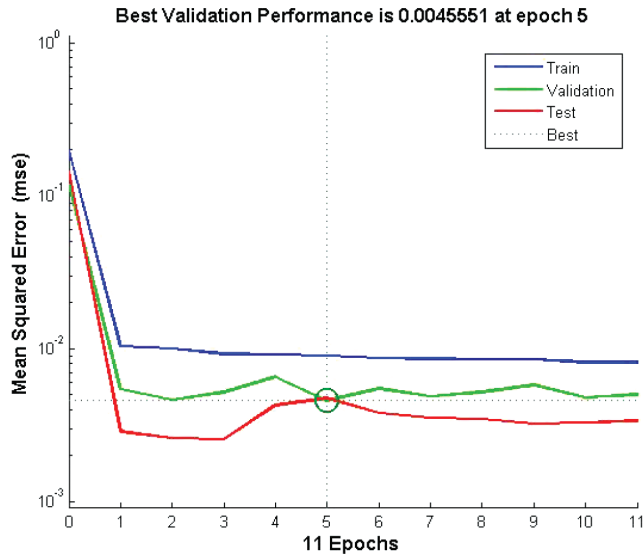
Fig. 11. Performance of the ANN (own work)

learning algorithm for another twelve epochs in order to confirm the alleged local minimum for the goal set for the created network structure (Fig. 9). From epoch 1 to 5, a downward trend in validation tests of the ANN learning can be seen.

Figure 12 depicts the regression results for the training, validation and test, and the regression for all data assigned to the ANN learning with a supervisor. Here, the ordinate axis represents the neural network output for the given input data. The abscissa axis shows values from the actual measurements (targets), to which the values returned by the ANN should be convergent.

The $R = 1$ regression result means that there is an unequivocal relationship between the actual value (target – from measurement or simulation) and the neural network output value.

The regression results for the discussed case are as follows. The regression for the data assigned to the training reached $R = 0.69866$. The data constituted about 70% of all data assigned to the ANN learning with a supervisor. The regression for the validation was $R = 0.80432$. The data used for this step were about 15% of all data. Lastly, the regression for the test was $R = 0,74238$. Consequently, the data used in this stage was about 15% of all data. One more regression value was calculated; this represents all data and was $R = 0.7109$.

The training, validation and test are performed during the procedure of neural network learning.

Figure 13 presents the results obtained from the approximation process (function fitting process) performed by artificial neural network learning. In this figure, dots represent the actual values of the substitute thermal factor obtained from measurements (targets), while cross marks represent the results of the approximation. Vertical lines indicate absolute errors between actual values and the corresponding results obtained by the function fitting process. The solid line is the plot of the resulting approximating function.
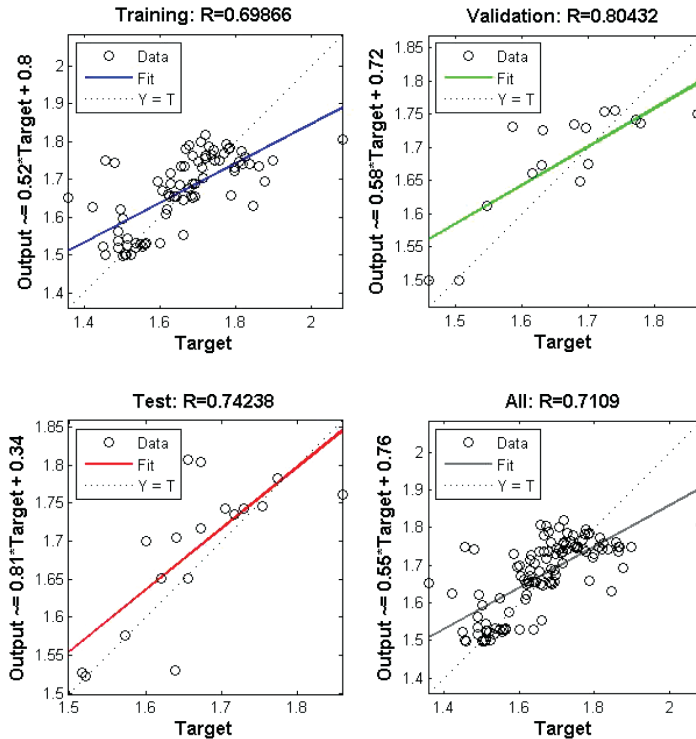
Fig. 12. Regression results for the training, validation and test and the regression for all data assigned to the ANN learning with a teacher (own work)
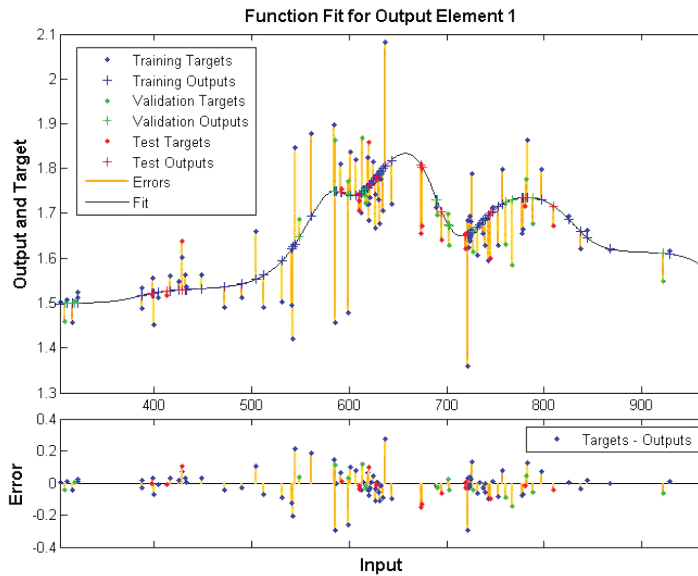

Fig. 13. Results of function fitting with the use of the ANN; output – substitute thermal factor; input – the temperature (Own work)

129

5. Summary

The results of the analysis relating to the character of the overload conditions of the traction substation using neural networks allow continuous development itself. Compared to previous articles [12], the data presented in this paper has improved consider stating how it has improved; this is because it is based on a new model of SSN. This is an example of regression calculated for all of the measurement data. In the article [12], the value of that regression was R = 0.68304, now it is R= 0.72248. The improvement was achieved by extension (more neurons) of the hidden layer.

The presented studies imply the necessity to conduct further research across a wider range. Authors in subsequent articles will undertake analyses of the influence of the structure on the results achieved through modelling the phenomenon.

References

[1]   Białoń A., Chrabąszcz I., Hudym W., Kaczmarczyk A., Prusak J., *Wpływ odległości kolejowych podstacji trakcyjnych na rozkład obciążeń między nimi – symulacyjna ocena wybranych przypadków*, TTS Technika Transportu Szynowego, 7-8/2015, 80–82.

[2]   Chrabąszcz I., Drapik S., Dudzik M., Kaczmarczyk A., Prusak J., *Analiza obciążeń zespołów prostownikowych, dla „inteligentnych" kolejowych podstacji trakcyjnych DC – wstępne badania symulacyjne wybranych przypadków*, Logistyka 6/2015, 990–999.

[3]   Chrabąszcz I., Prusak J., Drapik S., *Trakcja elektryczna prądu stałego. Układy zasilania.* Podręcznik INPE dla elektryków, Zeszyt nr 27, Kraków – Bełchatów, 2009.

[4]   Drapik S., Dudzik M., Kobielski A., Prusak J., *Komparatywna ocena zmienności obciążeń kolejowych podstacji trakcyjnych.* 11th International Conference „Modern Electric Traction" MET'2013, Poland Warsaw, October 10 – 12. 2013; materiały konferencyjne, 62–67.

[5]   Drapik S., Kaczmarczyk A., Kobielski A., Prusak J., *Charakter zmienności obciążeń tramwajowych podstacji trakcyjnych zasilających linie o różnej specyfice ruchu pojazdów*, TTS Technika Transportu Szynowego, 6/2015, 43–48.

[6]   Drapik S., Kobielski A., Prusak J., *Fluktuacja obciążeń podstacji trakcyjnych w ujęciu teorii szeregów czasowych.* TTS Technika Transportu Szynowego, 7–8/2010, 59–64.

[7]   Drapik S., Kobielski A., Prusak J., *Selected issues of traction substation load* variability, Chapter 5, 47–58, Monografia Politechniki Gdańskiej Modern Electric Traction, Power Supply, Edited by Krzysztof Karwowski, Adam Szeląg, Gdańsk University of Technology, Faculty of Electrical and Control Engineering, Gdańsk 2009.

[8]   Drapik S., Kobielski A., Prusak J., *Wybrane aspekty zmienności obciążeń kolejowych podstacji trakcyjnych.* TTS Technika Transportu Szynowego 4/2010, 27–31.

[9]   Drapik S., Kuzniecow W., Markowski P., Prusak J., Woszczyna B., *Badanie skali zmienności obciążeń wybranej tramwajowej podstacji trakcyjnej na podstawie rzeczywistych wyników pomiarowych dla spójnego okresu czasowego obejmującego szesnaście tygodni*, Logistyka 6/2015, 1026–1035.

[10] Drapik S., Markowski P., Prusak J., Woszczyna B., *Analiza obciążeń zespołów prostownikowych przed i po wystąpieniu przeciążenia na przykładzie wybranej tramwajowej podstacji trakcyjnej*, TTS Technika Transportu Szynowego, 12/2015, 427–434.

[11] Drapik S., Markowski P., Prusak J., Woszczyna B., *Tramwajowe podstacje trakcyjne – wybrane problemy bezpieczeństwa ekologicznego w świetle oceny ich obciążeń*, Logistyka 4/2015, 3017–3027.

[12] Dudzik M., Drapik S., Prusak J., *Approximation of overloads for a selected tram traction substation using artificial neural network algorithms*, not published.

[13] Hilgard E.R., *Wprowadzenie do psychologii*, Państwowe Wydawnictwo Naukowe, Warszawa 1973.

[14] Jagiełło A.S., Chrabąszcz I., Drapik S., Dudzik M., Kobielski A., Prusak J., *System do aktywnej regulacji obciążenia zespołów prostownikowych kolejowej podstacji trakcyjnej. Sposób aktywnej regulacji obciążenia zespołów prostownikowych kolejowej podstacji trakcyjnej*, Rozwiązanie zarejestrowane w Urzędzie Patentowym RP na rzecz Politechniki Krakowskiej pod numerem P.511511,objęte ochroną prawną od dnia 10.03.2015.

[15] Kałuża E., Bartodziej G., Ginalski Z., *Układy zasilania i podstacje trakcyjne*, Skrypty uczelniane Politechniki Śląskiej nr 1220, Gliwice, 1985

[16] Kobielski A., Drapik S., Dudzik M. Prusak J., *Time Series as an Aid to Research of traction Substation Load*, JEPE Journal of Energy and Power Engineering, Volume 7, Number 5, May 2013 (Serial Number 66), David Publishing Company, El Monte, USA, 979–986.

[17] Kobielski A., Drapik S., Dudzik M., Prusak J., *Niektóre problemy analizy i modelowania zmienności obciążeń kolejowych podstacji trakcyjnych*, Monografia 450: Elektrotechnika w Zastosowaniach Trakcyjnych; seria: Inżynieria Elektryczna i Komputerowa, edited by A.S. Jagiełło, Politechnika Krakowska, Kraków 2014, 237–249.

[18] Kobielski A., Drapik S., Dudzik M., Prusak J., *Wstępne studium efektywności zastosowania sieci neuronowych w badaniach obciążeń kolejowych podstacji trakcyjnych*, TTS Technika Transportu Szynowego, 10/2014, 40–43.

[19] Korbicz J., Obuchowicz A., Uciński D., *Sztuczne sieci neuronowe. Podstawy i zastosowania*, Akademicka Oficyna Wydawnicza PLJ, Warszawa 1994.

[20] Mierzejewski L., Szeląg A., Gałuszewski M., *System zasilania trakcji elektrycznej prądu stałego*, Wydawnictwo Politechniki Warszawskiej, Warszawa 1989.

[21] Tadeusiewicz R., *Sieci neuronowe*, Akademicka Oficyna Wydaw. RM, Kraków 1992.

[22] Wyniki pomiarów prądów obciążeń trakcyjnych kabli zasilających podstacji tramwajowej nr „01" („Czyżyny"), materiały udostępnione przez ZIKiT w Krakowie, 2015.

Dominik Oćwieja
    Independent expert

Paweł Markowski
    Graduate studies, Faculty of Mechanics, Cracow University of Technology

Janusz Prusak orcid.org/0000-0001-8037-1378

Bartosz Woszczyna orcid.org/ 0000-0002-2355-4175
bwoszczyna@pk.edu.pl
    Department of Traction and Traffic Control, Faculty of Electrical and Computer
    Engineering, Cracow University of Technology

THE RANGE OF LOAD VARIABILITY OF RECTIFIER UNITS WITH
A CONCENTRATED DISPOSITION OF TRAM SUBSTATIONS AS EXEMPLIFIED
BY A REAL TRAM LINE

PODSTACJE TRAMWAJOWE O ZAGĘSZCZONEJ LOKALIZACJI – ZAKRES
ZMIENNOŚCI OBCIĄŻEŃ ZESPOŁÓW PROSTOWNIKOWYCH,
NA PRZYKŁADZIE RZECZYWISTEJ LINII TRAMWAJOWEJ

Abstract

The first part of this paper presents a comparison of the measured and simulated results of the load variability of rectifier units of a tram traction substation. The subject of the tests was a power supply substation for the contact line of a tramway, the profile and traffic of which was known. After a positive appraisal of the applied simulation method, an assessment of the range of load variability for the rectifier units took place for a hypothetical situation involving the concentrated disposition (layout) of the traction substations (so-called micro-substations). The results acquired under the described circumstances are presented in the second part of this paper.

Keywords: tram traction substation, traction load variability, traction micro-substation

Streszczenie

W pierwszej części artykułu dokonano porównania wyników pomiarowych i symulacyjnych dotyczących zakresu zmienności obciążania zespołów prostownikowych tramwajowej podstacji trakcyjnej. Obiektem badań była rzeczywista podstacja zasilająca sieć trakcyjną na linii o znanym profilu i występującym na niej ruchem tramwajów. Po pozytywnej ocenie zastosowanej metody symulacyjnej – przeprowadzono ocenę zakresu zmienności obciążeń zespołów prostownikowych dla hipotetycznej sytuacji, polegającej na zagęszczeniu lokalizacji podstacji trakcyjnych (tzw. mikropodstacji). Uzyskane dla tych okoliczności wyniki znajdują się w drugiej części artykułu.

Słowa kluczowe: tramwajowa podstacja trakcyjna, zmienność obciążeń trakcyjnych, mikro-podstacja trakcyjna,

1. Introduction

Tram traction power supply systems used in our country consider changing to 'Poland' as this would be clearer and more conventional are all based on the same diagram [13, 24, 16] which has been in operation for a few dozen years. Also trams have been operating equally efficiently (more accurately, DC rail vehicles, equipped with resistor start-up systems and DC serial engines). Industry experts (but not only they) know that modern tram rolling stock has and asynchronous motors. Clearly, invested means into tests and design works as well as common acceptance of new solutions in opinion making and decision making environments bring positive results. Moreover, in the case of power supply systems, new solutions which are better adjusted to the specific loads they are subjected to must be based on extensive testing and analyses [3, 4, 8, 10, 12, 15, 17, 21, 22, 23].

Interesting results of tests [11] regarding use of, to a certain extent, doubled power supply in Warsaw trams concern mainly increase in efficiency of the railing stock under new circumstances.

During examinations and testing, researchers pay attention to the nature of traction loads, in particular, loads placed on rectifier units at substations [1, 9, 22, 23]. Research findings form the basis for solutions intended to improve the power supply to tram systems via overhead lines. In this paper, at the example of a real (active) tram line there was assessed an impact of application of other (selected) system solutions, concerning power supply for the tram contact line, on specificity of the traction.

2. Route profile and tram traffic

Traction loads depend on many factors [13, 14, 16]. Hereunder presented the most essential data reflecting the specifics of the considered tram line section. In the case of other sections of tram line, the acquired results may differ; this is because of their dissimilarity (just to mention the characteristics data hereunder)

The selected section of the tram line is supplied by a single traction substation; it is an ultimate double track extreme line with a loop at its end [7]. The length of the cruising section is 1800 m and the length of the loop is 300 m. In Fig. 1, there is presented course of the line at the background of the city plan, where the yellow color means the cruising section and the red one means the loop.

The tram line is located at 234 m a.s.l. 'at the loop' the track then rises to 262 m a.s.l. at a distance of approx. 1200 m from the loop. The track then drops to 252 m a.s.l. at the end of the power supply section. From the presented data, the difference between the highest and the lowest points at the track is 28 m.

Table 1 presents data regarding the profile of the vertical track that is inclination of the track-way to the level. In this case it is a product of change of the track height in meters and the length of the section where it exists, in km. Consequently, the result is in per promil.

Fig. 1. Course and location of the studied tram line section [19]

Table 1. Vertical profile of the track [19, 20]

	Distance [m]	Length	[‰]
1	Pętla	300	0
2	0	43	10
3	43	46	13
4	89	84	15,5
5	173	49	9
6	222	171	5
7	393	49	13.5
8	442	125	22
9	567	52	33.5
10	619	234	45
11	853	29	37.7
12	882	38	30
13	920	38	28
14	958	101	26
15	1059	41	22.5
16	1100	38	19
17	1138	110	6.5
18	1248	32	–6
19	1280	41	–9
20	1321	41	–11
21	1362	107	–13
22	1469	81	–27
23	1550	11	–40
24	1561	55	–32.5
25	1616	113	–25
26	1729	41	–13.5
27	1770	35	3

It can be observed that the vertical profile of the track is rather varied. The steepest uphill section is located at the 619th meter of the track as measured from the loop and it is 45 per promils In the track there are a total of 14 sections with an inclination which exceeds 15 per promils.

Table 2 presents data relating to the horizontal profile of the track. This is information regarding for which points on the track it is necessary to include additional resistances when doing calculations since the tram is not travelling in a straight line.

Table 2. Horizontal profile of the track [19, 20]

	Distance [m]	Length [m]	Radius [m]
1	Pętla	300	40
2	0.0	370	∞
3	370	105	186.2
4	475	288.75	452
5	763.75	96.25	186.2
6	860	280	∞
7	1140	43.75	45.2
8	1183.75	17.5	∞
9	1201.25	17	79.8
10	1218.25	43.75	42.5
11	1262	105	∞
12	1367	165	1048
13	1532	268	∞

At the tram loop there is a sharp turn (radius 40 m) and the trams must turn back onto a relatively short section (300 m). On the track there are 7 bends and 5 straight sections. The sharpest bends are situated at 1140 m (radius 45 m) and 1218 (radius 42 m) from the loop.

Data in the above table is necessary for simulation calculations with the applied theoretical drive method [16]. Obviously, some other data is required, such as data relating to stops on the tram-line or technical parameters of the vehicles themselves. In this paper, exemplary results of simulations are presented for the type 105N tram (Fig. 2) and the type NGT-6 tram (Fig. 3) for a drive from the loop (Fig. 1) to the downtown area.

Applying, among others, the above diagrams there were acquired certain resultant loads on the power supply cables and rectifier units described in the further part of the paper. It should be remembered that other circumstances, such as other track profiles, other tram railing stock and other data, type of which is not a secret for experts, may result in different final results.

A factor which has an impact on a value and a nature of loads on rectifier units there are also time-tables acc. to which trams drive (they should drive), in the area of the power supply of every traction substation. In Table 3, in a collective manner there is presented quantity of tram vehicles within the power supply area of the examined traction substation, with the assumption that trams drive in accordance with their scheduled timetables [20].
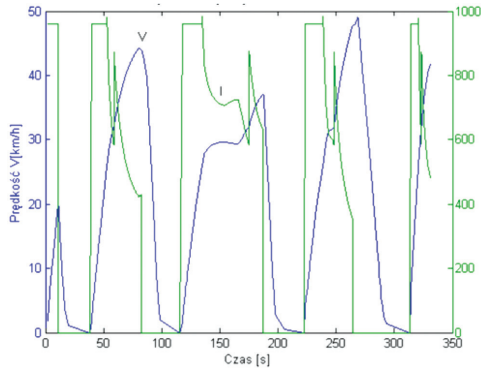

Fig. 2. Diagram of the current and speed
for a theoretical drive of the type 105N tram
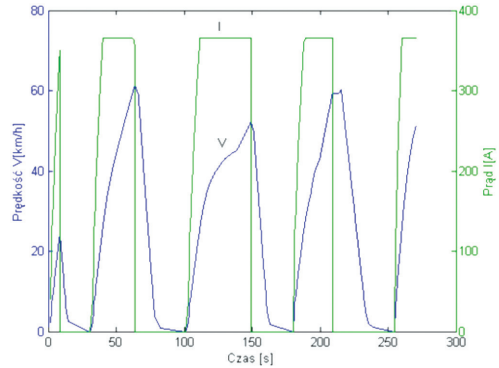(Blue – V(t); green – I(t)) (own materials)

Fig. 3. Diagram of the current and speed
for a theoretical drive of the type NGT-6 tram
(Blue – V(t); green – I(t)) (own materials)

Table 3. Number of drives for particular lines (own materials)

Line no.	Number of drives from the loop	Number of drives to the loop	Total
Business days			
6	73	76	149
24	57	55	112
50	144	144	288
Total	274	275	**549**
Saturdays			
6	36	36	72
24	54	53	107
50	87	86	173
Total	177	175	**352**
Sundays and holidays			
6	-	-	-
24	51	49	100
50	84	83	167
Total	135	132	**267**

As can be concluded from the above table, at the time of tram driving (04:30 to 23:50, according to the timetables) during a business day, a total of 549 trams drive which works

out as being 0.47 vehicles per minute. At the peak time, there was an average of 0.7 vehicles driving along the track per minute; this is a fairly high concentration of tram traffic.

The statement above is important in the context of the assessment of the specifics of existing rectifier unit loads, in particular in terms of applying their rated parameters which are described later in this paper.

3. Traction loads – results of measurements and calculations

This section presents the traction loads placed on the rectifier units of the operated traction substation calculated both on the basis of the measured results [7] and acquired by means of computer simulation based predominantly on the theoretical drive method [16].

The authors used a rather rare opportunity to compare the measured and computational results in order to have a reference to applied computational method.

Analysing the results herein it should be noted that there are various complex factors which temporarily affect the course of tractions loads [13, 14, 16]; this means that the recorded loads may seriously differ on different for the same timetable and the same remaining parameters (these have been partially described previously) [1, 3].

Figure 4 presents a diagram of traction current loads calculated on the basis of currents from 'feeders', with a frequency of 1 Hz for a business day.
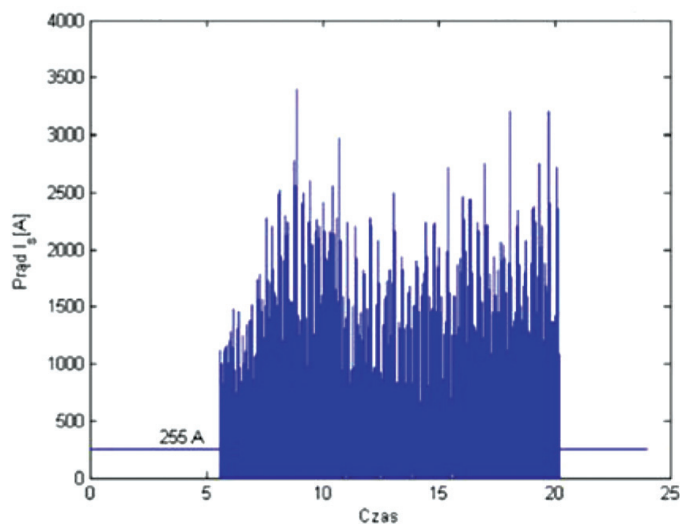

Fig. 4. Diagram of temporary currents on bus bars of the DC switchgear of the traction substation during a business day (own materials)

On the basis of the measurement data, it was determined that the average value of the current consumed by trams over 24 hrs was 255 A and the maximum value of the current was 3400 A – this occurred at around 9.00 am.

Figure 5 presents the course of the actual current capacity at the background of limits arising from the application of three rectifier units rated [9] at the substation [5].
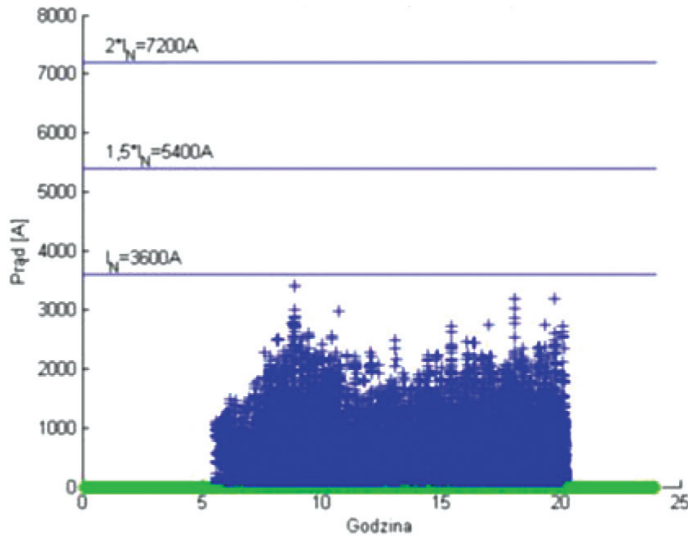

Fig. 5. Diagram presenting comparison of short-currents with rated data of the three rectifier units (own materials)

As shown in the above diagram, the total load placed on the rectifier units over a period of 24 hrs remains below the maximum long-term permissible load (I_N = 3600 A). Calculations revealed that for the presented case, the total time of no load (current of 0 A) was 50.4% of the 24 hr period. For 48.8% of the 24 hr period, the current did not exceed 1200 A. In order to secure such a load, it would be enough to have a single rectifier unit without the need to use its overload capabilities.

Figure 6 presents a diagram of simulated traction loads for rectifier units according to drive timetables valid on a business day.

In this case, the average value of the current over 24 hrs was 291 A, which is 14% higher than the measured value (255 A, Fig. 4). The highest temporary value of the current occurred before 5:00 p.m. and was 3,015 A. This is lower than the measured value (3,400 A, fig. 4) by approx. 11%.

Additionally, for the simulated course of the traction current (Fig. 6) there was checked total time (during 24h) of non-existence of the load (current equal 0 A). The obtained result of 45.7% was slightly lower than the measured data (50.4%). For 51.5% of the 24 hr time period, the current did not exceed 1,200 A. In this case, the value was slightly higher than the measured data (45.8%).

Previous experiences of the authors regarding the analysis of loads on tram traction substations [1, 3] prove that the loads in question may differ from each other on successive days. For the examined substations, it is possible to find days when measured results are close to simulated results, but opposite examples can also be found. The assessment of the nature of traction loads is still open

Continuing the comparison of the course of loads (Figs. 4 & 6), Table 4 shows values of shape and peak coefficients characterising the variability of electric runs [6].

Table 4. Comparison of the shape coefficient and peak coefficient for measured and simulated currents (own materials)

Type of a coefficient	Measurements	Simulation
Shape coefficient k_{kszt}	1.86	1.60
Peak coefficient k_{sz}	7.18	6.46

Both of the coefficients for the measured currents are slightly higher than the simulated currents; in particular, the shape coefficient is higher by approx. 14% and the peak coefficient by approx. 10%. This means that under actual conditions, the runs are more variable than those acquired theoretically.

Figures 7 & 8 present an assessment of the results acquired in a manner not described in the literature (this also apples to Fig. 5). The relationship between traction loads for successive hours and the rated parameters that is the long-term current load of the rectifier units of the examined traction substation is graphically presented.
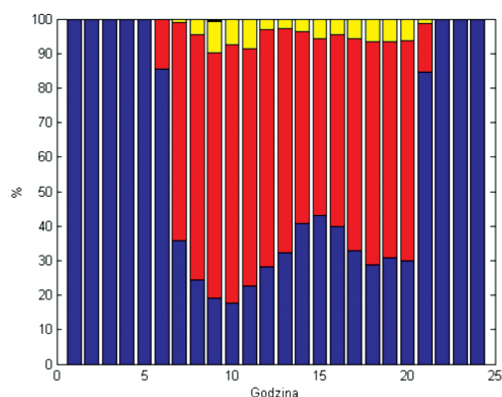

Fig. 7. Diagram of percentage content of currents in ranges for successive hours at bus bars of the examined substation on a business day – results of measurements (own materials)
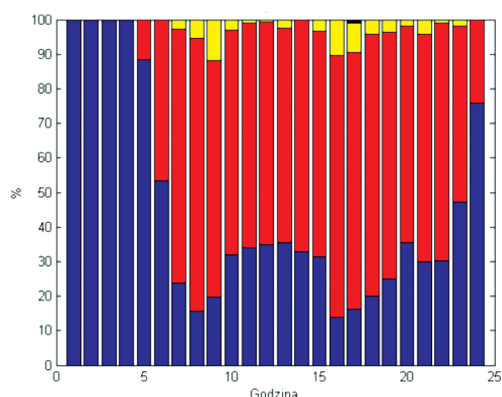
Fig. 8. Diagram of percentage content of currents in ranges for successive hours at bus bars of the examined substation on a business day – results of calculations (own materials)

Blue indicates the percentage time at every hour of the day when the short-term current is 0 A (no tractions load). Red indicates current from 0 A to 1,200 A (range of long-term load of a single rectifier unit). Yellow refers to current from 1,200 A to 2,400 A (it concerns two rectifier units), while black refers to currents exceeding 2,400 A (three rectifier units).

The results presented in the previous two figures can be interpreted in various ways, depending upon requirements. For example, similarities and differences between measured values and computed values can be identified in a measurable way. It is also possible to see the

timescale, for example, when rectifier units are not loaded, or for how long a single unit would be sufficient for a substation if only its long-term load was considered (without taking overload risk into account).

The results presented herein can provide the basis for interpreting other results, which can be achieved only by means of simulations; this concerns cases demonstrated below.

4. Concentrated location traction substations

Figure 9 presents the configuration of a contact line power supply which exists in the area of supply of the selected tram traction substation [5, 11].

As can be observed in Fig. 9, this substation is connected with a contact line by means of power supply cables, so-called 'feeders', which are individually named. Particular sections of the contact line supply are electrically separated by sectional isolators. Disconnecting switches visible in the schematic design, shunting the section isolators, at the time of normal use are open. For example, section isolator no. 8502 separates sections of the contact line powered by various neighbouring traction substations.
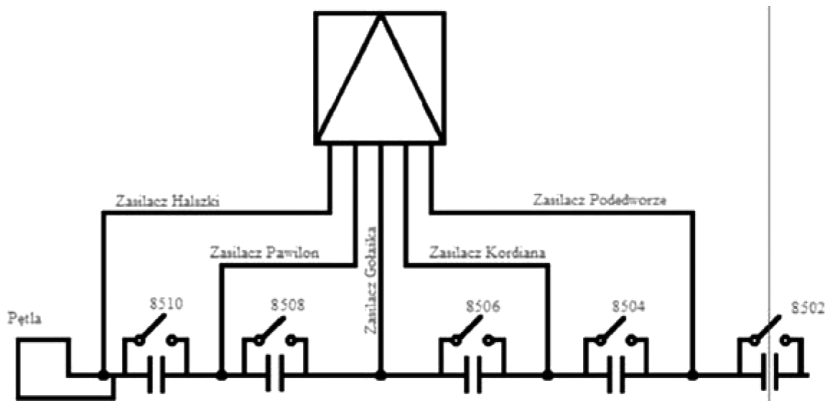
Fig. 9. Schematic design of the contact line power supply for the case under examination [5]

Certain aspects regarding the specifics of load variability of the traction substation's rectifier units supplying the contact line according to the diagram in Fig. 9 have already been demonstrated in this paper.

In Fig. 10, a proposal for the contact line power supply is presented for the same power supply area, but from separate miniaturised substations characterised by a concentrated disposition (layout).

It is noticeable that miniaturised sub-stations, marked as micro-substations in Fig. 10 (μP), are functionally assigned to existing feeders (Fig. 9) supplying energy to *five separate sections* of the contact line. As a result of such a power supply system, neighbouring micro-substations can carry out doubled (double side) energy supply for selected power supply sections by means of disconnecting switches which shunt the sectional isolators.
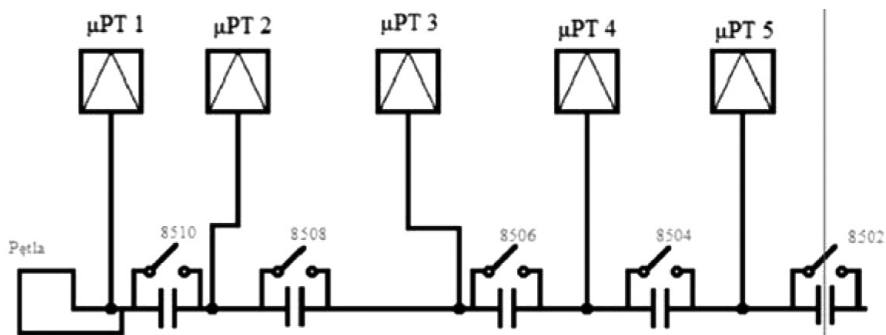
Fig. 10. A scheme design of the contact line power supply in the case of concentrated disposition of miniaturised substations (own materials)

Figure 11 presents a simulated course of the load of micro-substation no. 2, powering the section between sectional isolators nos. 8510 and 8508.

In Fig. 11, it is also marked that the average value of the load current over the 24-hour period was 83 A and the maximum value was 2,247 A. It was also calculated that the total time of no load was 76.8% of the day.
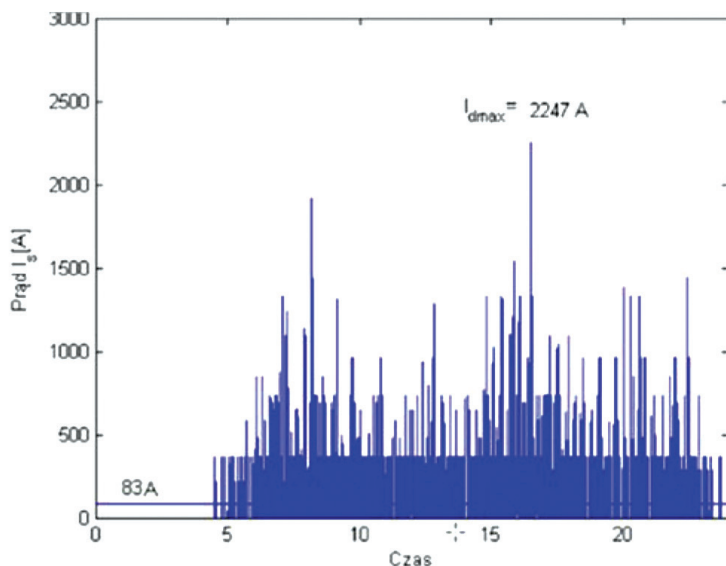
Fig. 11. Diagram of traction currents posing a load for the micro-substation no. 2 (own materials)

Assessment of the above simulated results can be extended on the basis of the previous point, which concerns data acquired by means of measurements and simulations.

Table 5 shows the coefficients of the shape and the peak [6] for the course of traction loads of micro-substations nos. 2 and 3, in the case of individual operation (single supply) and parallel operation (doubled supply), after switching off the sectional disconnecting switch no. 8508 (Fig. 10).

Table 5. Coefficients of the shape and peak of traction load currents for varied systems of contact line power supply from micro-substations nos. 2 and 3 (own materials)

Traction substation	Shape coefficient k_{kszt}	Peak coefficient k_{sz}
Micro-substation no. 2	2.51	10.48
Micro-substation no. 2 (parallel operation)	2.09	9.72
Micro-substation no. 3	2.44	9.46
Micro-substation no. 3 (parallel operation)	2.05	8.61

On the basis of the values of the coefficients in Table 5, it is clear that in the case of the doubled (two-side) power supply, the variability of traction loads is limited. Additionally, the total no load time concerning micro-substation no. 2 was shortened over the course of 24 hrs by up to 61.9%. One can expect reduced voltage limitation at tram current collectors [14, 16, 13, 18] and other benefits arising from a doubled power supply system.

Calculations were also performed regarding the selection of rectifier units for micro-substation no. 2 with the assumption of there being a doubled power supply that is for parallel operation with micro-substation no. 3.

The presented results concern a variant with a miniaturised rectifier unit. It was decided that the unit in question will be rated 5th overload class as the presently used rectifier unit [9]. However, the constant load current will be three times less that is it equals 400 A [5]. Figure 12 presents a course of simulated load at the background of limits arising from the application of two miniaturised rectifier units at a micro-substation.
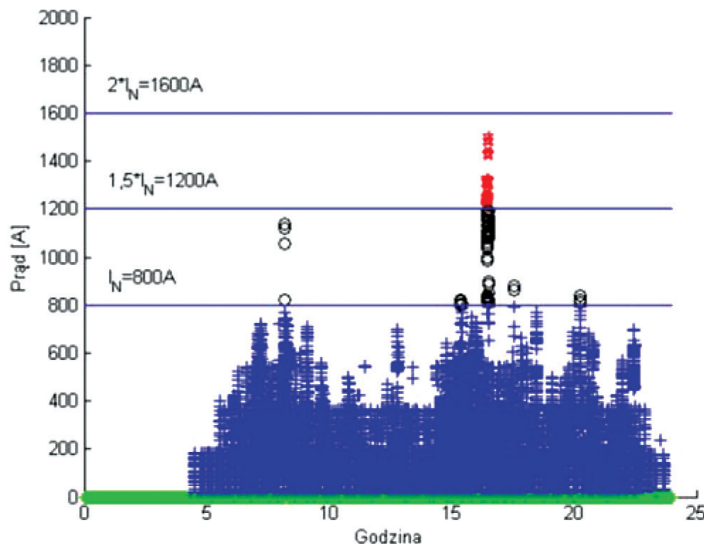

Fig. 12. Graph presenting a comparison of short-term currents and assumed rated data of two miniaturised rectifier units (own materials)

As observed in Fig. 12, the resultant rated parameters of two rectifier units will not be *again,* exceeded in the examined case. Most of the time, short-term currents have values below the rated value ($I_N = 2 \times 400\,A = 800\,A$).

In five cases, short-term currents stay within the range between the rated current value ($800\,A$), and value of the long-term overload ($1.5 \times I_N = 1200\,A$). However, in one case, short-term currents were within a range exceeding the long-term load ($1200\,A$), but they did not exceed the value of the short-term load ($2 \times I_N = 1600\,A$).

Comparing the diagrams presented in Figs. 12 & 5, it can be observed (optical value) that the range of use of parameters of micro-substation no. 2 rectifier units is better (more complete) than the currently used traction substation.

In the Faculty of Tractions and Traffic Control at the Technical University in Kraków a prototype model (mock-up) was erected representing a section of the tram control line power supply system. A unique attribute of this mock-up is that it has been designed and erected in order to test phenomena (currents, voltages) occurring in the elements of the power supply system. Existing in Europe (e.g. in Poland: experimental track of the Institute for Railway in Żmigród – Węglewo) testing grounds are designed to test railing stock this. The testing of new ideas for power supply systems is not possible in the field. Figure 13 presents a picture of the erected mock-up from the side of the front plate; the basic functional panels designed to expand the measurement capabilities that can be performed are indicated.
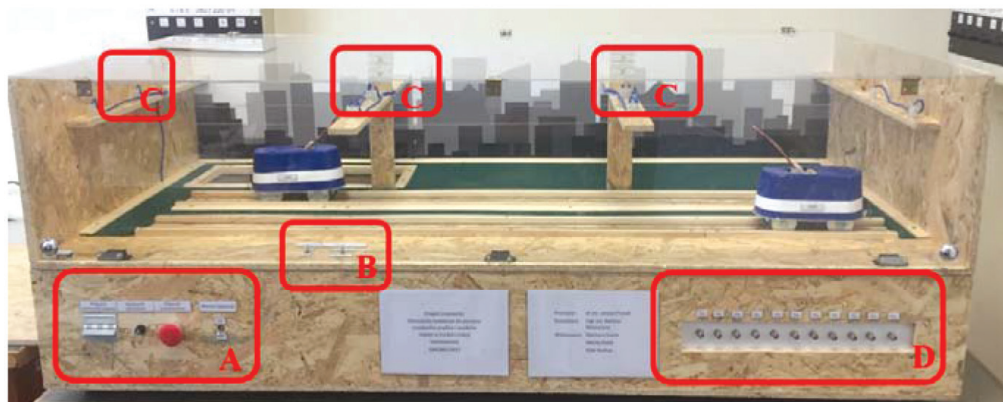
Fig. 13. General view of the mock-up, where: A – panel switching on the stand; B – substation additional resistance control panel; C – line and sectional disconnecting switch; D – measurement lines panel

Either state what or simply delete this with use of the mock-up, certain measurements were made for typical (for a present operation) connections in the DC power supply system. Satisfactory results had been acquired which means results were expected. It can be expected that results for atypical connections that are worthy of examination will also be reliable. The performed measurements enabled us to identify imperfections within the erected model; however, this is the typical situation in the case of prototypes.

The presented idea for the application of traction micro-substations to supply tram contact lines could be a stage of works focused on improvement of the municipal transport electrical power supply system.

5. Summary

The application of simulation methods for determining traction loads based on a theoretical drive brings results which, at the present stage of analyses, can be considered to be sufficiently accurate.

Application of the tram power supply system based on the concentrated disposition (layout) traction substations (so-called micro-stations) requires the erection of rectifier units with parameters suitably adjusted for the new solutions. This remark also concerns remaining technical equipment for these substations this is confusing as I can't work out exactly what point you are trying to make here.

Presented specificity (nature) again, this doesn't work – I'm not sure what you are referring to of short-term traction substations enables, among other things, the identification of time periods with zero load currents.

The presented solution of a supply system based on the traction micro-stations enables the non-complicated application of a doubled, railway type supply, with all the advantages associated with this solution.

Application of the mock-ups reflecting DC electric traction power supply systems (here, for trams), due to observances may promote didactic and training processes as well as R&D goals resulting in modernization of such systems in order to increase, e.g. their efficiency. Obviously, tests, particularly tests of new solutions on properly erected mock-ups do not pose a competition, but they are intended and desired supplementation of results acquired by means of simulation calculations. The most important and valuable results are those acquired from measurements of 1:1 scale objects. The application of mock-ups before tests in real conditions will, in the authors' opinion, reduce the costs of the tests due to the possibility of initial choice of the best parameters solutions

The presented system solutions and results picturing a nature of traction loads may be the inspiration for further solutions for improving the efficiency of tram power supply systems. In the electric power supply systems of municipal and suburban transport, direct voltages are applied, although other types of voltages have been applied in railway transport in many countries. Commencing the modernisation of operations would mean large scale investments; this is unquestionably good news for business environments I'm which want to support this type of transport.

References

[1] Drapik S., Markowski P., Prusak J., Woszczyna B., *Analiza obciążeń zespołów prostownikowych przed i po wystąpieniu przeciążenia na przykładzie wybranej tramwajowej podstacji trakcyjnej*, TTS Technika Transportu Szynowego 12/2015, 427–434.

[2] Drapik S., Dudzik M., Kuzniecow W., Prusak J., *Efektywność wykorzystania sztucznych sieci neuronowych, typu feedforward o jednej warstwie ukrytej siedmio-neuronowej, do analizy przeciążeń wybranej tramwajowej podstacji trakcyjnej.* Materiały drukowane XVII Ogólnopolskiej Konferencji Naukowej z zakresu Trakcji Elektrycznej SEMTRAK 2016, Zakopane, październik 2016, 145–158.

[3] Drapik S., Kuzniecow W., Markowski P., Prusak J., Woszczyna B., *Badanie skali zmienności obciążeń wybranej tramwajowej podstacji trakcyjnej na podstawie rzeczywistych wyników pomiarowych dla spójnego okresu czasowego obejmującego szesnaście tygodni*, Logistyka 6/2015, 1026–1035.

[4] Drapik S., Kaczmarczyk A., Kobielski A., Prusak J., *Charakter zmienności obciążeń tramwajowych podstacji trakcyjnych zasilających linie o różnej specyfice ruchu pojazdów*, TTS Technika Transportu Szynowego 6/2015, 43–48.

[5] *Dokumentacja podstacji tramwajowej nr 35 „Witosa"*, ZIKiT Kraków.

[6] Cholewicki T., *Elektrotechnika teoretyczna*, Wydawnictwa Naukowo-Techniczne, Warszawa 1971.

[7] Materiały udostępnione przez ZIKiT w Krakowie.

[8] Dudzik M., Prusak J., *Ocena możliwości miniaturyzacji podstacji trakcyjnych tramwajowych*, Politechnika Śląska, Katedra Transportu Szynowego, Konferencja „Advectus 2012" Katowice–Ogrodzieniec, 20–21 kwietnia 2012, 63–70.

[9] Norma PN- IEC 146-1-1+AC Przekształtniki półprzewodnikowe - wymagania ogólne i przekształtniki o komutacji sieciowej.

[10] Chrabąszcz I., Prusak J., Stecyk M., *Rozkład obciążeń zasilaczy sieci trakcyjnej tramwajowej przy zmienionej konfiguracji zasilania*, TTS Technika Transportu Szynowego 9/2015, 45–48.

[11] Tuliński K. *Rozwój systemu zasilania w Tramwajach Warszawskich oraz doświadczenia z wykorzystaniem zasobników energii i rekuperacji na podstacjach*, Niepublikowany materiał przedstawiony na posiedzeniu Centralnego Kolegium Sekcji Trakcji Elektrycznej w siedzibie Stowarzyszenia Elektryków Polskich w Warszawie, w dniu 10.12.2015.

[12] Jagiełło A.St., Chrabąszcz I., Drapik S., Dudzik M., Kobielski A., Prusak J., *System do aktywnej regulacji obciążenia zespołów prostownikowych kolejowej podstacji trakcyjnej. Sposób aktywnej regulacji obciążenia zespołów prostownikowych kolejowej podstacji trakcyjnej*, Rozwiązanie zarejestrowane w Urzędzie Patentowym RP na rzecz Politechniki Krakowskiej pod numerem P.511511, objęte ochroną prawną od dnia 10.03.2015.

[13] Mierzejewski L., Szeląg A., Gałuszewski M., *System zasilania trakcji elektrycznej prądu stałego*, Wydawnictwo Politechniki Warszawskiej, Warszawa 1989.

[14] Chrabąszcz I., Prusak J., Drapik S., *Trakcja elektryczna prądu stałego. Układy zasilania*, Podręcznik INPE dla elektryków, Zeszyt nr 27, Kraków–Bełchatów 2009.

[15] Drapik S., Markowski P., Prusak J., Woszczyna B., *Tramwajowe podstacje trakcyjne – wybrane problemy bezpieczeństwa ekologicznego w świetle oceny ich obciążeń*, Logistyka 4/2015, 3017–3027.

[16] Kałuża E., Bartodziej G., Ginalski Z., *Układy zasilania i podstacje trakcyjne*, Skrypty uczelniane Politechniki Śląskiej nr 1220, Gliwice 1985.

[17] Chrabąszcz I., Dudzik M., Prusak J., Stec W. *Wstępna analiza możliwości zastąpienia obiektu wybranej podstacji tramwajowej kilkoma o mniejszych gabarytach*, Budownictwo Innowacyjne. Międzynarodowa Konferencja InBuild, Kraków, 15–17.10.2013.

[18] *Wyniki pomiarów prądów obciążeń trakcyjnych kabli zasilających podstacji tramwajowej nr „35" („Witosa")*, materiały udostępnione przez ZIKiT w Krakowie, 2015.

[19] http;//kmkrakow.atlaskolejowy.pl

[20] http://www.mpk.krakow.pl

[21] Oćwieja D., Markowski P., Prusak J., Woszczyna B., *Specyfika obciążeń zespołów prostownikowych tramwajowej podstacji trakcyjnej dla kilku wariantów pracy na przykładzie rzeczywistej linii tramwajowej.* Materiały drukowane XVII Ogólnopolskiej Konferencji Naukowej z zakresu Trakcji Elektrycznej SEMTRAK 2016, Zakopane, październik 2016, 215–224.

[22] Dudzik M., Drapik S., Prusak J., *Approximation of overloads for a selected tram traction substation using artificial neural networks,* Technical Transactions, 3-E/2016, 39–50.

[23] Kuznetsov V.G., *Elaboration of methodology for calculation of traction power-supply system with the help of renewal stream theory [Текст]*, V.G. Kuznetsov, G. Vaiciunas, Transbaltica 2009; Proceedings of the 6-th international scientific conference, Vilnus Gediminas Technical University, 123–128.

Barbara K. Wilk

barbara.wilk@pg.edu.pl
Department of Water and Wastewater Technology, Gdansk University of Technology

Aleksander J. Urbański

Institute of Geotechnics, Cracow University of Technology

The impact of the shape of screen openings on groundwater flow to a deep drilled well

Wpływ kształtu otworów filtru studni głębinowej na proces filtracji w jej otoczeniu

Abstract

The authors propose a supplementary method for modelling seepage flow around a deep drilled well screen. The study applies 3D numerical modelling (FEM) in order to provide an in-depth analysis of the seepage process. The analysis of flow parameters (flux distribution $\mathbf{q}(\mathbf{x}, t)$ and pressure distribution p) was conducted using the ZSoil.PC software system. The analysis indicates that the shape of perforation is of secondary importance during deep bore well screen selection.

Keywords: deep drilled well screen, FEM, ZSoil, groundwater flow

Streszczenie

Autorzy proponują uzupełniającą metodę modelowania filtracji wokół filtru studni głębinowej. W pracy zastosowano modelowanie numeryczne 3D (MES) w celu dogłębnej analizy parametrów procesu filtracji. Analizę parametrów filtracji (rozkład prędkości filtracji $\mathbf{q}(\mathbf{x}, t)$ oraz rozkład ciśnienia p) przeprowadzono za pomocą systemu MES ZSoil.PC. Analiza wykazała, że kształt perforacji ma drugorzędne znaczenie podczas selekcji filtru studni głębinowej.

Słowa kluczowe: filtr studni wierconej, MES, ZSoil, filtracja

1. Introduction

Groundwater, accessed through deep drilled wells, usually supplies water of a quality superior to surface water [8, 23]. The groundwater is a valuable natural resource, readily used in, for example, industrial, medical or municipal applications [2, 26]. Moreover, groundwater resources are more accessible than surface water. Therefore, it is crucial to develop and broaden knowledge on the quantity and quality of groundwater, and on the appropriate methods for its withdrawal [13].

The correct usage of groundwater resources requires in-depth knowledge on the construction and operation of deep drilled wells [1]. It should be pointed out that a screen is one of the key elements of the drilled well as it helps to maintain the required well performance and deliver water free of a fine soil fraction [7]. Therefore, when designing a deep drilled well, its technical parameters must be carefully considered [20].

A thorough literature review on the design of deep drilled well screens failed to answer the question of whether the shape of a screen perforation has a significant impact on the performance of a screen. The review of the available literature has only led to the conclusion that the key technical parameters of a deep drilled well screen include the total screen surface (working surface) area, total area of screen openings and the size of the openings (depending on a size of the aquifer grain or a filter pack fill adhering to the screen).

It should also be stressed that thus far, analyses of seepage flow in the vicinity of deep drilled well screens have been based mainly on empirical formulas. The design groundwater inflow rates, determined by individually laboratories, have significantly differed from each other. Therefore, a detailed analysis of seepage related fields (flow distribution $\mathbf{q}(\mathbf{x}, t)$, pressure distribution $p(\mathbf{x}, t)$ was conducted using the ZSoil PC software, which employs the 3D numerical modelling methodology (FEM) and a homogenisation technique.

2. Groundwater flow in full saturation conditions

Seepage, as the movement of groundwater, is influenced by a variety of factors, such as: grading of soil, soil structure, soil porosity and cracking [2, 23]. The filtering properties are determined with the permeability coefficient k. Assuming a full saturation of the porous medium, the average flow q in a one-dimensional situation can be determined from the following formula, commonly known as Darcy's law [8]. Assuming that the fluid's viscosity, temperature and density are constant, this takes the form:

$$q = -k \cdot J \qquad (1)$$

In this model, the seepage flow (Darcy velocity) is directly proportional to the hydraulic gradient J, and k is the proportionality coefficient. Darcy's law is applicable only to laminar flows and is invalid for rocks or soils with a very high permeability [8, 24, 14, 13]. These limitations of the validity of Darcy law can be expressed by the notion of dimensionless Reynolds number Re:

$$\text{Re} = \frac{\rho \cdot q \cdot d}{\eta} \qquad (2)$$

where:

ρ – water density,

η – dynamic viscosity of ground water (= 0.0013 kg/m/s),

d – diameter of flow channel.

In ground water seepage problems, parameter d corresponds to an average diameter of a 'channel' between solid soil particles. This characteristic dimension of a ground microstructure is related to soil porosity, grain sizes and its distribution curve. Different sources give different limiting values of Re preserving the laminar flow regime, with the range Re = 1–10 in Bear [3], to Re = 30 in Houben [10].

Considering a general, three-dimensional case with a constant permeability coefficient and an isotropic medium, the flow components can be calculated from the following formulas [18, 14]:

$$\mathbf{q} = -k \cdot \mathbf{grad}(p/\gamma_w + Y) \ \equiv \ q_i = -k(H+Y)_{,i} \qquad (3)$$

where:

γ_w – volumetric weight of the fluid,

Y – the potential of the gravity field, which is negligible in the analysed flow homogenisation case (close to the screen).

However, it is important while analysing groundwater flow in macroscopic systems (e.g. while looking at a free surface close to the screen or at a flow distribution up the screen height). Darcy's law, as a constitutive equation for seepage in a porous medium, must be supplemented by a balance equation, which in full saturation conditions, takes the following form:

$$div\mathbf{q} = \frac{\partial q_x}{\partial x} + \frac{\partial q_y}{\partial y} + \frac{\partial q_z}{\partial z} = 0 \ \equiv \ q_{i\,,i} = 0 \qquad (4)$$

Expressing equation (4) through pressure p or hydraulic head H, Laplace's equation is obtained:

$$\nabla p = \frac{\partial^2 p}{\partial x^2} + \frac{\partial^2 p}{\partial y^2} + \frac{\partial^2 p}{\partial y^2} = 0 \ \equiv \ p_{,ii} = 0 \ \equiv \ H_{,ii} = 0 \qquad (5)$$

This equation serves as the basis for a numerical analysis conducted using the finite elements method (FEM), which is discussed further in this paper. To solve the boundary problem, the conditions applicable to each point of the boundary of the calculation domain have to be determined. Thus, for the problem presented in Fig. 2, the first-type (Dirichlet) boundary condition (equation 6) applies to pressure (where its value is known, i.e. within the opening $\bar{p} = 0$ and $\bar{p} = 1$ on the outer surface:

$$p = \bar{p} \qquad (6)$$

The second-type (Neumann) boundary condition, for the flow perpendicular to the boundary (equation 7), applies to the remaining parts of the periodic cell boundary, where

a lack of normal flow is caused by the presence of a filter pipe, or by flow symmetry and periodicity.

$$\mathbf{n} \cdot \mathbf{q} \equiv n_i q_i = q_n = \overline{q}_n = 0 \qquad (7)$$

3. Screen in a deep drilled well

The screen is an element of the filter column which also comprises a subfilter pipe (which very often acts as a sedimentation basin) and an upper pipe, which connects the screen with the ground surface [20, 16]. The designing of deep drilled well screens focuses mainly on their following features: length, elevation, perforation, diameter and acceptable screen performance. The main objective of the screen is thus to let water pass from the aquifer into the well and prevent loose soil, sediment and rock from entering the well while minimising hydraulic resistance. With regard to the above, in the past, well screens were selected with the largest possible opening area (lowest entrance velocity) [14]. The most recent field experience and laboratory tests have shown that the average entrance velocity of water moving into the screen should not exceed 0.6-1.2 m/s (providing that the screens have open areas greater than 3-5%) [1, 5, 11, 16]. However, Water Well Construction Standard ANSI/NGWA-01-14 does not specify the maximum screen entrance velocity due to the fact that different variants of entrance velocity and screen open area can give similar values for the designed screen length [1, 11, 16]. Moreover, the document indicates that the perforation of the well screen should be as large as possible, providing a laminar flow entrance velocity.

The size of well screen perforation is also largely dependent on the type of aquifer and the use of a gravel pack [2, 19]. Additionally, well screens should be characterised by correct slot design to minimise blockage, they should be constructed from corrosion resistant material and have a structure that hinders the formation of sediments of mechanical, chemical or biochemical origin [18, 20]. They should also be designed to prevent sanding the well during its normal operation. A proper screen ensures longevity and trouble-free operation of the deep drilled well [13]. Therefore, the following types of screens may be used: framed screens, mesh screens, gravel screens, and various types of special structures (e.g. those constructed from porous concrete prefabricates).

The framed screens with a proper perforation are the most frequently used type of screen [14, 21].

4. Framed screen perforation

Framed well screens are usually in the form of' pipes with a series of openings (of a specific shape) to enable water to pass through. The openings can be round or rectangular (slots) [14]. The diameters or widths of screen openings are selected according to the grain size of the aquifer. The Abramow's formulas can be applied to calculate the dimensions of the screen

openings based on the uniformity coefficient of grains of a filter layer, which is in a direct contact with the filter (η) [7, 15, 17, 20]. It should be noted that the diameter of openings should not be smaller than 10 mm and not larger than 25 mm. The slot width should not exceed 10 mm. When designing a framed screen perforation, the screen flow rate coefficient must be calculated from the following formula [13]:

$$m_f = \frac{f}{F} \qquad (8)$$

where:

f – total area of the openings (active surface),

F – surface area with perforation, screen surface (working surface).

For round openings $m_f \leq 0.25$; for slots $m_f \leq 0.15$.

5. Materials & Methods

Modelling of a groundwater flow with the ZSoil.PC FEM software was preceded by calculations of technical parameters of a deep drilled well. The calculations were performed according to the groundwater intake design principles formulated by Wieczysty and Gabryszewski for the given input data. In this way, reliable and accurate data was obtained for further numerical calculations. Following the calculation of the screen length and diameter, the dimensions of three types of openings were determined. These were: round holes (chessboard), longitudinal slots and transversal slots. The openings were distributed on the screen surface and the total area of screen perforation was kept constant for each case. The appropriate filter pack grain size was selected to ensure that the grains did not pass through the screen, i.e. to protect the well against sand accumulation. Table 1 presents the conditions and results of further calculations in ZSoil.PC (FEM) (Table 1.).

Table 1. Input data and major results of deep drilled well screen calculations

Aquifer grain size	Screen openings	Water table	Calculated screen length, m	Calculated outer screen diameter, m	Calculated inner screen diameter, m	Calculated diameter of filter pack pipe (d_{50} = 4.0 mm), m
d_{10} = 0.32 mm d_{50} = 0.35 mm d_{60} = 0.39 mm	a) round hole perforation (chessboard) b) longitudinal slot perforation c) transversal slot perforation	Free water table 12 m BGL	2.80	0.195	0.175	0.395

Dimensions of the deep drilled well screen for the analysed options are provided below:
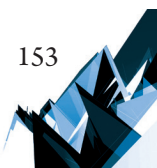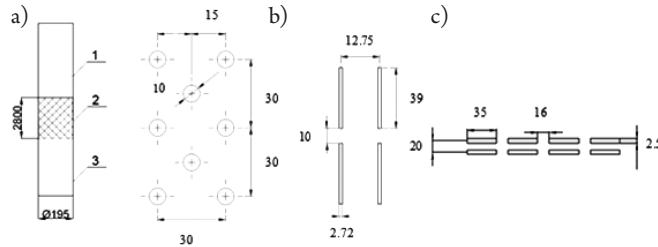
Fig. 1. Deep drilled well screen (1 – upper pipe, 2 – filter, 3 – subfilter pipe) with mf = 8.35%: a) round hole perforation (chessboard), b) longitudinal slot perforation, c) transversal slot perforation; all dimensions in [mm]

After determining the screen size for the given application, the groundwater flow was determined for three deep drilled well screens, differing in screen opening shapes; flow rate coefficients for each option were kept constant (mf ≈ 8.35%). The numerical analysis was based on flow homogenisation, assuming its periodicity both along and around the pipe. The periodic cell was created and defined as a section of a hollow cylinder with an internal radius of R1 = 97.5 mm and filter pack dimensions of a = 100 mm; this was identical for each type of perforation. A radius of R3 = 297.5 mm, for the outer cell surface was selected for cases in which any visible fluctuations of the flux vector **q** vanish.

Two permeability coefficients in the filter pack and the surrounding aquifer zone have been considered:

1) with different values: $k = 1.0$ [mm/s] $= 1.0e^{-3}$ [m/s] for a filter pack, $k_1 = 0.01$
   $k = 1.0e^{-5}$ [m/s] – for an aquifer strata, a medium sand was adopted in this study,
2) with a constant value of $k_1 = k = 1.0$ [mm/s] $= 1.0e^{-3}$ [m/s] assumed in both zones.

It is worth noting that these are just approximate, indicative values, roughly corresponding to real numbers. Nevertheless, due to linearity of the boundary problem, the obtained results correctly illustrate the nature of the phenomenon, and could be generalised to other data; however, this can only be done if the conditions of Darcy law validity, described in p.1, hold.

The 3D FEM models of a periodic cell for the three types of openings with the *adopted* boundary conditions (p – pressure [kN/m²], q_n – flux normal to the surface) are shown in Fig. 2.

It is assumed that the depth of the screen tube wall is so small that pressure distribution along the segment between the inner and outer surface of a tube may be approximated by a sudden drop to a value of $p = 0$ on the outer surface of the screen tube, which is also the inner surface of the periodic cell.

6. Results and discussion

The pressure field was determined for all six analysed cases (3 x 2 conditions). The pressure distribution for the three perforation types is very similar, i.e. the closer to the centre of the opening, the lower the pressure; pressure increases with the distance from the perforation. In the case of flow

setups 1a, 1b and 1c, a significant disproportion (100 x) of the permeability coefficient between the highly permeable layer of the filter pack and the aquifer close to the pipe is observed. This disproportion causes a drop in the value of the pressure close to the pipe (Fig. 3).
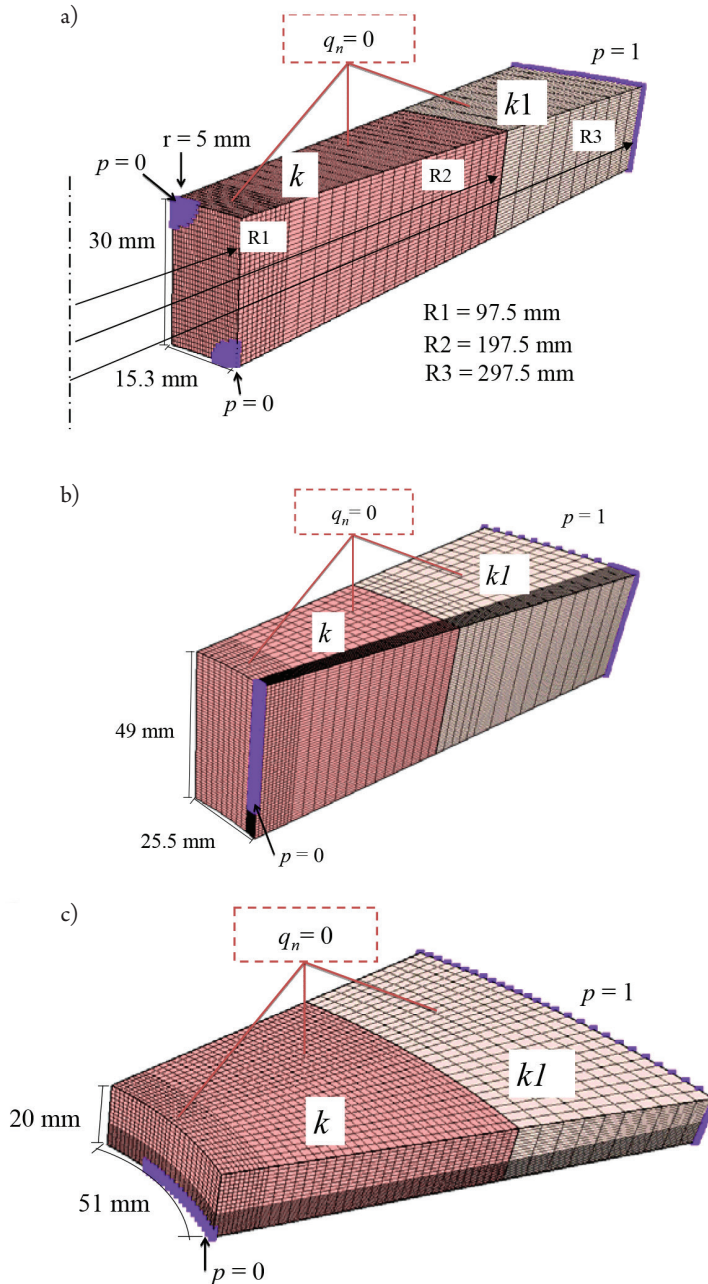

Fig. 2. A periodic cell of a deep drilled well screen with perforation and a screen adjacent zone: a) circular hole perforation, b) longitudinal slot perforation, c) transversal slot perforation
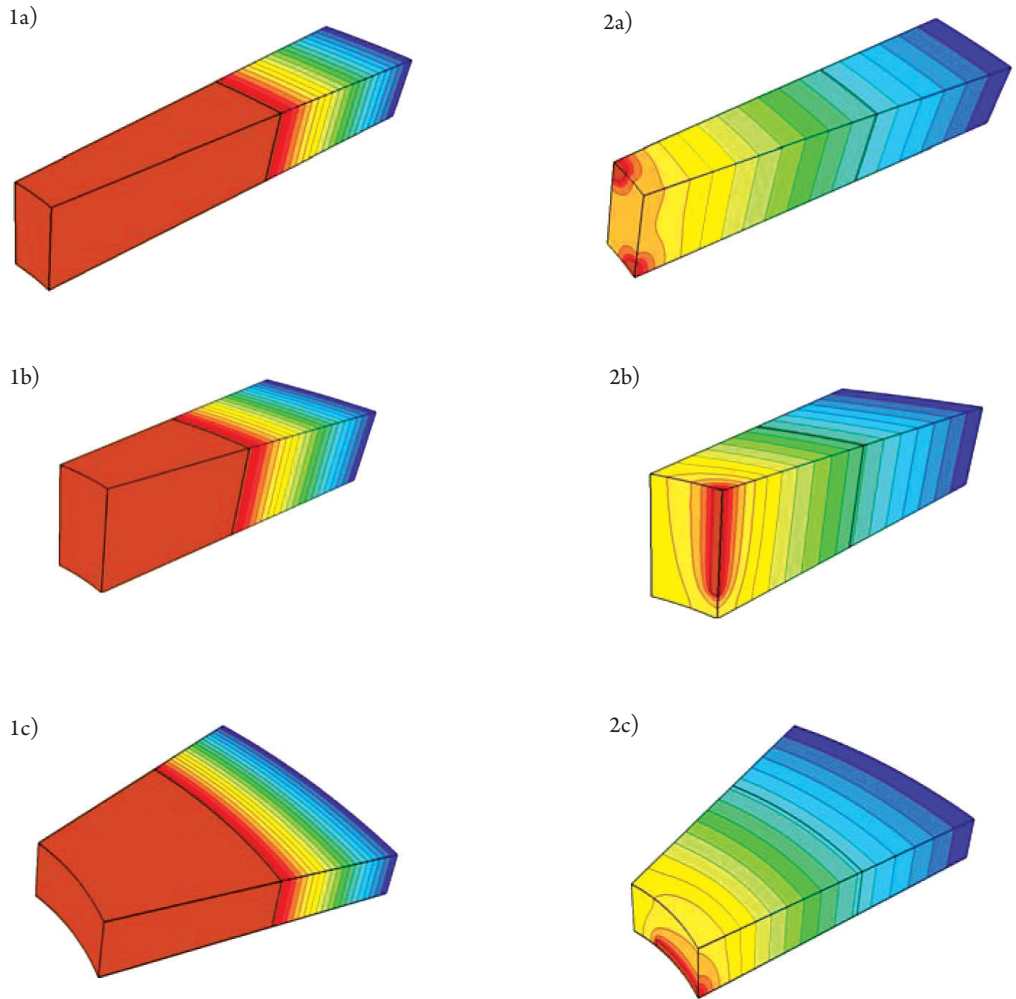
Fig. 3. Pressure distribution in the periodic cell: a) round hole perforation, b) longitudinal slot perforation, c) transversal slot perforation for both flow setups; maximum pressure value $p = 1 \text{ kN/mm}^2$ (dark blue), minimum pressure value $p = 0 \text{ kN/mm}^2$ (brown)

Numerical studies performed by a few authors [9, 13, 21, 22, 24] describe a drop in pressure in close proximity to the well screen. Szanyia et al. (2018) describe pressure distribution near the well screen (crude oil inflow to a horizontal drilling well), whereas the exact pressure distribution for different screen perforations has not been calculated on a micro-scale.

After specifying the boundary conditions, the results clearly indicate that the highest flow values were found at the well screen openings and in their immediate vicinity, also that they dropped with increasing distances from the screen openings. Additionally, the individual flux vectors $|\mathbf{q}|$ at the outer surface of the computational domain were read for each case presented below.
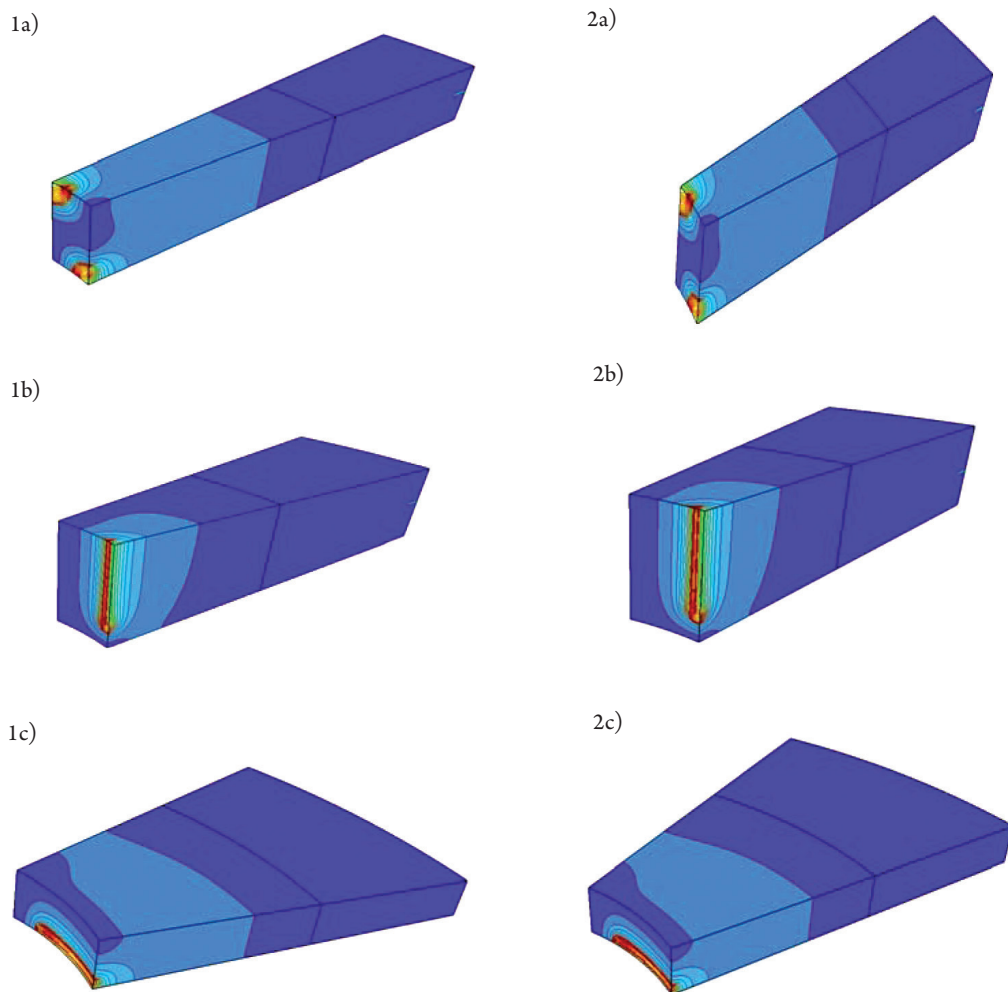
Fig. 4. Maps of individual flux vectors |**q**| distribution for three options of the periodic cell: a) round hole perforation, b) longitudinal slot perforation, c) transversal slot perforation

Table 2. Flow at the outer surface of the periodic cell (radius R = 297 mm)

perforation/set up of k type	1) $k1 = 0.01\ k = 0.01$ mm/s $\|\mathbf{q}\| \times 10^{10}$ [mm/s]	2) $k = k1 = 1$ mm/s $\|\mathbf{q}\| \times 10^{10}$ [mm/s]
a) circular	0.08153	2.47384
b) vertical	0.08136	2.32901
c) transversal	0.08143	2.39139

Interestingly, the values of flux vectors |**q**| at the outer surface of the cell (Table 2), obtained for the same unit pressure value p, were very close to each other for all types of perforation.
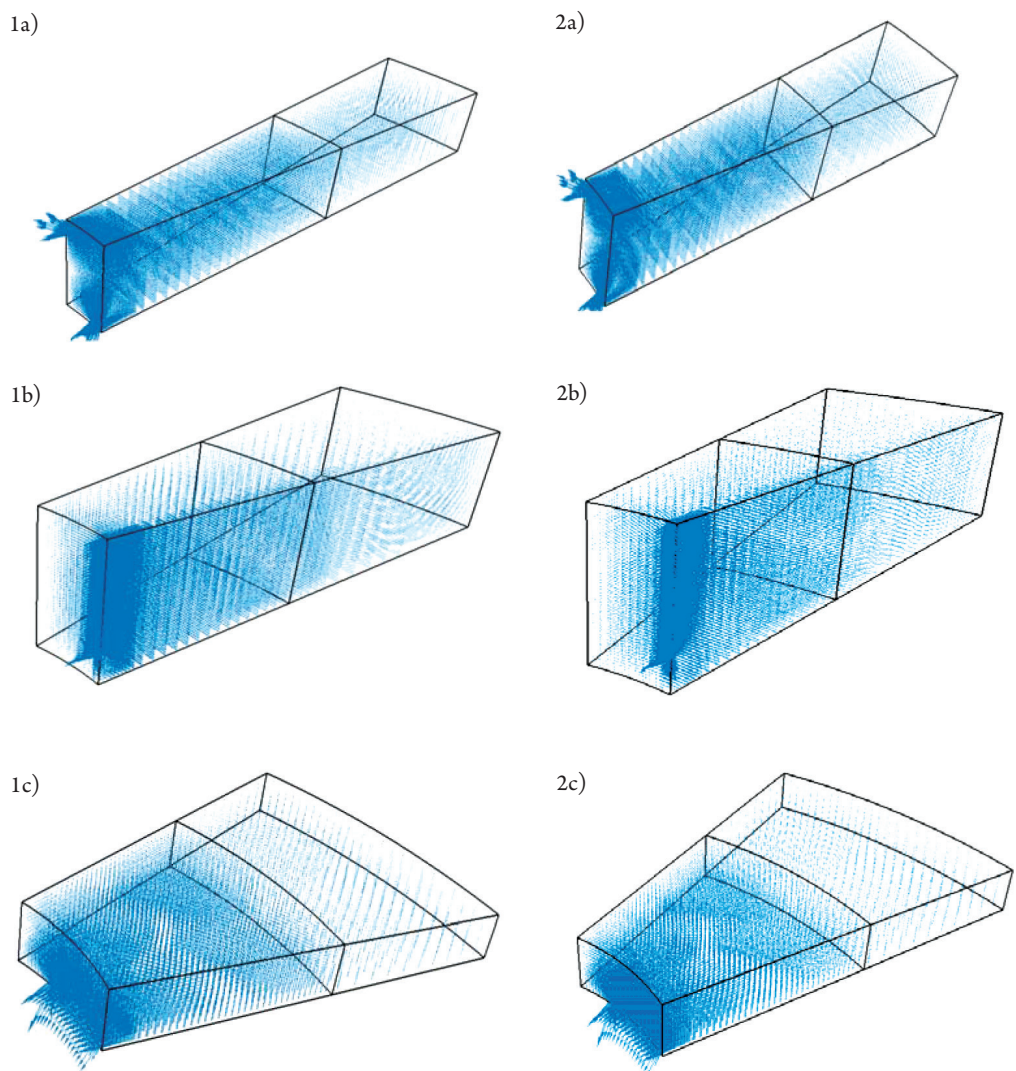
Fig. 5. Flux vectors $|\mathbf{q}|$ distribution for three options of the periodic cell: a) round hole perforation, b) longitudinal slot perforation, c) transversal slot perforation

Numerical modelling in the close proximity to the deep drilled well screen was discussed in several publications [13, 22, 24, 27]. However, the authors of the publications approach the subject differently due to the complexity of the issue and the diversity of situations that may occur in practice. Therefore, it is difficult to compare the results obtained in this publication with others. Most publications focus on determining the right water entrance velocity into the drilled well screen and there are many different opinions on this topic [6, 18, 10, 12, 15, 22]. There are also many publications on new analytical and numerical models explaining and quantifying the flow behaviour in aquifer systems [27]. These often include comparisons with analytical methods.

The currently available publications certainly confirm the results obtained by the authors with regard to the occurrence of the largest values of groundwater velocity vectors near the well screen. They also confirm the pressure distribution obtained in this publication and the distribution of flux vectors, although without taking into account the different types of perforation. The authors prove the abovementioned dependencies using other tools (e.g. Fluent program) and do not analyse it on a micro-scale.

It should be noted that the approach to the issue proposed by the authors is simplified, as it is based on Darcy's law (assumption of a laminar inflow into the well under full saturation conditions); however, it can be a good preliminary verification of empirical formulas, on the basis of which, the perforation of the screen is selected. It should be noted, however, that in close proximity to the screen, the groundwater flow may show some deviations from Darcy's law [11] and this will be covered in the next phase of authors research, along with other considerations. Other issue ignored are hydraulic losses at the openings, which in the case of the thin walls of the filter screen can be considered to be of minimal importance.

The presented computational analysis of seepage fields in a close neighbourhood of the screen (dimensions of finite elements are limited by slot width to 0.2 mm and analysis is performed on a domain of periodic cell with height $\sim 10^{-2}$m) can be seen as a micro-scale analysis, being the first step of a multi-scale analysis of the seepage problem The obtained results can be easily used for the identification of permeability properties of special finite elements by homogenisation. These linear (1D) finite elements, described in ZSoil [29], can represent drilled wells in 3D FEM computational models of a macro-scale system reaching hundred of meters, see Urbański [24, 25].

7. Conclusions

The obtained results indicate that the m_f coefficient is the key parameter for the selection of the opening of a deep drilled well screen. If the m_f value is maintained, the shapes and the distribution of openings are of a secondary importance. The velocity and the pressure distributions are nearly identical for the studied cases. The highest flow values are observed at the centre of the screen openings and in its immediate vicinity; flow rate drops proportionally to the distance from the perforation.

The simulations with the three-dimensional FEM showed that the engineering formulas where flows to the screen depended only on the m_f coefficient were of the most practical use.

References

[1] American Water Works Association, *AWWA Standard for Water* Wells. ANSI/NGWA-01-14, AWWA, Denver 2014.

[2] Antoniou A., Smits F., Stuyfzand P., *Quality assessment of deep-well recharge applications in the Netherlands*, Water Science and Technology: Water Supply 17(5) /2017, 1201–1211.

[3] Bear J., *Hydraulics of Groundwater*, Mineola, Dover 2007.

[4] Boyraz U., Kazezyılmaz-Alhan C.M., *Solutions for groundwater flow with sloping stream boundary: analytical, numerical and experimental models*, Hydrology Research 4(48)/2017, 258–267.

[5] Byung-Woo K., *Effect of Filter Designs on Hydraulic Properties and Well Efficiency*, Groundwater S1(52) /2014, 175–185.

[6] Castellazzi P., Martel R., Galloway D.L., Longuevergne L., Rivera A., *Assessing Groundwater Depletion and Dynamics Using GRACE and InSAR: Potential and Limitations*, Groundwater, 54(6)/2016, 768–780.

[7] Delleur J.W., *Elementary Groundwater Flow and Transport Processes, The Handbook of Groundwater Engineering*, Cushman, J. H. & Tartakovsky, D.M. (Eds.), CRC Press LLC, Florida 2016.

[8] Gabryszewski T., Wieczysty A., *Ujęcia wód podziemnych*, Arkady, Warszawa 1985.

[9] George R.M., *Bore Wells Vs. Open Wells: Water Crisis and Sustainable Alternatives in Kerala*, Journal of Management & Public Policy 7(2)/2016, 19–28.

[10] Houben G.J., Hauschild S. I., *Numerical modelling of the near-field hydraulics of water wells*, Hydrogeology Journal 49(4)/2011, 570–575.

[11] Houben G.J., *Hydraulics of water wells – flow laws and influence of geometry*, Hydrogeology Journal 23(8)/2015, 1633–1657.

[12] Houben G.J., *Review: Hydraulics of water wells – head losses of individual components*, Hydrogeology Journal 23(8)/2015, 1659–1675.

[13] Karatzas G.P., *Developments on Modeling of Groundwater Flow and Contaminant Transport*, Water Resources Management 31(10)/2017, 3235–3245.

[14] Knapik K., Bajer J., *Wodociągi*, Politechnika Krakowska, Kraków 2011.

[15] Lubowiecka T., *Mathematical model of deep drilled wells with confined aquifer and its empirical verification*, PhD dissertation, Cracow University of Technology, Kraków 1978.

[16] Mahasneh A.M., *Well Screens and Gravel Packs*, Global Journal Of Science Frontier Research 15-5-H/2015, 30–39.

[17] Manera D.B., Voltolini T.V., Menezes D.R., Leal de Araujo G.G., *Chemical Composition of Drilled Wells Water for Ruminants*, Journal of Agricultural Science 8(12)/2016, 127–132.

[18] Mansuy N., *Water Well Rehabilitation: A Practical Guide to Understanding Well Problems and Solutions*, Layne Geosciences Inc., USA 1999.

[19] Misstear B.D.R., Banks D., Clark L., *Water wells and boreholes*, Wiley, Chichester 2016.

[20] Nanteza J., de Linage C.R., Thomas B.F., Famiglietti J.S., *Monitoring groundwater storage changes in complex basement aquifers: An evaluation of the GRACE satellites over East Africa*, Water Resources Research 52(12)/2016, 9542–9564.

[21] Satora S., *Konstrukcje Studni Wierconych Ujmujących Wody Podziemne z Warstw Fliszowych*, III Konferencja Naukowo-Techniczna "Błękitny San", Dubiecko, 21–22 kwietnia 2006.

[22] Szanyi M.L., Hemmingsen,C.S., Yan,W., Walther, J.H., Glimberg, S.L., *Near-wellbore modeling of a horizontal well with Computational Fluid Dynamics*, Journal of Petroleum Science and Engineering 160/2018, 119–128.

[23] Tkaczenko A., *Studnie wiercone – część druga,* Wydawnictwo Geologiczne, Warszawa 1971.

[24] Urbański A., Podleś K., *The 2D/3D method of filtration and stability analysis of a slope with dewatering wells*, ZSoil Days, Lausanne 2017, https://www.zsoil.com/zsoil_day/2017/Urbanski-Podles_Wells_2D_3D.pdf (access: 15.10.2018).

[25] Urbański A., *Multi-scale analysis of a flow to drainage tubes*. ZSoil Days, Lausanne 2016, http://www.zsoil.com/zsoil_day/2016/A_Urbanski_Multi-scale_analysis.pdf (access: 15.10.2018).

[26] [Wilk B.K., *Ultrafiltration membranes made of: polyaniline, ionic liquid and cellulose*, Technical Transactions 1-Ś/2016, 171–187.

[27] Yeh H.D., Chang Y.C., *Recent advances in modeling of well hydraulics*, Advances in Water Resources 51/2013, 27–51.

Kinga Brózda
Jacek Selejdak

kbrozda@bud.pcz.pl

Department of Concrete Structures and Geotechnics, Faculty of Civil Engineering,
Czestochowa University of Technology

Peter Koteš

Department of Structures and Bridges, Faculty of Civil Engineering, University of Žilina

Analysis of the crack width of beams reinforced with FRP bars

Analiza zarysowania belek zbrojonych prętami FRP

Abstract

The paper investigates and compares a selected issue of Serviceability Limit State (SLS) of simply supported reinforced concrete (RC) beams subjected to various values of flexural stresses. Characteristic crack widths of beams reinforced with various types of bars were calculated. Beams reinforced with Glass Fiber Reinforced Polymer (GFRP), Carbon Fiber Reinforced Polymer (CFRP) and Aramid Fiber Reinforced Polymer (AFRP) were examined. The computational analysis of beams reinforced with FRP bars was based on Italian guideline for the design (CNR-DT 203/2006) and in accordance with the EC2 (EN 1992-1-1:2004). Based on the conducted analysis, the effect of changing the service live load on the increase in crack width was presented.

Keywords: FRP reinforcement, RC beam, crack width, design recommendations, CNR-DT 203/2006

Streszczenie

W artykule omówiono i porównano wybrane zagadnienie Stanu Granicznego Użytkowalności (SLS) swobodnie podpartej jednoprzęsłowej zbrojonej belki betonowej, poddanej różnym wartościom naprężeń zginających. W celu przeprowadzenia analizy dokonano obliczeń szerokości rozwarcia rys prostopadłych do osi belek zbrojonych prętami kompozytowymi. Do obliczeń przyjęto pręty zbrojeniowe polimerowe wzmocnione włóknem szklanym (GFRP – *Glass Fiber Reinforced Polymer*), węglowym (CFRP – *Carbon Fiber Reinforced Polymer*) oraz aramidowym (AFRP – *Aramid Fiber Reinforced Polymer*). Obliczenia wytrzymałościowe belek zbrojonych prętami FRP (*Fiber Reinforced Polymer*) wykonano zgodnie z włoskimi zaleceniami projektowymi (CNR-DT 203/2006) oraz w oparciu o obowiązującą normę europejską Eurokod 2 (PN-EN 1992-1-1:2008). Na podstawie przeprowadzonej analizy przedstawiono wpływ zmiany obciążenia użytkowego na wzrost szerokości rozwarcia rysy.

Słowa kluczowe: zbrojenie FRP, belka zbrojona, szerokość rozwarcia rysy, zalecenia projektowe, CNR-DT 203/2006

1. Introduction

Recently, an increased interest in the use of the fiber reinforced polymer (FRP) materials in building and engineering structures can be observed [1–4]. Among other things, the use of FRP rebar as the main reinforcement of concrete structures is increasingly common. This interest arises due to very good physical and mechanical characteristics of this material. Especially, low self-weight, good fatigue properties (parallel to the fibers orientation) due to the production method (pultrusion) [5, 6], very high resistance to the impact of aggressive environmental factors and high corrosion resistance generate intensified research of possibility to use FRP bars [1–3, 7–11]. Such material characteristics of a FRP rebar as strength and stiffness properties depend on the type of used fiber. There are FRP bars reinforced with the following types of fibers [2]: glass (GFRP), carbon (CFRP), aramid (AFRP) and basalt (BFRP).

The main purpose of this paper is to determine the possibility of using FRP reinforcement. Accordingly, a computational analysis of simply supported reinforced concrete beams affected by various values of flexural stresses was performed. The analysis consists in the comparison of results obtained for RC beams reinforced with FRP rebars. During the research, crack widths were taken into consideration. The results of the analysis allow for the specification of the most effective reinforcement under assumed conditions.

2. Computational analysis

It is worth noting that there is no available standard for strength calculations of sections reinforced with FRP rebars [11–13]. As a result of long-term experience of many researchers and designers, guidelines for the design of structural elements reinforced with FRP bars were elaborated. Among the available recommendations for design, four most popular guidelines could be distinguished: the Italian [14], the American [15], the Canadian [16] and the Japanese ones [17]. These design recommendations have been developed on the basis of analytical solutions and empirical equations, which are supported by experimental tests carried out on FRP bar samples and structural RC elements reinforced with FRP rebars [1–4, 12, 13]. The computational analysis of beams was made on the basis of applicable standards and design recommendations.

2.1. Calculation model

Simply supported beams with a rectangular cross-section were assumed. The outline of the static scheme and cross-section of the investigated beams are presented in Fig. 1. The dimensions of the cross-section are the following: $b = 180$ mm, $h = 350$ mm, and the effective length of the span is $L_{eff} = 4.0$ m. The beams are reinforced with 3Φ12 of the following bars: CFRP, ARFP and GFRP. The used concrete is specified by C20/25 compressive strength class and the concrete cover thickness is assumed as $c = 35$ mm. The

material characteristics of concrete were as follows: the characteristic compressive strength f_{ck} = 20 MPa, the mean value of axial tensile strength of concrete f_{ctm} = 2.2 MPa, the ultimate compressive strain in the concrete ε_{cu} = 0.0035 and the modulus of elasticity of normal weight concrete E_{cm} = 30·10³ MPa. The strength properties of the rebar are reported in accordance with the bar manufacturer's material data [18, 19]. The beam is designed to carry a service dead load equal to w_{SDL} = 3.0 kN/m and a various value of a service live load equal to w_L = {0.5; 2.0; 3.5; 5.0; 6.5; 8.0; 9.5; 11.0} kN/m. The limitation of the crack widths is assumed as $w_{k,lim}$ = 0.4 mm, in accordance with the EC2 standard [20]. The beam is not exposed to the moisture.
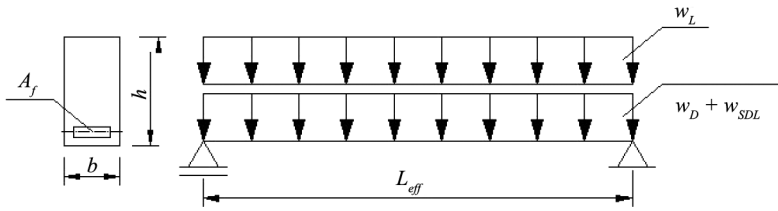

Fig. 1. The outline of the static scheme and cross-section of the investigated beams

2.2. Calculation method

The calculation method of beams reinforced with FRP was chosen in accordance with the Italian design recommendations [14], because of similarity thereof to the EC2 [20]. The material characteristics and environmental conversion factors of FRPs are specified by the manufacturer [18, 19] and shown in Table 1.

Table 1. The FRP's material characteristics

Type of rebar	The characteristic tensile strength of FRP f_{tk} [MPa]	The modulus of elasticity of FRP E_f [MPa]	The design strain of FRP ε_{fd} [–]	The environmental conversion factor η_a [–]
CFRP	2 300	130·10³	0.018	1.0
AFRP	1 400	60·10³	0.023	0.9
GFRP	1 300	55·10³	0.022	0.8

The characteristic crack widths w_k [mm] of the FRP reinforced element were calculated according to the Italian guidelines [14] using the following equation:

$$ \rule{4cm}{1.5pt} \tag{1}$$

and compared with the ultimate value of the crack widths $w_{k,lim}$. The non-dimensional coefficient β is relating the average crack width to the characteristic value and is assumed according to the design recommendation [14]. The final average distance between cracks s_{rm} [mm] was calculated using Eq. 2. It depends on bond properties of the FRP bars (non-

dimensional coefficient k_1) and the strain diagram (non-dimensional coefficient k_2). The suitability of the relationships provided by the EC2 standard [20] for computations of the distance between cracks was assumed.

$$s_{rm} = 50 + 0.25 \cdot k_1 \cdot k_2 \cdot \frac{d_b}{\rho_r} \qquad (2)$$

where:

d_b – the equivalent diameter of the FRP reinforcement, in mm;

ρ_r – the effective reinforcement ratio, equal to $\dfrac{A_f}{A_{c,eff}}$, where $A_{c,eff}$ is the effective concrete area in tension defined according to the EC2 standard [20] (the area around the tensile FRP reinforcement, which has a depth equal to the distance between FRP's centroid and tension fiber of concrete multiplied by 2.5).

The average strain accounting for tension stiffening, shrinkage, etc. is defined by ε_{fm} (Eq. 3). It depends on non-dimensional coefficients β_1 (accounting for bond properties of FRPs) and β_2 (accounting for the duration of loading).

$$\varepsilon_{fm} = \varepsilon_f \cdot \left(1 - \beta_1 \cdot \beta_2 \cdot \frac{\sigma_{fr}^m}{\sigma_f^m} \right) \qquad (3)$$

where:

ε_f – the strain of FRP reinforcement;

σ_f – the FRP reinforcement stress in tension of the cracked cross-section, in MPa;

σ_{fr} – the FRP reinforcement stress in tension of the cracked cross-section (when the first crack is observed), in MPa;

m – the coefficient, which equals 2.

2.3. The results of the analysis

The results of the characteristic crack widths w_k of the beams obtained during the theoretical analysis were compared in Table 2.

Table 2. The results of crack widths w_k depending on the type of rebar and live load level w_L

The live load level w_L [kN/m]	0.5	2.0	3.5	5.0	6.5	8.0	9.5	11.0
Type of rebar	w_k [mm]							
CFRP	0.006	0.182	0.259	0.299	0.322	0.337	0.347	0.355
AFRP	0.025	0.753	1.069	1.235	1.332	1.394	1.436	1.465
GFRP	0.034	1.020	1.448	1.673	1.804	1.888	1.945	1.985

Assuming that the limitation of the crack widths equals 0.4 mm, only beams reinforced with CFRP bars satisfied the condition. The beams reinforced with AFRP and GFRP bars
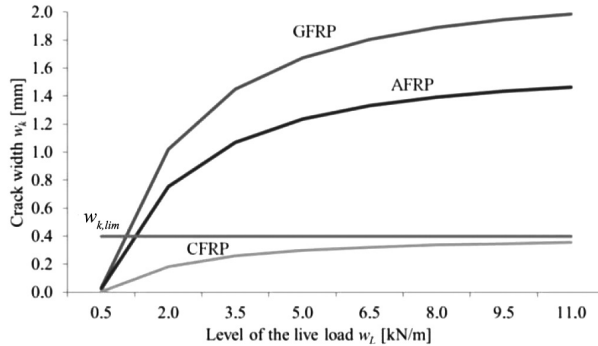
Fig. 2. The increase in value of the crack widths depends on the acting level of live load

exceed the limit value already at live load level equal to w_L = 2.0 kN/m. The reason of this phenomena is low values of modulus of elasticity of polymer rebar (AFRP and GFRP). The modulus of elasticity of CFRP is about two times higher than the ones of the other FRPs.

Interestingly, the increase in crack width of the beams reinforced with FRP seems to change as the logarithmical function. It means that the crack width growth at the initial load increase is more dynamic.

3. Summary

In this paper, an attempt to determine the most effective FRP reinforcement of a RC beam under assumed conditions was made. The characteristic crack widths which depend on the various level of service live load were calculated and compared. The calculations were done in accordance with the applicable standards and design recommendations [14-17, 20].

As it was suspected, during the computational analysis it was observed that the value of modulus of elasticity of the FRPs has the greatest impact on the growth of crack widths. Only beams reinforced with CFRP bars satisfy the condition of crack width limitations. It was noticed that the crack widths growth increased logarithmically as far as the intensity level of the acting live load increased. This is interesting due to the fact that in the case of steel reinforcement, as indicated by calculations made in accordance with EC2 [20], the crack width increased linearly. The obtained results will allow us to understand the flexural behavior of FRP RC members within SLS. In order to fully determine the effectiveness of FRP reinforcement under the SLS, further analysis is recommended.

References

[1]   Brózda K., Major M., Selejdak J., *Computational Analysis of Serviceability Limit State of Beams Reinforced with FRP Bars*, 23th International Conference Engineering Mechanics, Svratka, 15–18 May 2017, 218–221.

[2] Brózda K., Selejdak J., Koteš P., *The Analysis of Beam Reinforced with FRP Bars in Bending*, Procedia Engineering, vol. 192, 2016, 64–68.

[3] Bywalski C., Drzazga M., Kamiński M., *Obliczanie zginanych elementach zbrojonych prętami FRP*, Materiały budowlane, vol. 6, 2014, 72–73.

[4] Drzazga M., Kamiński M., *Pręty kompozytowe FRP jako główne zbrojenie zginanych elementów betonowych – przegląd zaleceń i efektywność projektowania*, Przegląd budowlany, vol. 3, 2015, 22–28.

[5] Brózda K., Selejdak J., *Analysis of FRP Bars Used as Reinforcement in Concrete Structures*, Production Engineering Archives, vol. 12(3), 2016, 2–4.

[6] Ulewicz R., Mazur M., *Fatigue testing structural steel as a factor of safety of technical facilities maintenance*, Production Engineering Archives, vol. 1(1), 2013, 32–34.

[7] Selejdak J., Ulewicz R., Ingaldi M., *The Evaluation of the Use of a Device for Producing Metal Elements Applied in Civil Engineering*, 23rd International Conference on Metallurgy and Materials, Brno, 21–23 May 2014, 1882–1888.

[8] Lipinski T., *Corrosion effect of 20 % NaCl solution on basic carbon structural S235JR steel*, 16th International Scientific Conference Engineering for Rural Development, Jelgava, 24–26 May 2017, 1069–1074.

[9] Pliszka I., Radek N., *Corrosion Resistance of WC–Cu Coatings Produced by Electrospark Deposition*, Procedia Engineering, vol. 192, 2017, 707–712.

[10] Szczotok A., Nawrocki J., Pietraszek J., *The Impact of the Thickness of the Ceramic Shell Mould on the $(\gamma + \gamma')$ Eutectic in the IN713C Superalloy Airfoil Blade Casting*, Archives of Metallurgy and Materials, vol. 62(2), 2017, 587–593.

[11] Barris C., Torres L., Miàs C., Vilanova I., *Design of FRP reinforced concrete beams for serviceability requirements*, Journal of Civil Engineering and Management, vol. 18(6), 2012, 843–857.

[12] Gravina R.J., Smith S.T., *Flexural behavior of indeterminate concrete beams reinforced with FRP bars*, Engineering Structures, vol. 30, 2008, 2370–2380.

[13] Toutanji H., Deng Y., *Deflection and crack–width prediction of concrete beams reinforced with glass FRP rods*, Construction and Building Materials, vol. 17, 2003, 69–74.

[14] CNR-DT 203/2006. Guide for the Design and Construction of Concrete Structures Reinforced with Fiber-Reinforced Polymer Bars.

[15] ACI 440.1R-06. Guide for the design and construction of concrete reinforced with FRP bars.

[16] CSA-S806-02. Design and Construction of Building Components with Fibre Reinforced Polymers.

[17] JSCE, Recommendation for design and construction of concrete structures using continuous fiber reinforcing materials, Concrete Engineering Series No. 23, 1997.

[18] Polprek Sp. z o.o. product data sheet, available at: www. polprek.pl (22.12.2016).

[19] Sireg Geotech S.r.l. product data sheet, available at: www.sireggeotech.it/en (22.12.2016).

[20] EN 1992-1-1:2004. Design of concrete structures. General rules and rules for buildings.

Ryszard Dindorf ⬤ orcid.org/0000-0002-2242-3288
dindorf@tu.kielce.pl

Piotr Woś
wos@tu.kielce.pl

Division of Mechatronics Devices, Department of Manufacturing Engineering and Metrology, Faculty of Mechatronics and Machine Building, Kielce University of Technology

Sᴇɴsᴏʀʟᴇss sᴛᴇᴘ ᴘᴏsɪᴛɪᴏɴɪɴɢ ᴏғ ʜʏᴅʀᴀᴜʟɪᴄ ʟɪɴᴇᴀʀ ᴀᴄᴛᴜᴀᴛᴏʀ

Bᴇᴢᴄᴢᴜᴊɴɪᴋᴏᴡᴇ ᴋʀᴏᴋᴏᴡᴇ ᴘᴏᴢʏᴄᴊᴏɴᴏᴡᴀɴɪᴇ ʜʏᴅʀᴀᴜʟɪᴄᴢɴᴇɢᴏ ᴀᴋᴛᴜᴀᴛᴏʀᴀ ʟɪɴɪᴏᴡᴇɢᴏ

Abstract

The paper presents a design, working principle and simulation of a sensorless position system whose hydraulic linear stepper actuator is controlled by a combination of single binary on/off valves. For dynamic modelling and digital simulation of stepper actuator, the bond graph method was used. Preliminary simulation tests were conducted to determine the dynamic characteristics and dynamic properties of the stepper actuator.

Keywords: stepper actuator, positioning system, sensorless control

Streszczenie

W artykule przedstawiono projekt, zasadę działania i symulację bezczujnikowego układu pozycjonowana hydraulicznego liniowego aktuatora krokowego sterowanego kombinacją pojedynczych binarnych zaworów włączających/wyłączających. Do modelowania dynamicznego i symulacji cyfrowej aktuatora krokowego wykorzystano metodę grafów wiązań (bond graph). Przeprowadzono wstępne testy symulacyjne w celu określenia charakterystyk dynamicznych i właściwości dynamicznych aktuatora krokowego.

Słowa kluczowe: aktuator krokowy, system pozycjonowania, sterowanie bezczujnikowe

1. Introduction

Hydraulic positioning systems should meet such requirements as precision position and high operational reliability irrespective of the load mass and the speed of the working movement. The sensorless control system for positioning hydraulic linear actuators (cylinders) and rotary actuators (motors) is presently an alternative to traditional servo control with servo or proportional valves. In the paper [3] a new type of a linear hydraulic stepper drive for sensorless positioning tasks in hydraulics is discussed. The paper [4] presents the idea of Digital Hydraulics (DH), which consists in replacing the expensive and sensitive servo valve with a combination of simple, robust and low-cost binary on/off valves. The advantages of Digital Hydraulic Systems (DHS) are as follows: potential increase of efficiency, redundancy, robustness and higher accuracy in machine movements. Furthermore, they include lower energy usage, fewer shutdowns, less lost production and lower initial investment and spare parts carrying cost. DHS focuses on unconventional control which involves the use of binary on/off valves for direct control of the hydraulic linear stepper actuator. The paper deals with a design, working principle and simulation of the sensorless step positioning with the hydraulic linear stepper actuator controlled by a combination of binary on/off valves. The practical use of hydraulic linear stepper actuators was considered, especially for moving an object and maintaining its position automatically in machine tools during manufacturing processes (welding, drilling, riveting, punching) and for precise positioning of lasers, sensors or limit switches.

2. Design and working principle of sensorless positioning of a hydraulic linear stepper actuator

The hydraulic linear stepper actuator is supplied from a hydraulic constant pressure source p_0 =const, representing an ideal source of hydraulic energy regardless of the flow rate. Two identical non-adjustable throttle valves are placed at the inlet of the right and left side of the actuator chamber. At the outlet of the hydraulic linear stepper actuator there are n binary on/off valves. The binary on/off (poppet-type) valves are similar to pilot-to-open check valves, but they work like bleed valves. As shown in the hydraulic diagram in Figure 2, the binary valve bleeds the flow in the ON state and stops the flow in the OFF state. The binary on/off valve is actuated by solenoid coil and returns to the starting position due to spring action. After turning on the power supply of the solenoid, the binary valve immediately opens the flow path from the outflow slots to the tank. In the case of a high speed on/off selenoid valve, this means switching delay time 5-20 ms. On the other hand, the on/off poppet valve opens as much as the flow goes through it needs. The poppet has less distance to move to stop the flow, thus its response is faster than that of other valves (i.e. spool valves). After opening of the i-th binary on/off valve, there is a pressure drop in one actuator chamber. As a result of pressure difference $\Delta p = |p_1 \text{-} p_2|$, the actuator piston moves to the place of flow through outflow slots 1 and 2. In the unsteady state the p_1 and p_2 pressures in the left and right cylinder chamber can

alternately increase and decrease until a fixed position of the actuator piston is achieved. The actuator piston moves until the steady state is reached in which there is a balance of forces acting on the actuator's piston, when the pressure p_1 in the left chamber and p_2 in the right chamber are the same. Outflow slots 1 and 2 with the actuator piston create symmetrical metering edge with negative overlap, as detail A in Figure 2 shows.

Different distinctive positions of the actuator piston in relation of outflow slots 1 i 2 are schematically shown in Figure 2. For each distinguished position of the actuator piston, flow rates q_{vij} (where: i –is the number of the actuator chambers, j – is the number of the outflow slots) have been marked.

On the basis of the actuator piston position (Fig. 2), the static characteristics of cross-sectional flow area A_{ij} were determined depending on the opening x and the outflow slots 1 and 2, which are shown in Figure 3.
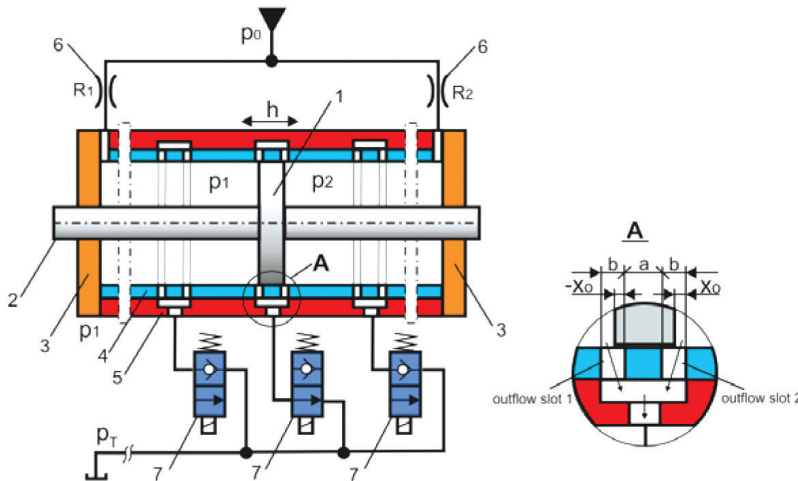

Fig. 1. Solution of sensorless positioning of hydraulic linear stepper actuator: 1 – piston, 2 – piston rod, 3 – and caps, 4 – sleeve, 5 – cylinder, 6 – throttle valves, 7 – binary on/off valves
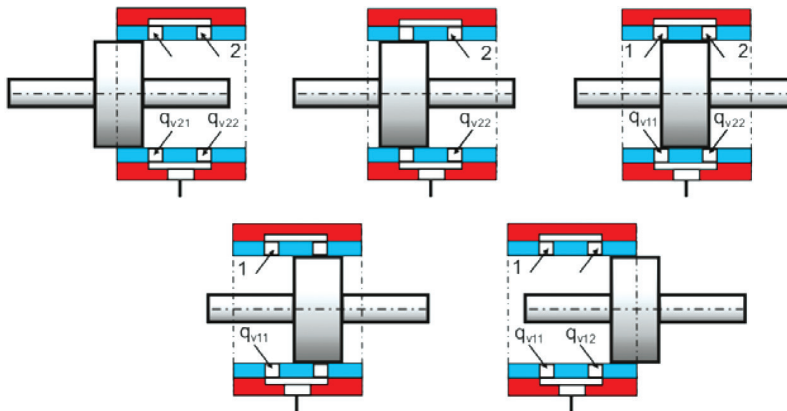

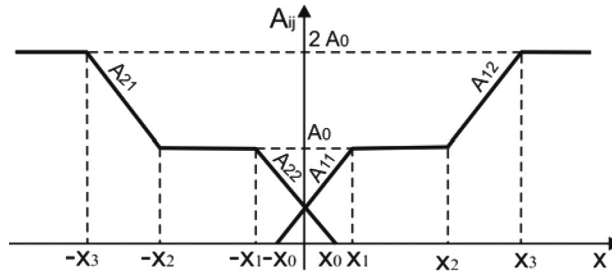
Fig. 2. Different distinctive positions of actuator piston

Fig. 3. Static characteristics of cross-sectional flow area A_{ij}

3. Bond graph modelling of sensorless position control of hydraulic linear stepper actuator

The method of Bond Graphs strictly identified with the functional structure of the hydraulic control systems is used for dynamic modelling of a sensorless position control system of a hydraulic linear stepper actuator. According to the definition, the bond graph represents an instantaneous energy flow, i.e. power between ports of different bond graph nodes [5]. The power transferred equals the product of two physical quantities, which are called effort e and flow f. Since the equations of kinematic and potential energy on bond graphs are described by means of time function, the bond graphs are applicable to digital simulation of a hydraulic linear stepper actuator. For the creation of a bond graph modelling of the hydraulic linear stepper actuator, the following denotations were introduced: SE_p – energy effort source which corresponds to pressure p_0; SE_c – effort source which corresponds to Coulomb friction; C_1, C_2 – hydraulic capacitances in actuator chambers; A – piston area; I – inertance in kinetic energy storage corresponds to the mass of piston and payloads; R_1, R_2 – hydraulic resistances of throttle valves; R_v – resistance corresponding to viscotic friction proportional to piston velocity v; R_{11}, R_{12}, R_{21}, R_{22} – hydraulic resistances dependent on variable flow rate between actuator chambers $(1, 2)$ and outflow slots $(1, 2)$: $q_{v11}(R_{11}), q_{v12}(R_{12}), q_{v21}(R_{21})$. In the bond graph such elements as transformer TF, modulated transformer MTF, integration component INT, function blocks FNC and multiplication block MUL are included. The transformer element TF is a two-port bond graph element transforming energy from one domain into another. $TF: A$ transforms hydraulic power into mechanical power. The modulated transformer element MTF is not constant, but depends on time or any other parameter. In order to obtain piston stroke h, the integrator component INT is introduced. The FNC blocks are used for a non-linear function with one variable and the MUL block for a non-linear function with several variables. The $FNC1$ and $FNC2$ blocks represent flow rate through the throttle valves at the actuator inlet. The $FNC3$ block represents flow rate through the on/off valve at the actuator outlet. In the papers [2], the bond graph model of a hydraulic stepper cylinder was extended by supply conduits. A bond graph model of sensorless position control system of hydraulic linear stepper actuator is represented in Figure 4.
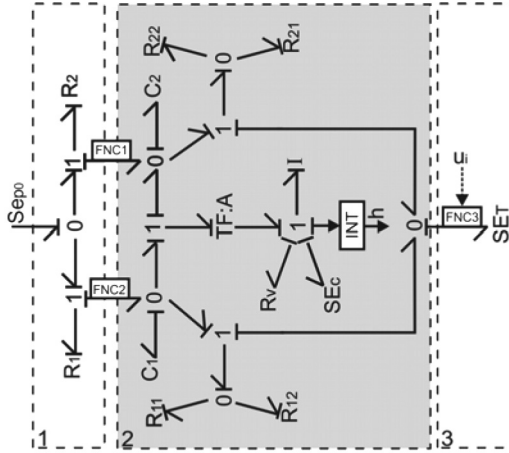
172

Fig. 4. Bond graph model of a sensorless position control system: 1 – throttle valves,
2 – hydraulic linear stepper actuator, 3 – on/off control valve

4. Simulation results of sensorless positioning of a hydraulic linear stepper actuator

The dynamic characteristics of a sensorless positioning system of a hydraulic linear stepper actuator was determined on the basis of the dynamic model represented by means of the bond graph method. The digital simulation was carried out using the available software, i.e. CAMPG (Computer Aided Modelling Program with Graphical Input) with interface to Matlab&Simulink environment [1]. CAMPG takes the topological description of a physical system model described by a Bond Graph, and transforms it into a dynamic simulation model of a hydraulic linear stepper actuator in the source code form. In digital simulation, the following basic parameter values were introduced: $SE_p = 15$ MPa, $SE_c = 100$ N, $A = 0.77 \ 10^{-3}$ m^2, $I = 12$ kg, $R_1 = R_2 = 0.41 \ 10^9$ Pas/m^3, $C_1 = 0.85 \ 10^{14}$, $C_2 = 0.42 \ 10^{-13}$ m^3/Pa. On the basis of the bond graph model from Figure 3 and the digital simulation using CAMPG, the dynamic characteristics of the hydraulic linear stepper actuator during step positioning were determined. The example of dynamic characteristics of a hydraulic linear stepper actuator in one step h_i of the piston is presented in Figure 5.
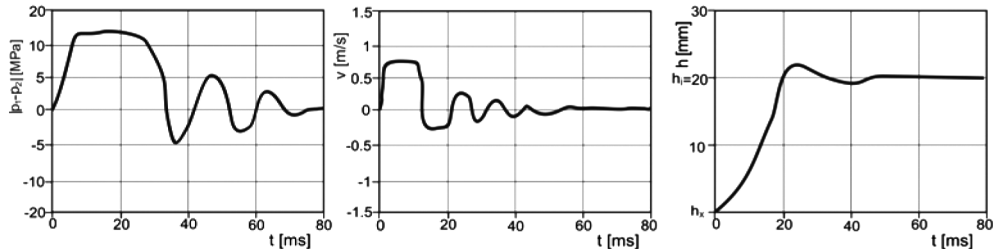

Fig. 5. Dynamic characteristics in one step positioning of the hydraulic linear stepper actuator

For the estimation of the dynamic properties of the hydraulic linear stepper actuator, the following control quality factors are assumed: δ_p – overshot, t_p – setting time, T – time constant, δ_o – oscillation and $|\delta h|$ – position deviation. The following values of quality factors are obtained for a linear hydraulic stepper actuator: δ_p = 5%, t_p = 80 ms, T = 33 ms, δ_o = 75%, $|\delta h|$ = 1.1 mm. The accuracy of the actuator piston position is within permissible 5% deviation, i.e. $|\delta h|$ = 0.05 h_i.

5. Summary

This paper presents a new solution and working principle of a sensorless positioning system of a hydraulic linear stepper actuator controlled by a combination of single binary on/off valves. The working principle of a hydraulic linear stepper actuator for the combination of single binary on/off valves is described. The binary (2/2-way) seat valves used to control the position of actuator piston have several benefits: they are inexpensive, reliable, insensitive to contamination and have zero leak. The control of the on/off valves is simpler in relation to the servo-valve and easier with the controller. The position control of a stepper actuator often requires making a step move to a new position and maintaining this position for a long time. A sensorless positioning system has the advantage of being controlled accurately in the open-loop position control without feedback needed to position a hydraulic linear stepper actuator. Since a position feedback sensor is not required, it allows cost savings when compared to the servo-control system. The bond graphs method was used for dynamic modelling and CAMPG/MATLAB environment for digital simulation of the sensorless position control system of a hydraulic linear stepper actuator. The solution of the sensorless position control system of a hydraulic linear stepper actuator will be patented. Next, the prototype model will be made and experimental tests will be carried out. The prototype of the sensorless hydraulic stepper actuator meets almost all design goals and shows a high potential for practical applications.

References

[1]   Borutzky W., *Bond graph modelling of engineering systems. Theory, applications and software support.* Springer Verlag, Berlin, New York 2011.
[2]   Dindorf R., *Dynamic modelling of w hydraulic positional cylinder by bond graph method.* 5th MMAR International Symposium. August 25–29, 1998, Miedzyzdroje, Poland, 267–272.
[3]   Gradl C., Plöckinger A., Scheidl R., *Sensorless position control with a hydraulic stepper drive – Concept, compression modeling and experimental investigation.* Mechatronics, 35, 2016, 91–101.
[4]   Linjama M., Laamanen A., Vilenius M., *Is it time for digital hydraulics?* 8th SICFP International Conference, May 7–9, 2003, Tampere, Finland, 1–4.
[5]   Thoma J.U., *Simulation by Bondgraphs.* Springer Verlag, Berlin, New York 1990.

Agata Dudek orcid.org/0000-0001-9115-028X
dudek@wip.pcz.pl

Barbara Lisiecka orcid.org/0000-0002-0945-3423

Katarzyna Strzelczak orcid.org/0000-0002-5869-2324

Institute of Materials Engineering, Faculty of Production Engineering and Materials
Technology, Czestochowa University of Technology

Assessment of the quality of epoxy coating in the automotive industry

Ocena jakości powłoki epoksydowej w przemyśle samochodowym

Abstract

Increasingly, many conventional and advanced automotive coatings applications demand materials with well-defined surface properties, fulfilling specific requirements and affecting automotive industrial development. The main assumption for the study was to analyze the microstructure and adhesion of epoxy powder coating on a steel substrate. The results of optical microscope metallographic, SEM/EDX, XRD analysis and adhesion test are presented.

Keywords: high strength low alloy (HSLA), S600 MC, epoxy powder coating, cross–cut test, ISO 2409:2013

Streszczenie

Coraz częściej, konwencjonalne i zaawansowane powłoki samochodowe wymagają materiałów o ściśle określonych właściwościach powierzchniowych, spełniających odpowiednie wymagania i wpływających na rozwój przemysłu samochodowego. Głównym założeniem badania była analiza mikrostruktury i przyczepności powłoki epoksydowej do podłoża stalowego. Uzyskano wyniki badań mikrostruktury za pomocą mikroskopii optycznej, skaningowej SEM/EDX, analizy XRD oraz przeprowadzono test adhezji powłoki.

Słowa kluczowe: wysokowytrzymała stal niskostopowa (HSLA), S600 MC, powłoka epoksydowa, test adhezji, ISO 2409:2013

1. Introduction

Nowadays, the selection of suitable material is a key decision in the automotive industry. The whole process is loaded with requirements in the field of good fuel efficiency, reduction in the weight of the vehicle, consumer safety standards imposed by government and consumer demands. Material needs to possess such qualities as good weldability, mechanical properties, good formability, joinability, good corrosion resistance, functional properties (e.g. hardness and wear resistance), etc. Steels are one of the most popular and important structural materials in the world. Their use in the automotive industry is constantly growing. In order to achieve good balance of low cost, light weight and good mechanical properties, high strength low alloys (HSLA) [1–2] are increasingly used.

High strength low alloy steels (HSLA) are not considered as alloy steels in the normal sense because their main feature which is emphasized is mechanical properties and not their chemical composition. HSLA steels are more interesting than conventional carbon steel due to better mechanical properties and greater resistance to atmospheric corrosion. HSLA steels are mainly used in structural elements for the production of car parts, heavy–duty highway and off–road vehicles, mine and railroad cars and many others. The structural S600 MC steel is one of the types of HSLA steel used in the automotive industry. This steel is characterized by exhibit excellent cold forming, high strength, good welding performance, low–temperature brittle fracture strength, excellent dimension accuracy and surface properties in production. S600 MC steel can be used in many industries, such as car fabrication (e.g. automobile parts, suspension systems, truck chassis), machine parts manufacturing and construction industry. The high strength of these steels is designed to reduce weight and/or to increase payload [3–5].

In order to protect HSLA steel against different environmental factors, various types of coatings, paint and lacquers have been developed. The automotive coatings are exposed to UV rays, heat and humidity, falling objects, scratches, chipping (e.g. rock hits) and rust from salt or road deicers. Technology aims at the production of automotive coatings that will be characterized by durable surfaces, exceeding customers' expectations of appearance, maximizing efficiency, and meeting environmental regulations. The factors influencing the development and use of automotive coatings and coating technologies include, among others: corrosion protection, aesthetic characteristics, appearance quality, durability, cost and environmental requirements. The corrosion protection of cars [6–7] is the main problem in the automotive industry of economic importance.

As is well known, the protection of metal by coating consists in the creation of an insulating layer between a metal surface and corrosive environment. The durability of the coating depends on the barrier effect, adhesion and inhibiting features and the presence of an active pigment. Therefore, epoxy paint containing such a pigments is one of the most inexpensive and effective anti–corrosion coatings. Additionally, pigments give color and luster; they help to establish thickness to the coatings. The effective protection will be provided if the coating is sufficiently impermeable and evenly stretched without any break. Depending on the final application of the coated element, the coating thickness can amount to several hundreds of micrometers [8–9].

Currently, the use of an epoxy coating is an interesting solution to ensure reliability and long-term performance of coated automobile parts. Because the resins synthetic and cross-linkers form a film coating, they can be used to protect metallic engineering structures exposed by natural or artificial environment. Epoxy resins are used as aqueous dispersions or emulsions in anticorrosive paints for steel substrates. Due to their excellent chemical stability, good adhesion to metals substrates, resistance to moisture, different solvents and chemical species, the epoxy powder coating is a popular candidate for the development of corrosion resistant coating on a suspension system in the automotive industry [10–11].

2. Material and Methods

The specimens for the investigations were performed from S600 MC steel. The chemical composition of the S600 MC steel is presented in Table 1.

Table 1. Chemical composition of the S600 MC steel (% wt.)

C	Si	Mn	P	S	Al	Nb	V	Ti	Mo	B
0.120	0.500	1.900	0.025	0.015	0.015	0.090	0.200	0.220	0.500	0.005

Before painting, the samples were degreased in acetone, left to dry at room temperature and washed with de–ionized water. The epoxy paint was applied using the powder coating method without any solvent. Two sets of samples were prepared in which the difference consisted in preparing the steel substrate. The steel in the first series of samples was polished in order to deprive the roughness surface. In the second series of samples, the steel had a rough surface to ensure better paint adhesion. After completion, the paint was allowed to cure for seven days. The epoxy powder coating thickness was measured after curing in order to ensure that the required values had been obtained (50 μm).

The analysis of microstructure was carried out using the Olympus GX41 optical microscope. The analysis of morphology of the surface after powder paint was performed by using an Olympus SZ61 stereo microscope and a Jeol JSM–6610LV scanning microscope.

The identification of the phase composition of the epoxy powder coating was made using an X–ray diffractometer (Seifert 3003 T–T) with a cobalt lamp with characteristic radiation wavelength of $\lambda_{cok\alpha}$ = 0.17902 nm. Other parameters are presented in Table 2.

Table 2. X–ray diffractometer parameters

	Parameters				
	Supply voltage (U_r)	Current intensity (I_r)	Angle range (2θ)	Measurement step	Pulse integration time (t_r)
Ranges	30÷40 [kV]	30÷40 [mA]	10÷120°	0.1°	10 [s]

In order to assess the quality of the epoxy powder coating, the adhesion test was made in accordance with the ISO 2409:2013 Paints and varnishes – Cross–cut test [12].

3. Results and Discussion

Figure 1 presents the microstructure obtained for specimens by an Olympus GX41 optical microscope. Taking into account the roughness surface of the steel substrate, Figure 1a shows better adhesion of the epoxy powder coating.
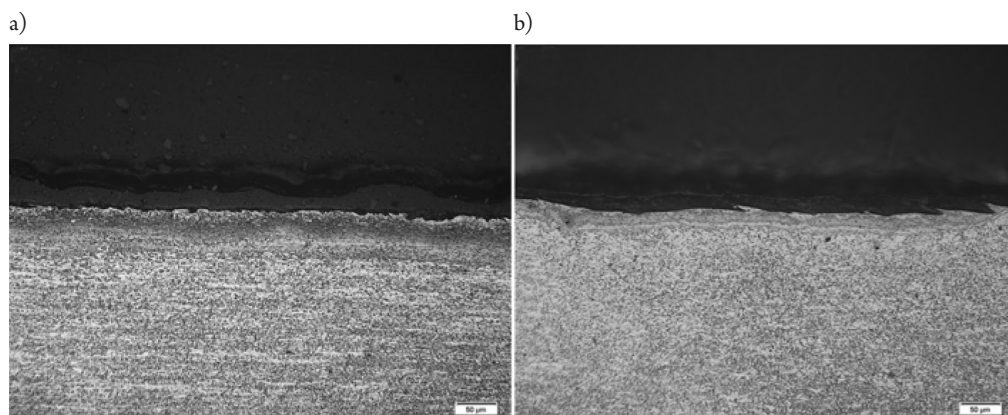
a)   b)

Fig. 1. Microstructure of epoxy powder coating with: a) good, b) poor quality of the steel substrate

Macroscopic examinations were used to evaluate the epoxy powder coating on the surface quality of the steel substrate. The analysis of the surface revealed numerous coating losses on the samples, whose steel substrate was completely smooth and did not have a rough surface. The quality of adhesion was confirmed by the adhesion test which was performed in accordance with the ISO 2409:2013. The samples were placed on a flat surface to prevent deformation during the test. On the surface, manual cutting was performed to gain a lattice pattern, following the specified procedure. The next step was to stick the adhesive tape on the surface and leave it for 5 minutes. After this time, the tape was removed. The obtained results were used to determine the resistance of the epoxy powder coating on the steel substrate. The samples with the epoxy powder coating on the rough surface of the steel substrate revealed a detachment of small flakes of the coating at the intersections of the cuts (below 5%). Whereas, the samples with poor surface preparation showed a loss of coating greater than 15%, but not greater than 35%.

Figure 2 presents SEM microstructure images and EDS spectra in the epoxy powder coating identified by EDX analysis areas by a Jeol JSM–6610LV scanning microscope. The analysis of chemical composition of the epoxy powder coating surface is presented in Table 3.

The phase composition analysis for individual specimens revealed the presence of the crystalline–amorphous crystallization, where the crystalline phase is carbon. The carbon crystallizes is a hexagonal cell of P (cell parameters: $a = b = 0.89$ nm, $c = 0.14$ nm, $\alpha = \beta = 90°$, $\gamma = 120°$).
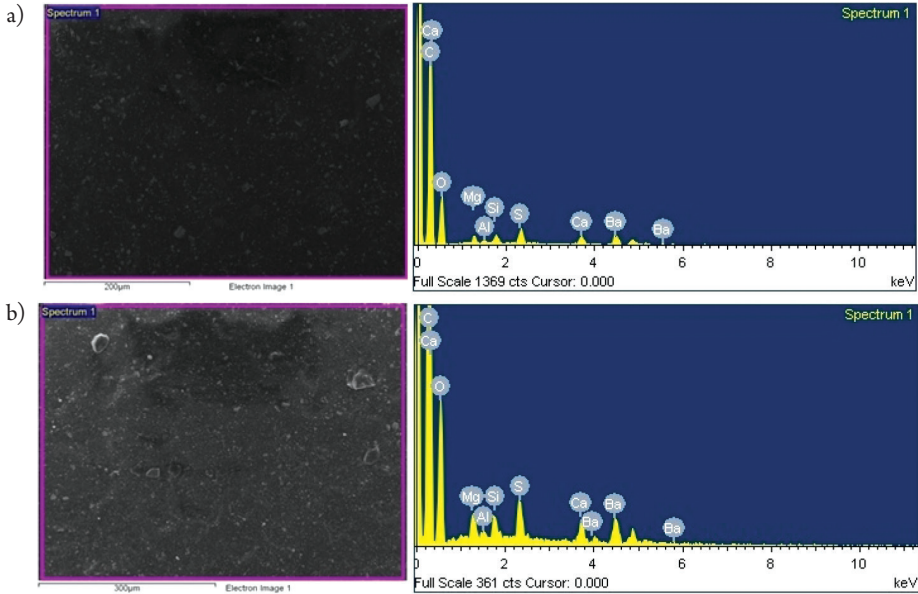
Fig. 1. Analysis of chemical composition of the surface in the epoxy powder coating (Spectrum 1) with: a) good, b) poor quality of the steel substrate

Table 3. EDX–analysis of chemical composition of the surface in the epoxy powder coating (location of the measurements is marked in Fig. 2)

Epoxy powder coating	Quality of the steel substrate	Element [weight %]							
		C	O	Mg	Al	Si	S	Ca	Ba
	good	66.12	23.90	0.78	0.09	0.59	1.56	1.07	5.89
	poor	68.33	23.65	0.70	0.14	0.38	1.26	1.05	4.49

Results of the analysis of phase composition of the epoxy powder coating are presented in Figure 3.
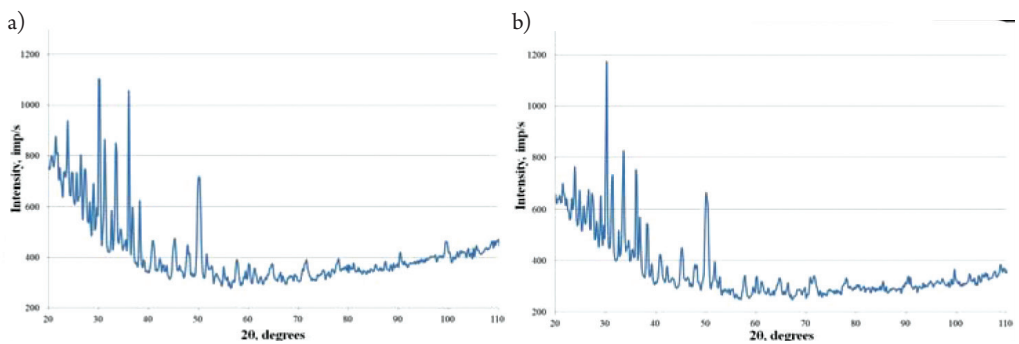

Fig. 3. Diffractogram of the epoxy powder coating with: a) good, b) poor quality of the steel substrate

4. Conclusions

Nowadays, automobile coatings are exposed to many factors. The quality of coatings depends on coating formula, durability of the exterior and interior paint finishes, intensities of the environment and many other factors. Application of coatings is the most widely used corrosion protection method for metallic surfaces. The strength and adhesion of coating depends on the method of preparation and application of the coating. As one of the most important parameters of quality of a coating is its adhesion, particular attention should be paid to the proper development of the surface of a steel substrate and determination of appropriate roughness.

References

[1]   Shirehjini F.T., Danaee I., Eskandari H., Zarei D., *Effect of Nano Clay on Corrosion Protection of Zinc-rich Epoxy Coatings on Steel 37*, Journal of Materials Science & Technology, vol. 32(11), 2016, 1152–1160.

[2]   Sutar V., Dharankar C.S., Thirupathi Raju B., *High Strength Steel for Automotive Applications*, International Research Journal of Engineering and Technology, vol. 3(5), 2016, 966–968.

[3]   Ranjbarnodeh E., Pouranvari M., Fischer A., *Influence of welding parameters on residual stresses in dissimilar HSLA steels welds*, Association of Metallurgical Engineers of Serbia, vol. 19(1), 2013, 33–43.

[4]   Saha D.C., Westerbaan D., Nayak S.S., Biro E., Gerlich A.P., Zhou Y., *Microstructure-properties correlation in fiber laser welding of dual-phase and HSLA steels*, Materials Science and Engineering A, vol. 607(23), 2014, 445–453.

[5]   Ulewicz R., Novy F., Mazur M., Szataniak P., *Fatigue properties of the HSLA steel in high and ultra-high cycle region*, Production Engineering Archives, vol. 4(3), 2014, 18–21.

[6]   Suay J.J., Rodriguez M.T., Razzaq K.A., Carpio J.J., Saura J.J., *The evaluation of anticorrosive automotive epoxy coatings by means of electrochemical impedance spectroscopy*, Progress in Organic Coatings, vol. 46(2), 2003, 121–129.

[7]   Akafuah N.K., Poozesh S., Salaimeh A., Patrick G., Lawler K., Saito K., *Evolution of the Automotive Body Coating Process – A Review*, Coatings, vol. 6(2), 2016, 1–22.

[8]   Canosa G., Alfieri P.V., Giudice C.A., *High-solids, one-coat paints based on aliphatic epoxy resin-siloxanes for steel protection*, Progress in Orgainc Coatings, vol. 77(9), 2014, 1459–1464.

[9]   Roselli S.N., Romagnoli R., Deya C., *The anti-corrosion performance of water-borne paints in long term tests*, Progress in Organic Coatings, vol. 109, 2017, 172–178.

[10] David R., Raja V.S., Singh S.K., Gore P., *Development of anti-corrosive paint with improved toughness using carboxyl terminated modified epoxy resin*, Progress in Organic Coatings, vol. 120, 2018, 58–70.

[11] Liu S., Chevali V.S., Xu Z., Hui D., Wang H., *A review of extending performance of epoxy resins using carbon nanomaterials*, Composites Part B: Engineering, vol. 136, 2018, 197–214.

[12] ISO 2409:2013 Paints and varnishes – Cross-cut test, fourth edition.

Czesław Kundera
Tomasz Kozior
tkozior@tu.kielce.pl
Faculty of Mechatronics and Mechanical Engineering, Department of Manufacturing Engineering and Metrology, Kielce University of Technology

Assessment of mechanical properties of PA 3200 GF polyamide models made by SLS

Ocena właściwości mechanicznych modeli wykonanych z poliamidu PA 3200 GF w technologii SLS

Abstract

The paper presents the results of mechanical properties research of samples made in the Selective Laser Sintering technology. Polyamide powder PA 3200 GF reinforced with glass fiber was the material used to build the model. Samples subjected to a uniaxial tensile test were made in accordance with ASTM D638 – V standard. The printing direction was the technological parameter of the study. The analysis of the results showed that the addition of fiberglass significantly influenced the improvement of mechanical properties, especially the isotropic of mechanical properties with respect to the printing direction.

Keywords: Additive Manufacturing, SLS, Polyamide PA 3200 GF, Formiga P100

Streszczenie

W artykule przedstawiono wyniki badań mechanicznych próbek wykonanych w technologii Selektywnego Spiekania Laserowego. Materiałem wykorzystanym do budowy modeli był poliamid PA 3200 GF wzmacniany włóknem szklanym. Próbki poddane jednoosiowej próbie rozciągania wykonane zostały zgodnie z norma ASTM D638-V. Parametrem technologicznym uwzględnionym podczas badań był kierunek budowy modeli. Analiza wyników badań wykazała, iż dodatek włókna szklanego w znaczny sposób wpływa na poprawę własności mechanicznych, przede wszystkim na izotropię własności mechanicznych w odniesieniu kierunku budowania modeli.

Słowa kluczowe: Technologie Przyrostowe, SLS, Poliamid PA 3200, Formiga P100

1. Introduction

Additive technologies allowing for the construction of physical objects directly from 3D models are increasingly being used not only in the building of prototypes, but also for the production of fully functional machine elements. Currently, layered technologies are used in many areas of industry such as, for example, prototype production [1] or construction of tools used in the production of conventional manufacturing technologies. Mechanical properties of the materials used are so good that they are also used to build components exposed to the wear process [2]. Due to the layered nature of a model construction, most additive technologies using materials based on plastics have anisotropic in both mechanical properties and dimensional-shape accuracy [3–6].

Due to the high degree of complexity in the construction of models using SLS technology, the current state of art describing the impact of technological parameters on mechanical properties does not sufficiently cover the presented topic. Selected manufacturing problems, related to mechanical properties of materials used for construction in SLS technology are described in papers [7–9].

The authors of the research [7] presented in their work the results of strength tests, with particular emphasis on the influence of selected technological parameters on tensile strength. The PA 2200 polyamide powder based on the known construction PA 12 polyamide was used to build the sample models. The research results confirmed that the direction of the models on the building platform directly influences the tensile strength and the Young's modulus.

Another studies related to determining the influence of technological parameters on selected mechanical properties are presented in paper [8]. The authors of the research have tested samples made in SLS technology. A mixture of two polyamide powders based on PA6 and P12 construction polyamides was analyzed. The technological parameters were as follows: laser power, energy density and temperature of the process chamber. The authors also determined basic mechanical properties such as tensile strength and Young's modulus for variable proportions of mixed materials.

This work describes the preliminary tests based on the determination of the impact of the "printing direction" technological parameter on the strength of the models during the uniaxial tensile test. PA 3200 GF material, which is based on pure PA 2200 polyamide, was used in the tests, but it was reinforced with the addition of glass fiber. The analysis of the test results compares the results obtained for polyamide reinforced with glass fiber with the results obtained for pure PA 2200 polyamide presented in work [9].

2. SLS Technology

Selective Laser Sintering SLS is one of the oldest additive technologies. The technology developed in the 1980s is also one of the most complex layered methods. A large number of variable technological parameters that have a direct impact on the manufacturing process and functional properties is one of the largest in relation to other generative technologies, in particular those based on plastics.

In this method, a polyamide powder with a grain diameter of only 0.056 mm is spread on the machine working platform over the shoulder, and then a focused CO_2 laser beam scanning the selected cross section sinter the currently built layer, combining it with the previously created and thus creating the model. During the tests, a Formiga P100 (3D printer, machine from EOS) was used to make the sample models. The mechanical properties of materials used in the construction of samples are shown in Table 1.

Table 1. Mechanical properties of materials: PA 2200/PA3200 GF [10]

Mechanical properties	Value	Unit	Standard
Young's modulus	1700/3200	MPa	EN ISO 527
Impact strength	4.4/5.4	kJ/m^2	ISO 180/1A
Shore'a hardness(15s)	75/80	–	ISO 868/Scale D
Denisty	0.930/1.22	g/cm^3	EOS method

3. Research

Tensile strength tests of samples made in SLS technology were carried out using an Inspekt Mini 3kN strength testing machine. The samples were made in accordance with ASTM D638-V. The initial strength tests presented in [9] indicated large differences in the strength of the sample models made with the variable parameter of the orientation of the models on the building platform (printing direction). In connection therewith, technological parameter included in the presented research was the direction of the models on the building platform. Three directional were chosen, i.e. 0°, 45° and 90°, shown in Figure 1.
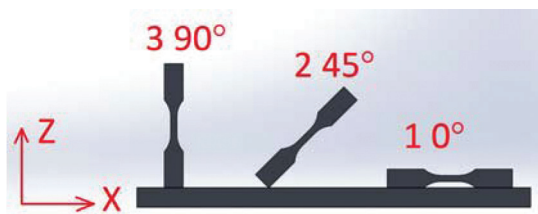

Fig. 1. Samples on the platform

Each type of samples was made in the amount of 5 pieces to perform statistical calculations. For each direction, tensile strength was determined experimentally in the form of the parameter – *Rm*, Young modulus – *E*, and relative elongation of the samples – *A*, whose results are shown in Table 2. The table also shows the calculated values of standard deviation. A graphical representation of the test results is presented in Figures 2–4, where the tensile results of the samples are compared, depending on the printing direction.
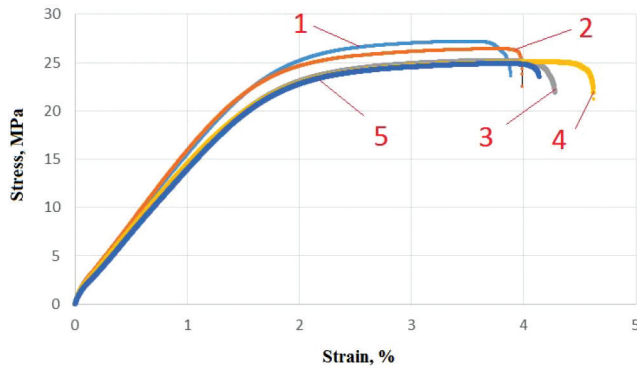
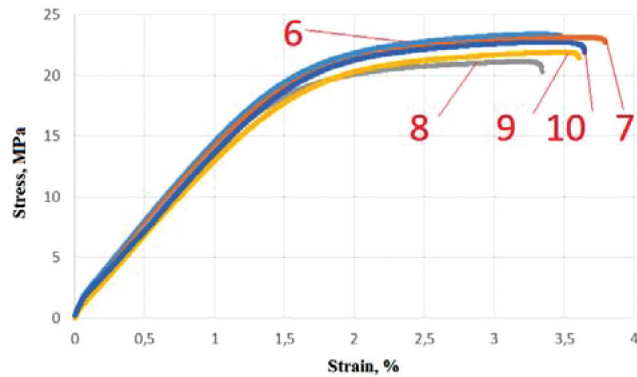Fig. 2. Tensile test result for the first type of placement

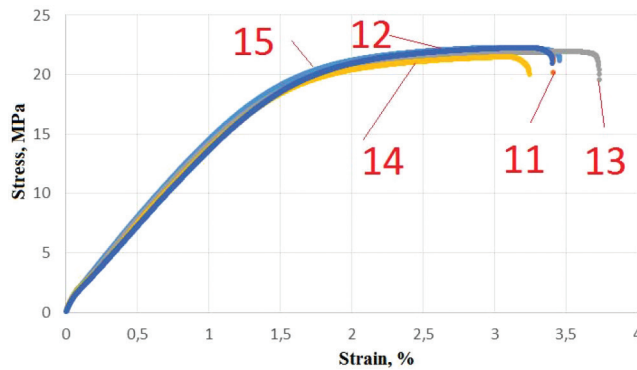Fig. 3. Tensile test result for the second type of placement

Fig. 4. Tensile test result for the third type of placement

Analyzing quantitatively the results of the research, it can be concluded that with the increase of the angle of placing the models on the building platform, the tensile strength of polyamide decreases. In the case of samples made with a given angle of 0°, the average tensile strength value is 22.05 MPa. In the case of samples made with a given angle of 45°, the average strength value is 21.05 MPa. The least advantageous variant of placing the models

relative to the building platform is the angle of 90°, where the average value of the strength is 20.75 MPa. Comparing the test results for those obtained for pure polyamide PA 2200 [9], it can be concluded that the addition of glass fiber clearly affects the improvement of the strength of the samples, in particular the phenomenon of anisotropy. In the case of pure PA 2200 polyamide, the average measurement results for the same location and the same type of test varied by up to 50% depending on the direction of the models on the building platform. At the same time, pure polyamide was characterized by very different elongation of samples during the test ranging from 1% to 15%. The presented test results for glass fiber reinforced polyamide clearly indicate that the addition of glass fiber minimizes the influence of printing direction on the strength of the samples. The test results presented in Table 2 indicate that the highest elongation value was recorded for samples made at an angle of 0°, however, the results obtained for 45° and 90° differ slightly. After analyzing the data on the percentage elongation of the tested samples, it can be stated that the addition of glass fiber reduces anisotropic in mechanical properties also in this aspect.

Fig. 5.

Table 2. Research results for polyamide PA 3200 GF

No.	Rm, MPa	E, MPa	A, %
1	22.59	0.59	9.40
2	21.96	0.60	9.01
3	20.98	0.49	9.78
4	22.1	0.58	10.78
5	22.65	0.53	9.76
$\bar{x}$	22.05	0.56	9.75
s	0.6	0.04	0.59
6	19.44	0.57	7.96
7	21.62	0.56	8.33
8	19.16	0.51	7.72
9	21.76	0.52	8.48
10	23.3	0.63	8.73
$\bar{x}$	21.05	0.56	8.24
s	1.55	0.04	0.36
11	18.53	0.54	7.84
12	19.91	0.55	8.07
13	21.81	0.61	8.88
14	21.35	0.59	7.49
15	22.13	0.58	7.46
$\bar{x}$	20.75	0.57	7.94
s	1.34	0.02	0.52

4. Conclusion

After analyzing the results of tensile tests of polyamide reinforced with glass fiber samples, and comparing the results with previously performed tests for pure polyamide, the following general conclusions can be formulated:

The tensile strength expressed by the Rm parameter is the highest for samples made with a given angle of 0°. As the value of the angle increases, the tensile strength decreases. Statical analysis allows us to state that the standard deviation of the test results is also the smallest for the above-mentioned positioning of the models, which positively affects the reproducibility of the test results.

Samples made at an angle of 90° are characterized by almost 20% lower elongation compared to samples with a given angle of 0°.

The value of the Young's modulus for all the made models of samples remains at a similar level regardless of the direction of the models' location on the building platform.

The results of the presented tests in comparison to those obtained for pure PA 2200 polyamide are characterized by a very high degree of isotropy.

References

[1] Leu M.C., Guo N., *Additive manufacturing: technology, Applications and research needs, Frontiers of Mechanical Engineering*, Vol. 8, 2013, 215–243.

[2] Kundera Cz., Kozior T., *Assessment of tribological properties of polymers used in additive technologies SLS and PJM*, Tribologia, Vol. 5, 2016, 73–84.

[3] Polák R., Sedláček F., Raz K., *Determination of FDM Printer Settings with Regard to Geometrical Accuracy*, Proceedings of the 28th DAAAM International Symposium, 0561–0566, Vienna, Austria.

[4] Kozior T., Kundera Cz., *Evaluation of the Influence of Parameters of FDM Technology on the Selected Mechanical Properties of Models*, Procedia Engineering, Vol. 192, 2017, 463–468.

[5] Salazar–Martín A.G., Pérez M.A., García-Granada A.A., Reyes G, Puigoriol-Forcada J.M., *A Study of Creep in Polycarbonate Fused Deposition Modelling Parts*, Materials & Design, Vol. 141, 2018, 414–425.

[6] Adamczak S., Makieła W., Stępień K., *Investing advantages and disadvantages of the analysis of a geometrical surface structure with the use of Fourier and wavelet transform*, Metrology and Measurement System, Vol. XVII, 2010, 233–244.

[7] Pilipović A., Valentan B., Brajlih T., Haramina T., Balić J., Kodvanj J., Sercer M., Drstvenśek I., *Influence of laser sintering parameters on mechanical properties of polymer products*, International Conference on Additive Technologies ICAT, 2010.

[8] Salmoria G.V., Leite J.L., Veira L.F., Pires A.T.N., Roesler C.R.M., *Mechanical properties of PA6/PA12 blend specimens prepared by selective laser sintering*, Polymer Testing, Vol. 31, 2012, 411–416.

[9] Kundera Cz., Kozior T., *Influence of the amount of energy provided to sintered polyamide layer in SLS technology on mechanical properties*, Logistyka, Vol. 6, 2014, 6374–6380.

[10] EOS company, *Formiga P100 – User Manual*, Munich 2008.

Dominik Kwiatkowski
dkwiatkowski@pk.edu.pl
Institute of Applied Informatics, Faculty of Mechanical Engineering, Cracow University of Technology

Air consumption survey for pneumatic cushion in different nozzle configurations during moving loads

Pomiar zużycia powietrza dla poduszki pneumatycznej w różnych konfiguracjach dysz podczas przemieszczania ładunku

Abstract

The subject of this paper concerns the search for structural solutions of pneumatic cushions [1, 2] in order to minimize the air consumption, operate at the lowest admissible pressure and compensate for the unevenness of the floor. The paper presents the solution with a multi-nozzle air outflow. This solution was obtained by a theoretical analysis, then a prototype of the device was made and laboratory tests were carried out.

Keywords: pneumatic cushions, air consumption, multi-nozzle air outflow

Streszczenie

Tematyka podjęta w referacie dotyczy poszukiwania rozwiązań konstrukcyjnych poduszek pneumatycznych [1, 2] w celu minimalizacji zużycia powietrza, pracy przy możliwie niskim ciśnieniu oraz uniezależnienia poduszki od wrażliwości na nierówności posadzki. W niniejszym artykule przedstawiono rozwiązanie z wielostrumieniowym wypływem powietrza. Rozwiązanie to uzyskano w wyniku analizy teoretycznej, następnie wykonano prototyp urządzenia i przeprowadzono badania stanowiskowe.

Słowa kluczowe: poduszki pneumatyczne, zużycie powietrza, wielostrumieniowy wypływ

1. Introduction

In industrial companies lifting equipment, such as overhead cranes, winches, conveyors, is often used to transport heavy loads. It is usually characterized by large sizes, limited reach and high purchase costs. Today's industrial halls built with the use of modern technologies allow for obtaining horizontal and smooth work surfaces, including tilt α ≤ 0.1o and a roughness of Ra ≤ 12.5 μm.

This condition allows for applying transport systems with a pneumatic cushion. Pneumatic cushions are devices of small size, characterized by low height, which ranges from 30 to 40. This simple design allows for sliding cushions under large loads and devices easily. In the laboratory of the Institute of Applied Informatics in the University of Technology, research is conducted on improving the parameters of pneumatic cushions through structural changes and the use of new control systems [2, 3]. A research stand in the form of a transport platform (Fig. 1) allows for testing new solutions at different load values.

During operation, a pneumatic cushion creates a film of air which reduces friction with the ground. This film is produced by air that flows radially from the chambers in the lower part of the cushion. In the standard design of the air cushion [6], the air flows through one nozzle, placed in the central axis. Such a solution has some disadvantages, which include difficulties in achieving position stability and high sensitivity to surface irregularities. As part of this work, a solution consisting in increasing the number of outflow nozzles was proposed. Prototypes of a cushion with additional three and eight symmetrically placed nozzles were made. Then, a research was carried out on the impact of the number and deployment of nozzles on air demand through a pneumatic cushion depending on the load.
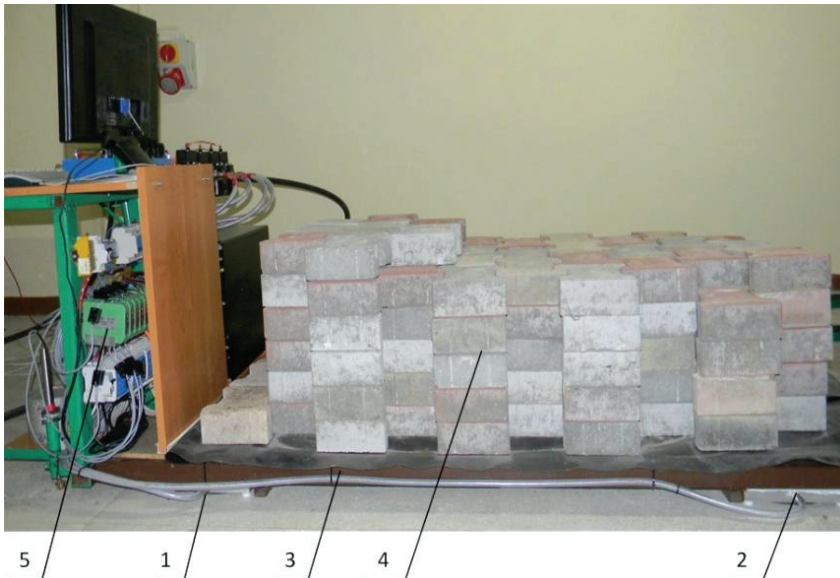

Fig. 1. Transport platform on pneumatic cushions, where: 1, 2 – pneumatic cushions,
3 – frame, 4 – load, 5 – measuring system

2. Mathematical model

Before the start of the research, a mathematical model of a pneumatic cushion with one outlet nozzle, a model with four outlet nozzles and a model with nine nozzles were built. The models were used to determine the theoretical value of the required volume air flow at set values of other parameters such as pressure and temperature.

2.1. Model of the pneumatic cushion with a single outlet

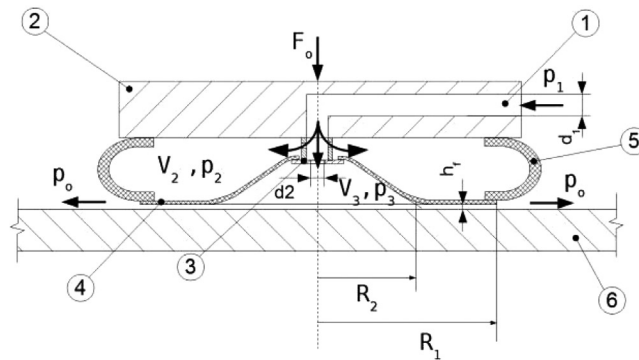The simplified cross section of the pneumatic cushion is shown in Figure 2.

Fig. 2.View of the pneumatic cushion in cross section: 1 – supply collector, 2 – carrying plate, 3 – outlet nozzle, 4 – the bearing surface of the air chamber, 5 – the side surface of the air chamber, 6 – rigid surface

The mathematical model of the pneumatic cushion with one outlet nozzle included the following geometric parameters: d_1 – diameter of the supply collector, p_1 - inlet pressure, d_2 – diameter of the outlet nozzle, F_o – force from the load, p_2, p_3 – pressure in the air chambers, V_2, V_3 – volume of the air chambers, h_f – height of the air gap, p_o – pressure ambient, R_1, R_2 – external and internal radius of the surface cooperating with the floor.

The calculation of the volume flow through the outlet nozzle was performed for the constant state, when the pressure in the side air chamber equalized $(p_1 = p_2)$. With this assumption, the volumetric flow rate was calculated for the slit outlet nozzle [4, 6]:

$$Q_1 = \mu_1 \cdot A_1 \cdot v_1 = \frac{\mu_1 \cdot \pi \cdot d_2^2}{4} \cdot \sqrt{\frac{2}{\rho_p} \cdot (p_1 - p_3)} \qquad (1)$$

where

A_1	– cross-sectional area of the nozzle,
v_1	– flow velocity,
μ_1	– discharge coefficient,
d_2	– diameter of the nozzle,
p_1, p_3	– pressure at the nozzle inlet and in the outlet chamber,
ρ_p	– air density.

The flow of air Q_3 through the annular slit formed between the lower surface of the pneumatic cushion and the rigid surface was calculated by integrating the elementary flow q_r through a segment of the ring-shaped surface of the thickness of dr within limits from R_2 to [5, 6]. After performing simple transformations, a formula was obtained describing the air flow rate at the pneumatic cushion outlet for a constant state:

$$Q_3 = \frac{\pi \cdot p_3}{6 \cdot \eta \cdot \ln\left(\dfrac{R_1}{R_2}\right)} \cdot h_f^3 \tag{2}$$

where

h_f – height of the air gap,
p_3 – pressure at the outlet chamber,
η – coefficient of dynamic,
R_1, R_2 – external and internal radius of the surface cooperating with the floor.

2.2. Model of the pneumatic cushion with the quad outlets

In this case, in the pneumatic cushion, apart from the main outlet nozzle to the lower chamber, three additional outlet nozzles were made, which were arranged on the lower surface of the cushion evenly at 120 degrees on the circle of radius $R_d = 150$ mm. The mathematical model of a pneumatic cushion with four nozzles is defined according to the indications shown in Fig. 3. Assuming flow continuity in constant, volumetric flow rates at individual points of the pneumatic cushion can be noted using formulas (3)–(7). The flow rate through the supply channel nozzle can be noted in the following equation:

$$Q_1 = \mu_1 \cdot A_1 \cdot v_1 = \mu_1 \cdot \frac{\pi \cdot d_1^2}{4} \cdot \sqrt{\frac{2}{\rho_0} \cdot (p_{zas} - p_1)} \tag{3}$$

The flow through the nozzles according to the side and bottom chambers is expressed by the following equations:

$$Q_2 = \mu_2 \cdot A_2 \cdot v_2 = \mu_2 \cdot \frac{\pi \cdot d_2^2}{4} \cdot \varphi \cdot \sqrt{v_1^2 + \frac{2 \cdot \kappa}{\kappa - 1} \cdot \left(\frac{p_1}{\rho_1} - \frac{p_2}{\rho_2}\right)} \tag{4}$$

$$Q_3 = \mu_3 \cdot A_3 \cdot v_3 = \mu_3 \cdot \frac{\pi \cdot d_3^2}{4} \cdot \varphi \cdot \sqrt{v_1^2 + \frac{2 \cdot \kappa}{\kappa - 1} \cdot \left(\frac{p_1}{\rho_1} - \frac{p_3}{\rho_3}\right)} = Q_5 \tag{5}$$

The flow rate through each of the three nozzles placed in the lower part of the side chamber assuming uniformity of load and symmetry of the system:

$$Q_4 = \mu_4 \cdot A_4 \cdot v_4 = \mu_4 \cdot \frac{\pi \cdot d_4^2}{4} \cdot \sqrt{\frac{2}{\rho_2} \cdot (p_2 - p_3)} \tag{6}$$

The total flow of air through the gap between the pneumatic cushion and the ground:

$$Q_6 = Q_5 + 3 \cdot Q_4 = \frac{\pi \cdot p_3}{6 \cdot \eta \cdot \ln\left(R_1 / R_2\right)} \cdot h_f^3 \qquad (7)$$

where

A_i, v_i – area and flow velocity,
ϕ – velocity coefficient,
μ_i – discharge coefficient,
d_i – diameter of the nozzle,
p_1, p_2, p_3 – pressure at the inlet, in the side chamber and in the bottom chamber,
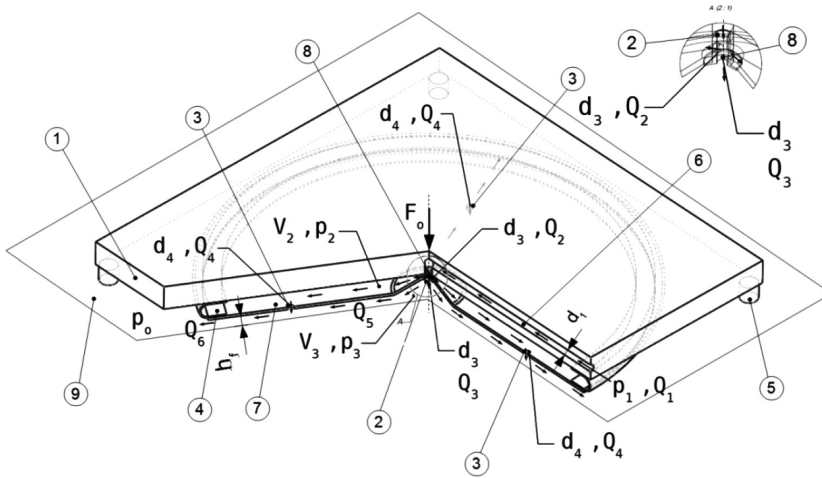ρ_i – air density,
κ – adiabatic coefficient.

Fig. 3. A simplified model of the pneumatic cushion with the quad outlets: 1 – carrying plate,
2, 3 – nozzle, 4 – the side surface of the air chamber, 5 – support, 6 – supply collector, 7 – the bearing surface of
the air chamber, 8 – mounting plate, 9 – rigid surface

2.3. Model of the pneumatic cushion with nine outlet nozzles

The model with nine nozzles was made analogously to the model with four nozzles, with eight nozzles evenly distributed on the circle every 45 degrees. The mathematical model of a pneumatic cushion with four nozzles is defined according to the indications shown in Fig. 4.

The flow rate in this case is described by equations (4)–(6), supplemented by the equation of the total air flow intensity, which in this case has the following form:

$$Q_6 = Q_5 + 8 \cdot Q_4 = \frac{\pi \cdot p_3}{6 \cdot \eta \cdot \ln\left(\dfrac{R_1}{R_2}\right)} \cdot h_f^3 \qquad (8)$$
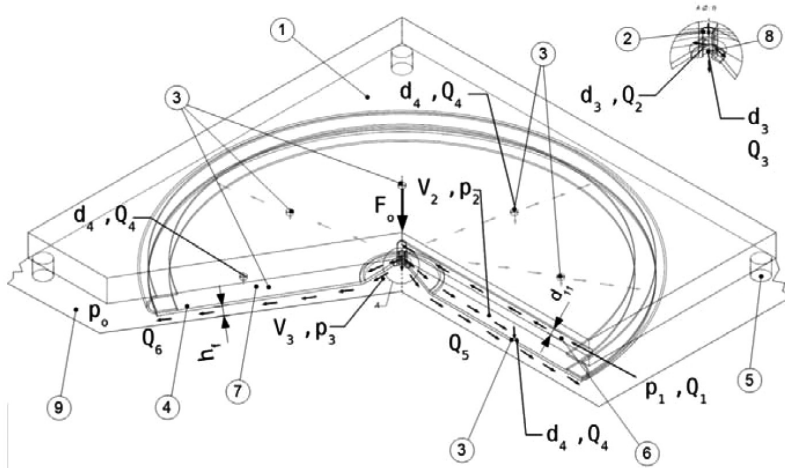
191

Fig. 4. A simplified model of the pneumatic cushion with nine outlet nozzles: 1 – carrying plate,
2, 3 – nozzle, 4 – the side surface of the air chamber, 5 – support, 6 – supply collector,
7 – the bearing surface of the air chamber, 8 – mounting plate, 9 – rigid surface

The constructed mathematical models were used to determine the volume value of the flow rate as a function of supply pressure using the Maple [1] program.

3. Experimental research

In order to conduct experimental research, three prototypes of cushions with an external radius of $R_1 = 250$ mm were built with one, four and nine outlet nozzles respectively. The appearance of the cushion with four nozzles is shown in Figure 5.
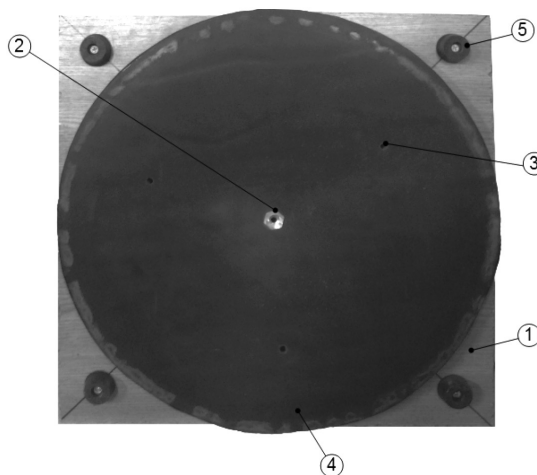

Fig. 5. The air cushion with the quad outlets: 1 – carrying plate, 2, 3 – outlet nozzle,
4 – the bearing surface of the air chamber, 5 – support

The research plan included the determination of the volume flow rate for three pneumatic cushion prototypes made at different load and supply pressure values. The load was in each case carried out by means of a mass placed on the cushion: $m_1 = 202.5$ kg, $m_2 = 252.0$ kg, $m_3 = 324.0$ kg.

During the research, volumetric flow rates were determined depending on the supply pressure. Each graph contains the following curves: 1 – experimental testing at a standstill (without moving the system), 2 – experimental test during the movement of the pneumatic cushion, 3 – theoretical calculation at a standstill (without moving the system), 4 – theoretical calculation during the movement of the air cushion. Sample results of pneumatic cushion tests for the load of $m_3 = 324.0$ kg, are shown in Fig. 6–8.
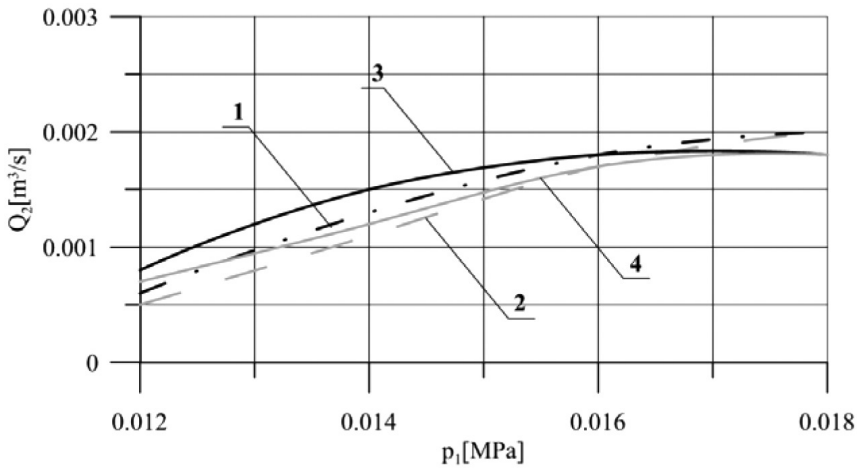

Fig. 6. The volumetric flow rate for the pneumatic cushion with a single outlet, loaded mass $m_3 = 324.0$ kg
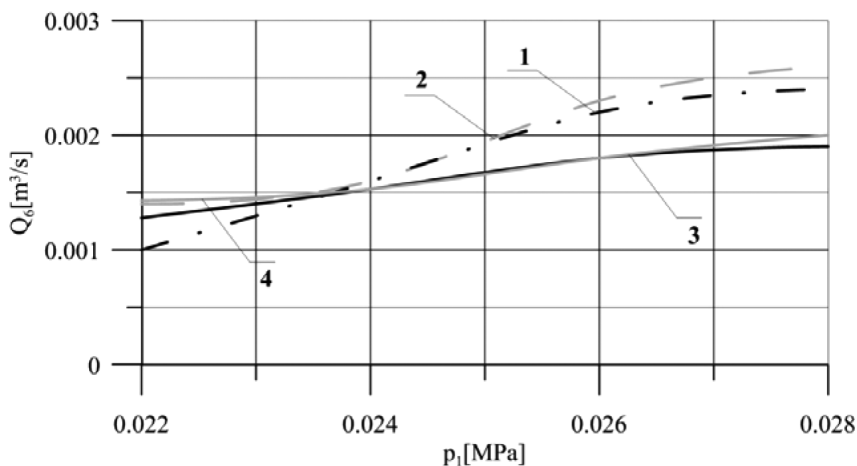

Fig. 7. The volumetric flow rate for the pneumatic cushion with quad outlets, loaded mass $m_3 = 324.0$ kg
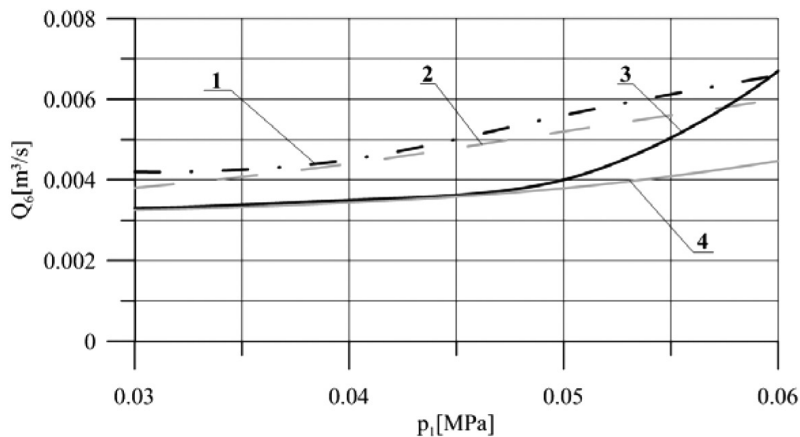
Fig. 8. The volumetric flow rate for the pneumatic cushion with nine outlet nozzles,
loaded mass $m_3 = 324.0$ kg

The presented research results show a good correlation between theoretical calculations and experimental tests. The maximum difference is up to 10% for the single-nozzle pneumatic cushion nd up to 20% for cushions with four and nine nozzles. Slightly larger differences can be observed during the movement of the cushions. This may be caused by surface irregularities which were not included in the mathematical model.

4. Conclusions

The paper studied air cushions with different numbers of nozzles. The dependence of the flow rate as a function of supply pressure for different loads was obtained. The comparison of test results showed that increasing the number of nozzles to four means about twice the increase in air flow required to create the air gap. In the case of a cushion with nine holes, this is an increase of about six fold. At the same time, increasing the number of nozzles leads to a significant improvement in the stabilization of the position of a pneumatic cushion. When lifting the load with the single-nozzle cushion, there was a visible waving effect. This effect was significantly reduced after using the cushion with four nozzles and practically disappeared after using the cushion with nine nozzles. Increasing the number of nozzles also led to a reduction in the force necessary to move the cushion with the load. The use of the cushion with four nozzles allowed for the reduction of force by about 20%, while the cushion with nine nozzles enabledthe reduction of this force by about 50%.

References

[1] Krowiak A., *Maple. Podręcznik*, Helion, Gliwice 2012.

[2] Lisowski E., Filo G., *Pressure control in air cushions of the mobile platform*, Journal of KONES Powertrain and Transport, vol. 18 (2)/2011, 261–270.

[3] Lisowski E., Kwiatkowski D., *Określenie podstawowych parametrów systemu pneumatycznego platformy transportowej na poduszkach pneumatycznych*, Przegląd Mechaniczny, vol. 2 (12)/2012, 45–48.

[4] Messina A., Giannoccaro N., Gentile A., *Experimenting and modeling the dynamics of pneumatic actuators controlled by the pulse width modulation (PWM) technique*, Mechatronics, vol. 15 (7), 2005, 859–881.

[5] Moon J.-H., Lee B.-G., *Modeling and sensitivity analysis of a pneumatic vibration isolation system with two air chambers*, Mechanism and Machine Theory, vol. 45 (12)/2010, 1828-1850.

[6] Wołkow J., Dindorf R., *Teoria i Obliczenia układów pneumatycznych*, Wydawnictwo PK, Kraków 1995.